SINGLE- AND MULTI- CAVITY BEAM MASERS FOR MICROWAVE AND ULTRAMICROWAVE FREQUENCIES

Thesis submitted for the Degree of Doctor of Philosophy

at the University of Keele

by

ANTHONY LEWIS STAPLEY SMITH

Department of Physics,
University of Keele.

June, 1966

ABSTRACT

An ammonia beam maser with a single resonant cavity and with two cascaded cavities is investigated.

A single cavity microwave beam maser is described and its characteristics of operation determined. This maser is constructed so that a second resonant structure can be inserted between the state separator and the main cavity. This second structure can either be another cylindrical microwave cavity or a Fabry-Perot spherical mirror interferometer.

With the two microwave cavity system 'molecular ringing' effects are observed and these have been examined in detail. The system is found to act as an amplifier and as a very sensitive spectrometer. Previously unresolved hyperfine structure of ammonia is observed.

The normal microwave ammonia beam maser uses the inversion splitting of the $J = K = 3$ rotational level. Other rotational levels are also split and molecules in certain of these can be state selected by a multi-pole or ring electrostatic separator. A double resonance experiment using common rotational and inversion levels is considered as a means of detecting ultramicrowave stimulated emission by monitoring the oscillation at the microwave inversion transition frequency.

The design of separators and resonators for ultramicrowave (125μ) radiation is reported and the construction of a far infrared grating spectrometer to test components and systems for the double resonance maser is described.

Preliminary experiments are described for a double resonance

system, with the first resonator taking the form of a half confocal cavity. The sensitivity of this detection system is evaluated.

ACKNOWLEDGEMENTS

The Author would like to thank

Professor D. J. E. Ingram for the provision of experimental facilities.

Dr. D. C. Lainé for his supervision and encouragement.

Many academic and technical staff of the Department for their continued help.

The Ministry of Aviation for provision of equipment.

The S.R.C. and the University for personal finance.

Miss V. M. Cook and Miss E. Evans for their help in the preparation of this thesis.

CONTENTS

Chapter 1. Stimulated emission and Masers

1:1 Stimulated emission and absorption[1-6]

Atoms, ions and molecules can exist in arrangements with considerable variations in energy. Investigation has shown that the particles (henceforth called 'molecules') exist in discrete energy states; that is, the internal energy of such systems is quantised. The energy of such an assembly can change if the electrons or nucleons change their motion or orientation, but this can only happen if the resultant state is a permitted quantum state of the system. Normally the initial and final states of any change will have different energies so the excess energy must be emitted or absorbed. Frequently the excess energy is in the form of radiant energy and there is an interaction between an electromagnetic field and a charged or uncharged molecule.

If the final energy state of the molecular system is higher than the initial state then the excess energy is supplied by the radiation field and absorption takes place. If the final energy state is lower than the initial state then energy is supplied to the field and the process is called emission. If the initial state is 2 (energy W_2), the final state 1 (W_1) and W_2 is greater than W_1, then the emitted energy is $W_2 - W_1$ and this appears as a photon in the quantised field with energy

$$hf = W_2 - W_1 \qquad 1$$

where h is Planck's constant and f is the frequency of the emitted radiation. This is only an approximate relation; Heisenberg's uncertainty relation shows that for any such field-matter interaction lasting a finite time the energies cannot be determined exactly and so the frequency of emission is

not monochromatic.

For there to be a fluctuation or change in the electromagnetic field there must be a change in the electronic structure of the assembly. Thus for radiative transitions either there must be a change of the overall electronic charge of the system, or the spatial charge or moment (dipole or quadrupole usually) must assume a new state. The former process has been used for traditional oscillators and amplifiers at low frequencies (up to 300 GHz), whereas the latter process has until recently only been of use at optical frequencies as a generator and for spectroscopy. But 13 years ago it was pointed out[7] that molecular as opposed to electronic devices might under suitable circumstances be used as amplifiers and oscillators. The acronym MASER[8] was coined, this is now usually taken to stand for 'Molecular Amplification by Stimulated Emission of Radiation', although it can be still used to specifically apply to Microwave frequency devices. Other regions of the electromagnetic spectrum are covered by the terms IRASER for the infrared, LASER for the optical region and UVASER for the Ultraviolet. All these terms are taken to apply to oscillators as well as amplifiers.

In Section 2 below it will be seen that when there is an interaction between a simple oscillator and a field, a definite phase relationship exists between the two and in Section 3 the relationships between the various interaction processes will be introduced and the possibility of practical devices considered.

1:2 The Harmonic Oscillator and phase coherence[6]

To understand the process of molecular emission and absorption of

radiation it is helpful to consider the simple classical model of the harmonic oscillator. This can be considered as an analogue of the electron bound to the atomic nucleus.

Consider the electron vibrating with a resonant frequency ω_0 in the x direction, if there is no damping the equation of motion is

$$\ddot{x} + \omega_0^2 x = 0. \qquad 2$$

However, if there is a field present,

$$E = E_\omega \cos(\omega t + b) \qquad 3$$

where ω is the frequency of the field and b is a phase angle. The equation for the driven oscillator is

$$\ddot{x} + \omega_0^2 x = eE/m \qquad 4$$

where e is the charge of the electron of mass m.

With the appropriate boundary conditions (time is 0 when the wave encounters the oscillator at amplitude a and phase c)

$$\dot{x} = \frac{eE}{m(\omega_0^2 - \omega^2)} \left[\omega_0 \sin(\omega_0 t + b) - \omega \sin(\omega t + b) \right] + a\omega_0 \cos(\omega_0 t + c) \; . \qquad 5$$

There will be a transfer of energy between the field and particle given by

$$W = \dot{x}\, e\, E \text{ per second per frequency interval.} \qquad 6$$

On substituting 5 in 6 one has the integral below for the exchange of energy over the period t,

$$W = \frac{e^2 E^2 \omega}{m(\omega_0^2 - \omega^2)} \int_0^t \left[\omega_0 \sin(\omega_0 t + b) \cos(\omega_0 t + b) - \omega \sin(\omega t + b) \cos(\omega t + b) \right] dt$$

$$+ ae\omega_0 E_\omega \int_0^t \cos(\omega t + b) \cos(\omega t + c)\, dt \; . \qquad 7$$

When W is positive in value there is net absorption of wave energy by the oscillator and when W is negative there is net emission. This sign is determined by the relative values of the phase constants b and c, that is the relative phase of the oscillation and the field.

Consider the situation when the field is exactly at the resonant frequency, $\omega = \omega_0$. Then the first two terms cancel out and the exchange of energy is dependent on the third term. If b and c are of different phase (one positive the other negative) then the third term will be negative and W will be negative and the molecular system will give up energy to the field, that is induced or stimulated emission will take place. It is clear that the induced emission will always be in phase with the field and hence the radiation can be said to be coherent.

If b and c are of the same phase then W will be positive and the radiation field loses energy to the oscillator; absorption takes place. Thus for absorption (as for emission) there is a fixed phase relation between the field and the assembly.

To summarise, in a two state system when a radiant field interacts with a molecular assembly, molecules in the lower state may absorb radiation from the field and molecules in the upper state may emit radiation to the field which is coherent with the field. A certain amount of emission will also take place from the assembly even when there is no incident field, this emission, called spontaneous emission, would correspond to the radiation damping of the electrons in the above analogue.

1:3 Thermodynamic Derivation of A/B[1, 4, 5, 6, 9]

In 1917 Einstein introduced the idea of stimulated emission in order

to be able to describe adequately the interaction of radiation and matter. His argument is thermodynamic and phenomenological and for a microscopic description a quantum mechanical method must be used. Einstein's method introduces most of the concepts required for understanding maser action.

In a black body enclosure the total energy density is only dependent on the absolute temperature of the system. This total energy exists as radiation of a range of frequencies given by

$$U_f df = 8\pi f^2/c^3 \left[\frac{hf}{\exp(hf/kt) - 1} \right] df \qquad 8$$

where U_f is the energy density of the radiation per unit frequency interval at the frequency f, c is the velocity of light, k Boltzman's constant and t the absolute temperature.

The expression $\frac{hf}{\exp(hf/kt) - 1}$ is the average energy in a mode of oscillation at the frequency f and $\frac{8\pi f^2 df}{c^3}$ is the number of modes of oscillation per unit volume in the frequency interval df at frequency f. At microwave frequencies $hf << kt$ for normal temperatures and the average energy per mode, or thermal noise, is kt. At optical frequencies $hf >> kt$ but the average mode energy does not become 0, but rather hf; to obtain this, quantum fluctuation theory is required. Hence it can be seen that at microwave frequencies the zero point fluctuations are negligible but at optical frequencies these provide nearly all the noise.

Einstein considered an assembly of molecules in such an equilibrium black body enclosure. Since the molecules are in equilibrium with their surroundings the molecules when they make transitions between states

must obey Planck's radiation law, equation 8. Consider a two state system with the molecules able to make radiative transitions between the states. For equilibrium, the total probability of transitions from the upper state, 2, to the lower state, 1, (P_{21}) with the emission of a quantum of radiation, $hf_{21} = W_2 - W_1$, must equal the total probability of transitions of 1 to 2 (P_{12}).

Assuming both states have the same statistical weights and if C is a temperature dependent constant the probabilities will depend on the number of molecules in each state so one has

$$P_2 = C \exp(-W_2/kt) \quad \text{and} \quad P_1 = C \exp(-W_1/kt). \qquad 9$$

There will be three types of transition. If there is no radiation present then a molecule in state 2 (upper) may spontaneously emit a photon (so called zero point fluctuation in the electromagnetic field) with a probability $A_{21}dt$ where dt is the time of observation and A_{21} the spontaneous emission coefficient. If radiation is present (density U_f) then the probability for stimulated emission from state 2 to 1 is $U_f B_{21}dt$ where B_{21} is the coefficient of induced emission. Similarly the probability of absorption from state 1 to 2 is given by $U_f B_{12}dt$.

Hence the total probability for an upward transition is the absorption probability multiplied by the probability of occupation of the lower state, thus

$$\text{Probability}_{12} = U_f B_{12} C \exp(-W_1/kt)dt \qquad 10$$

and the emission probability is the sum of the spontaneous and stimulated components

$$\text{Probability}_{21} = U_f B_{21} C \exp(-W_2/kt)dt + A_{21} C \exp(-W_2/kt)dt. \qquad 11$$

In thermal equilibrium these two probabilities are the same (and from 10 and 11)

$$U_f B_{12} \exp(-W_1/kt) = (U_f B_{21} + A_{21}) \exp(-W_2/kt). \qquad 12$$

B_{12}, B_{21} and A_{21} can be evaluated quantum mechanically, but it can be seen immediately that if t becomes large, the exponential terms tend to equality and (by equation 8) U_f becomes large so for thermal equilibrium

$$B_{12} = B_{21} \qquad 13$$

and so equation 12 becomes

$$U_f B \exp(W_2 - W_1/kt) = A \exp(-W_2/kt) \qquad 14$$

which with 8 gives

$$A = \frac{8\pi f^2}{c^3} hfB \ . \qquad 15$$

Now $8\pi f^2/c^3$ is the number of radiation modes per unit volume per unit frequency range and hf is the energy of the appropriate quantum so equation 15 can be expressed as

(A) = (mode density per unit frequency range) × (transition quantum energy) × (B) .

16

This latter expression is more uniformly applicable because it can be used for any structure, not only a black body enclosure: in particular in the microwave region in a resonant cavity the term 'mode density per unit frequency range' will have the value of the reciprocal of the half

power frequency response range.

The individual values of A and B can be obtained by quantum mechanics as

$$A = \frac{64\pi^4 f^3}{3hc^3} |\mu|^2 \qquad B = \frac{8\pi^3}{3h^2} |\mu|^2 \ . \qquad 17$$

But the relative importance of stimulated and spontaneous emission in various parts of the spectrum may be obtained by comparing equation 15 with equation 8

$$A/(BU_f) = \exp(hf/kt) - 1 \qquad 18$$

$hf/kt \sim 5 \times 10^{-3}$ at 1 centimetre (30 GHz or 10,000 μm)

0,5 at 100 μm (3 THz or 0.1 mm)

50 at 1 μm (300 THz or 1,000 nm)

for normal room temperatures. Thus at microwave frequencies spontaneous emission will be negligible and in the far infrared it will be small compared with stimulated emission, provided that the stimulating field is not too small. But at optical frequencies the spontaneous emission is considerably greater than stimulated emission unless the field is considerable.

For the two state situation when spontaneous emission can be neglected the population of states may be given by

$$N_1 + N_2 = N \qquad 19$$

and the normal Boltzman distribution gives

$$N_2/N_1 = \exp(-(W_2 - W_1)/kt) = \exp(-hf/kt). \qquad 20$$

The molecules can be 'paired off' to give the excess population as

$$N_1 - N_2 \sim hfN/2kt \ . \qquad 21$$

Thus at normal temperatures and at 1.25 cms $N_1 - N_2$ is only N/500. This means that effectively in absorption spectroscopy only one in 500 active molecules can contribute towards the observable absorption: the remaining 'absorptions' are 'paired off' by 'stimulated emissions'. If in some way the populations are altered to non-thermal values the observed signal might be increased by a factor up to 500. The creation of such non-thermal distribution systems has been achieved in several ways with Masers.

1:4 Masers[10]

The first devices to be constructed which created inverted populations and from which stimulated emission was observed are attributed to Bloch[11] and Purcell and Pound[12]. These were transient systems and no amplification was achieved; it was not until 1953 when Weber[7] pointed out the possibilities of amplification and oscillation with non-Boltzman populations that the first serious consideration was given to practical and useful devices in the open literature. But several suggestions seem to have been circulating in 1952. Nethercot gave a paper (on behalf of Townes) at a sympsium on submillimetre waves at Illinois and Basov and Prokhorov[13] also suggested a molecular amplifier.

In 1954 Gordon, Zeiger and Townes[8, 14] published their first results on a successful microwave amplifier and oscillator (at 24 GHz) using ammonia gas. They realised that they had a very low noise amplifier ($< 10^{o}$K), a very stable oscillator (~ $1/10^{10}$) and a gas spectrometer with a resolution (~ 7 KHz) nearly an order of magnitude better than any achieved previously. Work was also going on to create a useful two

level pulsed system and a Phosphorous doped silicon crystal was used as an adiabatic fast passage maser by Combrisson, Honig and Townes[15].

The first proposals for three level systems and pumping to obtain continuous operation devices came from Basov and Prokhorov[16] and Bloembergen[17] and in 1957 Scovil, Feher and Seidel[18] produced a 9 GHz continuously operating three level solid state maser using the paramagnetic spin levels of gadolinium in a crystal of lanthanum ethyl sulphate. Since then solid state masers using ruby crystals and several other materials have been developed. Since 1960 Ramsey[19] and others have developed the atomic hydrogen beam maser.

Masers working at infrared and optical frequencies were first proposed by Schawlow and Townes[20] and later by Basov, Krokhin and Popov[21]. In 1960 Maiman[22] demonstrated laser action with a pulsed ruby device optically pumped with a Xenon flash lamp and Javan, Bennett and Herriott[23] obtained continuous oscillation in a mixture of Helium and Neon in a gas discharge in the near infrared. More recently lasers have been made using semiconductors and double quantum transitions. The frequency range of the various devices now extends from the ultraviolet to the far infrared.

In the following sections of this chapter the different types of devices will be considered. In Section 1:5 special consideration will be given to beam masers (also treated in Chapters 4 and 5) but no mention will be made of multi-cavity masers which are treated in some detail in Chapter 6. In Section 1:6 other microwave masers are considered and in Section 1:7 lasers, Uvasers and Irasers. In Section 1:8 various double quantum systems are mentioned. All these sections are very brief and emphasis is given to the possibilities of laser action in the region of

the electromagnetic spectrum between microwave and infrared, the far infrared (50-1000 μm). This region of the spectrum is considered in more detail in Chapter 2, where the direction of the investigation described in this thesis will be discussed.

1:5 Beam Masers

In the Ammonia beam maser a non equilibrium population condition is obtained by passing a beam of molecules through a very strong inhomogeneous electric field (~ 100,000 volts/cm): this both creates a second order Stark effect for the molecule and physically separates molecules in various energy states. Each rotational state of the molecule (quantum numbers J for total rotation and K for resolved component about the molecular axis) is split by the inversion of the nitrogen about the plane of the hydrogens (see Chapter 3). With a suitably designed electrostatic system the upper state molecules are concentrated along the axis of the beam and the lower state molecules move away from the axis. This 'focusing' effect is strongest for the lower energy rotational 'inversion pairs' and Gordon, Zeiger and Townes used the J = K = 3 inversion transition at 23.870 GHz. After state separation the beam enters a resonant structure, in this case a resonant cavity, and if the flux, separation and quality factor of the cavity are sufficient oscillation takes place with a power of about 10^{-11} watts. Since the oscillation is observed nearly normally to the beam axis the normal Doppler broadening is much reduced and a spectrometer with about 4 KHz linewidth is obtained. Gordon[24] used the spectrometer to observe the hyperfine structure of the ammonia molecule by operating it below

oscillation threshold. It has also been used as an amplifier[25] since it has an intrinsic noise temperature of only a few degrees absolute (this is usually masked by considerably more thermal apparatus and circuit noise) but its bandwidth is only about 300 Hz so this is a rather restricted application. The oscillation is very stable and has been studied experimentally[26-32] and theoretically[33-36] by a considerable number of people. It has been used as a frequency standard with a stability of about one in 10^{10}, but with an accuracy rather worse than this. Apart from variations due to changes in device operating conditions the $N^{14}H_3$ 3-3 Maser has the drawback that the oscillation line is made up of three hyperfine components (see Chapter 3) with a spread of about 2 KHz. This quadrupole nuclear interaction[37] can be removed by using the J = 3, K = 2 inversion transition or by using $N^{15}H_3$. The former is undesirable because a greater flux of molecules is required and this leads to greater device instabilities, but an accuracy of a few parts in 10^{11} has been achieved[38]. The use of the nitrogen-15 isotope produces a stability of about the same amount[39], but both oscillators are subject to travelling wave effects; recently attempts have been made to reduce these by using multi-cavity and opposed beam systems (see Chapter 6 below), but there is some doubt as to if ammonia will be adopted as a frequency standard[40]. The main rivals are the atomic hydrogen beam maser, the rubidium gas cell controlled oscillator, the Caesium beam standard and the thallium beam standard. Of these the atomic hydrogen beam maser seems to have the best short term and long term stability and the best reproducibility,

but it is large, heavy and expensive. The caesium beam standard has poor short term stability and the rubidium standard's reproducibility is poor, but it is suggested[40] that the thallium standard may be good. All these devices have stabilities in the range one in 10^{12} to one in 10^{14}.

The Hydrogen maser[41-44] operates between the ground state hyperfine levels of atomic hydrogen at 1420 MHz. A magnetic state separator is used to focus the upper state atoms into a teflon coated quartz bulb which is inside a cylindrical radio frequency cavity, radiation is produced when the cavity is tuned correctly, and the line Q is very large because the atoms exist in the bulb for about one second. The rubidium frequency standard has existed for several years[45-48], but only recently has the device achieved sufficient gain to achieve self-sustained maser oscillation[49]. A rubidium lamp is used to pump a mixture of rubidium-87 and a buffer gas in a cell mounted in a cavity tuned to the 6835 MHz transition. With correct filtering and polarisation of the optical radiation an inverted population is obtained and an oscillation power of about 10^{-10} watts.

A beam maser can be constructed for many different substances provided that a resonant structure can be made for the appropriate frequency and that the energy levels are such that a magnetic or electrostatic separater can be used as a focuser. Shimoda[50-52] has used a parallel plate condensor resonator and an electrostatic state separator on the K-type doubling transitions of formaldehyde at 4.6 MHz and 18.3 MHz and Thaddeus[53-54] has examined the hyperfine structure of HDO at 10.3 GHz, HDS at 11.3 GHz, CH_2O at 14.5 GHz and

CHDO at 16.0 GHz.

In general there are no reasons why similar techniques should not be used for higher frequency beam masers, provided that the transitions are strong enough and adequate state separation can be obtained. But higher field gradients in the separator are required and it is less efficient for states with larger J values and also the population of higher energy states is smaller. Krupnov and Skvortsov have operated a formaldehyde maser at 72.838 GHz using a normal single mode cavity[55] and a multi-mode plane parallel Fabry-Perot resonator[56-57]. Marcuse has used the rotational levels of HCN at 88.6 GHz, again with electrostatic state separation and a multi-mode cavity. But in this case he had to use a multi beam focuser arrangement in order to obtain sufficient flux; and a low loss confocal cavity (see Chapter 4).

Several proposals have been made for using similar systems for even higher frequencies[62-64], and Gorog[65] and Basov and Letokhov[66] have proposed optical beam masers. Because of the greater spontaneous emission at optical frequencies and because of beam transit time effects Basov and Letokhov suggest that forbidden transitions with lifetimes of 10^{-3} to 10^{-5} seconds will be most suitable. They suggest levels in the alkali-earths, zinc and the group V elements: these would be pumped with intense spectral lamps, or their own radiation suitably amplified in another laser amplifier. Gorog's suggestion is that the required inverted population might be achieved by photodissociation, in particular from rubidium iodide to an excited state of rubidium.

Gordy and Cowan[67] have suggested that the problems of obtaining inverted populations for far infrared masers could be overcome by using

two inverting fields rather than one and Bergmann has suggested a multi level pumping system for Sodium[68]. Such a multi level pumping or double quantum system has been used by Shimoda and Wang[69] for examining the hyperfine structure of ammonia at 24 GHz.

Schulten has pointed out[70] that a conventional electrostatic separator is not necessary if a field perturbation is applied for a carefully calculated length of time, and has proposed a OCS Maser at 73 GHz. Laine[71] has pointed out that if consideration is given to the coherent nature of the information in such a system a self pumping sensitive spectrometer might be obtained provided that two resonant structures are used.

1:6 Microwave solid state masers[1, 2, 10]

The first solid state masers were two level devices using paramagnetic spin systems in a magnetic field. Inversion was obtained by pulse techniques and Bolef and Chester[72] have reviewed the various inversion methods: 'Adiabatic fast passage', '180° pulse inversion' and 'sudden field reversal'. These devices usually had to be operated at low temperatures and the 'amplification time' and repetition frequency were controlled by the various relaxation times. Bolef and Chester suggested several methods, such as the use of mechanical feed systems and rotating crystallite assemblies, for converting these two level systems to continuous operation; but these methods became unattractive when the continuously operating 3 level masers were introduced. However, they may still be used when a pulsed oscillator or amplifier is acceptable, either because of lack of alternatives such as in the sub-

millimetre region of the spectrum or because of the nature of the signals being examined[73]. Hirschfield and Wachtel[74] have made a continuously operating two level electron cyclotron maser at 5.8 GHz producing 10 milliwatts, and such a system might be extended to higher frequencies[74a].

In the microwave region of the spectrum solid state masers have to compete with many existing amplifiers and sources of coherent power as well as the more recently developed parametric amplifiers[75], transistor amplifiers and oscillators, avalanche transit time diodes (Read devices) and Gunn oscillators[76]. Thus it appears that masers will be selected as oscillators only at high frequencies (> 30 GHz) or very low noise amplifiers (< 15°K below 4 GHz, < 30°K from 4 GHz to 10 GHz)[77-79].

Most continuously operating solid state masers have used the paramagnetic ions Cr^{3+}, Fe^{3+} or Gd^{3+} at low temperatures in a magnetic field to produce a 3 or 4 level system. The paramagnetic ion in a suitable host crystal is mounted in a cavity (or waveguide) resonant to two (or more) frequencies, the signal frequency and the pump frequency. In the 3 level system with energies $E_3 > E_2 > E_1$ (and populations n_3, n_2 and n_1) and with a normal thermal distribution of populations one has $n_1 > n_2 > n_3$. If radiation of energy $E_3 - E_1$ is incident on the system such that this transition is saturated (usually at low temperatures) then $n_1 = n_3$ and either $n_2 < n_3$ or $n_1 < n_2$ and stimulated emission can be obtained: if the pumping is continuous and the system is suitably cooled to make the relaxation time for the non maser transitions appropriate an amplifier or

oscillator can be made. Frequently it is found that a more convenient system is obtained if a four level system is used, the pumping can be achieved in various ways, but one common mode of operation is to pump to both populate the upper maser level and depopulate the lower maser level.

Normally the pump frequency must be greater than the signal frequency but with complicated pumping schemes this need not be so and Minkowski[80] has operated a 9.6 GHz amplifier with a 5.7 GHz pump and Hughes[81] achieved maser action in an iron doped rutile crystal at 91 GHz with a 65 GHz pump. More recently Odehnal[82] has suggested a double quantum system and this is discussed in section 1.8 below.

The paramagnetic crystal for a maser amplifier may be placed in a resonant cavity or in a travelling wave structure, the latter configuration is now considered to be the best since the system can be made unidirectional and hence there is good isolation of input and output, the bandwidth is larger and the system has a greater dynamic range. Also the gain will be greater and the noise output less. The main disadvantage is the greater interaction length of field and crystal required, this problem is overcome by using a slow wave structure or a crystal material of large dielectric constant. For some specialist applications cavity masers are still used, thus Hughes and Richards[83] have used ferric ions in polycrystalline and powdered aluminium nitrate at 9.35 GHz, obtaining 25 dB gain with a bandwidth of 4.5 MHz at 4.2°K and a tuning range of 200 MHz. Similarly Hughes and Deal[84] have operated a Fe^{3+} in TiO_2 zero field maser at 81.3 GHz with a 20 MHz bandwidth.

Travelling wave masers[10, 85] have been operated over most of the range 1 GHz to 50 GHz as low noise amplifiers, frequently for radio astronomy. Thus Yngvesson and Kollberg[86] have made an L band amplifier of Chromium doped rutile at 1.2 to 1.5 GHz with gain greater than 20 dB, bandwidth 5 MHz and a noise temperature of less than 10^{o}K. Matveenko[87] and others have obtained 20 dB with a 15 MHz bandwidth at 2^{o}K at 8 cms. wavelength. Norris and Miller[88] have obtained 55 dB gain with 14 MHz bandwidth in C band with iron doped rutile in a meander line; and Arams and Peyton[89] have used chromium doped rutile with 20 dB gain and a noise temperature of about 20^{o}K for a 75 MHz bandwidth and a tuning range from 35 to 40 GHz. McEvoy and others[89a] have developed a magnetic stagger tuned wide bandwidth maser at 5 GHz with iron doped rutile at 4.2^{o}K. The gain and bandwidth varies from 78 dB with 12 MHz to 33 dB with 66 MHz.

1:7 Laser oscillators

A large amount of literature has been published on lasers in the last five years so this short review will concentrate on near and far infrared laser action and emission obtained as a difference frequency between two higher frequency sources. Many general review articles have been written[10, 20, 21, 90-97] and because of the coherence[98] and directivity and high powers available the possible applications are considerable. Applications[99-100] include non-linear optics[101-103] and dielectric breakdown[104], communication[105-107], amplification[108-114], scattering and interferometry[115], plasma diagnostics[116], machining[117], computation[118], rotation sensing[119], determination of the velocity of

light[120], holography[121], surveying and radar[122], besides the investigation of effects such as laser speckle patterns[123-127] and the self trapping of optical beams[128-131].

The first laser to work was the ruby laser of Maiman, since then many liquid and other solid systems[10, 100, 132, 133] have lased but the majority of non-gaseous systems have used Transition, Lanthanide or Actinide ions in glass or crystal lattices. The crystal is usually of the order of 10 cms. long, a few millimetres in diameter and has its end faces polished flat and parallel to form a Fabry-Perot resonator, alternatively an external Fabry-Perot or spherical mirror assembly is used. The output is normally pulsed because of the difficulty of obtaining sufficient population inversion with the incoherent radiant pump lamps available, and the system may be 'Q' switched to increase the peak intensity of the output. Normally a 3 or 4 level system is used at liquid nitrogen or room temperatures with a few pump pulses per minute and output pulses lasting a few milliseconds. Normally the crystal field splittings of the ion spectra are quite large (very large for the transition ions) and the laser action depends both on the crystal lattice and on the doping ions. The most powerful solid state lasers are still those using chromium doped aluminium oxide, energies of 1500 Joules have been produced with peak powers of 55 MWatts, or 6 GW with a ruby amplifier following the oscillator. This system works at 693.4 to 694.3 nm and the Nd-doped glass laser at 1.06 μm produces nearly as much power. Nd-doped systems are interesting for two reasons; first Nd^{3+} and another dopant (such as Yb^{3+}) have been used to double dope Gadolinium Tungstate crystals, such that the radiation

pump can be used to pump the Yb^{3+} ions which then resonantly couple to the Nd^{3+} such that the pulse energy and lifetime are increased; in fact Nd^{3+} has been used in a CeF_3 host such that the rare earth in the lattice is used to pump the Nd^{3+}.[100] The second interest is that Zernike and Berman have used a neodynium glass laser to generate a difference frequency in the far infrared[137], using quartz as the non linear mixing element.

The other large group of solid state lasers are the semiconductor lasers[138-140], the first of these to work were made from Gallium Arsenide doped with Zinc and Tellurium to produce highly degenerate diodes. Three groups in the United States produced the first diode lasers in the autumn of 1962 by forward biasing the diodes at liquid nitrogen temperature and with pulsed currents of the order 10^4 amps per square centimetre. The 840 nm light propogated in the plane of the junction and average power of the order of a watt was obtained. Later room temperature pulsed operation and liquid hydrogen and helium temperature continuous operation were obtained. Other III-V compounds to have lased include InAs, InP and InSb (at 5.3 μm). Holonyak and Bevacqua[141] have made a series of lasers with frequencies of 660 to 840 nm by varying the ratio of Arsenic and Phosphorous in a Gallium arsenide-phosphide diode. Group IV-VI compounds have also lased, PbTe at 6.5 μm and PbSe at 8.5 μm.

The InSb laser is interesting because the emission has been obtained normal to the plane of the junction such that the emitted radiation only has to be transmitted through a few micrometers of semi-

conductor, and also because the emission wavelength is tunable by 5% with a magnetic field (~ 13 kGauss)[142].

Most of these diodes require low temperature operation, but it appears that magnetic fields and pressure may be able to tune these devices over several microns[143]. More recently diodes have been pumped by electron beams[144] and optical radiation and it appears that coherent radiation should be obtainable from the optical region to about 14 μm and possibly further, and throughout the middle and far infrared as a beat frequency[140].

The only optically pumped gas system to have lased is a Caesium laser at 7.18 μm[145]. All the other gas systems have used electron excitation either with an R.F. or D.C. discharge, frequently with a second species acting as a resonant transfer medium. The first gas laser system, the helium neon laser, has lased from 590 nm downwards in frequency, typically with a tube about a metre long, one centimetre in diameter and with spherical mirror geometries. Output powers of only 1 to 50 mWatts are achieved in any one line[146]. Patel has extended the number of neon lines observed into the middle and far infrared, the longest wavelength lines being at 124.4, 126.1 and 132.8 μm. A typical cavity for such lasers is five metres long, 5 cms. diameter with silvered mirrors and a single output coupling hole in one mirror. Pumping is by electron excitation and individual lines have powers of less than a nanowatt[147-152]. Many other noble gas lines have been observed in the near infrared, and the argon ion laser[153] produces several watts of continuous wave power in the optical region. Some of the noble ion lasers are the highest frequency coherent sources at the

moment and a pulsed discharge through neon has produced oscillations at 337 nm[154]. But several suggestions have been made for higher frequency lasers, using chemical systems[155], Quartz[156], excitons[157] and other materials and mechanisms[158-160].

In 1963 several laboratories obtained laser action in vibrational-rotational bands of molecules in the infrared; Mathias and Parker used a D.C. pulse discharge system in confocal resonators with one of the mirror's aluminium surfaces partially transmitting. They found numerous lines from 0.8 to 1.1 μm in Nitrogen[161] and from 0.5 to 0.8 μm in Carbon monoxide[162] with peak powers of a few watts and average powers of tens of microwatts. Patel used a 5 metre discharge tube with coupling either through one of the metallic mirrors or through a small coupling hole in one of the mirrors: he found numerous transitions in the vibrational-rotational band of carbon dioxide near ten microns and a very strong line at 10.6 μm which produced 1 mW of continuous power[163-164] and one milliwatt when pumped with an R.F. discharge in a one metre long tube with selective excitation with nitrogen[165].

Mathias, Crocker and Wills used diffraction coupling round a limited area mirror in a nitrous oxide laser at 10.9 μm[166] and Patel has obtained 10 mW of continuous power from a continuous flow gas system of Nitrogen and CS_2 at 11.5 μm[167]. Very recently Moeller and Rigden[168] have obtained 18 watts in a CO_2, He, N_2 mixture in a one metre tube, two centimetres in diameter using a continuous flow system and Patel and others have operated a similar mixture in a 230 centimetre long tube, 7.7 cms. in diameter to produce more than a hundred watts of continuous power (at

10.6 μm)[169].

In 1964 Gebbie and others obtained laser action in a 480 cms. long tube at a number of wavelengths between 23 and 79 μm in water vapour with a peak output of 40 watts per pulse at 27.7 μm[170]. Later a further line was found at 119 μm[171] with an even larger system and Mathias and Crocker have used a better resolution system to obtain lines from 16.9 μm to 120.08 m with lines at 115.42 μm and 118.65 μm, but with peak output powers of less than a milliwatt at the longer wavelengths[172]. Since then these lines have lased continuously[173] and in smaller systems[174].

Laser lines have been found among the ground electronic state vibration-rotation levels of ammonia between 21 and 32 μm with peak powers of several watts lasting for a few microseconds[175], and Gebbie and others have obtained laser action in H, C and N compounds at 337 μm. They used a 930 cms. discharge tube and obtained peak powers of about 10 watts[176-177]. Several other lines have since been found in dimethylamine and deuterium plus bromine cyanide: from peak power lines of about one watt at 126.24 μm, 128.75 μm and 130.95 μm to rather less power at 372.80 μm and half a watt at 538 μm, the longest wave length laser so far recorded[178-179].

1:8 Multi-Quantum devices

The optically pumped rubidium maser has already been described, this is a three level system where an inverted microwave energy level population is obtained by using an intense optical lamp. Thus the pumping frequency is very much greater than the signal frequency and

the energy efficiency of the oscillator is very small. But this type of pumping does provide the possibility of a far infrared maser and several people have investigated the energy levels of ruby. Devor and others[180] have obtained stimulated emission at 22.4 GHz with optical pumping and proposed extension to the millimetre region[181]. Scabo[182] has obtained maser action at 9.4 GHz at liquid nitrogen temperature using a ruby laser pump and Prokhorov and others have used a similar system to obtain about 10^{-5} watts of power in the millimetre region[183]. Strain and Coleman have used a ruby sample at liquid helium temperatures to observe stimulated emission at 426 and 612 GHz[184].

Phelan and Rediker pumped a 5.3 μm InSb laser with a Gallium Arsenide laser and possibly obtained a quantum efficiency of greater than one[185]. All these devices are basically double resonance devices and only one metastable level is required[186-187], whereas in 1959 Bloembergen[188] proposed another type of device, the quantum counter, which requires two metastable levels for operation. The quantum counter depends for its action on receiving two signals (usually infrared or optical) at nearly the same time (one 'signal', one 'pump') and having suitable energy levels matching these energies. Thus double excitation takes place and the system decays by fluorescence. The advantages of this system are low noise operation and conversion of a possibly difficult to observe infrared signal to an easily observable optical quantum[189]. Several systems have worked[190-191], and similar effects have been observed amongst competing laser transitions[192].

Harmonic generation can be achieved by using a non linear element or the non linear relationship between the polarisation of a particle system and its driving field, this latter effect becomes less efficient

at millimetre wave frequencies and it has been found that third harmonic generation is greatly enhanced if at least one of the energies involved coincides with a quantum transition energy of the particle system[193]. Thus the inversion transition of ammonia[194] has been used and Akitt and Coleman[195] have generated one and a half watts at 104 GHz and Andresen[196] has proposed this method for the generation of submillimetre radiation. A similar but different process is used in the double quantum device where two quanta (photons or phonons) add or subtract to coincide with the energy gap in a system, but with no energy gaps corresponding to the individual quanta. Such effects[197] have been observed in the optical region of the spectrum with laser beams and in 1964 it was proposed that a laser could be made from such a system. In fact such maser amplification was first observed recently in the microwave region of the spectrum using a photon-phonon effect in MgO[198].

Chapter 2. The Far Infrared Region

2:1 Introduction

The far infrared region of the electromagnetic spectrum (50 microns to 1000 microns) is virtually uninvestigated, principally due to the lack of any sources of appreciable power. Few microwave electron tubes have been constructed to work at less than 2,500 μm and the only other sources of coherent radiation in the region are harmonics generated from lower frequency electron oscillators and gas lasers. Spectroscopy in the region has relied on incoherent and thermal radiation, frequently from a mercury discharge tube. This is of insufficient intensity to allow a resolution better than one part in a hundred for most of the region.

In this section there will be a general discussion of the reasons for interest in this region of the spectrum and the material systems which have energies of this order. In Section 2 the problems of sources, transmission and detection will be considered and possible designs for a spectrometer presented. Section 3 is a brief survey of non-thermal sources which have been proposed for operation in this region and in Section 4 a detailed proposal for a stimulated emission device using the rotational states of ammonia gas is considered. In Section 5 the construction and use of a grating spectrometer to test materials and systems in connection with the ammonia Iraser is described.

There have been a number of survey articles on the far infrared or sub-mm region of the spectrum[199-210] and specific references will only be made to more recent developments.

The energies associated with gaseous molecular rotational transitions correspond to microwave or far infrared frequencies according to the mass of the molecule. The lighter molecules, such as hydrogen iodide, ammonia, nitrous oxide, water vapour and simple organic molecules have their lower energy transitions in the far infrared and the slightly heavier molecules which have small quantum transitions in the millimetre region have their higher transitions in the submillimetre region.

Ionic crystal lattice vibrations occur in the infrared and far infrared, thus RbI has an absorption peak at 75 cm^{-1} and Sodium Chloride resonates at 164 cm^{-1}. Other halides also have lattice vibrations in this region (AgBr at 85 cm^{-1}) and spectroscopic examination of these absorption spectra has shown that the alkali halides are by no means ideally ionic crystals and that considerable information about lattice vibrations and structure can be obtained.

Simple organic molecules have vibrational frequencies in the near infrared and these are used by organic chemists to determine their structure, and very large bodies have acoustic modes in the audio frequency range. Chain molecules, about a hundred atoms long, have skeletal twisting motions in the far infrared which can be observed spectroscopically if the charge distribution is assymetric. At even lower frequencies (~ 10 cm^{-1}) resonances have been observed in anti-ferromagnetic crystals at low temperatures. Also at low temperatures the 'superconducting edge' has been examined in the 25 cm^{-1} region for

some metals and evidence has been found for the correlation of the behaviour of the electrons.

Semiconductors have their intrinsic absorption edge in the optical or near infrared region of the spectrum, but various impurities and multi photon effects can produce lower energy absorptions, especially at low temperatures; and cyclotron resonance can be observed if a suitable magnetic field is used.

Plasma densities and temperatures can be measured by observing the reflected and transmitted components of suitable frequency radiation. The ideal frequency increases with plasma density and with plasma densities of 10^{14} to 10^{16} particles per cubic centimetre ultramicrowave radiation is desirable.

For communication systems higher frequencies can carry more information content and the ultramicrowave band could, ideally, carry a hundred times as much information as the present radio and microwave frequency bands; but problems of coherent sources, modulation and atmospheric attenuation are considerable and it would seem that any such system would have to use guided propogation in 'light pipes', except possibly at about 1 mm and 350 μm.[211]

2:2. Ultramicrowave transmission and detection

To produce radiation between 200 cm^{-1} and 10 cm^{-1} is difficult, the only sources using the intrinsic properties of materials are the gas lasers mentioned in the last chapter; but these only work at specific frequencies, are virtually untunable and are frequently of very low power. Thus they are unsuitable for general spectroscopy.

In the microwave region of the spectrum, devices, such as Klystrons, which use the interaction of electrons with fields are used, but at higher frequencies very small resonant structures are required. Thus at 5.5 mm a typical Klystron will have cavity dimensions of hundredths of an inch and require potentials of about 2 KV. Other possible sources of power are discussed in Section 3 below, but at the moment for spectroscopy the best source available is a high temperature black body radiator. Typically this means (according to Planck's radiation law) that the maximum power available for the band 900 to 1000 microns is 10^{-8} watts. This is very much less than that available in the near infrared or optical region. Thus for a 10^{4} ^{o}K source only one part in 10^{8} of its output is in the region of 200-400 μm. Since the source is so weak, a black body at as high a temperature as possible is required, thus a Nernst filament, Globar or mercury discharge tube is used[212-215]. The best at wavelengths more than 100 μm is a medium pressure mercury discharge lamp with a fused quartz (silica) window. Silica because glass could not withstand the temperature and is completely opaque to sub-mm radiation.

For a spectrometer in the 100-500 micron region transmission components such as lenses cannot be used because nearly all materials absorb too greatly; the best transmitters such as crystal quartz, polyethylene, melinex and polystyrene typically absorb 50% per millimetre. Thus transmission components[216-219] are only used as filters and windows, and a spectrometer will use metallic surfaced mirrors and components as large as possible. Nearly all far infrared spectroscopy

has used diffraction grating spectrometers, but some Fourier transform, Michelson type interferometers have been constructed[220]. Ideally these have a higher resolving power than grating instruments (principally because they do not use power limiting slits or filters), but their outputs have to be transformed by a computer to produce a wavelength spectrum and they are rather inflexible. The grating spectrometers use metallic echelette gratings to put as much as possible of the energy in one desired order of the spectrum, either in a Czerny-Turner or Ebert configuration[221-223]. Typically the telescope and collimator mirrors will be 20 cms in diameter and have focal lengths of 40 to 80 centimetres. Symmetric entrance and exit slits a few centimetres high will be used with a mercury-quartz lamp source and both transmission and reflection filtering. Because of the larger amount of higher frequency radiation to be removed the filtering must be very efficient. Unfortunately normal transmission filters for the region have rather gradual out-offs, and although crystal quartz, sapphire, polyethylene and carbon loaded polyethylene ('black polythene') are used[224-226], they have to be supplemented by rather more specific filters. Thus Restrahlen filters are used both in reflection and transmission[227-230]; and filter gratings, meshes and scatter plates are used[231-234]. Various guided propagation systems have been proposed for the ultramicrowave region, but the only 'quasi-optical' techniques[235-236] to be much used are light pipes and cone channel condenser systems[237-240], especially for guiding the radiation to the energy detector.

The detection of sub-mm radiation has recently been reviewed by

Putley[241]. The most usually used detector is the Golay thermal cell[242-243]. The radiation is transmitted through a quartz or diamond window into a small zenon gas cell, the gas is heated and expands and one of the walls of the cell, which is made of a thin membrane, distorts. The other side of the membrane is ruled with a series of reflecting strips forming part of a Moire amplifier, and since the incoming radiation is chopped at some low frequency (< 15 Hz) and the time constant of the cell is about a tenth of a second the membrane vibrates. The Moire system amplifies this and it is converted to an electrical fluctuation by a photo cell. This system is very efficient and its sensitivity (~ 10^{-10} watts) is better than can be achieved by a bolometer or a crystal detector at less than a millimetre. More sensitive detectors have been made with sensitivities of about 10^{-12} watts and response times of about a microsecond. These are either bolometers using the superconductor resistivity edge of a metal or photoconductive semiconductors using either the intrinsic edge or one of the impurity levels. Unfortunately all these more sensitive detectors require liquid helium temperatures for operation. There is one other major problem in the construction of a far infrared spectrometer. Water vapour strongly absorbs throughout most of the region, so the spectrometer has to be either continuously flushed with dry nitrogen, or more usually evacuated to less than 0.1 torr.

2:3 Ultramicrowave Sources of Energy

As indicated in Section 2 conventional microwave oscillators such as klystrons and magnetrons would have to have components of very small

dimensions to operate below a few millimetres. But not only must the resonator structure be smaller (~ frequency) but the radiation currents have to flow in an increasingly thin skin depth (~ $f^{\frac{1}{2}}$) and the electron beam has to have a density which varies somewhere between f^2 and f^3 with frequency. Thus the total heat dissipation varies as about $f^{3\frac{1}{2}}$ and it does not seem likely that a tube operating below one millimetre wavelength will be constructed: the limit achieved at the moment being about $2\frac{1}{2}$ mm. But the problem can be eased if an extended interaction time device is used, such as a travelling wave oscillator. Thus Convert has constructed a series of backward wave oscillators producing tens of milliwatts c.w. power at 0.9 mm and a few milliwatts at 0.5 mm with a ten percent tuning range per device; and Bott[244-245] has produced watts of power in the 2 to 4 mm region. Various types of harmonic generators have been used to produce small amounts of submillimetre radiation from high power millimetre klystrons and magnetrons. Thus Gordy[246] has used a 100 mWatt 5 mm klystron to produce a twelfth harmonic in a silicon crystal and this has been used for spectroscopy of Carbon monoxide at 0.43 mm. Froome has used the nonlinearities of the cathode region of a tungsten-mercury arc to produce the 29th harmonic of an 8 mm klystron at 0.3 mm with a resolution of one in 10^4.

Numerous other sources have been suggested including plasma oscillators, Cerenkov radiators, cyclotron resonance, various semiconductor methods, spark oscillators, parametric amplifiers, irasers and laser beat frequencies. But only the spark oscillator (0.22 mm in 1923), various gas irasers already mentioned and laser beat frequency

methods have worked.

Various proposals for beating optical masers to produce a far infrared difference frequency have been made[247-249] but only recently has a device been successfully operated[250]. The main difficulties seem to be to find two tunable high power sources, a non linear medium which is both transparent to optical and far infrared radiation and the inefficiency of any such system due to the frequency ratios involved. Zernicke and Berman used the output of one neodymium glass laser with a quartz crystal inside the laser resonator and a liquid helium temperature photoconductive detector detecting the radiation (about one hundred microns).

2:4 Proposed Beam Iraser[251]

Light molecules have inter-rotational level energies in the far infrared region of the spectrum. After the first maser using ammonia gas had been operated it was suggested that maser action between rotational levels of ammonia should be possible. The inversion splitting of the J = 3, K = 3 rotational level of ammonia is used for the microwave (23,870 MHz) beam maser.

In a beam of ammonia molecules the upper (+) and lower (-) inversion levels are almost equally populated; but if the beam is passed through an inhomogeneous electric field the lower state molecules are deflected towards the region of highest field and the upper state ones towards the region of lowest field. Hence, with a suitably designed electrostatic focuser the upper energy molecules are physically separated from the (-) molecules and a negative temperature system is

obtained. The beam of upper state molecules can be induced to emit energy to the field of a resonant structure tuned to the inversion frequency, and, with sufficient feedback, oscillation can be obtained.

Not only is the J = K = 3 level split by inversion, but most of the other rotational levels are split; in particular the J = 4, K = 3 level. This is separated from J = 3, K = 3 by an energy corresponding to 125 microns (see Figure 1). Hence, when a beam of ammonia molecules is passed through an inhomogeneous electric field

J = 4, K = 3 (+) is populated and

J = 3, K = 3 (-) is unpopulated.

Thus in a suitable resonant structure it should be possible to stimulate emission between these levels. A low order mode microwave type cavity would be too small to construct for this region, so a high order mode structure is used. Two have been constructed, one confocal, the other half confocal (see Chapter 4). Both resonators are tuned by slightly altering the spacing between the mirrors by thermally expanding the brass spacer which retains the mirrors in position.

It has been calculated that it will not be possible to have a sufficient number of stimulated transitions with one beam in the far infrared cavity for self-sustained oscillation to take place. This is for two reasons, there cannot be sufficient flux of molecules in a single beam of molecules if the collimator nozzle and electrostatic state separator are to work efficiently. Second, the interaction time between the molecular beam and the field of the resonant structure will be too short. However, a certain amount of stimuated emission will take place in the resonant structure and hence J = K = 3 (-) will be

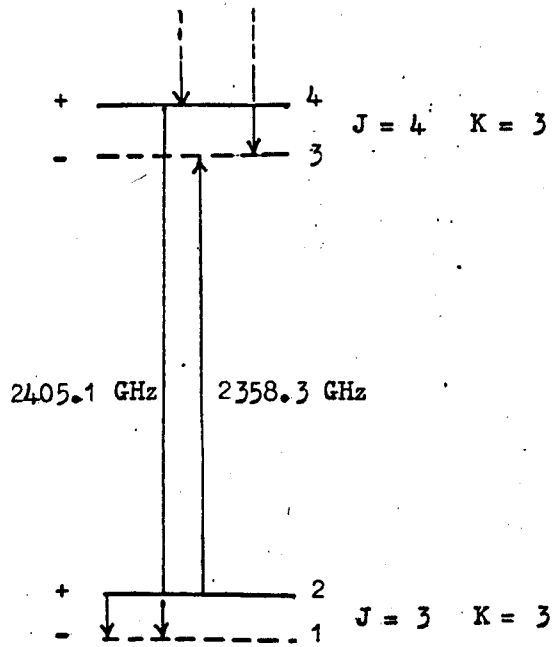

Figure 2:1

Rotation and Inversion energy levels of the Ammonia molecule

partially populated when the far infrared resonator is on tune. It would be difficult to detect the stimulated emission directly because the best detectors in this region are comparatively insensitive, but it is possible to use a 'double resonance' type technique to transfer the detection problem to the microwave region.

A microwave beam maser has been designed so that the molecular beam after leaving the state separator passes through the far infrared resonant structure before entering a microwave cavity. If conditions are such that microwave oscillation is taking place between J = K = 3 (+) and (-), then if the population of J = K = 3 (-) is increased due to far infrared transitions there will be a reduction in the excess of molecules in J = K = 3 (+) over those in J = K = 3 (-) and the amplitude of the microwave oscillation will decrease.

For the far infrared transition to be stimulated a field must be present, this can be the thermal field of the resonant structure. But this field is small and the microwave detection system must observe D.C. changes. A better system can be obtained by coupling A.C. modulated radiation into the far infrared cavity and looking for a component of this frequency in the microwave maser output.

In Chapter 3 the ammonia molecule is considered and in Chapter 4 beam collimation and resonant structures for microwave and ultramicrowave use. In particular various schemes for coupling energy to a half confocal cavity are considered. It will be seen that it is desirable to know the transmission of various crystal quartz and black polythene filters and windows, the efficiency of a vacuum system for removing

atmospheric water vapour absorption lines and the best thermal source operating conditions. It is also desirable to be able to measure the frequency of any emitted radiation from the beam iraser. So a far infrared grating spectrometer has been constructed; it is described in Section 5.

In Chapter 5 a single cavity beam maser is described in detail and unexpected effects due to the separation of resonant structure and beam separator are discussed. The average velocity of the beam molecules is measured and the optimum A.C. modulation operating frequency determined, and the sensitivity of the microwave detection system measured. In Chapter 6 the unusual effects due to the insertion of a second microwave cavity between the microwave detector cavity and the beam separator are measured and the possibility of a three cavity maser system considered. The resolution of a 2 cavity system is found to be extremely good and previously unobserved hyperfine structure of ammonia is detected. In Chapter 7 the first microwave cavity is replaced by one of the ultramicrowave cavities and detection of ultra-microwave stimulated emission is attempted.

2:5 Grating Spectrometer

A far infrared grating spectrometer has been constructed. To remove the atmospheric water vapour the instrument is mounted in a vacuum system. A double stage rotary vacuum pump with displacement of 10 cubic metres per hour (at atmospheric pressure) and ultimate pressure of better than 10^{-3} torr, is used to pump the spectrometer,

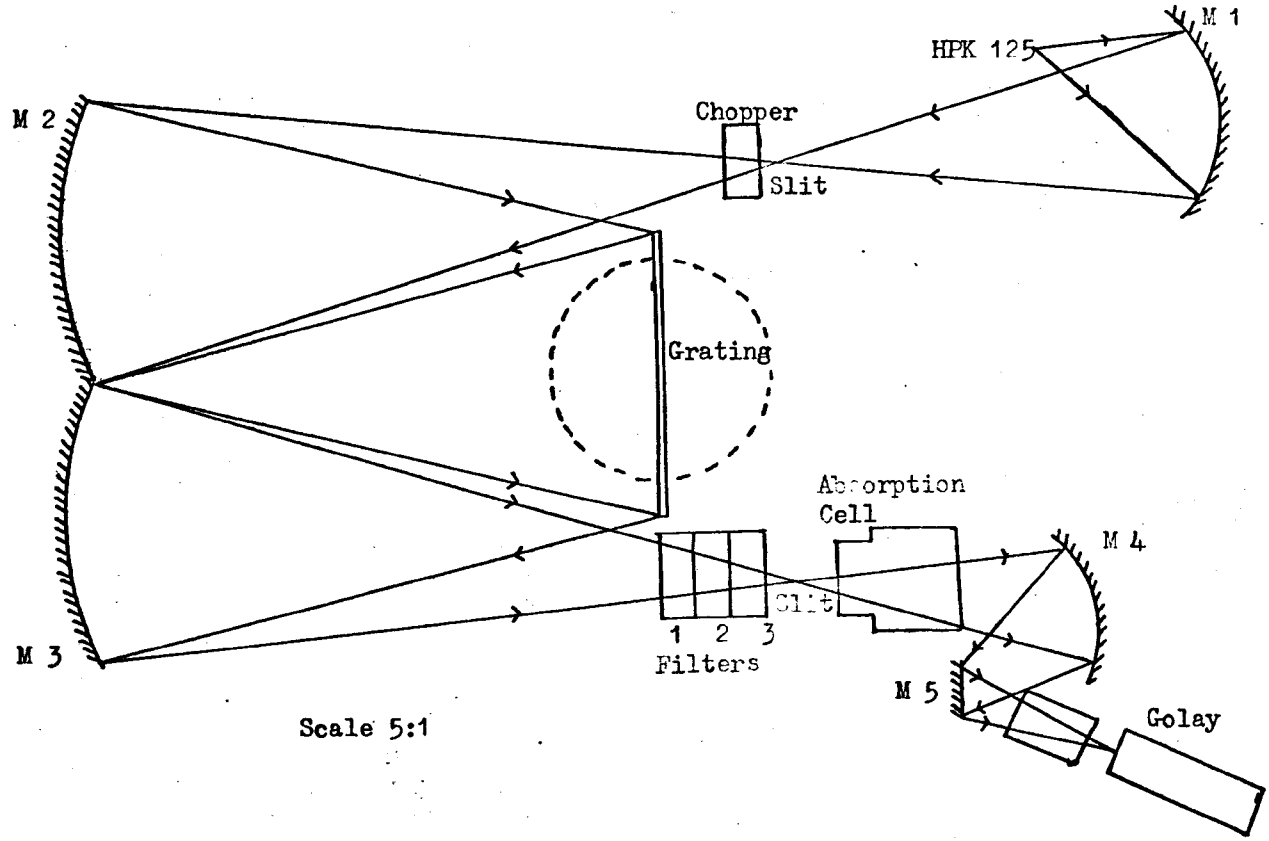

Figure 2:2

Czerny-Turner grating spectrometer

which is enclosed in three metal cylinders mounted on a central metal plate and sealed with rubber 'O' rings. The vacuum pump is equipped with gas ballast to help the pumping of water vapour and an automatic air admittance valve to admit air into the system if the pump stops. This avoids any contamination of optical components with pump oil. Silica gel is used to help dry the system. A sealed capsule [illegible] pressure dial gauge and a Pirani gauge are used to measure pressures from atmospheric down to 10^{-3} torr. These gauges are either connected to the spectrometer or to the vacuum system used to introduce gases into the absorption cell in the spectrometer.

Figure 2 is a diagrammatical representation of the optical system of the Czerny-Turner spectrometer[201-202, 213, 226-227, 252-256]. The radiation source is a Philips HPK 125 mercury lamp. All the mirrors are surface aluminised and the 6" × 6" reflection echelette grating has 125 lines per inch, blazed at 20° in Pb-Sn-Sb alloy. Mirror 5 is either surface aluminised or a reflection filter, usually a Caesium Bromide restrahlen plate. Filters 1, 2 and 3 are absorption filters: normally several thicknesses of 500 gauge black polythene and several millimetres of crystal quartz. The slits open symmetrically and are adjusted from outside the vacuum system. A mechanical chopper is situated behind the entrance slit, this both chops the radiation and provides a reference frequency and phase for use in the Golay electronic amplifier. The detector is a Golay thermal cell using a Unicam 10Hz amplifier and phase sensitive detector and time constants up to 45 seconds. The Unicam amplifier and phase detector were unstable

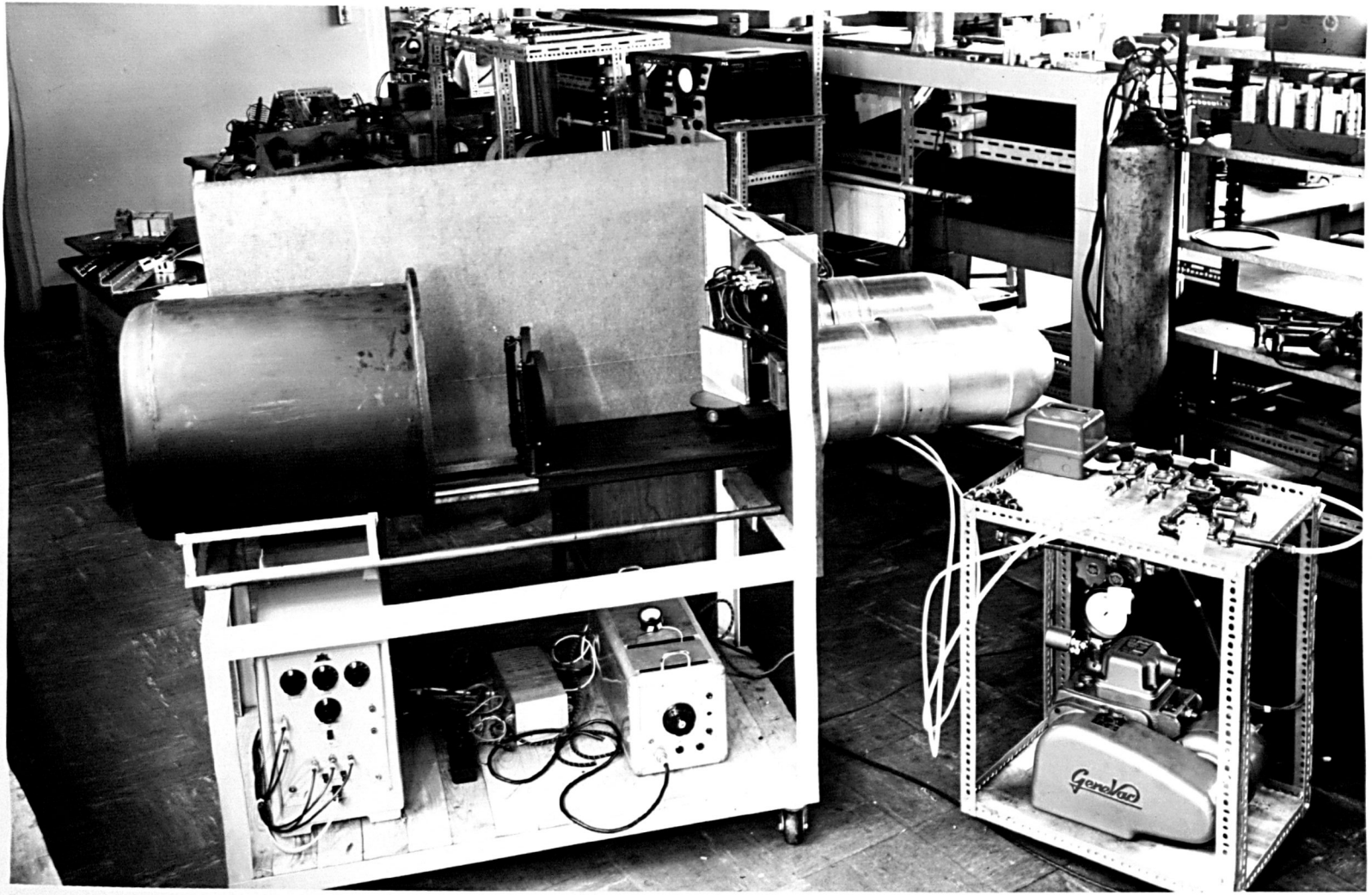

Figure 2:3 Grating spectrometer

and the D.C. amplifier drifted, so for later runs of the spectrometer a Princeton JB5 amplifier and CR4 preamplifier were used (see Chapter 5 for details). Figure 3 is a general photograph of the spectrometer, Figures 4 and 5 are close-up photographs of the grating area and the collection and detection area.

The diffraction condition for a reflection grating is given by

$$\sin(x + y) - \sin(x - y) = n\lambda/d \qquad 1$$

where d is the grating constant, x the angle between the incident beam and the spectrometer axis of symmetry (= $13^{o}30'$) and y is the angle between the grating normal and the spectrometer axis. Hence

$$2 \cos x \sin y = n\lambda/d \quad \text{and} \quad 2 \cos x \cos y \, dy = \frac{n}{d} d\lambda \, . \qquad 2$$

Thus the angular dispersion

$$dy/d\lambda = n/(2d \cos y) \, . \qquad 3$$

Also[257]

$$D\lambda = s/(2F \, dy/d\lambda) \, . \qquad 4$$

Where F is the focal length of the collimating system, s is the exist slit width and $D\lambda$ is the band of wavelengths which will pass through the slit. Since

$$D\lambda = \lambda^2 \, Df \qquad 5$$

where Df is the wave number range passed by the exit slit. Then

$$Df = \frac{s}{2F\lambda^2 \, . \, dy/d\lambda} = \frac{s \, d \cos y}{F\lambda^2 n} \qquad 6$$

which for 3mm slits, 100 lines per inch grating blazed at 15^{o}, 52 cm

Figure 2:4

focal length mirrors in the first order at 125 microns gives $Df \sim 0.9\ cm^{-1}$.

According to the Rayleigh Jeans radiation formula the energy per unit volume within a black body enclosure, in the wavelength range $D\lambda$ is

$$E_\lambda = 8\pi kt\lambda^{-4} \quad . \tag{7}$$

If the energy comes from a single source of emissivity e, then the radiation per unit solid angle is

$$E'_\lambda = 8\pi kt\lambda^{-4}\ ce/4\pi = 2kct\lambda^{-4}\ e \text{ watt.cm}^{-2} \text{ steradian cm.} \tag{8}$$

and the energy received by the detector will be

$$E''_\lambda = 2ekct\lambda^{-4}\ XYZ\ spA'\ D\lambda/F^2 \text{ watts} \tag{9}$$

where X is the energy efficiency of the monochromator, with acceptance area A', with equivalent slits of height p. Y is the efficiency of the source to entrance slit optics and Z is the efficiency of the exit slit to detector optics. From equation 5

$$1/\lambda^4 = D\lambda^2/Df^2 \tag{10}$$

so

$$E''_\lambda = \frac{2ekcTpXYZ\ sA'\ Df^2}{D\lambda F^2} \quad . \tag{11}$$

Thus with equation 5

$$E''_\lambda = \frac{4ekcT\ Df^2\ XYZ\ p\ A'}{F}\ dy/d\lambda \tag{12}$$

and with equation 3

$$E'' = \frac{2ekcT\ Df^2\ nXYZ\ pA'}{F\ d\ \cos y} \tag{13}$$

Figure 2:5

If the grating area is A then A cos y = A' and

$$E'' = \frac{2ekcT\ Df^2\ nXYZ\ pA}{Fd} \text{ watts .} \qquad 14$$

If the following numerical values are substituted in equation 14 e = 1, n = 1, F = 52, p = 2, A = 52^2, Y = 3, X = Z = 1/3, d = 0.0254 cm, Df = 0.9 cm^{-1}, T = 2000°K and k = 1,38 × 10^{-23} joules.deg^{-1}, then the spectrometer transmits E'' = 10^{-7} watts. Thus the spectrometer with 3 mm slits and Golay cell detection should have a resolution of about 1 cm^{-1} and a good signal to noise (depending on the phase sensitive detector time constant).

The grating is driven from outside the vacuum system by an electric motor and gearbox, this produces a linear grating drive, thus the resulting spectra are non linear with wavelength. Figures 6a and b are two early atmospheric water vapour spectra obtained with the spectrometer unevacuated and the Unicam amplifier; the zero drift of the system can be seen as well as the almost total absorption at several wavelengths. The higher resolution was obtained by narrowing down the slits to 5 millimetres. For filtering 5 thicknesses of 150 gauge black polythene and 3.2 cms.of crystal quartz were used, the spectra taking about 30 minutes to record. These spectra were obtained by using a Unicam Pfund condensor unit to focus radiation on to the Golay cell, rather than mirrors M4 and M5. A cone light pipe (electroformed in copper) was also tried but this was only about 60% as efficient. The most efficient and flexible system was that using M4 and M5 plus a rectangular cross section silvered mirror

BEST COPY AVAILABLE.

VARIABLE PRINT QUALITY

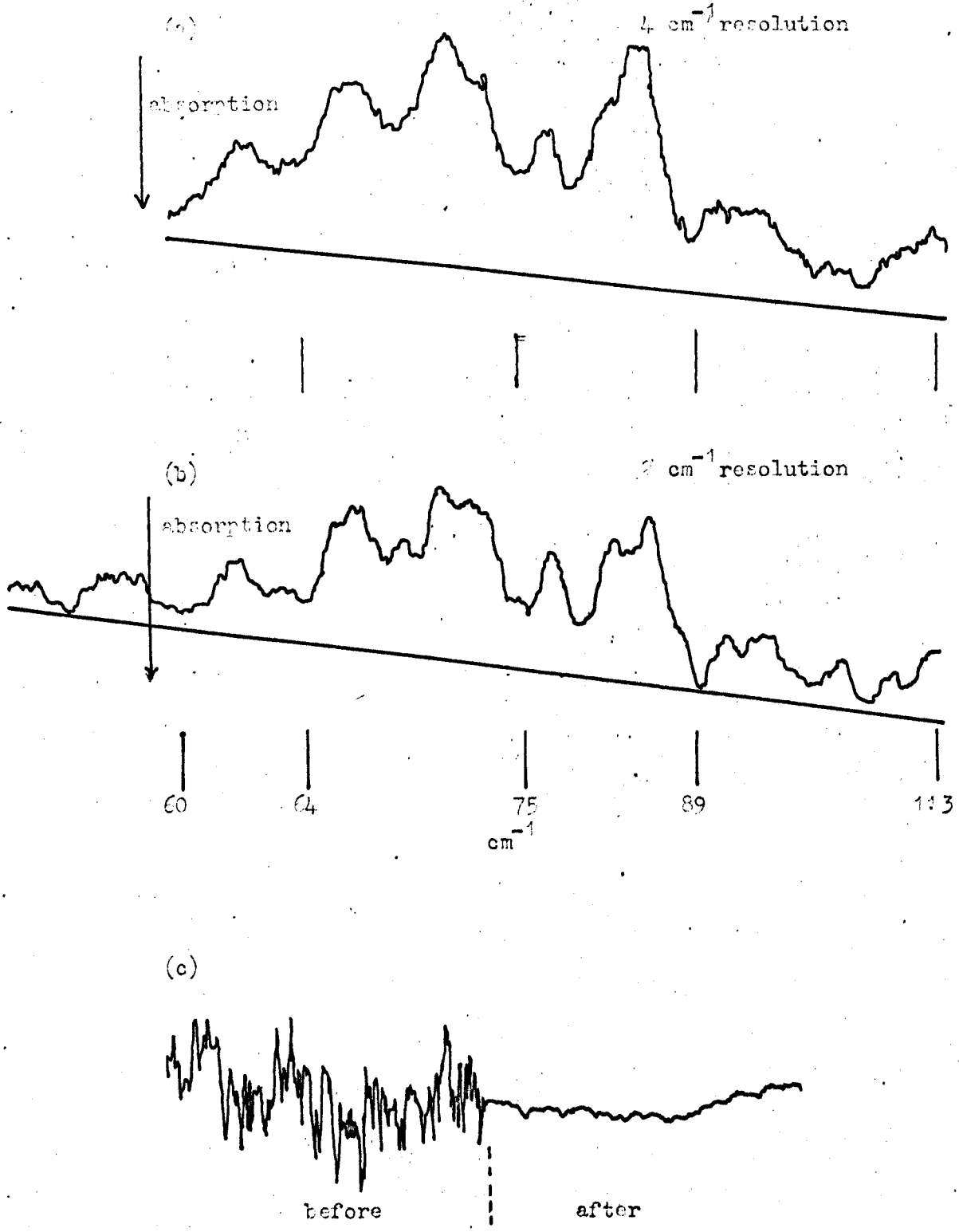

Figure 2:6

(a) and (b), Atmospheric Water Vapour absorption spectra

(c), Golay stability and noise, before and after electronic improvements

light condensor between M5 and the Golay. For the remaining spectra the Princeton phase sensitive detector system was used and the Golay cell Moiré preamplifier light source and the heater of the first amplifier valve were run off an accumulator supply. Figure 6c illustrates the improvement in signal to noise achieved with this system, and the remaining spectra exhibit an almost drift free system.

The far infrared output of the HPK 125 Mercury-Quartz lamp was checked for both A.C. and D.C. operation and it was found that the output varied by less than ten percent for equal power inputs (although in the near infrared the output was 75% modulated by the A.C. mains frequency at 100 HZ.). The far infrared power output of the lamp was found to be directly proportional to the power input to the lamp, so a water jacket was made for the lamp and it was run at as high a temperature as possible without devitrefying the quartz envelope too quickly.

Figure 7 is an atmospheric water vapour absorption spectrum from 60 to 120 cm^{-1} with the improved system and 1 cm^{-1} slit width limited resolution. A ten second time constant was used in conjunction with the phase sensitive detector and the complete sweep took 80 minutes. The wavelengths are crudely obtained by geometrical measurement and then the lines are accurately matched to published spectra[252-253, 258-260]. The filtering used was 8.5 millimetres of crystal quartz, 2 sheets of 150 gauge black polythene and 2 sheets of 500 gauge black polythene. It can be seen that around 80 cm^{-1} the atmospheric absorption is almost complete (path length about two metres). The central part of this spectrum is reproduced in Figure 8b with the addition of one reflection

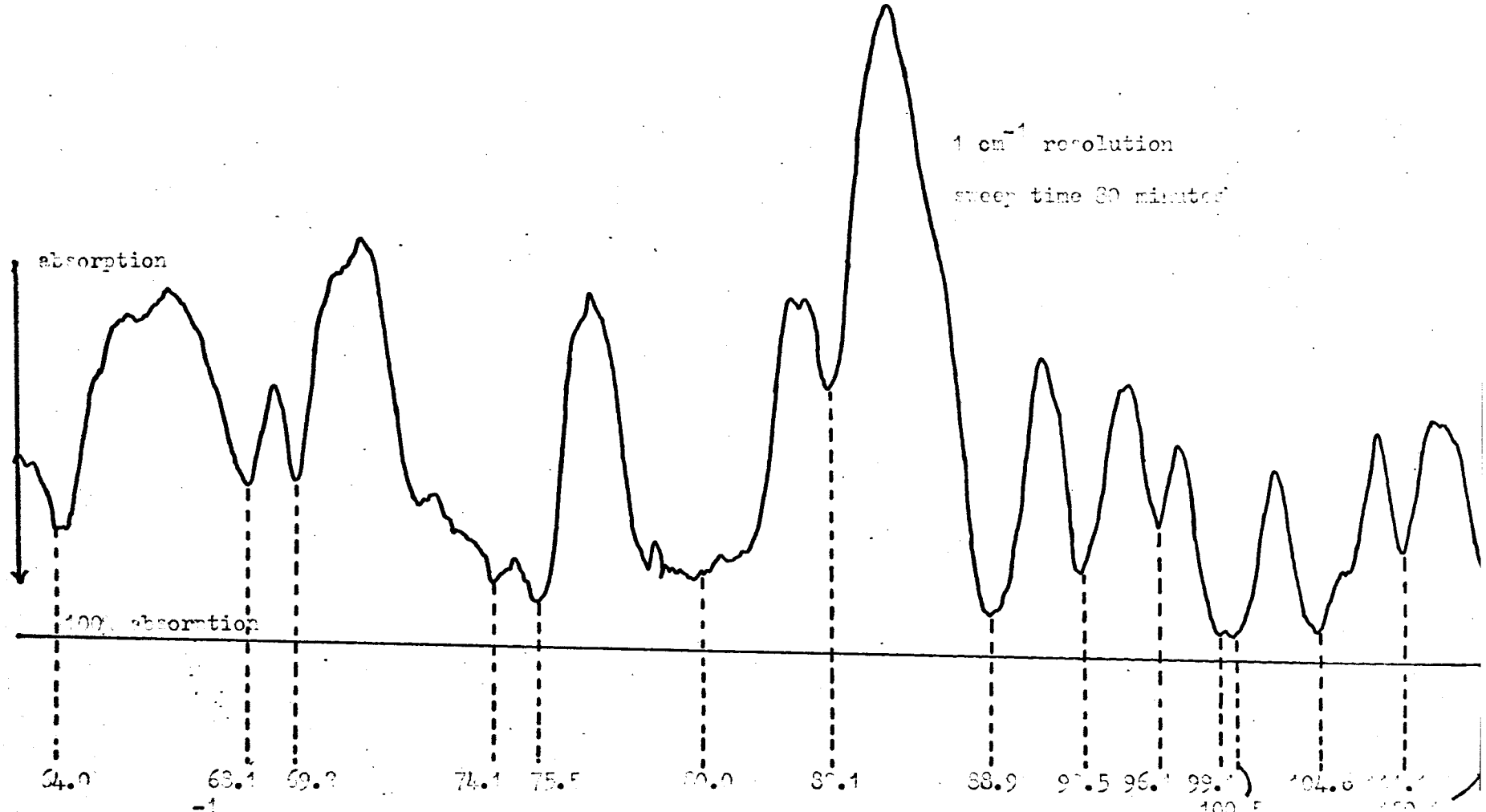

Figure 3:7

Atmospheric Water Vapour absorption spectrum

from a Gaesium bromide restrahlen plate. It can be seen that a certain amount of background radiation has been eliminated (see for instance the line at 82.1 cm^{-1}), but that the quartz and black polythene are at least 80% efficient without the addition of the restrahlen plate.

Figure 8a illustrates the effect of evacuating the spectrometer. The 'blaze' of the spectrometer is now much more pronounced and the atmospheric water vapour lines have disappeared. In fact a vacuum of about 10^{-1} torr removes at least 90% of the water absorption.

Thus the water cooled HPK 125 lamp produces about the expected amount of radiation at 80 cm^{-1} and should be run as hot as possible; adequate filtering is obtained with crystal quartz and black polythene transmission filters and atmospheric water vapour absorption can be removed with a vacuum of 10^{-1} torr.

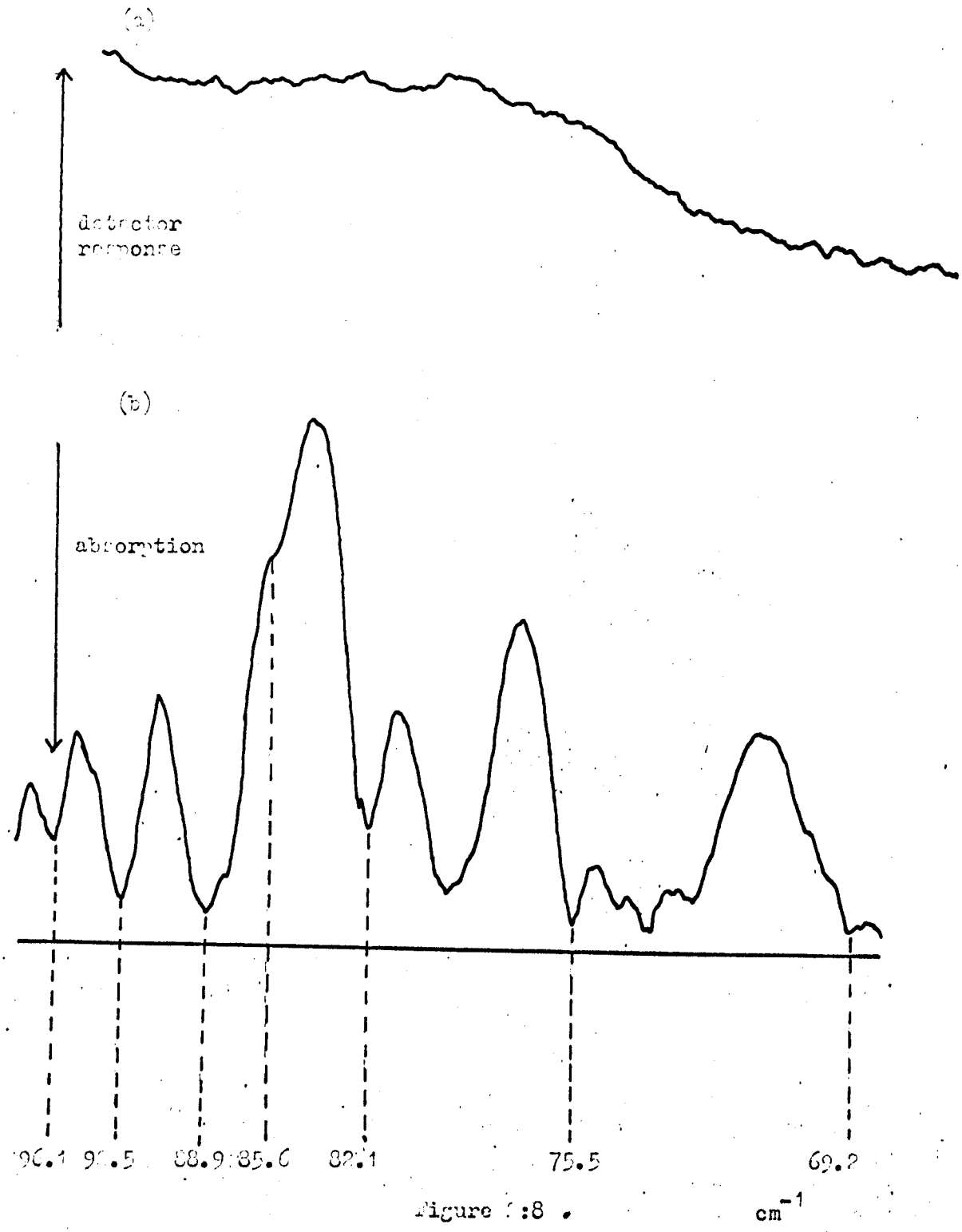

Figure 7:8 .

(a), Blaze of the grating with evacuated spectrometer and restrahlen filter

(b), Atmospheric water vapour absorption with CsBr restrahlen filtering

Chapter 3. The Ammonia Molecule

3:1 Introduction[24, 261-267]

The general properties and structure of the ammonia molecule have been established by chemical examination and both infrared and Raman spectroscopy. The nitrogen atom ($1s^2$, $2s^2$, $2p^3$) is covalently bound to three hydrogen atoms ($1s^1$) so that each hydrogen completes its K shell and the nitrogen completes its octet to have a neon like structure. The nitrogen L electrons have a valency electron distribution derived from q hybrid orbitals which are directed towards the apices of a regular tetrahedron (tetrahedral angle $109^\circ 28^\circ$). In the NH_3 molecule the bond angle is only $106^\circ 47'$ because there is a slightly greater repulsion between the non-bonding electrons and the hydrogen bonding electrons than the mutual repulsion between the hydrogen bonding electron pairs.[261-262]

The ammonia molecule is a non-rigid, non-planar, oblate symmetric top with the three hydrogen atoms at the corners of the base equilateral triangle and the nitrogen at the apex of the tetrahedron (see Figure 1a). The distance between hydrogen atoms is $1.014^\circ A$ and the angle b is $67^\circ 58'$. The energy of the molecule, H, can be expressed as

$$H = H_T + H_V + H_R + H_I \qquad 1$$

where H_T, H_V and H_R are the translational, vibrational and rotational energies and H_I represents the interaction energy between the rotation and the vibration. A molecule has 3N degrees of freedom, where N is the total number of atoms. Three of the twelve for ammonia represent translation, three rotation and six internal vibrational modes.

(a) The ammonia molecule

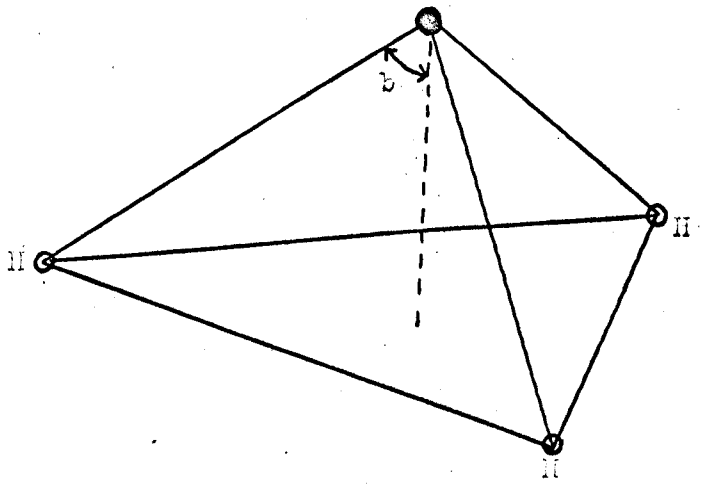

(b) Vector diagram of the rotational motion of the ammonia molecule

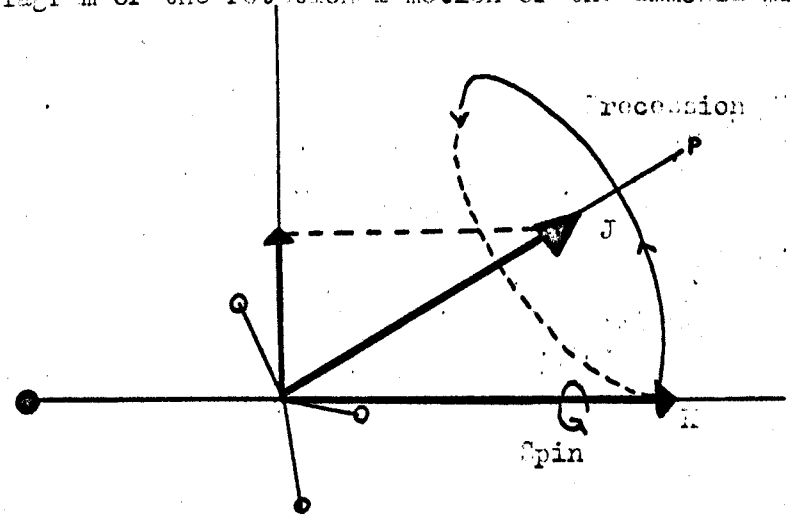

Figure 3:1

The moments of inertia of any system of masses may be represented by an ellipsoid whose centre coincides with the centre of mass and whose orientation is fixed in the mass (or molecular) system. The molecular moment of inertia about any axis through the centre is equal to half the distance between the intersects of this axis and the ellipsoid. With a coordinate system with x, y and z along the principal axes of the ellipsoid, and I_x, I_y and I_z the moments of inertia along these axes, the equation of the ellipsoid of inertia may be written.

$$\frac{x^2}{I_x^2} + \frac{y^2}{I_y^2} + \frac{z^2}{I_z^2} = 1 . \qquad 2$$

A molecular rotation is usually easiest to describe in terms of the principal axes of such an ellipsoid of inertia. An axis of symmetry in a molecule is always a principal axis of the system; and for the ammonia molecule an axis passing through the nitrogen atom and which is equidistant between the hydrogen atoms is an axis of symmetry. Since the molecular configuration is unchanged when the molecule is rotated by $2\pi/3$ radians about this axis it is a 3 fold axis of symmetry. This is only possible if the other two moments of inertia are equal, thus $I_x = I_y = I_B$. Since the ammonia molecule is an oblate symmetric top, its moment of inertia about the principal axis, I_z, is larger than the other two moments and $I_z = I_C$.

3:2 Rotational Spectrum[268]

The rotational energy of a symmetric top can be obtained by con-

sidering it as a rigid rotor and treating it as a classical problem with quantised angular momentum restrictions. The top spins about its main axis, and this axis nutates about the total angular momentum vector P, as shown in Figure 1b.

The energy of rotation is given by

$$W = \tfrac{1}{2} I_x w_x^2 + \tfrac{1}{2} I_y w_y^2 + \tfrac{1}{2} I_z w_z^2$$

$$= \frac{P_x^2}{2I_x} + \frac{P_y^2}{2I_y} + \frac{P_z^2}{2I_z} \qquad 3$$

$$= \frac{P^2}{2I_B} + P_z^2 (1/2I_C - 1/2I_B) \text{ for ammonia,}$$

where $P^2 = P_x^2 + P_y^2 + P_z^2$, the sum of the squares of the Cartesian angular momentum vectors, is quantised and given by $P^2 = J(J + 1)h^2/4\pi^2$. J is an integer called the Total Angular Momentum (excluding nuclear spin) quantum number. Similarly the angular momentum along the z axis is quantised, $P_z^2 = K^2 h^2/4\pi^2$, where K is an integer and is the projection of J on the molecular axis of symmetry, and takes the values $K = J, J - 1, \ldots\ldots - J + 1, - J$. Hence

$$W = \frac{J(J + 1)h^2}{8\pi^2 I_B} + \left[\frac{h^2}{8\pi^2 I_C} - \frac{h^2}{8\pi^2 I_B}\right] K^2 \qquad 4$$

and

$$W/h = BJ(J + 1) + (C - B)K^2$$

where the rotational constants are defined by

$$B = h/8\pi^2 I_B \quad \text{and} \quad C = h/8\pi^2 I_C. \qquad 5$$

Since the energy is dependent on K^2 the allowed energy levels for $K > 0$ are doubly degenerate and for each K value there will be a series of energy levels corresponding with the appropriate J values. Although for each K series the exact energies for corresponding J levels will be different, the separations between equivalent levels are constant so only one series spectrum will be observed, with the selection rules

$$\text{for } K \neq 0 \quad \Delta K = 0 \quad \Delta J = 0, +1, -1$$

$$\text{for } K = 0 \quad \Delta K = 0 \quad \Delta J = +1, -1.$$

The energies above were obtained for a rigid symmetric top molecule. The ammonia molecule is not quite rigid and centrifugally distorts. Since the distortion cannot depend on the sign of the direction of rotation the modifications to the energy equation can only involve even powers of the momentum, and the energy is usually given as

$$W(J, K) = BJ(J + 1) + (C - B)K^2 - D_J J^2(J + 1)^2 - D_{JK} J(J + 1)K^2 - D_K K^4 \qquad 6$$

where D_J is a measure of the centrifugal distortion due to end over end rotation of the molecule, D_K that due to rotation about the symmetry axis and D_{JK} a measure of the distortion due to the interaction of these two rotations. B (= 298,000 MHz) >> D_J (= 19 MHz) and D_{JK} (= -28 MHz).

For rotational transitions $J + 1 \leftarrow J$, $\Delta K = 0$ and from the above equations the transition frequencies are given by

$$f = 2(J + 1)(B - D_{JK}K^2) - 4D_J(J + 1)^3 \qquad 7$$

and the rotational spectrum for ammonia in the far infrared region of the spectrum is no longer degenerate for different values of K.

3:3 Vibration

Ammonia has six normal modes of vibration, two of which, ν_1 and ν_2, involve the nitrogen atom oscillating along the principal axis of the system (see Figure 2). The other four modes, ν_3, ν_4, ν_5, ν_6 are degenerate in pairs and have a considerably greater frequency (1627 cm^{-1}, 3414 cm^{-1}) than ν_2 which vibrates at about 950 cm^{-1}, whereas ν_1 is more energetic (3335 cm^{-1}).

In the previous section the rotational structure of the ground vibrational state (V = 0) was discussed, in a similar way each excited vibrational state has a rotational structure and vibrational-rotational transition bands are obtained, Mould, Price and Wilkinson[267] have studied the V = 0 to V = 1 ν_2 band in some detail. It is found that this band and the far infrared rotational spectrum[269] have a structure which cannot be explained by rotation or simple vibrational-rotational interactions, but requires a very much lower frequency (microwave) molecular vibration. This had already been observed, in 1934, by Cleeton and Williams[270] in the 0.8 cm^{-1} region.

The nitrogen atom in the ammonia molecule is at the apex of the regular trigonal pyramid. There is another position of equilibrium for the nitrogen atom, this is on the opposite side of the hydrogen plane. From Figure 3 it can be seen that considerable energy is

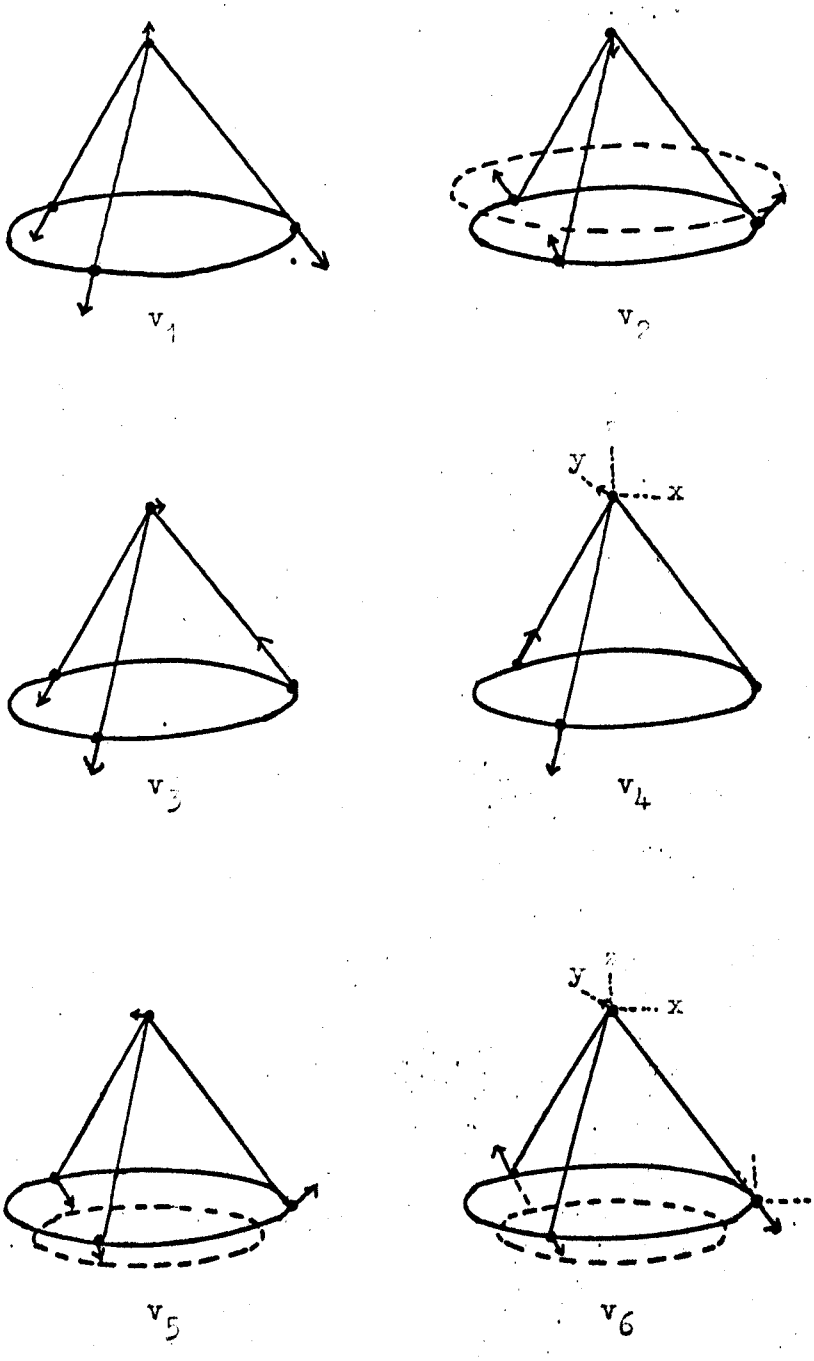

Figure 3:2

Vibrational modes of the ammonia molecule (after figure 6:4 in 'Symmetry' by R.McWeeny, Pergamon 1963)

required for the nitrogen to move from one position of equilibrium to the other, even the lower excited vibrational states will not have enough energy classically.

The energy levels of a particle in a parabolic potential well are illustrated in Figure 3 together with a representation of the two simplest wave functions. If a potential barrier is raised in the centre of the well then the spacing of the energy levels and shape of the wave functions change and a series of split levels results. The transitions between the components of these levels are called 'inversion transitions' because classically they correspond to the molecule inverting - 'turning inside out' - about a plane through the molecular centre of mass. Of course classically such a motion cannot take place and such an effect can only be explained wave mechanically.

If the wave function for the ground simple harmonic oscillator state on the 'left hand side' of the hydrogens is U_L and for the nitrogen on the right U_R, then the true molecular wave function, which must be symmetric or anti-symmetric with respect to inversion, is given for the two lowest energy states as

$$Y_0 = 1/\sqrt{2}.(U_L + U_R) \text{ and } Y_1 = 1/\sqrt{2}.(U_L - U_R) \qquad 8$$

and if the nitrogen is definitely on the left at time t = 0

$$Y = U_L = 1/2^{\frac{1}{2}} . (Y_0 + Y_1) \qquad 9$$

or with time variation included, where W_0 is the energy of Y_0 and d (= hf) is the energy separation of the two levels, such that the two

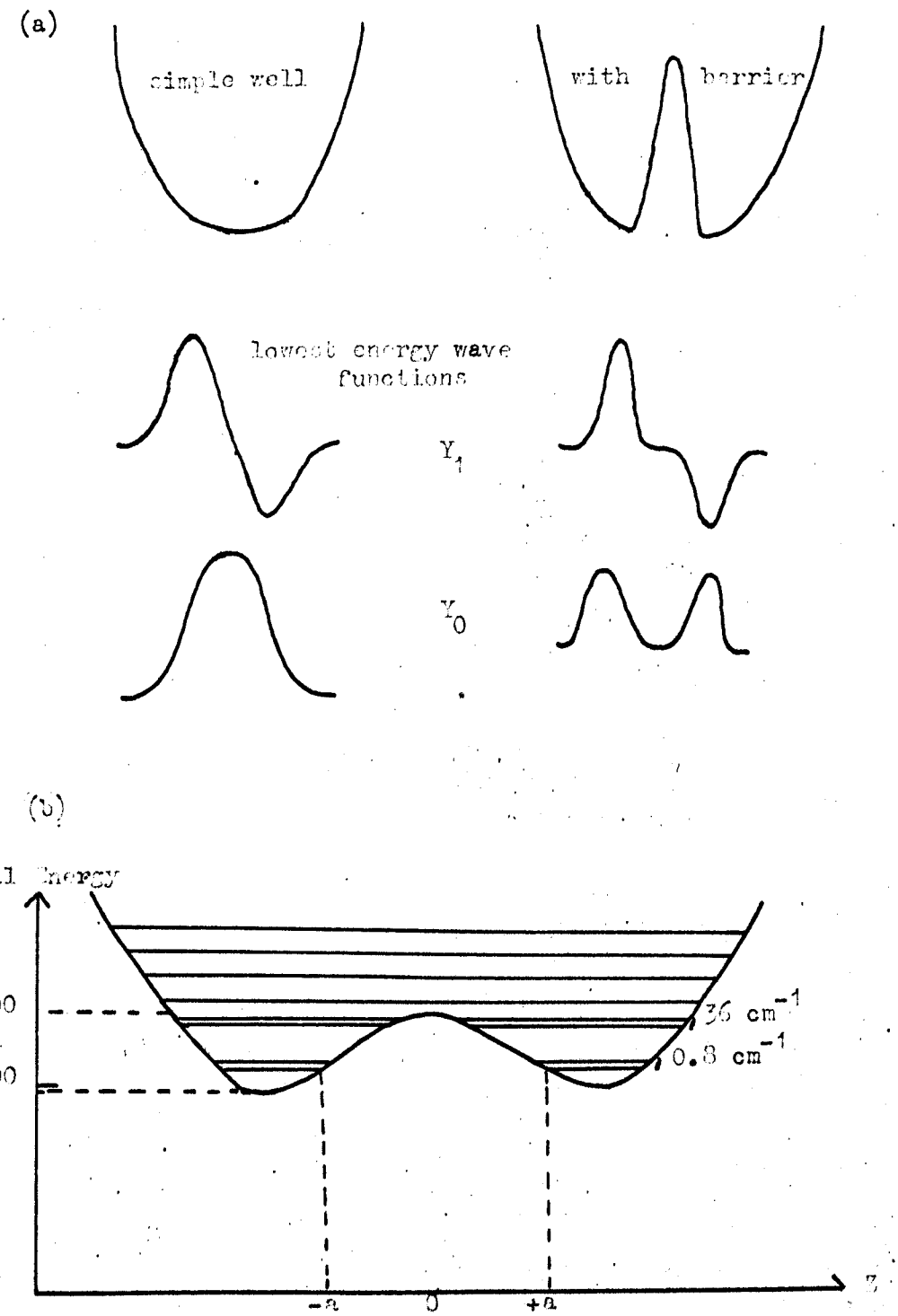

Figure 3:3

(a), Potential well and simple wave functions, with and without central barrier. (b), Lowest energy states of the ammonia molecule (after Townes and Schawlow [64] pages 66 and 301)

functions are $Y_0 e^{2\pi i W_o t/h}$ and $Y_1 e^{2\pi i (W_o + d)t/h}$ then

$$Y = 2^{-\frac{1}{2}} (Y_0 + Y_1 e^{2\pi i f t}) e^{2\pi i W_o t/h} \qquad 10$$

and after time t = 1/2f

$$Y = 2^{-\frac{1}{2}} (Y_0 + Y_1) e^{2\pi i W_o t/h} = U_R e^{2\pi i W_o t/h} \qquad 11$$

which corresponds to the nitrogen being on the right of the hydrogen plane.

Thus in two limiting cases the position of the nitrogen is on opposite sides of the hydrogen plane. For intermediate cases the wave function has components on both sides of the forbidden region and a component in the energetically (classically) central forbidden region. Dennison and Uhlenbeck[271] first considered this problem theoretically in 1932. They found that they could approximate the ammonia molecule inversion energy diagram by two equal parabolas connected by a straight line. Since then it has been found that the exact solution is very dependent on the height of the barrier between the two equal regions but insensitive to the exact shapes of the permitted potential walls and forbidden barrier. In fact Vuylsteke[265] has obtained a solution by using a square well approximation. Approximate solutions of the Schrodinger equation, such as

$$Y = \exp\{- h^{-1} \int_{-a}^{+a} [2m'(V_z - W)]^{\frac{1}{2}} dz \} \qquad 12$$

(where m' is the reduced mass of the molecule and V is the potential

energy of the central barrier, along the z axis from -a to +a, and W is the vibrational energy) show that the small component of the wave function in the forbidden region exponentially decreases from the values at the boundaries with the permitted region. For ammonia in the ground state $1/2f \sim 2 \times 10^{-11}$, corresponding to 0.8 cm^{-1} wave number, and if the vibration frequency, ν_2, (= 950 cm^{-1}) is thought of as the nitrogen oscillating in the well on one side of the plane, then this vibration can be thought of as penetrating the barrier at the much slower rate of 0.8 cm^{-1}.[272-273]

The transmitted amplitude of the wave function is

$$Y_a = \exp\left\{-2\hbar^{-1} \int_0^a \left[2m'(V - W)\right]^{\frac{1}{2}} dz\right\} = A^{-2}, \qquad 13$$

so the total amplitude transmitted after time t is $\nu_2 t\, A^{-2}$ and the frequency of oscillation is $\nu_2 \pi^{-1} A^{-2}$.

Since, to a good approximation, during the vibration the N - H bond length remains constant and the H - N - H angle changes, m' is given by

$$m' = \frac{3m(M + 3m \sin^2 a)}{(3m + M)} \qquad 14$$

where m is the mass of each hydrogen atom, M the nitrogen mass and 'a' is the angle between the hydrogen plane and an N - H bond.

If the wave equation is

$$H_{op} Y = WY \qquad 15$$

where H_{op} is the Hamiltonian operator (which is unchanged when the coordinate system is inverted) and W is the energy, then if the coordinates are changed $x \rightarrow x'$, $y \rightarrow y'$, $z \rightarrow z'$, the new wave function Y'

must be a solution of equation 15 for the same energy W. Thus for a nondegenerate system $Y = cY'$ where c is a constant.

If the further transformation $x' \rightarrow x''$, $y' \rightarrow y''$, $z' \rightarrow z''$, is made,

$$Y'' = cY' = c^2Y. \qquad 16$$

Then, since Y'' must be Y, $c^2 = 1$, thus $c = \pm 1$. If $c = +1$, Y is unchanged on inversion and is said to be symmetric, if $c = -1$, Y just changes its sign on inversion and is said to be antisymmetric. Thus the inversion levels can be designated (+) or (-), and one can establish the selection rules

$$+ \leftrightarrow - \qquad + \nleftrightarrow + \qquad - \nleftrightarrow -. \qquad 17$$

3:4 Fine structure

Since the ammonia molecule is not a completely rigid roter there is a rotational-vibrational interaction and each inversion frequency is different for different rotational states. The energy of the rotational transitions are considerably greater (far infrared) than that of the inversion transitions (microwave) so no resonant interactions occur and a perturbation description is adequate.

If the molecule rotates about the symmetry axis, the H - N - H angle will increase with angular momentum and, since the centrifugal force is proportional to the square of the angular momentum there will be a term in K^2, and the potential barrier formed by the hydrogen atoms will be lowered as they move further apart so the inversion frequency will increase and $f \propto aK^2$. Likewise if rotation is considered about

axes perpendicular to the symmetry axis, the hydrogen atoms will move further from the nitrogen atom, the inversion frequency will be decreased and $f \propto a\left[J(J+1) - K^2\right]$. Thus the inversion frequency is of the form

$$f = f_0 - a\left[J(J+1) - K^2\right] + bK^2 + \ldots \qquad 18$$

with several terms with higher powers of J and K.

Sheng, Barker and Dennison[274] and Newton and Thomas[275] have attempted numerical solutions of the modified wave equation for the inversion of the non rigid roter, but they were unable to match the observed spectrum to better than about ten percent. More recently Swalen and Ibers[276] have obtained a rather better solution for a harmonic oscillator potential well with a Gaussian barrier and Bagdanskis and Bulanin[277] have produced a generalised treatment for possible inversion states of ammonia molecules in solution.

The best fitting empirical formula seems to be that of Costain[278]

$$f = f_o \exp\left[aJ(J+1) + bK^2 + cJ^2(J+1)^2 + dJ(J+1)K^2 + eK^4\right] \text{MHz} \qquad 19$$

where a, b, c, d, e are constants numerically determined from experimentally determined microwave frequencies

$$f = 23{,}785.88 \text{ MHz}$$

$$a = -6.36996 \times 10^{-3}$$

$$b = +8.88986 \times 10^{-3}$$

$$c = +8.6922 \times 10^{-7}$$

$$d = -1.7845 \times 10^{-6}$$

$$e = +5.3075 \times 10^{-7}.$$

The mean deviation of this formula from 64 of the inversion lines is 1.3 MHz, omitting the K = 3 lines.

The anomalous deviation of the J = 3, K = 3 line is -0.21 MHz and similarly for 4, 3 = +1.76 MHz, 5, 3 = -7.03 MHz, 6, 3 = +21.18 MHz and 7, 3 = -52.39 MHz. These can be closely matched by a deviation formula

$$\Delta f = AF(J) \qquad 20$$

where A = 0.252 and F(J) = -1 for J = 3

+7 = 4

-28 = 5

+84 = 6

-210 = 7.

The K = 3 (and to a very much smaller extent K = 6 and K = 9) deviations are due to a higher order rotation-vibration interaction. This interaction lifts the $\pm K$ degeneracy, and because of the symmetry of the hydrogen nuclei only one of each pair of levels is possible, so the lines appear to be slightly shifted. Similar symmetry considerations lead to the additional transition selection rule for K = 0,

$$\text{(even J)}, - \not\to +, + \not\to - \qquad \text{(odd J)}, + \not\to -, - \not\to + \ . \qquad 21$$

Because the inversion splitting is normally greater than the splitting of the far infrared lines due to lifting of the K degeneracy (centrifugal distortion), the rotational parameters B, C, D_J, D_{JK} and D_K are normally replaced by B_0, C_0, D_0^J, D_0^{JK} and D_0^K, which are the mean values of the constants for the symmetric and antisymmetric states:

and the rotational spectrum is given by

$$f = 2B_0(J + 1) - 4D_0^J(J + 1)^3 - 2D_0^{JK}(J + 1)K^2 \pm \left[E_{inv}(0, J, K) + E_{inv}(0, J + 1, K)\right] \qquad 22$$

with constants

$$B_0 = 9.9440 \text{ cm}^{-1}$$
$$D_0^J = 0.000811 \text{ cm}^{-1}$$
$$D_0^{JK} = -0.00151 \text{ cm}^{-1} .$$

The inversion splitting of the 3.3 level is 23,870.11 MHz and for the 4,3 level 22,688.24 MHz, so for the rotational transitions $J = 3 \rightarrow 4$, $K = 3$ one has

$$f = 78.676 \text{ and } 80.230 \text{ cm}^{-1}. \qquad 23$$

for the two permitted transitions. This spectrum has been observed by Hansler and Oetjen[279], and the spectra for other ammonia rotational states by Barnes[280], Wright and Randall[26], McCubbin[281] and Sinton and McCubbin[282].

3:5 Hyperfine structure

In 1946 Good[273] found that the 3,3 line of ammonia at 0.8 cm^{-1} had a hyperfine structure, and Gordon[24], Gunther-Mohr and others[283-285] have examined this in some detail.

There is coupling between the quadrupole charge distribution on the nitrogen nucleus and the gradient of the electric field of the molecule. If the spin of the nucleus is I_N then F_I (= I_N + J) is a

good quantum number (in other than strong fields) and is subject to selection rules

$$\Delta F_I = 0, +1, -1 \qquad 24$$

The 3,3 and 4,3 doublets of ammonia will be split and the exact values of the splittings have been obtained by Gunther-Mohr et al, who found that a simple quadrupole interaction did not completely fit the data and that allowance had to be made for a change in the quadrupole coupling constant (eq Q) due to centrifugal distortion of the molecule, and a term had to be added to the Hamiltonian to allow for the magnetic interaction of the nitrogen nucleus with the molecular rotation. For the 3,3 line the inner quadrupole satellites ($\Delta F_I = \pm 1$, F_I 4 $\leftrightarrow$ 3) are 1690 KHz from the centre line ($\Delta F_I = 0$) and the outer quadrupole satellites ($\Delta F_I = \pm 1$, F_I 2 $\leftrightarrow$ 3) are 2350 KHz from the centre line.

The quadrupole splittings for the 4,3 inversion are rather less, ± 460 KHz for the F_I 5 $\leftrightarrow$ 4 transitions and ± 640 KHz for the F_I 4 $\leftrightarrow$ 3 transitions, (see Figure 4.).

In 1955 Gordon using a beam maser with 7 KHz resolution found additional structure in the inversion spectrum; in particular he found structure in the quadrupole satellites of the 3,3 and 4,3 transitions. This structure was explained in terms of hydrogen magnetic interaction with the molecular rotation. If I is the sum of the spins of the three hydrogen nuclei then F (= F_I + I) is a good quantum number and each quadrupole level is split into sublevels. For the 3,3 transitions the outer quadrupole satellites are split over the range ± 50 KHz and

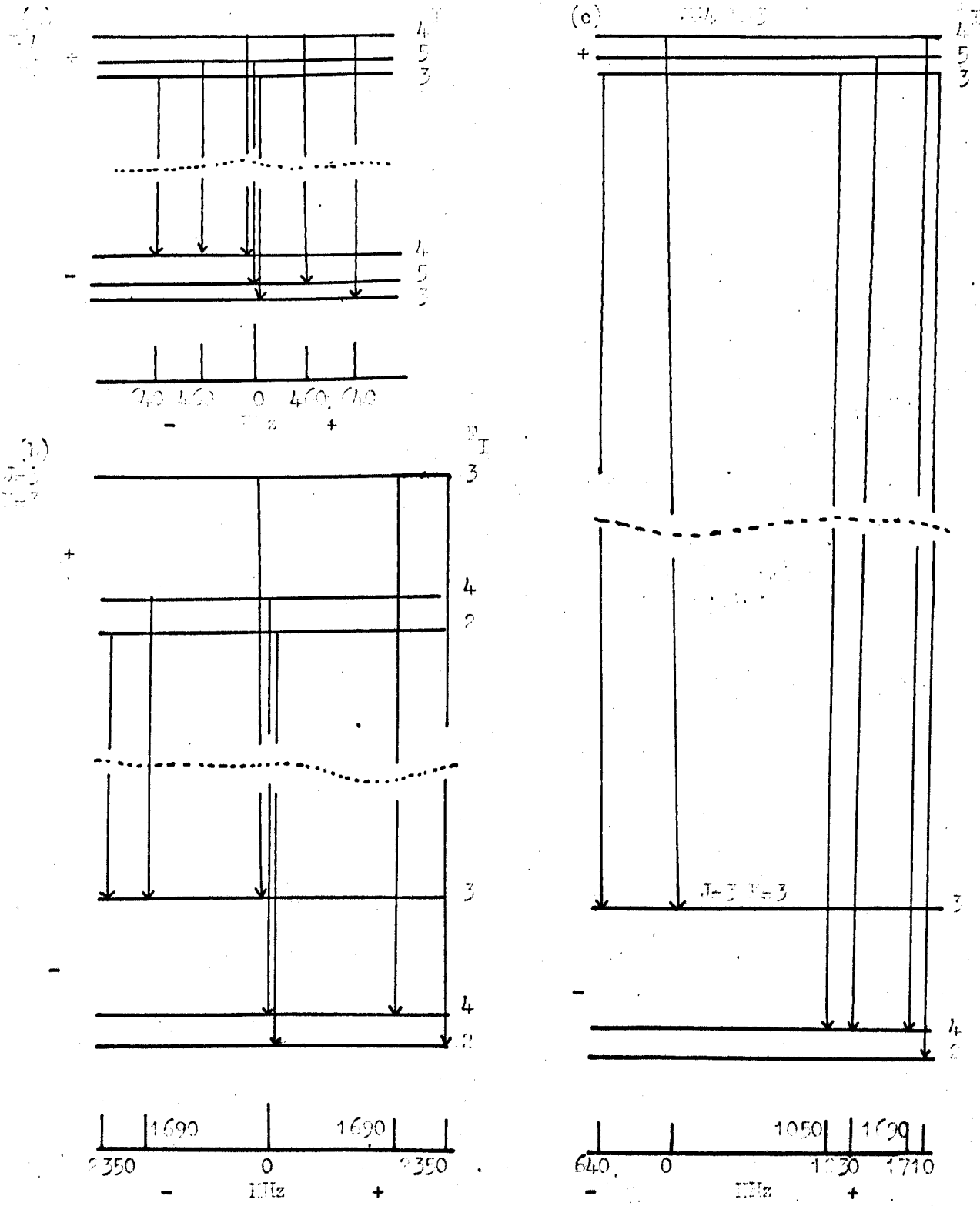

Figure 3:4

Hyperfine structure of the ammonia molecule. (a), The 4,3 inversion transition. (b), The 3,3 Inversion transition. (c), The 4,3(+) to 3,3(-) Rotational transition

the inner satellites by ± 10 KHz; but the satellites of the 4,3 transitions are only split by ± 5 KHz.

The $J = K = 3$, $\Delta F_I = 0$ transition has a centre $\Delta F = 0$ line and two magnetic satellites 65 KHz on each side of it corresponding to $\Delta F = \pm 1$ transitions. Gordon was not able to resolve any structure in the $J = K = 3$, $\Delta F_I = \Delta F = 0$ transition, but he did observe a slight assymetry in the line which would be explained if the eq Q quadrupole coupling constant was slightly different (by 4 KHz) for the upper and lower inversion levels, due to centrifugal distortion of the molecule.

The hyperfine interaction energy between the nitrogen and the remainder of the ammonia molecule is given by

$$W_{JKF_I} = - eq\, Q \left[1 - \frac{3K^2}{J(J+1)}\right] \Omega \cdot (\underline{J}, \underline{I}_N) + \left[a + \frac{(b-a)K^2}{J(J+1)}\right] \underline{I}_N \cdot \underline{J} \qquad 25$$

where Q is the nitrogen quadrupole moment, q is the electric field gradient at the nucleus and a (= 6.1 KHz) and b (= 6.5 KHz) are constants.

$$\Omega \cdot (\underline{J}, \underline{I}_N) = \frac{3(\underline{I}_N \cdot \underline{J})^2 + 3/2\,(\underline{I}_N \cdot \underline{J}) - I_N(I_N+1)\,J(J+1)}{2I_N(2I_N-1)\,(2J-1)\,(2J+3)} \qquad 26$$

and

$$2\underline{I}_N \cdot \underline{J} = F_I(F_I+1) - J(J+1) - I_N(I_N+1). \qquad 27$$

The variation of eq Q with inversion level will lead to a splitting of the $F_I = 3$, $F_I = 4$ and $F_I = 2$ lines and one has from the above equations

F_I	$\underline{I}_H \cdot \underline{J}$	$\Omega \cdot (\underline{J} \cdot \underline{I}_N)$	ΔW for Δeq Q = 4 KHz	ΔW for Δeq Q = 3 KHz	ΔW for Δeq Q = 2 KHz
3	-1	- 45/2	- 1.25 KHz	- 0.94	- 0.63
4	+3	+ 15/2	+ 0.42	+ 0.31	+ 0.21
2	-4	+ 18	+ 1.00	+ 0.75	+ 0.50

Gordon[6] found Δeq Q should be 4 KHz ± 1 KHz, and more recently[34] Bonanomi[286-287] has obtained 3 KHz ±0.7 KHz and experiments of Holuj, Daams and Kalra[288] suggest an even smaller value.

3:6 Stark effect[289]

Because of its inversion the ammonia molecule does not display a first order Stark effect, classically it resembles a rapidly reversing dipole with zero average dipole moment. If a strong field (> 1000 volts/cm) is applied the inversion is partially quenched and an average dipole moment is created. If hyperfine effects are neglected the inversion states have energies

$$W = W_0 \pm \left[(hf/2)^2 + \left[\frac{\mu E M_J K}{J(J+1)} \right] 2 \right]^{\frac{1}{2}} \qquad 28$$

where W_0 is the average energy of the upper and lower inversion levels, μ is the 'permanent' dipole moment that the molecule would have if inversion did not take place, E is the electric field strength and M_J is the projection of J on the direction of the applied field.

It can be seen that $M_J = 0$ states will not be affected by an applied field but $M_J > 0$ states will have different energies (greater for upper inversion states, less for lower inversion states) and in an

inhomogeneous field there will be a force on the molecules given by

$$F = -\operatorname{grad} W = \mp \frac{\left[\mu MK/(J(J+1))\right]^2 E \operatorname{grad} E}{\left[(hf/2)^2 + \left[\mu EMK/(J(J+1))\right]^2\right]^{\frac{1}{2}}} \quad . \qquad 29$$

Thus upper inversion state molecules will experience a force directed towards a region of minimum electric field gradient and lower inversion state molecules will move towards the maximum field gradient.

3:7 Thermal equilibrium populations

The fraction of molecules in any particular inversion state of ammonia is given by

$$f = f_v \times f_r \times f_s \qquad 30$$

for thermal equilibrium, where f_v is the fraction of molecules in the particular vibrational state, f_r is the fraction of molecules in the particular rotational state, given approximately by

$$f_r = \frac{(2J+1)}{4I^2 + 4I + 1} \left[\frac{B^2 Ch^3}{\pi (kT)^3}\right]^{\frac{1}{2}} \qquad 31$$

for low values of J and K. f_s is the degeneracy due to spin and 'K degeneracy' and is given by

$$\begin{aligned} K = 3n \neq 0 \qquad & f_s = 2(4I^2 + 4I + 3) \\ K \neq 3n \qquad & \quad 2(4I^2 + 4I) \\ K = 0 \qquad & \quad (4I^2 + 4I + 3) \end{aligned} \qquad 32$$

where I is the spin of a hydrogen nucleus.

The J = K = 3 ground vibrational state is the most populated level at room temperature, having 6% of the total number of molecules.

From equation 21 of Chapter 1 the ratio of the number of molecules in the lower inversion level to the number in the upper is 1.004.

The probability of a molecule being in a state J,K is accurately proportional to

$$(2J + 1) \exp - \left[\left[BJ(J + 1) + (C - B)K^2 \right] h/(KT) \right] \quad . \qquad 33$$

Thus the exact ratio of the number of molecules in the 4,3 state and 3,3 state is 0.870 at 300°K.

3:8 Transition probabilities[290]

Transition probabilities for symmetric top radiative transitions with $\Delta K = 0$ are given by

$$A_{J+1 \leftarrow J} = \frac{(J + 1)^2 - K^2}{(J + 1)(2J + 1)} \qquad A_{J \leftarrow J} = \frac{K^2}{J(J + 1)} \qquad 34$$

If hyperfine structure is taken into consideration, for $\Delta M = 0$, transitions the latter equation ($J \leftarrow J$) becomes

$$\text{for } \Delta F_I = 0 \qquad A_{J \leftarrow J} = \frac{K^2}{J^2(J + 1)^2} \quad \frac{M^2 \left[J(J + 1) - I_N(I_N + 1) + F_I(F_I + 1) \right]^2}{4F^2(F + 1)^2} \qquad 35$$

$$\text{for } \Delta F_I = +1 \quad A_{J \leftarrow J} = \frac{K^2}{J^2(J + 1)^2} \quad \left[(F_I + 1)^2 - M^2 \right] \times \frac{(F_I + 1 - I_N + J)(F_I + 1 + I_N - J)(I_N + J + 2 + F_I)(I_N + J - F_I)}{4(F_I + 1)^2(2F_I + 1)(2F_I + 3)} \qquad 36$$

If the M states are degenerate (no field), M^2 can be averaged over the various states

$$\sum_{-F_I}^{+F_I} M^2 = 1/3\left[F_I(F_I + 1)(2F_I + 1)\right] , \qquad 37$$

and for the 3,3 centre line ($\Delta F_I = \Delta F = 0$) inversion

$$A_{F_I = 2} : A_{F_I = 3} : A_{F_I = 4} = \frac{640}{576} : \frac{847}{576} : \frac{1225}{576} . \qquad 38$$

Chapter 4. Resonators and Beam Separators

4:1 Introduction

In Chapter 2 it was seen that for an ammonia double resonance detector resonant structures for 1/80 cm and 5/4 cm wavelengths would be required. Resonators for ammonia beam masers at 5/4 cm are normally single mode cylindrical cavities with single hole coupling. Such structures are described in Section 4 below. However 1/80 cm wavelength single mode microwave type cavities cannot be fabricated, they would be only about 1/100 cm in diameter; so either an overmoded cylindrical cavity must be used (Section 5) or Fabry Perot type multimode structures (Section 7). In Section 7 various schemes for coupling power to or from a Fabry Perot structure are discussed.

In Section 2 methods of obtaining a beam of upper state molecules are discussed and the normal multi-pole focuser described. Ring and spiral separators which have properties which should prove useful for supplying molecular beams to Fabry Perot type structures are discussed in Section 3.

4:2 Collimation and Separation[294-296]

In Section 3:6 it was seen that ammonia molecules in different inversion states have different Stark energies, and that the force on a molecule in an electric field is such that upper (+) inversion state molecules experience a force towards a region of lower field gradient and lower (-) state molecules experience a force towards a region of greater field gradient. If a thermal equilibrium beam of ammonia

molecules passes through a strong inhomogeneous electric field the molecules in the different inversion states assume different trajectories and the field may be arranged so that the (+) and (-) populations are almost completely separated from each other. Such state selection takes place if the beam passes down the axis of a system which produces a weaker field in the inner part of the beam and a stronger field in the outer part of the beam, lower state molecules move towards the outer part of the beam and upper state molecules to the inner. Such a field system can be created with a system of parallel rods, alternately charged positive and negative, arranged round the circumference of a cylinder. If there are 2n rods the electrostatic potential is approximately given by

$$P = \frac{V_{2n}}{2R^n} \, \mathrm{Re}(x + iy)^n \qquad 1$$

where R is the radius of the focuser, $\pm V_{2n}/2$ the voltage on alternate electrodes and x and y the coordinate position in the cross section of the focuser. The field at radius r is

$$E_r = \frac{nr^{n-1} V_{2n}}{2R^n} \qquad 2$$

and the maximum field is at the inner surface of the rods (R = r),

$$E_R = \frac{n V_{2n}}{2R} \quad . \qquad 3$$

The molecules in the beam will have a velocity v_z along the axis of the separator and v_r at right angles to it; and molecules in the

upper (+) state will be trapped by the separator if they have kinetic energy ($\frac{1}{2}mv_{rc}^2$) less than the maximum Stark energy. From 3:6 the Stark energy

$$W_E = W - W_0 = \pm \left[(hf/2)^2 + \left[\frac{\mu E M_J K}{J(J+1)} \right] 2 \right]^{\frac{1}{2}} \qquad 4$$

will have a maximum

$$W_{E\ max} = \pm \left[(hf/2)^2 + \left[\frac{\mu n\ V_{2n}\ M_J K}{2RJ(J+1)} \right] 2 \right]^{\frac{1}{2}} . \qquad 5$$

Exact trajectories for different directions and states of molecules have been plotted by Vonbun[291]. Molecules emerging from the separator have a definite maximum transverse velocity, which depends on their high field quantum state (M_J).

Figure 1 shows that an 8-pole (n = 4) focuser is a reasonable compromise between a quadrupole focuser which has small values of v_{rc}, but reasonable field values (and hence separation) along the axis; and a multi-pole focuser which has much larger values of v_{rc} but very little field near the axis of the focuser. An octapole separator has been used consisting of eight silver plated 26 swg steel electrodes on a 1 cm diameter circle. Each set of alternate electrodes is connected to a pair of metal rings which are accurately spaced and insulated from one another with ceramic rods (see Figure 2a). The separator is ten centimetres long and when cleaned and out-gassed it will support 30 KV between the electrodes (at about 10^{-5} torr). Such a potential creates a maximum field of about 120,000 volts/cm, but only 960 volts/cm at a distance of 1 mm from the axis.

Assuming that the molecules effuse from the source with a Maxwell-

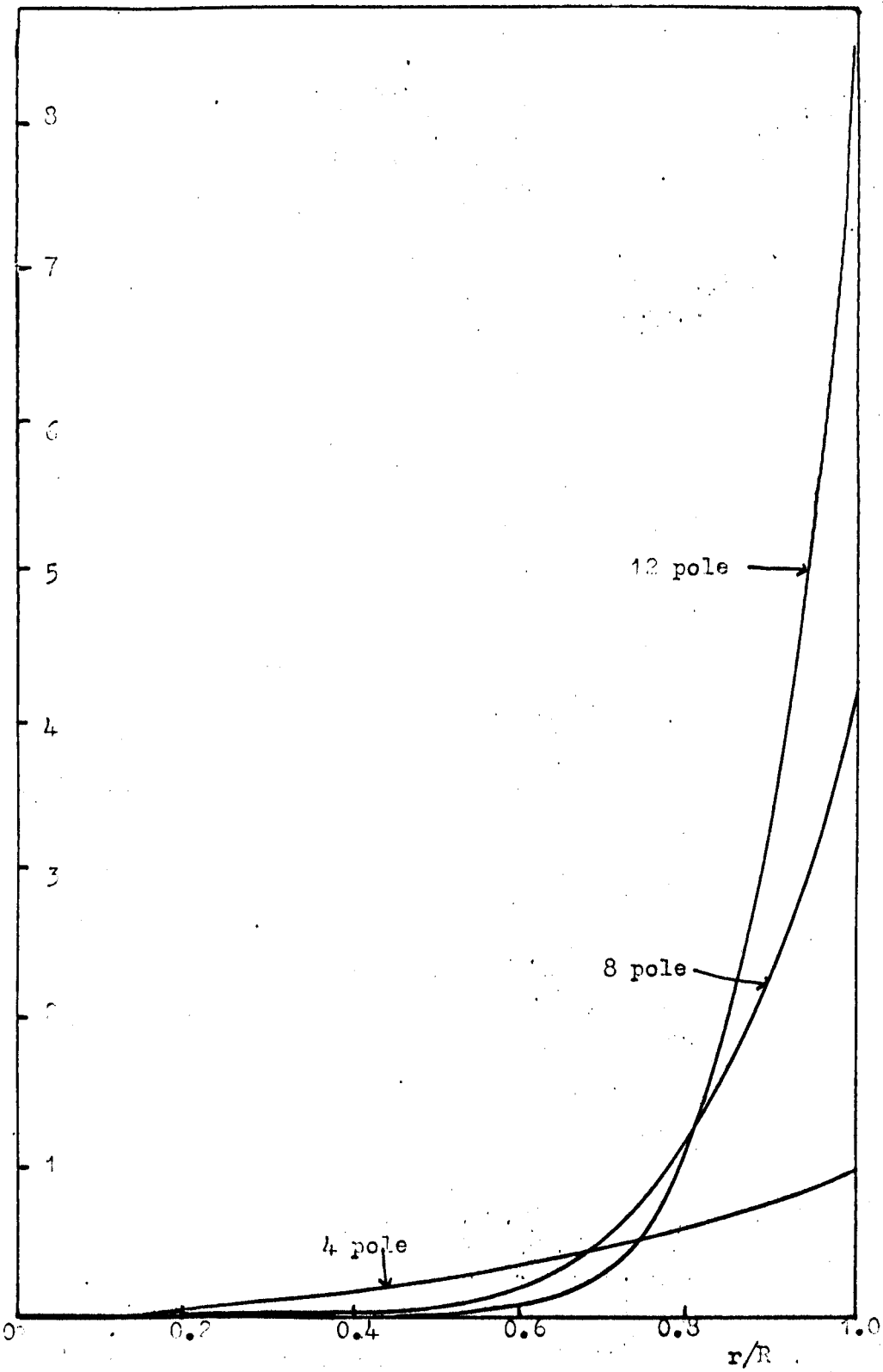

Figure 4:1

Distribution of field(E) in multi pole focusers (after Shimoda [34])

Boltzmann distribution of velocities and directions, the number of molecules[292] in a unit volume having velocity components v_r and v_z (> 0) is

$$N(v_r, v_z)dv_r\, dv_z = \frac{4Nv_r \exp(-v^2/\alpha^2)dv_r\, dv_z}{\alpha^3\pi^{\frac{1}{2}}} , \qquad 6$$

where $v^2 = v_r^2 + v_z^2$ and $\frac{1}{2}m\alpha^2 = kt$, with '$\alpha$' as the most probable velocity, m the molecular mass and N the number of molecules per unit volume.

The total flux from the source is

$$N_0 = \int_0^\infty \int_0^\infty A_0\, Nv_z\, dv_z\, dv_r = A_0\, N\alpha\pi^{-1} \qquad 7$$

where A_0 is the cross section area of the source.

The number of molecules, N_i, in a particular state, E_i, with a statistical fraction f_i (= N_i/N) which pass through a stop of area A is given by

$$N_i = f_i \int_0^{v_{rc}} \int_0^{(2L/\pi R)v_{rc}} AN(v_r, v_z)v_z\, dv_r\, dv_z \qquad 8$$

where the limit to the longitudinal velocity v_z is given by

$$v_z \leq \frac{2L}{\pi R} v_c \qquad 9$$

with L as the length of the focuser. This limit is caused by the fact that separation will be incomplete if the molecules do not spend sufficient time in the state separator. Thus

$$N_i = \frac{A}{A_0} f_i N_0 \frac{W_E}{kt} \left[1 - \exp\left[-\left[\frac{2L}{\pi R}\right]^2 \frac{W_E}{kt} \right] \right] \qquad 10$$

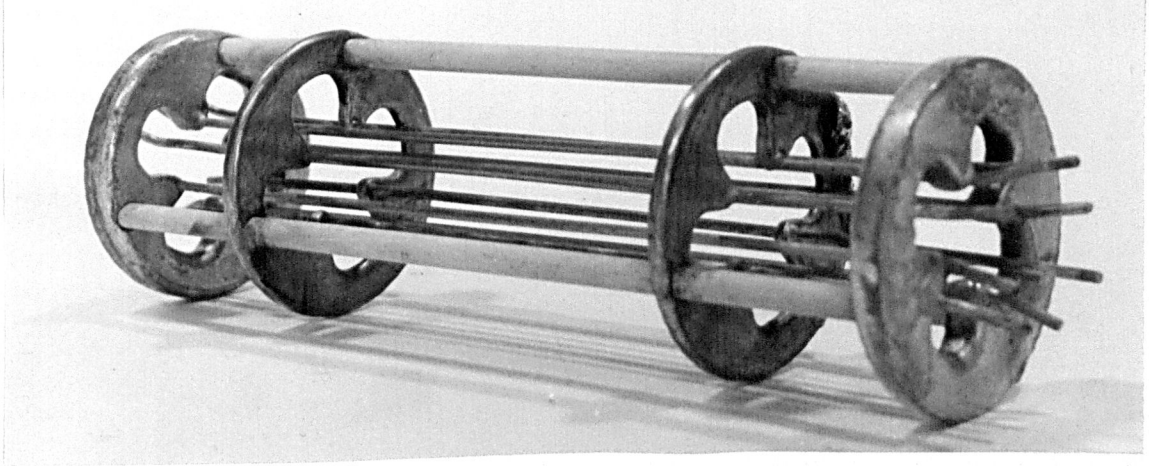

(a) 8 pole state separator

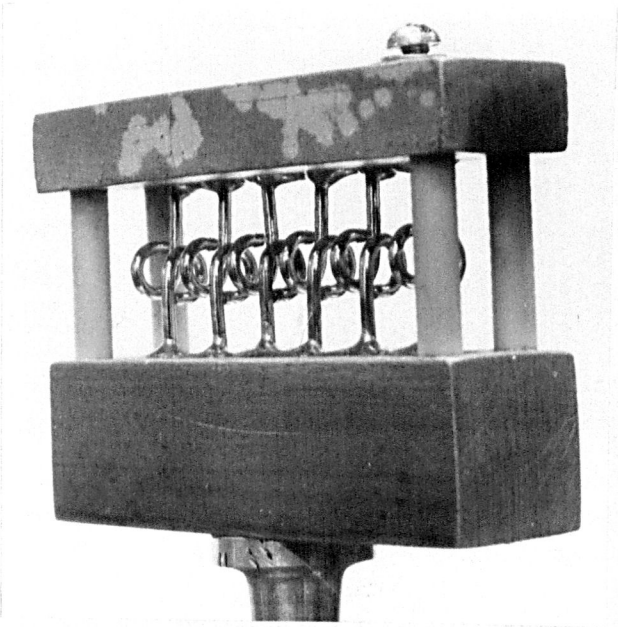

(b) Ring separator

(c) Confocal Resonator

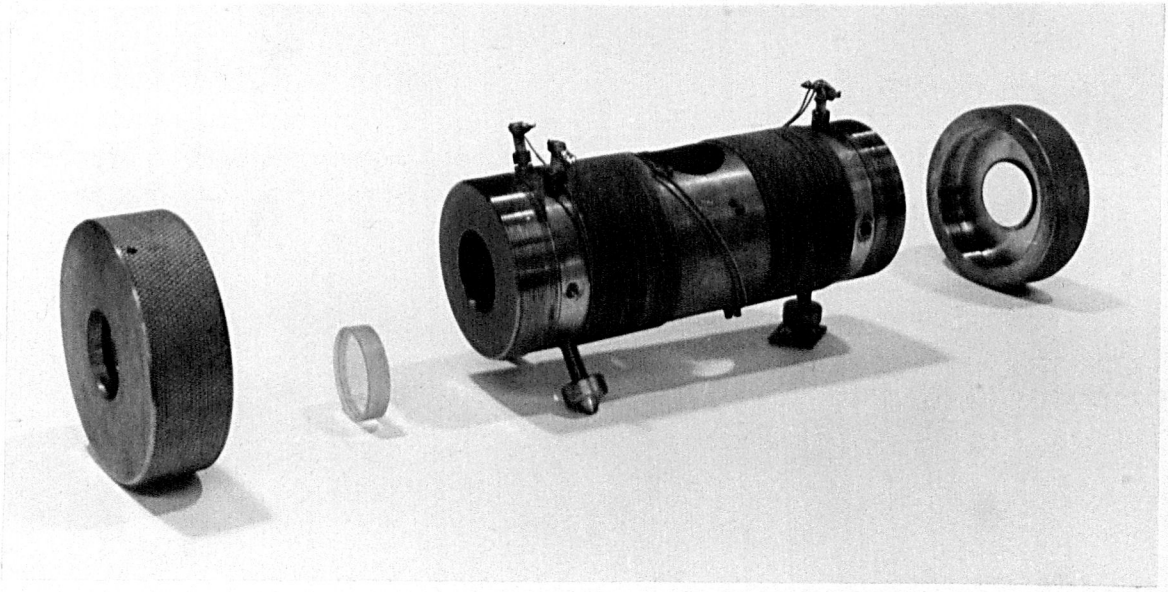

Figure 4:2

and if $\left[\frac{2L}{\pi R}\right] \cdot \left[\frac{W_E}{kt}\right] \ll 1$

$$N_i \simeq f_i \frac{A}{A_O} N_O \left[\frac{2L}{\pi R}\right]^2 \left[\frac{W_E}{kt}\right]^2 , \qquad 11$$

and if $\frac{\mu E M_J K}{J(J+1)} \gg (hf/2)^2$

$$W_E = \frac{\mu M_J K}{J(J+1)} E . \qquad 12$$

In the above it was assumed that the molecules effused from the source with a Maxwell-Boltzmann distribution, this is not true if the source has directional properties.

The peak intensity from a non-directional source is about 10^{19} molecules per second per steradian, whereas Giordmaine and Wang[293] found that this could be increased by a factor of about 20 if the source consisted of an array of long parallel tubes. In normal beam maser systems the mean free path of the molecules is less than the length of the collimating tubes, and is only greater than the radius, a, of the tube for part of the length of the tube, called the critical source length, given by

$$\text{critical source length} = \frac{2.5\ 2^{\frac{1}{4}}\ \alpha a^2}{8\pi^2\ \sigma^2\ I(0)} \qquad 13$$

where I(0) is the peak intensity per single tube, σ is the molecular diameter and α the average molecular velocity. ($\alpha_{ammonia}$ = 53,000 cm/sec.) So for an I(0) of 10^{16} molecules per second the critical source length is about 10 cm for a 1 mm radius tube, and 1 mm for a 0.1 mm radius tube.

If the source is long enough for Knudsen type flow to take place, then the molecules tend to be collimated, with a peak intensity proportional to the square root of the total number of molecules flowing and the half-intensity width of the beam also proportional to the square root of the number of molecules.

For a particular system the separator will collect a given percentage of the molecules from the source, according to the geometry of the system and flux flowing, thus in equation (11) N_0 should be replaced by N_0^x, where $x \sim 1$ for low flux and $\sim \frac{1}{2}$ for large flux; Becker[297] has suggested that in typical masers $x \sim 2/3$. Equation 11 should thus be amended to

$$N_i = f_i \frac{A}{A_0} N_0^x \left[\frac{2L}{\pi R}\right]^2 \left[\frac{\mu E M_J K}{kt\, J(J+1)}\right]^2 , \qquad 14$$

and since

$$\tfrac{1}{2}mv_{rc}^2 = W_{E\,max} = \frac{\mu E M_J K}{J(J+1)} \qquad 15$$

and

$$\tfrac{1}{2}m\alpha^2 = kt \quad . \qquad 16$$

Thus

$$\frac{v_{rc}^2}{\alpha^2} = \frac{\mu E M_J K}{kt\, J(J+1)} \quad . \qquad 17$$

The nozzle which has been used is 5 mm long and 3.3 mm in diameter and consists of a honeycomb of fine parallel copper tubes, about 0.25 mm in diameter.

From equation 14 the sensitivity of the number of focused

molecules to change in separator potential is found to be

$$\frac{dN_i}{dE} = \frac{2N_i}{E} \quad . \qquad 18$$

4:3 Ring and Spiral separators

More recently Becker[297], Piekara Stankowski Smolinska and Galica[298], Basov and Zuev[299] and Kazachok[300] have used spiral and ring state separators. In a ring separator the molecular beam passes through a series of equally spaced identical rings which are alternately charged positive and negative. The inhomogeneous fields focus the upper state molecules along the axis and defocus the lower state molecules. Spiral separators consist of 2 parallel spiral wires, one charged positive the other negative, which also create a strong inhomogeneous field along their common axis (see Figure 2b).

The field in a ring system is given by

$$E = \frac{V_0 \sin \frac{\pi}{2}\left(1 - \frac{2\delta}{L}\right) \frac{2\pi}{L} Z}{I_0\left(\frac{2\pi R}{L}\right) \frac{\pi}{2}\left(1 - \frac{2\delta}{L}\right)} \qquad 19$$

where

$$Z^2 = I_0^2\left(\frac{2\pi r}{L}\right) \cos^2 \frac{2\pi z}{L} + (I_0')^2 \left(\frac{2\pi r}{L}\right) \sin^2 \frac{2\pi z}{L} \qquad 20$$

and

$$I_0(x) = 1 + \frac{x^2}{4} - \frac{x^4}{2^4(2!)} + \ldots \qquad 21$$

is a modified Bessel function of the first kind of zero order, which becomes $\approx 1 + x^2/4$ if x is small. L is the period of the ring system, δ is the ring thickness and z the axis along the separator. Letting

$\delta = 0$

$$E = \frac{4V_0 Z}{\left[1 + \frac{\pi^2 R^2}{L^2}\right] L} \qquad 22$$

with Z varying periodically from $(\cos \frac{2\pi z}{L})(1 + \frac{4\pi^2 r^2}{L^2})$ to $\frac{8\pi^2 r}{L^2}$ along the z direction. If R = 0.17 cm, L = 0.5 cm and V_0 = 30,000 volts. on the axis the field varies from 0 to 120,000 volts/cm. Thus a great advantage of ring (and spiral) separators is that they produce an inhomogeneous field along the axis of the separator, thus axial molecules are well separated. Such separators are very efficient and comparatively insensitive to variations of separator potential ($dN/N \leq dE/10E$).

For state separation with ring and spiral separators Becker[297] has shown that the diameter, z, of the molecular beam of upper state molecules is given by

$$z = \frac{eB}{a}\left[1 - \frac{a(e - a)}{ef}\right] \qquad 23$$

where e is the distance between the source nozzle (diameter d) and the diaphragm (diameter D) at the entrance to the resonator, a is the distance between the nozzle and the centre of the separator (internal diameter B), f is the focal length of the 'lens equivalent' of the separator given by

$$B/f = bmU \qquad 24$$

where U is the potential difference between the rings or spiral wires,

m is the number of rings or windings of a single electrode and $b = 0.87 \times 10^{-6}$ per volt for ring and 1.03×10^{-6} per volt for spiral separators.

Thus if m = 6 for a ring separator with U = 20 KV, f ~ 3.5 cm and if e = 10 cm and a = 2.0 cm, z is about 0.4 cm. Thus it is seen that such a narrow diameter separator can produce a highly directional narrow beam.

4:4 Cylindrical cavities

The modes which can exist in cylindrical metal cavities are numerous, but they can be divided into two classes, TE or H modes where there is no electric field parallel to the axis of the resonator and TM or E modes where there is no magnetic field parallel to the axis of the resonator. The resonant condition for E modes is given by

$$\lambda_o = \frac{4}{\left[\left[\frac{L}{z_0}\right]^2 + \left[\frac{2U_{m,\,n}}{\pi a}\right]^2\right]^{\frac{1}{2}}} \qquad 25$$

where L is an integer equivalent to the number of half wave variations along the axis of the resonator of length $2z_0$, a is the radius of the cylinder and $U_{m,\,n}$ is the n^{th} root of the m^{th} order Bessel function $J_m(U) = 0$.[301] If L = 0, that is for the $E_{m,\,n,\,0}$ mode (where m is the total number of full period variations of either field component along a circular path concentric with the cylinder wall and n is one more than the number of reversals of sign of a field component along a radius)

$$\lambda_0 = 2\pi a/U_{m,\,n}\,, \qquad 26$$

and if m = 0, 2a = 0.9614 cm for a frequency of 23.87 GHz. This is a convenient diameter to match the typical half width of a beam produced by a multi-pole separator. A structure with a high quality factor should be long and made from a high conductivity metal. This must be made to a precision of ± 1/10 thou (thousandths of an inch) diameter, which cannot easily be drilled or bored, so a mandrel is made in S 80 stainless steel and electroplated, first with a layer of silver and then with copper. When the electroform is about an inch in diameter it is removed from the plating solution, machined externally and then removed from the mandrel by heating it in hot water or oil. The mandrels used have been 0.9619 cm in diameter, the extra diameter being necessary to correct for slight end effects of the cavities. This produces a cavity slightly too small, the final tuning being achieved by heating the cavity (for electroformed copper the cavity will tune by 0.4 MHz ± 10% for each 1° C change in temperature). The Quality Factor of the cavity is improved if metal rings or end-caps are inserted in each end of the cavity and adjusted for maximum Q. Several such cavities have been made, the longest being 12.5 cm. Typically they have loaded quality factors of 3 to 5 thousand compared with a theoretical value of 10,800 (with a small coupling hole 1/10 to 1/8 th inch diameter in the middle of the cavity).

A cavity oscillating in the E_{011} mode has also been used, this has a diameter of 0.9687 cm and a length of about 6 cm, this also tunes thermally, but the tuning is dependent on both radius and length.

Shimoda, Wang and Townes[33] have derived what they call a figure of metit (M) for a cavity resonator (length L) used with a beam (area A) maser.,

$$M = \frac{LQ_0}{A}\left[\frac{8}{\pi^2}\right]L \quad . \qquad 27$$

The factor $\left(\frac{8}{\pi^2}\right)L$ is due to the broadening of the resonance line width if the field is less concentrated along the axis than in the $E_{m,\,m,\,0}$ modes and the factor $\frac{L}{A}$ is derived from the sensitivity equation for a beam maser (see Chapter 5). For a broad beam filling the whole cavity this gives an E_{010} cavity a value of M = 7.7 and 6.0 for E_{011}, 5.9 for H_{111} and 4.1 for H_{011}. For a narrower beam the E_{010} mode is even better.

4:5 Ultramicrowave cylindrical cavities

When a resonant structure is required in the microwave region, it is normal to have the dimensions comparable to the wavelength of the radiation, with at least one of the cavity dimensions of the order of $\lambda/2$. However, in the ultramicrowave region it is not possible to manufacture structures with such small dimensions and one has to use a microwave-type cavity in a high order mode. Typically a cylindrical cavity operating in the TM_{0n0} mode of 0.960996 cm diameter will be resonant in mode 76 at 2362 GHz, in mode 77 at 2393 GHz and at 2424 GHz in the 78th mode, but there is considerable possibility of oscillation in other than the TM_{0n0} modes.

Thus for thermal tuning there must be a range of about 700° C, or a cavity can be specially made to tune to the 2404 GHz transition. A

cavity of diameter 0.9687 cm should tune to the 77th mode at a moderate temperature.

Alternatively one can use a Fabry-Perot interferometer as a resonator. The name Fabry-Perot would seem now to cover a whole class of interferometers which may be any resonant structure composed of two mirrors where the mirrors need not be plane or parallel.

4:6 Fabry-Perot Resonators

It is traditional to consider the plane-parallel Fabry-Perot resonator as a problem in geometric optics. Likewise Connes[302] has shown that two identical spherical concave mirrors with coincident focal points will form a resonant structure. Jackson[303] obtained interference effects with such a structure in the visible region and observed concentric ring patterns similar to those of the plane-parallel interferometer. Figure 3 illustrates the confocal arrangement, where radius of curvature b_1 equals radius of curvature b_2 and $d = b_1 = b_2$. If the two concave mirrors AC and BD are semi-transparent, then a plane-parallel beam entering along the Z axis in the positive direction will be partially transmitted at BD and partially reflected from BD and then AC to be transmitted or reflected at BD. The path difference between the two sets of rays is 4d with an error of $\frac{d}{16}\left[\frac{2a}{d}\right]^4$. Thus a high Q structure may be formed if this difference is small.

The Finesse, F, of an interferometer is the ratio of the fringe separation to the fringe half intensity width. For the plane-parallel case this will be of the order of 60 for good reflectors, thus for the

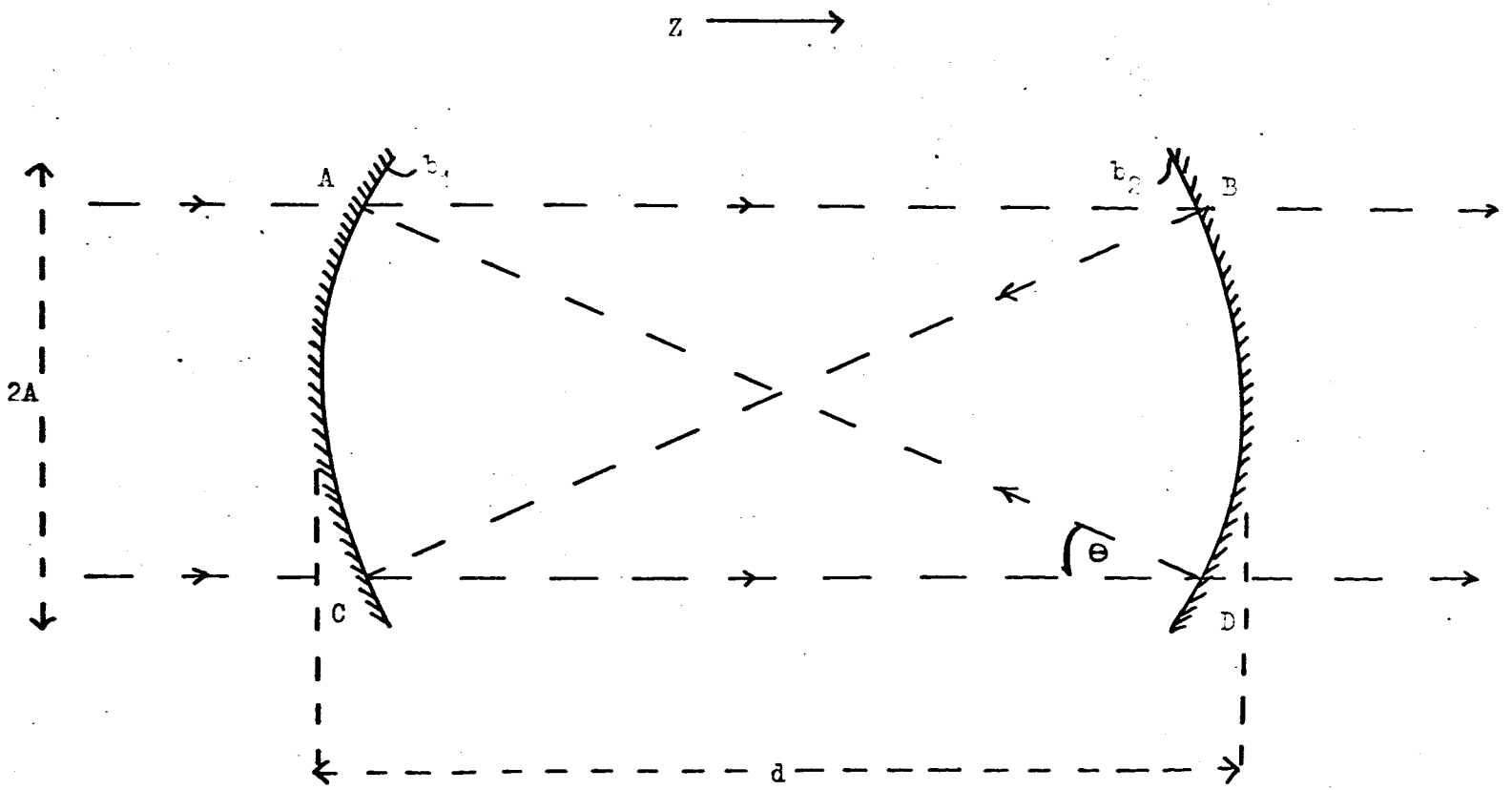

Figure 4:3

Confocal Resonator

comparable confocal system with half the Finesse,

$$\frac{d}{16}\left[\frac{2a}{d}\right]^4 \lesssim 1/50 \quad . \qquad 28$$

At 125μ with d = 10 cm, a will be 0.8 cm maximum. Thus the mirror diameters must not exceed 1.6 cm if the spherical nature of the mirrors is not to limit the Finesse of the interferometer. If bigger mirrors are used they must be parabolic.

Fox and Li[304] and Schawlow and Townes[20] have shown that the plane-parallel Fabry-Perot etalon will support discrete mode patterns and have indicated that this approach is useful for masers. They point out that each ring of the normal Fabry-Perot pattern does not indicate a discrete mode, but a summation of an infinite number of such modes. This is important for the plane-parallel case because each of these mode patterns will resonate at a slightly different frequency. This is not so for the confocal resonator, which is frequency degenerate. This degeneracy is lifted for a confocal system with imperfect mirrors or a system with non-confocal spherical mirrors.

Fox and Li have shown that assuming small diffraction and reflection losses the resonator quality factor is

$$Q = \frac{2\pi d}{\phi\lambda} \qquad 29$$

where ϕ is the fractional power loss per bounce from a reflector. This loss is the sum of the reflection and diffraction losses due to mirror imperfections, misalignments and finite apertures. It will be seen below that diffraction losses for a resonator with large Fresnel number, $N = \left[\frac{a^2}{d\lambda}\right]$, are an order of magnitude less than reflection losses.

Thus at 125μ for d = 10 cm and 99% reflectivity the resonator should have a Q of 500,000. The practical Q may be less than this; Zimmerer[305] has found for the millimetre region with a confocal resonator of Fresnel number 1.5 and with mirrors true to a few parts in 10^4, the practical Q is only 40% of the theoretical Q. Thus at 125μ with d = 10, n = 4 and mirrors flat and true to 1/25 optical wavelength a Q of 250,000 might be expected. With much care Welling and Andresen[306] at 70 GHz have obtained Q values of 160,000 (with q' = 180 - see below) for plane-parallel resonators; for higher orders of interference their system (N ~ 7 for the 100th order) was diffraction loss limited.

The value of Q obtained will be considerably less if a poor reflecting material is used. The reflectivity R is given by

$$R \sim 1 - 2(f\rho)^{\frac{1}{2}} \qquad 30$$

where ρ is the resistivity in ohm-cm with values of 1.4 to 1.6 × 10^{-6} for silver, 2.4 to 2.7 × 10^{-6} for aluminium and 60 × 10^{-6} for stainless steel. For the latter the power reflectivity will only be about 97% and the effective Q will be nearer 100,000.

The effective Q will also be considerably less if an inefficient means of coupling radiation in or out of the cavity is used, (see Section 7/p83 below); in particular for good reflectors, with 5% radiation coupled in or out using a poor coupling, a Q of only about 20,000 might be achieved.

For evaluating the usefulness of a structure for use as a resonator it is often helpful to replace Q by q' given by

$$q' = \frac{1}{\phi} = \frac{Q}{\pi q} \qquad 31$$

where q is the number of half wavelengths along the z direction. Thus provided the diffraction losses remain constant (N constant) the half confocal, confocal and concentric arrangements would all have the same q', whereas their quality factors would be in the ratio 1 : 2 : 4.

Fox and Li considered the propagation of a wave which was reflected back and forth between two parallel mirrors and between confocal spherical mirrors. They found that for both cases, discrete field distributions appeared, with the field amplitude tending to increase along the resonator axis and the phase shift being an integral multiple of 2π for certain discrete mirror separations. They found that the actual dimensions of the interferometer are unimportant in determining the field distribution and only the Fresnel number (which is approximately equal to the number of Fresnel zones seen in one mirror from the centre of the other) is important. These field variations are best regarded as transverse mode patterns, linearly polarised. The mode patterns representing standing wave patterns inside the interferometer are designated TEM_{mnq}, m, n and q being integral mode numbers, m and n representing orthogonal directions at right angles to q (Z direction) (alternatively m and n are sometimes used in mode designation as for circular waveguide). Kogelnik and Rigrod[307] have experimentally verified these mode patterns and confirmed that the modes with the least loss are those with m and n equal to zero or a small integer. Figure 4a illustrates this; it can be seen that the diffraction losses

of the confocal system may be orders of magnitude less than those for plane-parallel mirrors, and the losses of this system are less than that suggested by geometric optics.

Further, Vanyukov and others[308] have examined the effect of tilting one of the mirrors of a plane-parallel Fabry-Perot and derived the empirical formula

$$-\log(1-\phi) = 10^{-2}\ \alpha L^{0.42} \qquad 32$$

where α is the angle between the mirrors in seconds and L is the cavity length in metres. Thus for a $\frac{1}{2}$ minute angle of tilt losses will approach 10% per pass for a 12 cm resonator. Losses for a half confocal system (see below) are at least an order of magnitude less than this, the loss being only a few percent for the TEM_{002} mode for a 10 minute angle between the plates[309].

The reason for the low diffraction losses is that the field distribution tends to concentrate near the axis of the resonator system; this phenomenon is most marked for spherical mirror systems.

The radial distance from the axis for the field to fall to 1/e of its maximum value is called the spot size, and quantitatively Boyd and Kogelnik[310] have determined this as

$$W_s^1 = W_0 \left[1 + \frac{d^2}{b^2}\right]^{\frac{1}{2}} \qquad 33$$

for the fundamental mode (m = n = 0) for a spherical mirror system at a distance d/2 from the symmetric centre of the system, where W_0 is the spot size at the centre given by

$$W_0 = \left[\frac{b\lambda}{2\pi}\right]^{\frac{1}{2}} . \qquad 34$$

Thus the spot size of the fundamental mode of the confocal system at the reflectors is $W_0 2^{\frac{1}{2}}$. Hence for b = 10 at 125μ, W_s^1 is 0.2 cm, which is a factor of four less than the Connes-Jackson diffraction limitation for sufficient Finesse, which would be expected because Boyd and Kogelnik are limiting themselves to small values of θ.

From Figure 4a it can be seen that most of the energy will be stored in the lowest (dominant) mode for the confocal resonator because its losses are considerably less than those of the next mode (TEM_{01q}). This difference is very much greater than for the lowest modes of the plane parallel etalon, hence the spherical Fabry-Perot should oscillate in only the dominant mode or a very few low order modes.

Boyd and Gordon[311] have obtained the resonance condition for the confocal resonator as

$$\frac{4b}{\lambda} = 2q + (1 + m + n). \qquad 35$$

Thus although there will be resonances at integer values of $4b/\lambda$, the resonance in the TEM_{00q} mode can take place only at alternate resonance conditions; or in general, at any particular resonance condition all the odd order modes or all the even modes can resonate, but not both sets. Hence if the Fabry-Perot is being scanned by altering d it is possible that alternate conditions of $4b/\lambda$ will have different patterns or only one set of alternate resonances will be observed.

Boyd and Gordon extended their treatment of the confocal case to that of non-confocal spacings by showing that there exist constant phase surfaces in the confocal resonator (apart from those at the mirror surfaces) and hence if any one of these is replaced by a mirror a

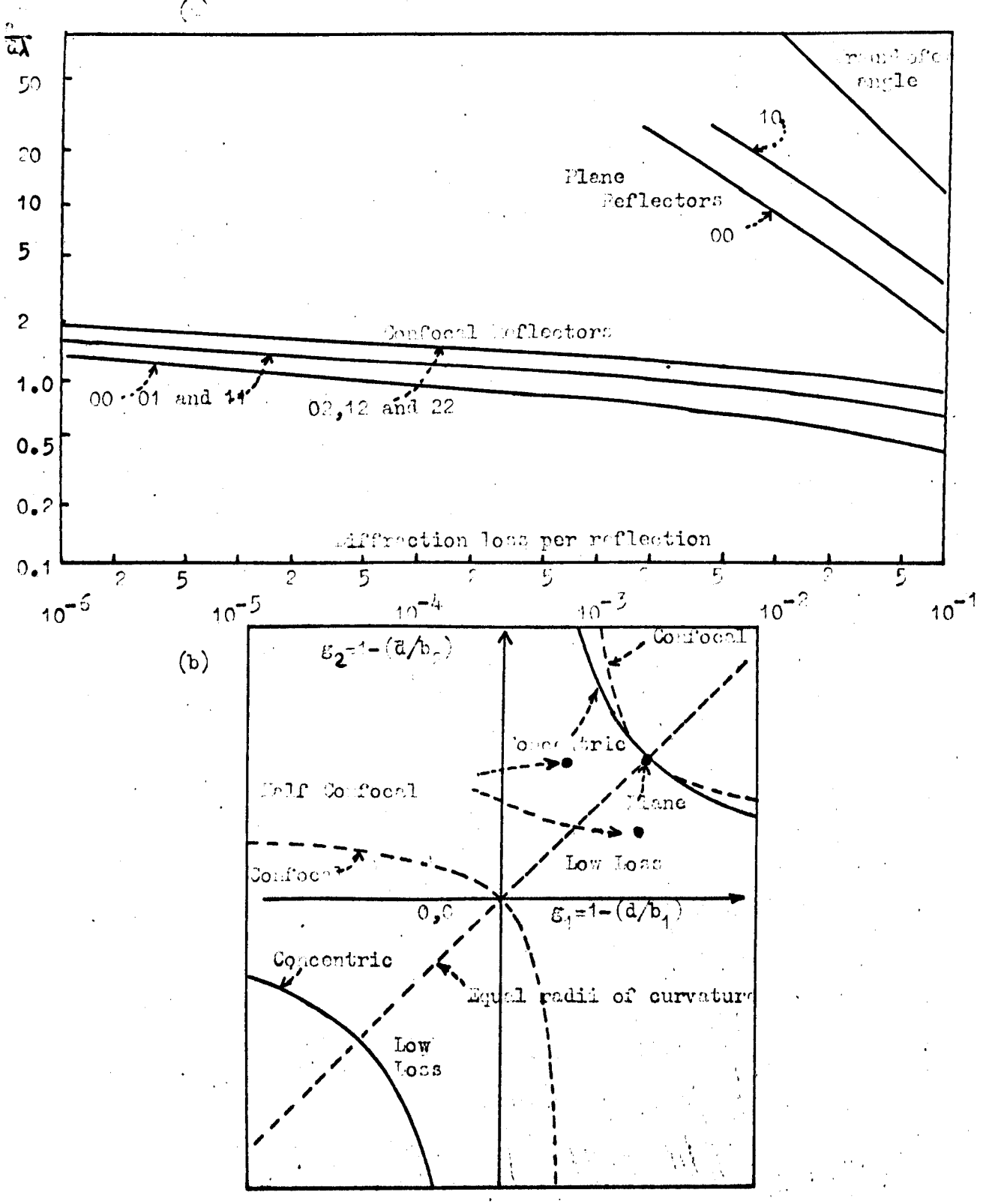

Figure 4:4

(a), Diffraction loss variation with Fresnel number

(b), Spherical mirror interferometer loss regions

resonant structure can be obtained. The minimum diffraction losses occur for the confocal case, but are of the same order of magnitude as those for adjacent spacings.

For the non-confocal case $4d/\lambda$ is no longer necessarily an integer at resonance, instead

$$\frac{4d}{\lambda} = 2q + (1 + m + n)\left[1 - \frac{4}{\pi}\tan^{-1}\frac{b - d}{b + d}\right] \qquad 36$$

and

$$\Delta(1/\lambda) = \frac{1}{4d}\left[2\pi q + (1 - \frac{4}{\pi}\tan^{-1}\frac{b - d}{b + d})\right]\Delta(m + n) \quad , \qquad 37$$

which illustrates the point made earlier that for the non-confocal case the modes are no longer degenerate in frequency. The splitting is comparable with that produced by the plane-parallel resonator for a 3% variation of d from b.

Unfortunately when various aberrations are considered the picture becomes more complex. Boyd and Kogelnik[310] have found that if the two spherical mirrors are of unequal aperture then the diffraction losses increase but the resonance conditions are not changed, but if the two mirrors are of unequal radii of curvature the diffraction losses tend towards infinity at d spacings between b_1 and b_2, that is, the confocal condition. Thus if a confocal interferometer is to be used a separation a few percent greater than the confocal should be used. Soohoo[312] has suggested that for $\mathfrak{m}N = 1$ system the least loss arrangement may be obtained with d about (3/2)b.

In fact Fox and Li in a later paper[313] have shown that the confocal

region is only a region of high loss, not a complete stop band. They point out that the concentric (coincident centres of curvature) system is also on the edge of a high loss region. Figure 4b is a two-dimensional section of a three-dimensional diffraction loss model. It can be seen that a twin spherical mirror system can be constructed for low loss, but it can only approach that of the perfect confocal system.

Boyd and Kogelnik have suggested that a resonator with all the low loss properties of the confocal system can be obtained by replacing one of the spherical mirrors with a plane mirror at the focal plane. The resonance condition for the generalised confocal resonator is

$$f = \frac{c}{2d}\left[q + (1 + m + n)\pi^{-1} \cos^{-1} \left[\left(1 - \frac{d}{b_1}\right)\left(1 - \frac{d}{b_2}\right)\right]^{\frac{1}{2}} \right] \qquad 38$$

where f is the resonant frequency. For a half confocal resonator b_2 is infinity and $2d = b_1$, from which it follows that

$$d = \frac{\lambda}{2}\left(q + \tfrac{1}{4}(1 + m + n)\right). \qquad 39$$

Thus longitudinal modes (lowest loss modes) will be separated by $\lambda/2$ and higher order ones will be spaced at $\lambda/8$ intervals, some coinciding in frequency with the pure longitudinal modes. There will be $\frac{13.2 \times 8}{125 \times 10^{-4}}$ one hundred and twenty five micron $\lambda/8$ modes along the axis of a 13.2 cm resonator, and the spectral separation between the $\lambda/8$ resonances will be 300 MHz. Since the bandwidth of the Fabry-Perot is 10 to 50 MHz the resonator will be tuned to a resonant mode for one sixth to one thirtieth of its scan, and a movement of less than a

micron of one mirror will shift the cavity from a resonant peak.

A half confocal resonator has been made (see Figure 2c) from a concave spherical mirror and a flat dielectric plate, separated by a brass former and held in position by silicon rubber 'O' rings mounted on brass end-caps. The end faces of the former are flat to better than 6 microns, parallel, and separated by 13.2205 ± 0.0010 cm. The resonator is tuned by heating the former with glass fibre insulated resistance wire wound round its circumference. The spherical mirror is surface aluminised and spherical to a tenth of an optical wavelength: the flat plate varies according to the radiation coupling scheme being used.

4:7 Fabry-Perot coupling

If a half confocal Fabry-Perot resonator is to be used to scan through a resonance line in a double cavity interferometer it is desirable to modulate the field intensity and tuning of the resonator in some way so that the resulting signal in the second cavity is not obscured in low frequency (~DC) noise at the scan frequency. This can be done by either having a rotating vane inside the cavity or by vibrating one of the mirrors out of alignment. The former technique (using a piezo-electric or mechanical system) leads to severe microphonic problems and the latter is difficult to achieve when the mirror alignment is dependent on a rigid spacer between the mirrors. Alterantively the active medium, rather than the resonator Q, can be modulated with a Stark or Zeeman system[314], but such a system may modulate the efficiency of the state separator or the output of the second cavity directly.

Another method is to use as the stimulating field radiation coupled into the resonant structure from outside. This can be easily modulated with a mechanical chopping system and the problem is then one of coupling. Since the Fabry-Perot approximates a free space device coupling might be achieved by inserting a thin film into the resonator at an angle with the axis. But unfortunately for the hundred micron region no film is available with sufficiently good transmission properties. If one mirror is made small such that there is considerable diffraction round it then with a suitable external optical system a controlled amount of coupling can be achieved. The plane mirror can be made in the form of a metal diffraction reflection grating[315], at such an angle that the first order of the grating forms the resonant structure with the spherical mirror and the zero order couples power out of the resonator. Such a scheme should couple a few percent of the energy, but the maximum reflectivity of the grating in the first order would be only about 95% and hence the quality factor of the resulting cavity would be small.

The remaining techniques available require transmission 'through' one or other of the two mirrors. For correct mode matching it is easiest to couple through the spherical mirror[316], but it is rather easier to construct most of the coupling schemes which will be suggested below for the plane mirror.

The two commonest techniques in the optical region of the spectrum use dielectric plates and thin metal films. The former cannot be made for the 100 micron region because they would require dielectrics

about 1 thou thick of greater transparency than is currently available (at room temperatures)[317]. Metal films are very inefficient because they absorb considerably more than they transmit: thus at 100 microns values for a typical metal film are reflectivity 80%, transmittance 1% and absorption 19%[318]. Standard electromagnetic theory predicts a skin depth for aluminium at 125 microns of about 60 nm, but Korolev and Gridnev[319] have found that a thin film (20 - 30 nm) of silver is almost completely reflecting and similar results have been obtained for gold and copper in the microwave region; thus any metallic film to be used in the far infrared should have its properties experimentally determined before use.

The thin film methods are examples of 'above cut-off' systems, that is the transmission properties are dependent on the bulk properties of the materials and not on the transmission through structures with holes or gaps with separations of the order of (or less than) the wavelength of the radiation ('beyond cut-off'). An above cut-off system which has been used for gas irasers is that of a single coupling hole in one mirror with a size considerably greater than the wavelength[151, 320]. Assuming coupling only to the TEM_{00q} modes a central hole is required and the transmission through the hole will be given by the ratio of the hole area (A) to the mirror spot area

$$\text{fractional loss} = \frac{2A}{\pi W_0^2} \qquad 40$$

for the plane plate where W_0 is given by equation 34, so

$$\text{fractional loss} = \frac{4A}{b\lambda} \quad . \qquad 41$$

For 2% coupling at 125 μ in a 12.5 cm cavity (b = 25 cm) the hole diameter must be 0.8 mm. This value is increased if the hole is composed of a dielectric because of the reflection at the air-dielectric boundary.

The above calculation assumes that the input radiation only couples to the TEM_{00q} modes and that the coupling does not interfere with the mode patterns: usually this is not true. McCumber[321] has calculated the losses of several of the 'lowest loss' modes for confocal resonators for different size central coupling holes for different cavity Fresnel numbers. It would appear that several transverse modes (10, 20, 30, 40, 01, 11 etc.) will have lower losses than the 00 modes and that the central hole will require to be less than 10^{-2} cm in diameter for the 00 modes to be the lowest loss modes. The losses of the non 00 modes might be increased by decreasing the reflectivity (or adding further coupling holes) radially from the central hole[322] but this would mean a rather low Q resonator.

'Beyond cut-off' coupling systems have been extensively studied by Culshaw[323-226] for millimetre and sub-millimetre resonant structures. Several of the structures which he investigated are not feasible for 125 micron radiation because of the difficulties of construction, but one type merits further study. This is a two dimensional array of slits or holes in an otherwise completely reflecting thin metal film.

For a rectangular array of circular transparent holes in a thin metal film, of diameter d and spacings a and b the susceptance (e.m.u.) is

$$B = -\frac{3ab\lambda}{\pi d^3} \qquad 42$$

provided that $5(a, b) > \lambda > (a, b)$ and $d/(a, b) < 0.5$ [305, 323, 327].

Rank and Genzel and others[232-233] have obtained results in the far infrared for metal meshes with $\lambda/(a, b) \sim 1$ and $d/a \nless 0.5$ and found that they can be used as efficient short wave cut-off filters (as described in p30 Chapter 2). Möller and McKnight[231] have obtained similar results for transmission filter gratings and Balakhanov[328] has considered metal strip grids. Recently Vinogradov and others[329] have shown that in the millimetre region of the spectrum Fabry-Perot reflectors can be made from wire grids, but considerable losses take place because of the non-coplanarity of the wires, even so at 2.1 mm reflectivities greater than 99.8% can be easily achieved. This is likely to fall to less than 98% at 125 microns.

If a square array of holes in a thin (with respect to λ) metal film is required to couple energy between a TEM wave and a TEM mode in a resonator, the easiest way of determining the optimum coupling condition is to equate the admittance of the other surface of the resonator with the admittance of the coupling plate. Maximum coupling will be achieved when the 'transmission line' is matched to the quality factor of the cavity. This assumes a 'passive' resonator, whereas for an active (stimulated emission) system rather

weaker coupling is required. For an electromagnetic wave of frequency f in air normally incident on a metallic surface of conductivity σ, the admittance Y is given by

$$Y = \left[\frac{\sigma}{4\pi e_0 f}\right]^{\frac{1}{2}} (1 - j) \qquad 43$$

where e_0 is the permittivity of free space ($= 8.85 \times 10^{-12}$ F/m).

Since the resistivity of aluminium $\approx 2.83 \times 10^{-8}$ ohm-metre, the factor $\sigma/(4\pi e_0 f)^{\frac{1}{2}} = g \approx 350$ MKS units at 2.4 teracycles. For high Q modes the mirrors must be separated such that the admittance of the continuous face at the perforated surface has unit conductance and a positive susceptance equal and opposite to the negative susceptance of the perforated metal plate. Zimmerer has obtained[327] an approximation for the susceptance

$$B = -(2g)^{\frac{1}{2}}, \qquad 44$$

hence for aluminium the inductive susceptance is given by equations 44 and 43 as - 26.5 mho. Since the reflectivity R is given by

$$R = 1 - 2/g \qquad 45$$

and this corresponds to a Q of about 10^6 for a 12.5 cm resonator.

When a plane electromagnetic wave is incident normally on a plane metal surface the amount of energy dissipated, t_0, is given by 1 - R and if a lossless dielectric is placed in front of and in contact with the metal surface then the energy dissipated is

$$t = \frac{Kt_0}{1 + (K - 1)\cos^2\theta} \qquad 46$$

where K is the dielectric constant and $\theta = 2\pi L/\lambda'$ with L the dielectric thickness and λ' the wavelength in the dielectric. The power absorbed in the metal sheet is increased by t/t_0 and that transmitted by a perforated metal sheet will be increased by this amount, so the value of B may be increased by a factor of up to two according to

$$B_{dielectric} = (t_0/t)^{-\frac{1}{2}} B \ . \qquad 47$$

So assuming no stimulated emission the optimum coupling condition is

$$-58.3 \lesssim B \lesssim -26.5 \ , \qquad 48$$

and Figure 5 is a plot of the various possible hole and spacing combinations for 125μ radiation. The various coupling plates which have been made and used in conjunction with the half confocal resonator will be described in Chapter 7.

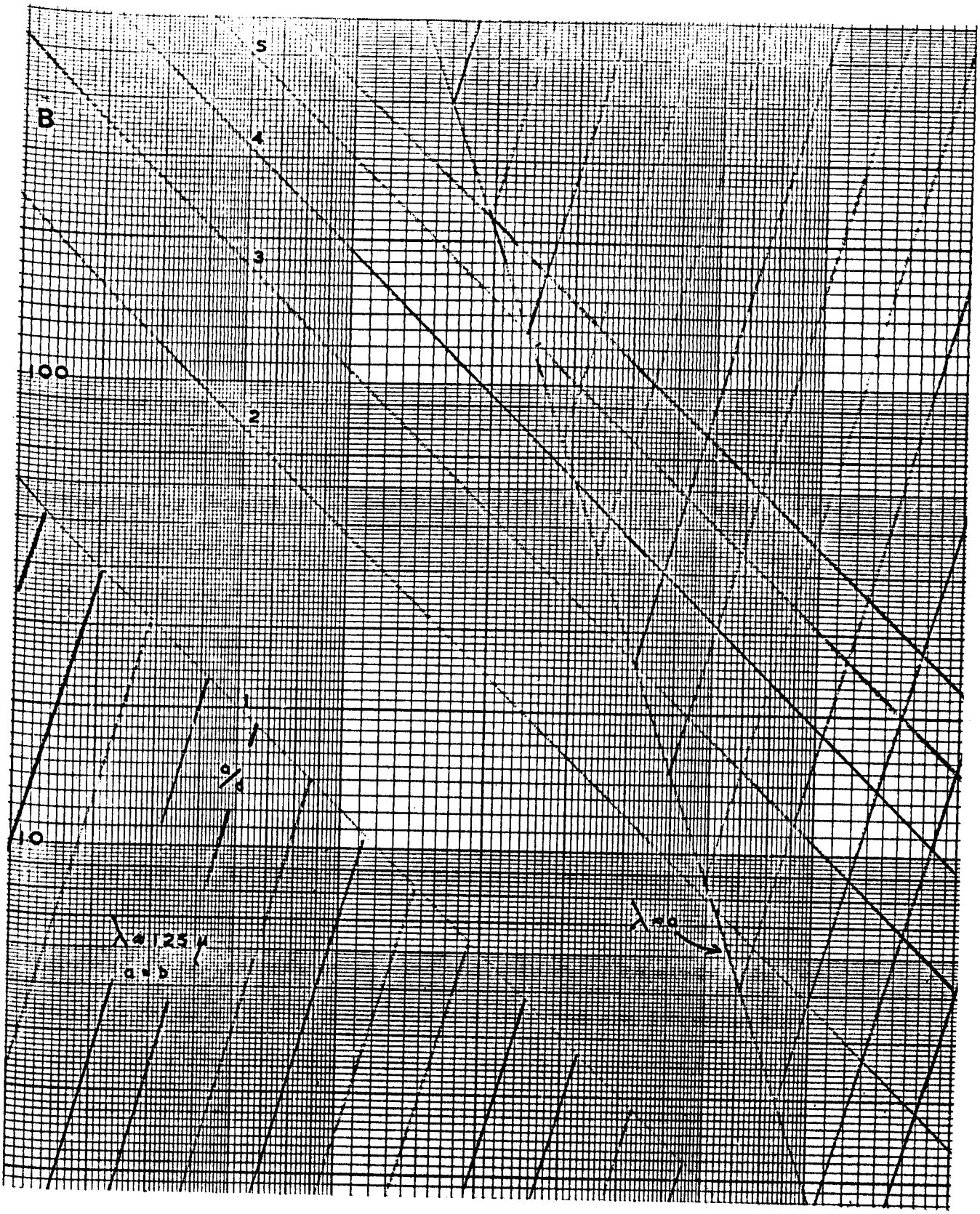
B
5
4
3
100
2
1
0/d
10
λ=0
a=b

Chapter 5. The Ammonia microwave beam maser

5:1 Introduction

The ammonia microwave beam maser was the first continuously operating stimulated emission device to work. In this chapter the construction of a single cavity microwave beam maser oscillator is described and some of its operating characteristics determined. In particular the effects of increasing the distance between the electrostatic separator and microwave cavity are examined.

If the state separator and the detector microwave cavity are separated by about 8 cm a second cavity, microwave or ultramicrowave, can be inserted in this gap and the beam will then pass through two resonant structures in succession. In Chapter 6 the effects due to an additional cavity similar to the detector cavity (resonant for the $J = K = 3$ ammonia inversion transition) will be described and in Chapter 7 the system with the additional cavity tuned for ultramicrowave ($J = 4, K = 3 \rightarrow J = 3, K = 3$) transitions will be considered and various experiments described.

In the single cavity ammonia microwave beam maser using the 3,3 inversion transition of ammonia a collimated beam of molecules is directed along the axis of an electrostatic state separator and the lower state molecules diverge from the axis and are frozen on the surface of a liquid nitrogen jacket; the upper state molecules are 'focused' into the microwave resonant structure, normally a single mode cylindrical cavity. The field in the cavity (initially thermal) stimulates transitions from the (+) to the (-) state and power is

delivered to the microwave field. If the cavity is correctly tuned and sufficient transitions take place the power delivered to the field may exceed the losses in the cavity and coupling hole and oscillation takes place.

The power delivered by the beam is very small (10^{-11} to 10^{-12} watts) so a sensitive detection scheme is needed. A 30 MHz intermediate frequency superheterodyne system is used with a microwave klystron (tuned 30 MHz from the 23,870 MHz maser frequency) as local oscillator. The two microwave oscillations pass via a 'magic T' to a silicon or germanium point contact diode and one of the 30 MHz sidebands is amplified in a low noise cascode pre-amplifier and main amplifier and then rectified and filtered. Normally some parameter of the maser system is modulated at a convenient audio range frequency so that the second rectifier gives an audio frequency output rather than a D.C. one.

The second diode (and suitable filtering) is followed by an audio amplifier and the signal can then either be recorded on an oscilloscope or pen recorder, or it may be compared with the frequency and phase of the original modulation in a synchronous amplifier and then recorded by a pen recorder. Figure 1 is a block diagram of the maser system.

For the ammonia beam to be formed and for collisions not to take place between ammonia molecules and other molecules, the background pressure between the nozzle and the cavity must be less than about 4×10^{-5} torr. Thus the nozzle, separator, cavity and nitrogen jacket are mounted in a vacuum system pumped by a 2" diffusion pump and

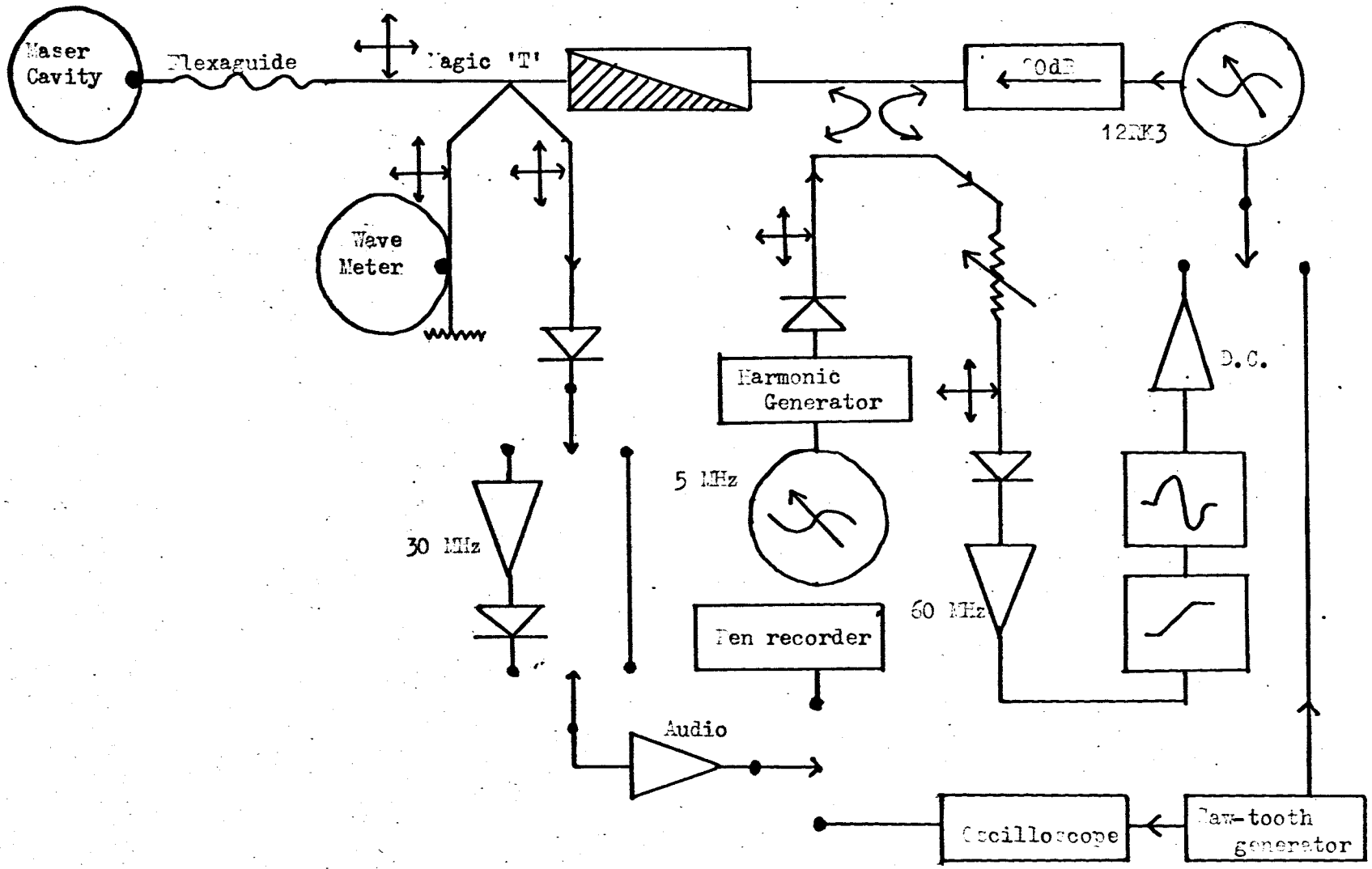

Figure 5:1

Block diagram of maser system

a two stage rotary backing pump. The main vacuum system is made of brass and the joints are either soldered or formed with rubber 'O' rings.

The nozzle, separator and cavity have been described in section 2:4 of Chapter 4: the vacuum, microwave and electronic systems are described in detail in section 4 below. In sections 2 and 3 the conditions necessary for oscillation are established and other parameters discussed. In section 5 the operation and characteristics of the maser are described and in section 6 the chief effects of the increased separation of nozzle and cavity are described and the molecular velocities established.

5:2 Power output and sensitivity[1, 33, 330]

A molecule in a pure energy state W_1 can be described by a wave function $Y(x_i)$, where x_i is dependent on position coordinates only. If a molecule exists in a superposition of two states then it can be described by a wave function $Y'(x_i, t)$ given by

$$Y'(x_i, t) = a_1(t)\, Y_1(x_i) + a_2(t)\, Y_2(x_i) \qquad 1$$

where Y' is dependent on position and time and $|a_1|^2$ is the probability of finding the molecule in energy state W_1 and $|a_2|^2$ the probability of finding it in W_2. With

$$|a_1|^2 + |a_2|^2 = 1 \quad \text{and} \quad hf_0 = W_2 - W_1 \qquad 2$$

where f_0 is the frequency of the emitted or absorbed radiation. It

has been shown[330] that if the molecule is subject to a perturbation

$$H' = E\mu \cos 2\pi ft \qquad 3$$

for a time t, where E is the exciting field and μ the dipole transition matrix element of the molecule, and if $a_1(0) = 0$ and $a_2(0) = 1$,

$$a_1(t)^2 = \frac{y^2 \sin^2 \pi zt}{z^2} \qquad 4$$

where

$$y = \frac{\mu E}{h} \qquad \text{and} \qquad z = \left[(f - f_0)^2 + y^2\right]^{\frac{1}{2}} \qquad 5$$

and f is the frequency of the field E. This transition probability is plotted in Figure 2a, it can be seen that on resonance ($f = f_0$) a molecule oscillates between the two states, hut off resonance the transition probability only varies between 0 and

$$\frac{(\mu E/h)^2}{(f - f_0)^2 + (\mu E/h)^2} \qquad 6$$

and a molecule which starts in one state has no certainty of reaching the other state.

Now if a beam with all the molecules (N) in the upper state enters a microwave cavity with average field E the power given up to the field is

$$P = Nhf_0 |a_1(t)|^2 \qquad 7$$

where t is the average time spent by a molecule in the cavity. If the average molecular velocity is v and the length of the cavity is L

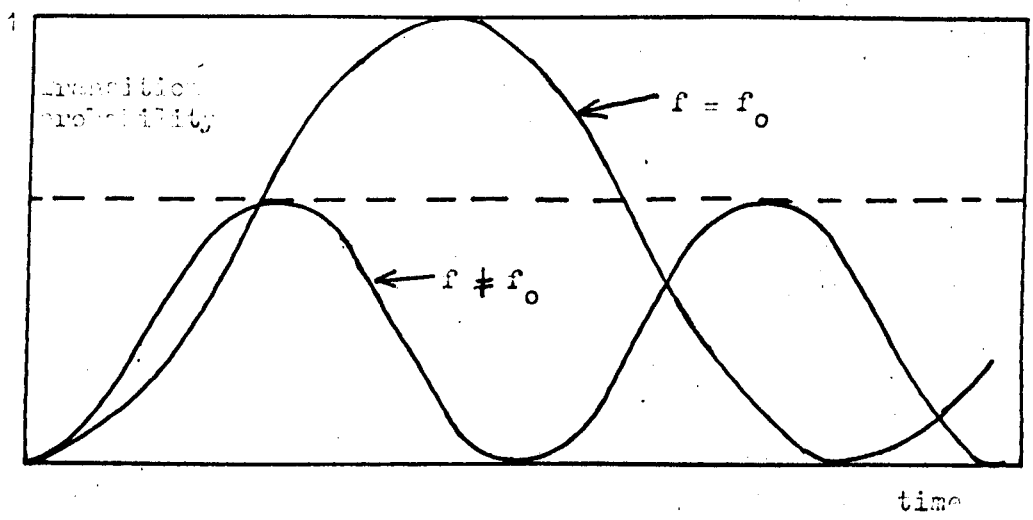

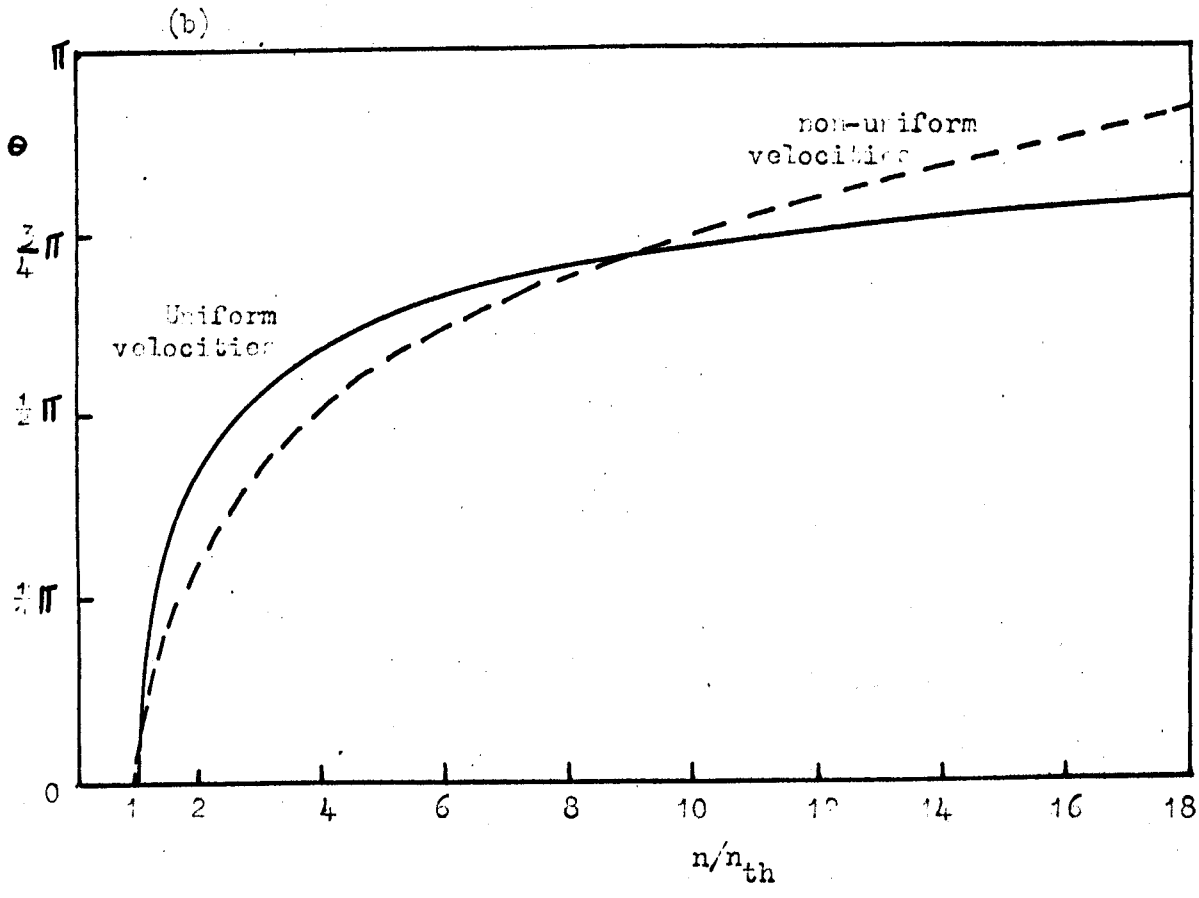

Figure 5:2

(a), Two quantum state transition probabilities, after Mittke[1]

(b), Maser amplitude of oscillation (θ) versus beam flux, after S.T.E.[35]

$$P = Nhf_0 \left|a\left(\frac{L}{v}\right)\right|^2 = \frac{Nhf_0\, y^2 \sin^2 \pi z\left(\frac{L}{v}\right)}{z^2} \quad . \qquad 8$$

The electric field, E, in the cavity is related to the stored energy in the cavity, W, by

$$W = \frac{E^2 AL}{8\pi} \qquad 9$$

where A is the cross section area of the cavity. Thus

$$y = \mu E/h = \mu \left[\frac{8\pi W}{AL}\right]^{\frac{1}{2}}/h \qquad 10$$

and

$$z = \left[(f - f_0)^2 + \frac{8\pi\mu^2 W}{h^2 AL}\right]^{\frac{1}{2}} \qquad 11$$

substituting these in equation 8 gives

$$P = Nhf_0 \quad \frac{\frac{\mu^2 8\pi W}{h^2 AL} \sin^2\left[\pi(L/v)\left[(f - f_0)^2 + \frac{8\pi\mu^2 W}{h^2 AL}\right]^{\frac{1}{2}}\right]}{(f - f_0)^2 + \frac{8\pi\mu^2 W}{h^2 AL}} \qquad 12$$

and letting

$$\pi^2 L^2 (f - f_0)^2/v^2 = d^2 \qquad 13$$

and

$$\theta = \frac{W}{W_a} \qquad \text{where } W_a = \frac{h^2 Av^2}{8\pi^3\mu^2 L} \qquad 14$$

then

$$P = Nhf_0 \left(\frac{\theta^2}{d^2 + \theta^2}\right) \sin^2 (d^2 + \theta^2)^{\frac{1}{2}} \quad . \qquad 15$$

Now at resonance $f = f_0$ and $d^2 = 0$, so from 15

$$\frac{P}{\theta^2} = Nhf_0 \frac{\sin^2 \theta}{\theta^2} \qquad 16$$

and since $\sin^2\theta/\theta^2 \sim 1$ for small values of θ and $\theta^2 = W/W_c$

$$\frac{P}{2\pi f_0 W} = \frac{Nh}{2\pi W_c} \quad . \tag{17}$$

At threshold of oscillation the losses of the cavity ($2\pi fW/Q$) are just matched by the power emitted from the beam and

$$N_{thresh} = \frac{2\pi W_c}{h\theta} = \frac{hv^2 A}{4\pi^2 \mu^2 L Q} \quad . \tag{18}$$

And for the 3,3 inversion transition of ammonia (with $\mu^2 = 1/3 \times 1.5 \times 10^{-36}$ c.g.s., A = 1 sq cm, L = 10 cm, Q = 4,000) for v = 40,000 cm/sec $N_{thresh} = 1.2 \times 10^{13}$ molecules per second or for v = 5,000 cm/sec $N_{thresh} = 2 \times 10^{11}$ molecules per second.

From equations 16 and 18

$$N/N_{thresh} = \theta^2/\sin^2\theta \tag{19}$$

and the oscillation amplitude saturates when $\theta = \pi$ and the oscillation characteristic may be plotted as in Figure 2b.

In the above derivation it has been assumed that all the molecules have the same velocity, they travel through the cavity parallel to the axis and that there are no collisions between molecules or with the cavity walls. Further it has been assumed that the molecular beam is of uniform cross section and the microwave field is uniform throughout the cavity. None of these assumptions are correct for an ammonia beam maser, but most of them are justified in first order theory; but it is found

that the saturation characteristic produced in a practical maser is considerably different from that of Figure 2b (see Figures 3 and 14) and this is attributed to non-uniform velocity distribution of the molecules. Such velocity effects are described in detail in Section 6 below.

The sensitivity of an ammonia beam maser oscillator can be estimated by equating the smallest detectable fluctuation in beam power with the noise power of the microwave superheterodyne detector. Thus according to Townes and Geshwind[331] the signal to be compared with noise is

$$\frac{(\Delta P_0)^2}{4P_0} = Fkt\Delta f \qquad 20$$

where ΔP_0 is the fluctuation in the total output power P_0 at the first detector, which has noise figure F and bandwidth Δf.

Now $P_0 = 2QP/Q_1$ where P is the beam power output, Q_1 is the output quality factor of the resonant cavity of loaded quality factor Q. So

$$\frac{Q(\Delta P)^2}{2Q_1 P} = Fkt\Delta f \quad . \qquad 21$$

By equations 14 and 16, at resonance,

$$Nhf_0 = \frac{P}{\sin^2 (xP)^{\frac{1}{2}}} \qquad 22$$

where $(x)^{\frac{1}{2}}$ is a slowly varying factor given by equations 9 and 14 which varies with operating conditions, but is in the range 10^{-1} to 10^{-2} and to a first approximation can be regarded as a constant, so

$$\frac{\Delta N}{N} = \Delta P(1/P - 2x^{\frac{1}{2}} \cot(xP)^{\frac{1}{2}} \qquad 23$$

and since for normal values of P (10^{-2} to 10^{-5} erg) $1/P > 5(2x^{\frac{1}{2}} \cot (xP)^{\frac{1}{2}})$ one can make the approximation $\Delta N/N \sim \Delta P/P$, and equation 21 becomes

$$(\Delta N/N)^2 = \frac{2Fkt\Delta fQ_1}{PQ} \quad . \qquad 24$$

For optimum sensitivity $Q_1 = 2Q$ and

$$\Delta N/N = \left[\frac{4Fkt\Delta f}{P}\right]^{\frac{1}{2}} = \left[\frac{4Fkt\Delta f}{Nhf_0 \sin^2 \theta}\right]^{\frac{1}{2}} \quad . \qquad 25$$

This theory assumes that the modification of the field is small so that there is no interaction between molecules; all stimulated emissions are sufficiently isolated to be considered as independent of each other and thus no 'amplification' takes place. Also it is assumed that any thermal fluctuations of the beam are less than the noise fluctuations in the superheterodyne receiver. For $\theta = \pi/2$, $N = 10^{12}$ molecules per second, $F = 10$, $\Delta f = 1/10$ Hz and with the usual values for the other parameters equation 25 gives $\Delta N/N \sim 3 \times 10^{-5}$.

Shimoda, Takahasi and Townes[77] have shown that the noise of a maser is given by an effective noise temperature T_N

$$T_N = \frac{hfa}{k(b - a)} \qquad 26$$

where a is the total probability of stimulated emission per unit time per photon and b is the probability of absorption per unit time per photon; and hf/k is the classical noise temperature for a system followed by a perfect amplifier and a/(b - a) is an amplification

factor due to the presence of the molecular population. As the power in a beam maser is increased so a increases and b - a becomes small and T_N becomes very large, and may exceed the noise of the following superheterodyne detector.

Townes[332] has considered the case when this is so, and when any fluctuations including spontaneous emission are amplified in the maser. When b $\rangle$ a the average number of photons in a cavity is given by

$$\bar{n} = c/(b - a) \qquad 27$$

where c is the probability per unit time of introducing by any process (including spontaneous emission, excluding stimulated emission) photons into the cavity, and the noise fluctuation is

$$n = \frac{(bc)^{\frac{1}{2}}}{(b - a)} \quad . \qquad 28$$

If (b - a) fluctuates by e, the signal will change by

$$S = \frac{ce}{(b - a)} \qquad 29$$

and for maximum sensitivity

$$\frac{ce_{min}}{(b - a)^2} = \frac{(bc)^{\frac{1}{2}}}{(b - a)} \qquad 30$$

$$\therefore \quad e_{min} = \frac{(b - a)(bc)^{\frac{1}{2}}}{c} = \frac{(bc)^{\frac{1}{2}}}{\bar{n}} \quad . \qquad 31$$

As a approaches b spontaneous emission is greatly amplified and the bandwidth of the system, Δf, is given by

$$\frac{\Delta f}{f} = \frac{b - a}{a} \qquad 32$$

so the effective quality factor of the system is increased and e_{min} is given by

$$e_{min} = \frac{b^{\frac{1}{2}}(b - a)^{\frac{1}{2}}}{n^{\frac{1}{2}}} = \frac{b^{\frac{1}{2}}a^{\frac{1}{2}}(\Delta f)^{\frac{1}{2}}}{n^{\frac{1}{2}}\, f^{\frac{1}{2}}} \qquad 33$$

and since $n = W/hf$

$$e_{min} = b^{\frac{1}{2}}a^{\frac{1}{2}}\Delta f^{\frac{1}{2}}h^{\frac{1}{2}}/W^{\frac{1}{2}} \qquad 34$$

and at threshold $a \sim b$

$$\therefore \quad e_{min} = b(h\Delta f/W)^{\frac{1}{2}} \quad . \qquad 35$$

This can be expressed in terms of minimum detectable beam flux,

$$n_{min} = \frac{8}{Q\mu} \cdot \frac{kT_o}{hf} \cdot \frac{kT_n}{hf} \left[\frac{3hV}{2\pi t}\right]^{\frac{1}{2}} \qquad 36$$

where Q is the cavity quality factor, t is the period of observation, V is volume of the cavity, T_o the temperature of the cavity and T_n the temperature of the beam given by

$$T_n = (hf/k)\ \ln(n_2/n_1) \qquad 37$$

where n_2 is the population of the upper level and n_1 of the lower level. Thus for experimental conditions (with t = 10 secs), T_n is 2 to 5°K and $n_{min} = 4 \times 10^4$ to 1×10^5 molecules/sec. For a threshold flux of 2×10^{11} molecules/sec this gives a sensitivity $\Delta n/n \gtrsim 2 \times 10^{-7}$.

5:3 Noise, Linewidth and Stability[14, 33, 78, 286, 334-337]

In the last section it was mentioned briefly that the noise of a practical maser system might be limited by fluctuations of the maser itself and not by the microwave detection system. In this section the noise of a beam maser is considered in more detail, the frequency pulling of the molecular oscillation by various factors is considered and the linewidth established.

The random noise generated in an ammonia beam maser can be considered as coming from five main sources, if one considers the beam and cavity system only and not any microwave and electronic detection system.

The beam of molecules may fluctuate in number of molecules flowing per second, because of mechanical vibrations and corona on the electrostatic separator, because of variations in the potential difference applied to the separator, because of fluctuations in the pressure behind the source nozzle and because of the finite number of molecules in the beam. All except the last can be reduced to insignificant amounts by careful design. If the number of molecules flowing per second in the upper energy state is n then the fluctuation in time t is $(nt)^{\frac{1}{2}}$ and if the total power generated by these molecules is $P_0 = Knhf$ where K is a constant for a given amplitude of oscillation, then the average fluctuation in power is

$$\Delta P_{av} = Khf\,(n/t)^{\frac{1}{2}} \qquad 38$$

and the electric field, E, in the cavity fluctuates by ΔE, given by

$$\Delta E/E = \frac{1}{2(nt)^{\frac{1}{2}}} \qquad 39$$

and if the speed of response is determined by the linewidth of the system, then with $n_{thresh} = 2 \times 10^{11}$ and $t = 1/3 \times 10^{-3}$, $\Delta E/E \sim 10^{-4}$. This fluctuation may be greater if it is amplified in the maser system, and will be less if it is time averaged ($\sim 10^{-6}$ for 10 second time constant).

The second source of noise is created by electric and magnetic fields in the cavity due to heaters and sensing elements and other stray fields (including the earth's field). These will tend to be cyclical according to the system and should normally be distinguishable from random noise.

The final three types of noise can all be classified as thermal noise. They are the noise generated in the cavity associated with the cavity losses, the noise coupled into the cavity from the microwave coupling hole and open ends of the resonator and lastly the spontaneous emission noise from the beam. The latter can be regarded as a zero point fluctuation in the cavity of order hf/k and is much less than the two former. Again assuming that there is no amplification or saturation in the system the field fluctuation due to thermal effects is given by

$$\frac{\Delta E_{av}}{E} = \left[\frac{kt\Delta f}{P_0}\right]^{\frac{1}{2}} \qquad 40$$

where $\Delta f \sim 1/t'$ with t' as the time of observation of the system, which will be put equal to $1/3 \times 10^{-3}$ to compare with beam 'shot' noise, P_0 is the power in the cavity and $\Delta E/E \sim 10^{-2}$.

Thus it is to be expected that the maser will be noise limited by thermal fluctuations, quantitative predictions based on this have been found to agree well with experiment for maser amplifiers, but it appears that the maser oscillator has been less well examined. For the present system the maser noise is definitely greater than the microwave superheterodyne noise for low oscillation amplitudes (see Figure 3) and the noise decreases with oscillation amplitude as predicted by Shimoda, Wang and Townes[33]. The thermal noise x_n decreasing according to

$$2x_n = \frac{x_i}{1 - \theta \cot \theta} \qquad 41$$

where x_i is the initial thermal fluctuation and θ is defined in section 2. Thus it appears that the present system is limited by thermal cavity noise at low amplitudes and superheterodyne detector noise at greater amplitudes.

Shimoda, Wang and Townes[33] derived an expression for the frequency of the molecular oscillator, f, in terms of the natural line frequency (f_0) and the resonant frequency (f_c) of the microwave cavity,

$$\frac{f - f_0}{f_0} = \frac{Q_c(v/L)(1 - \cos 2\theta)}{\pi f\,(1 - \sin 2\theta/2\theta)} \quad \frac{f_c - f}{f_0} \qquad 42$$

where Q_c is the cavity quality factor and a quality factor, Q_L, of the line is defined by

$$Q_L = \frac{f_0}{2\Delta f} = \frac{f_0}{nv/L} \qquad 43$$

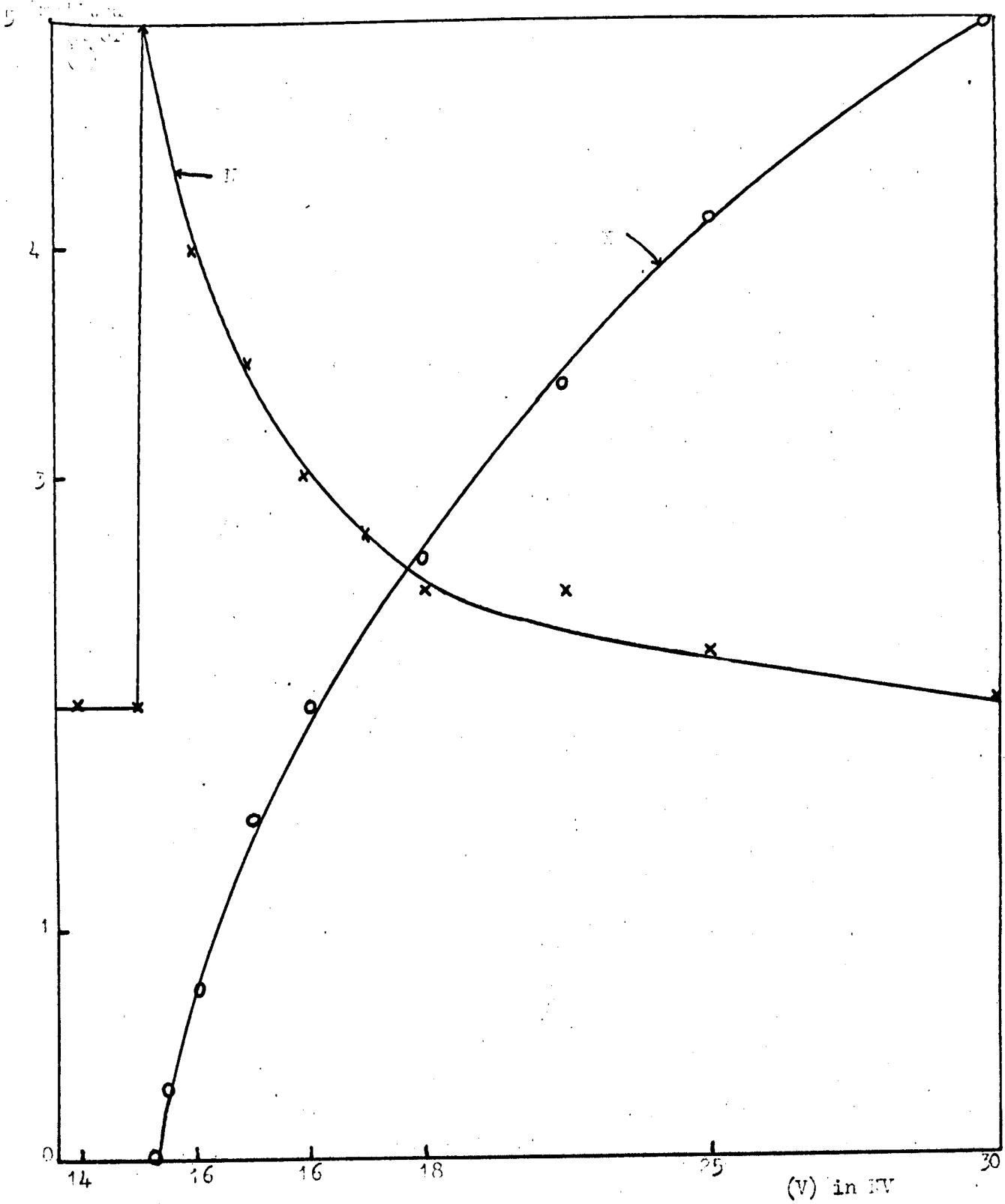

Figure 5:3

Single cavity beam maser noise. Noise amplitude (N) variation with separator potential (V). Maser oscillation amplitude (X) also plotted for comparison

with v as the mean velocity of the molecules and L the length of the cavity. n is a factor of the order of unity if $\theta \ll 1$, depending on the spread of the beam and the exact field distribution in the microwave cavity (n = 0.89 for a uniform field distribution along the axis and 1.19 for a TE mode variation). For the saturated line the linewidth is accurately expressed by

$$\Delta f = (0.8v^2/L^2 + E^2|\mu|^2/(3h^2)) \qquad 44$$

and equation 42 becomes

$$\frac{f - f_0}{f_0} = \frac{Q_c\,(1 - \cos 2\theta)}{n\pi Q_L(1 - \sin 2\theta/2\theta)} \quad \frac{f_c - f}{f_0} \quad . \qquad 45$$

When $\theta \ll 1$

$$\frac{(1 - \cos 2\theta)}{(1 - \sin 2\theta/2\theta)} \to 3 \quad . \qquad 46$$

Thus

$$(f - f_0) \propto \frac{Q_c}{Q_L}\ (f_c - f) \qquad 47$$

and since $Q_L \sim 10^7$ and $Q_c \sim 5 \times 10^3$, $Q_c/Q_L \sim 5 \times 10^{-4}$ and the output frequency of the maser is changed by very much less than the change in resonant frequency. It is important to have the cavity well stabilised because the total spectral width of the oscillation is considerably less than Δf, and the exact frequency of the oscillation is dependant on the cavity tuning. The total half power width of the oscillation is given by

$$2\Delta f' = \frac{8\pi kt(\Delta f)^2}{P_o} \qquad 48$$

where P_o is the power emitted by the beam. This gives a bandwidth of 10^{-1} to 10^{-3}Hz for a Δf of 1 KHz and normal operating conditions.

The ammonia beam maser has been used as a frequency standard and for this purpose it is necessary for its output frequency to be both stable and resettable. It was seen earlier in this section that the frequency pulling effect of the cavity disappeared when it was exactly tuned to the natural line frequency, Bonanomi[337] has shown that if two cavities are coupled together with the beam passing through one cavity, then there is a region with a zero temperature coefficient of expansion of the cavity system at resonance and the two cavities do not need to be so critically stabilised. It was also indicated that the frequency pulling was dependant on the beam flux, so variations in separator potential and source pressure may both change the frequency, but these effects should vanish when $f_o = f_c$. Unfortunately this is not so for the 3,3 line of ammonia because of the hyperfine structure of the central line.

Another important frequency pulling effect is due to unbalanced travelling waves in the microwave cavity. The power emitted by the molecular beam is not emitted uniformly along the length of the cavity, so there is a power flow along the cavity. To minimise this effect for an E_{010} cavity the coupling hole is placed in the middle of the cavity, this is a compromise because only at a particular flux will the power flow in each direction be equal. At low flux more power will be emitted towards the exit of the cavity and at higher flux more power nearer the entrance, this can produce a fractional frequency

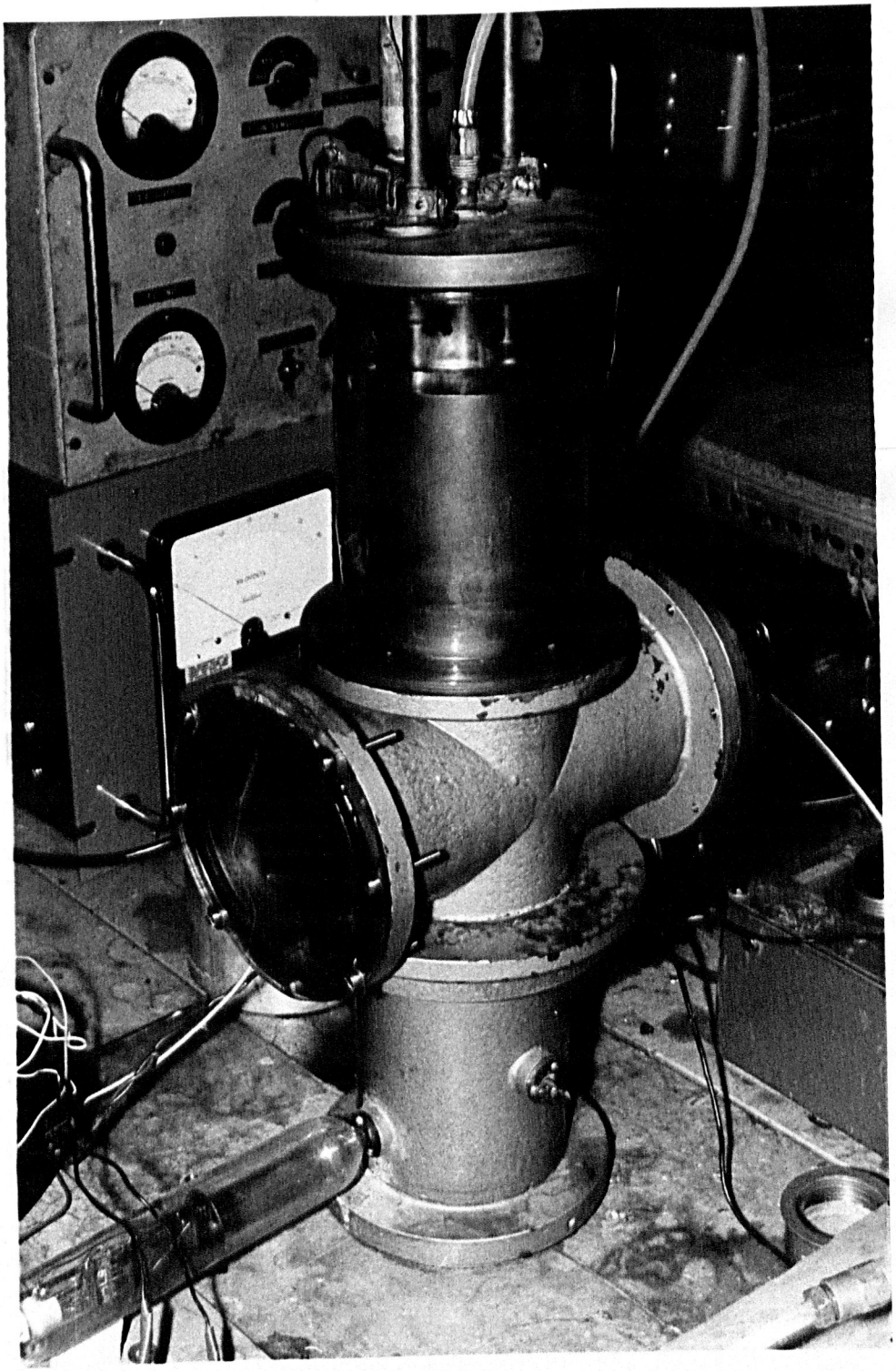

Figure 5:4

change of 2×10^{-9}. Thus a short cavity will be an advantage, but then a higher flux is required. Another advantage of a short cavity is that the effects of the change in numbers of focused molecules in different F_I states is minimised for changes in flux. This is because the different F_I states have different angular distributions on leaving the separator and if the cavity is long it will very definitely select lower F_I states.

There are several other effects, such as the dielectric loading of the cavity due to the ammonia beam, the loading of the cavity by changes in output coupling, pressure broadening effects and the variation of rotational level populations with separator potential. There are of course also Stark and Zeeman effects. Frequency changes of about one part in 10^{10} for 1 volt/cm fields and symmetric splittings of the hyperfine structure of 1 KH_z per oersted if the system is on tune, and a frequency shift as well if it is off tune.

5:4 Experimental apparatus

a. General

The maser vacuum housing is mounted on the top of a Dexion frame about four feet square and four feet from the ground. The apparatus is vertical with the beam nozzle above the separator, cavity and diffusion pump. The dexion frame also supports the remainder of the vacuum and ammonia supply system. The microwave and intermediate frequency apparatus are both mounted on a separate trolley only connected to the frame by the flexible waveguide carrying the maser signal. Most of the electrical apparatus is mounted in three 'post

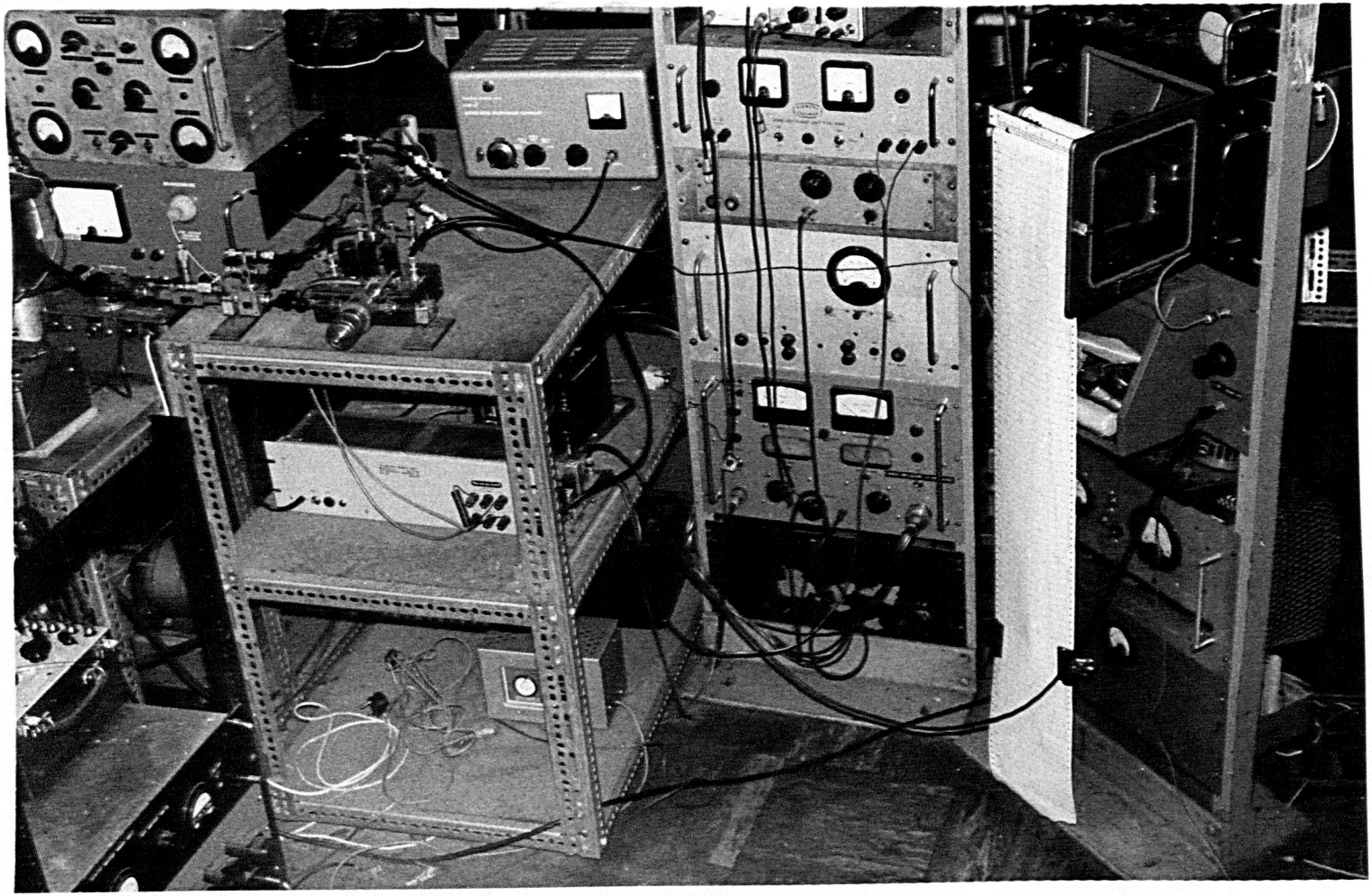

Figure 5:5

office' racks. Figures 4 and 5 are general photographs of the experimental equipment.

b. Vacuum and Ammonia System

Figure 6a is a diagram of the maser vacuum system. The maser chamber is made of brass and glass units with the junctions sealed with rubber 'O' rings (Figure 6b). The main cylinder has an internal diameter of 10 cm and an overall length of 50 cm. Two microwave cavities can be mounted in it, one immediately below the separator and the other 13 cm from the end of the separator. The 'K' band waveguide attached to the cavities is soldered to the vacuum housing and internally sealed with mica discs between the flanges and 'O' rings of a waveguide junction coupler. The supply line for the beam nozzle, the nozzle, the separator, the liquid nitrogen jacket and the E.H.T. lead in are all mounted from the top brass plate. All these connections and the electrical lead-ins are sealed with small 'O' rings. The 'O' rings round the liquid nitrogen pipes are kept warm by small electrical heaters and blown hot air. The E.H.T. lead-in is a long reach sparking plug suitably machined and with the atmospheric end extended with an araldite casting.

The vacuum connecting pipes are made from $\frac{1}{2}$" diameter copper pipe with 'Yorkshire' lead solder sealed junctions and 'Genevac' or 'Edwards' pressure actuated hand valves are used. The Edwards 2" diameter 704 oil diffusion pump (70 litres/sec) is connected to the 'Metrovac' 2 stage rotary pump (1 litre/sec) by a 1" diameter copper pipe and flexible coupling.

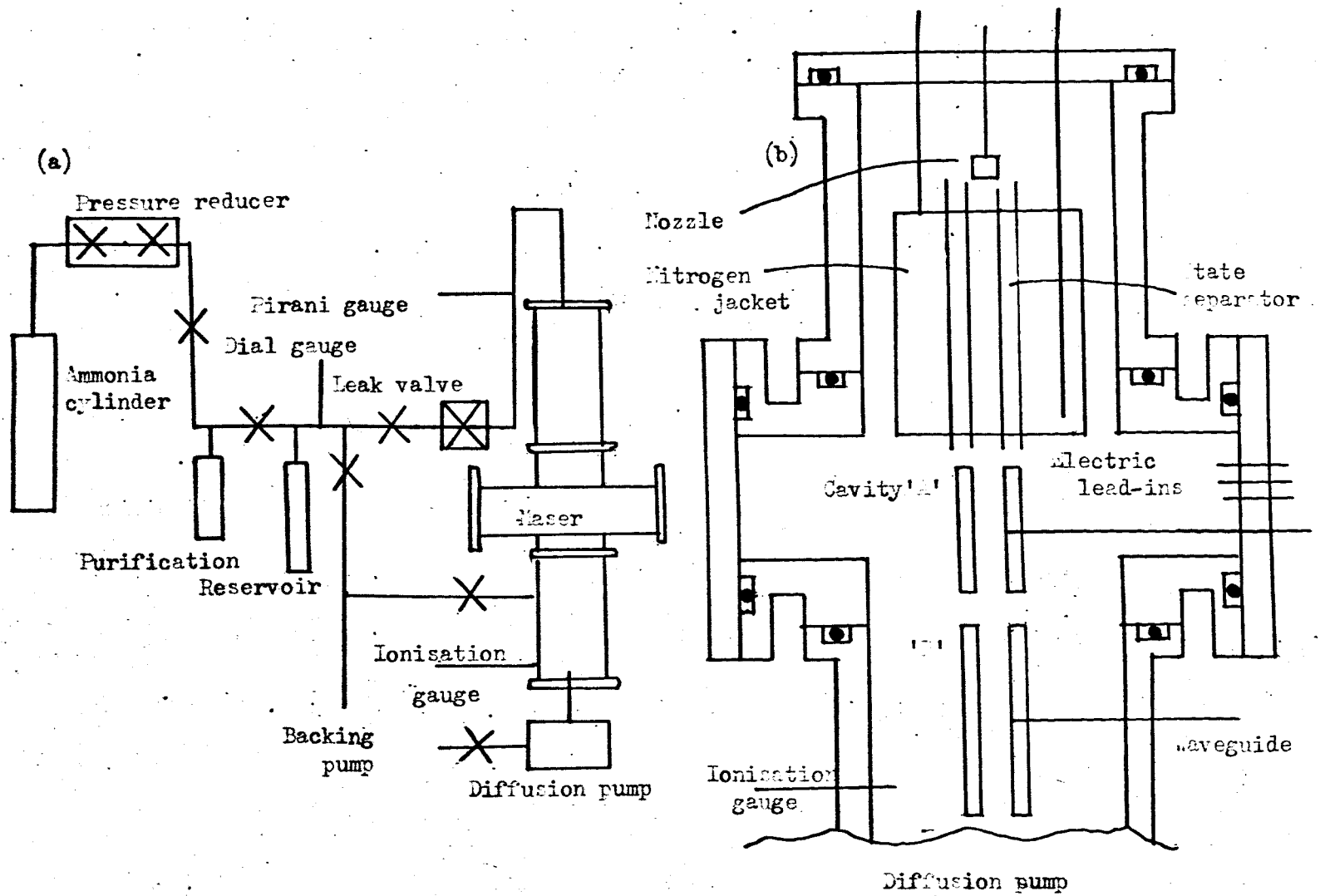

Figure 5:6

(a), Ammonia source and vacuum system. (b), Maser vacuum housing

The ammonia source is a 120 atmosphere pressure cylinder of anhydrous liquid ammonia. This cylinder is connected to a pressure reducing valve which is adjusted for about 30 lb/sq. inch output pressure. The ammonia is frozen in a liquid nitrogen trap and water vapour and air impurities removed; it is then stored at a pressure greater than atmospheric in a 3 litre glass reservoir. The flow from the reservoir to the nozzle is controlled by a fine control needle valve and the pressure (0.5 to 10 torr) is measured by an Edwards Pirani thermal gauge (head M5C, 10^{-3} to 10 torr). The control valve is connected to the top of the maser housing by a 'Nitex' $\frac{1}{4}$" diameter thick walled flexible nylon tube, so that the system may be moved and adjusted freely.

Initially the background pressure in the main vacuum system was monitored with a Penning gauge, but this required a permanent magnet which produced a sufficiently strong stray field to interfere with the operation of the maser. The Penning gauge was subsequently replaced with an Edwards IG2HB Ionisation gauge head. The filament is run from a 6 volt supply at about 2 amps and if the grid is at about 100 volts D.C. there will be a plate current of a few microamps for a grid current of a few milliamps, depending on the background pressure. This measures pressures from 10^{-2} to 10^{-6} torr. At low pressures the amplifier used for the plate current becomes unstable and at higher pressures the filament burns out. To prevent this happening accidentally a relay circuit was constructed to switch off the mains supply to the ionisation gauge control when the anode current exceeded 10 μa.

The backing pump reduces the pressure of the whole system to about

10^{-1} torr and the diffusion pump reduces the pressure in the main maser housing to about 10^{-5} torr in 2 hours, if the nitrogen jacket is filled with liquid nitrogen the pressure drops to about 4×10^{-6} torr.

c. Cavity Stabilisation

The K band cylindrical microwave cavity is thermally expanded until it is tuned to the ammonia transition. The silver plated copper cavity is heated by a current flowing in a 26 ohm bifilar wound coil of glass insulated 'Eureka' wire round it. Initially the heater current was controlled by a G25 glass insulated bead thermistor embedded in the cavity wall, but it was found that the D.C. control and supply circuit drifted slowly with time, so it had to be reset about once an hour. Now the coil is supplied from a low potential D.C. source which delivers a quarter to a third of an ampere. The input potential is switched on and off by a relay system ('Airmec' type 299) operated by a copper resistance thermometer (8.9 ohm at 20°C) attached to the cavity. If the heater current is so adjusted that it is flowing for about 80% of the time (very little control circuit 'overshoot') the cavity can be set and stabilised at any value between 24°C and 26°C (which is required for resonance) to within 1/10°C.

For a copper cavity the resonant frequency will change by 0.4 MHz per °C, thus the microwave cavity should be stable to ±20 KHz. Thus by equation 47 the maser output frequency should only vary by ±8 Hz, or less than 1 in 10^9 in overall frequency. This is two orders of magnitude more stable than the frequency of the local oscillator klystron (see section f below), hence noise in the system due to

frequency variations should be due to klystron or intermediate amplifier frequency drift.

Since the cavity can drift by ±20 KHz and has a half power band width of about 5 MHz there will be amplitude variations of the maser system of about 1% when the cavity is accurately tuned and considerably greater when it is detuned. This can be seen in Figure 7a which is a record of the amplitude of oscillation of the maser output as the cavity is detuned; the increased effects of the controller $1/10^{o}C$ regular variation can be seen as the cavity is detuned from the ammonia resonance.

d. Microwave system

Figure 1 is a representation of the microwave and electronic detection system. The cylindrical microwave cavity is connected to the microwave bridge by twelve inches of flexible waveguide of V.S.W.R. less than 1.15. The power from the maser is mixed with the output of a stabilised klystron (see section f below) in a silicon or germanium diode and the resulting signal amplified and displayed or recorded. The two signals are combined in a 'Mid-Century' Magic T, which is balanced with several slide screw tuners (see Figure 8). There are three modes of operation of the system, 'crystal video', 'unstabilised seperheterodyne' and 'stabilised superheterodyne'.

In the crystal video mode of operation a saw-tooth waveform of up to 100 volts peak potential is applied to the reflector of the klystron, this is sufficient to sweep the output of the klystron through a complete mode. Thus the frequency of the klystron varies

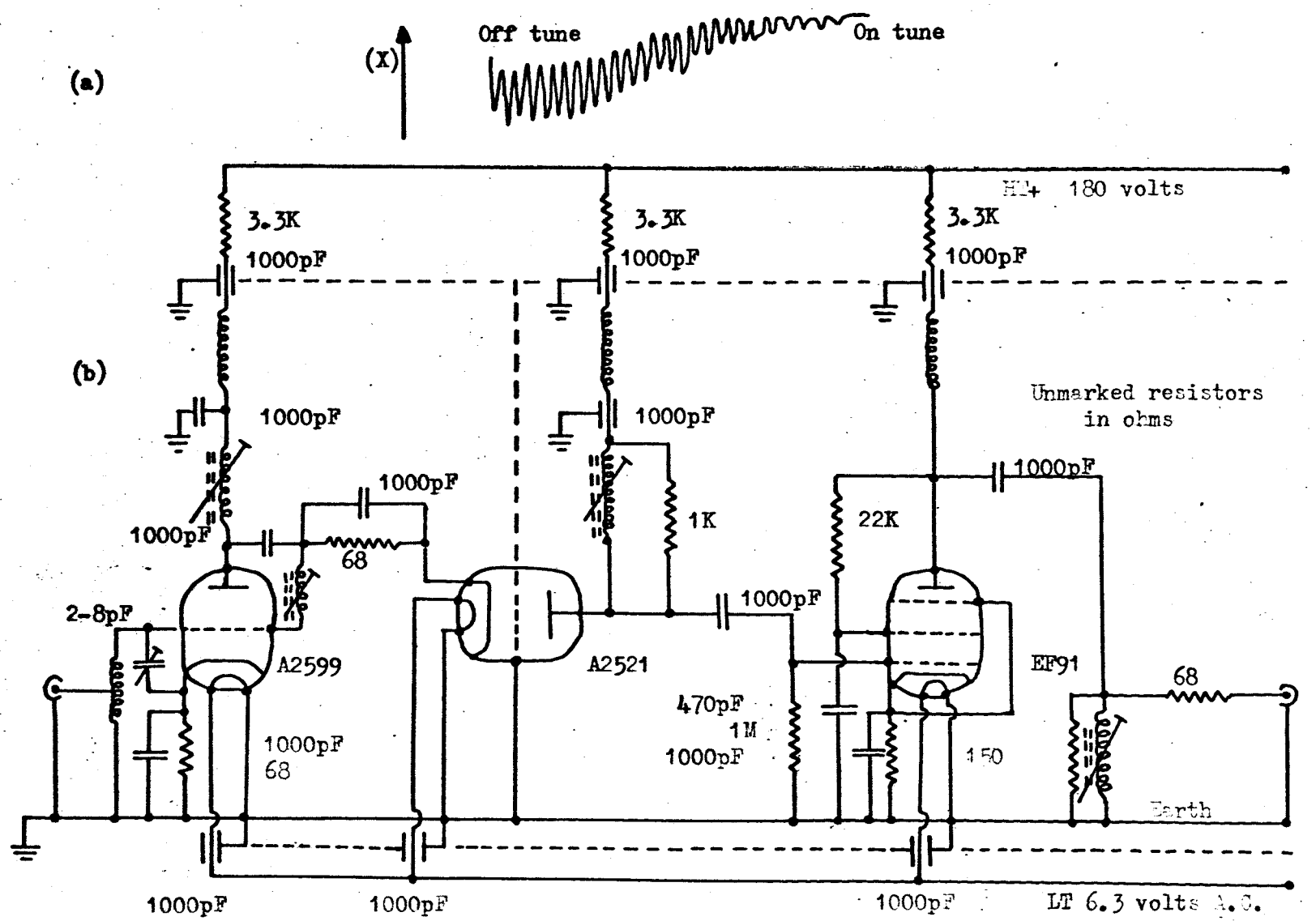

Figure 5:7

(a), Variation of maser amplitude (X) with cavity tuning. (b), 30 MHz preamplifier

with the sawtooth potential by about 50 MHz about a mean frequency of 23,870 MHz. If the audio amplifier is directly connected to the first detector and the output displayed on an oscilloscope, with the X sweep controlled by the original sawtooth, and the microwave cavity is on tune, the mode of the klystron is displayed and a small dip corresponding to the microwave cavity absorption is seen. The microwave system can then be 'tuned-up' for maximum cavity absorption and the frequency measured with a cavity wavemeter in the fourth arm of the bridge. The response of the wavemeter can either be observed in absorption as a second dip on the klystron mode or by a crystal detector connected to its reaction waveguide output and the signal displayed as a resonance on the second beam of the oscilloscope. If ammonia at 10^{-1} to 10^{-3} torr is introduced into the microwave cavity it produces an absorption dip superimposed on the cavity absorption and the cavity temperature controller can be adjusted so that the cavity is exactly tuned to the emission frequency.

The 'unstabilised superheterodyne' mode of operation is obtained by inserting the 30 MHz preamplifier and main amplifier and the second detector between the first detector and the audio amplifier. Then as the frequency of the klystron is swept only the noise output of the klystron, first detector and preamplifier is seen on the oscilloscope screen. If the klystron is detuned by 30 MHz from the maser frequency (this can be observed with the crystal video mode and calibrated wavemeter absorption) by adjusting the klystron resonant cavity and if the maser is oscillating a signal corresponding in shape to the bandpass

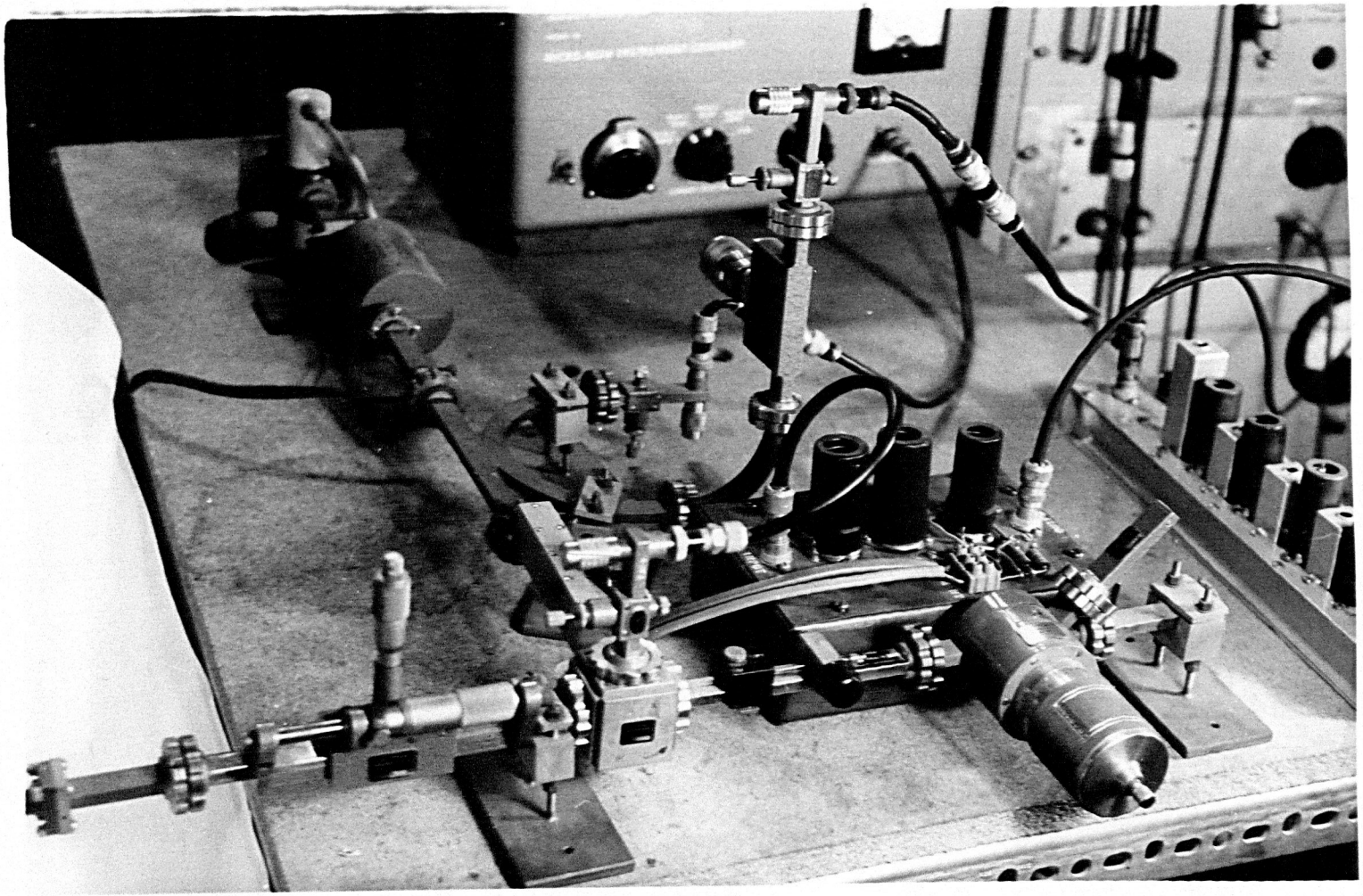

Figure 5:8

of the I.F. amplifier will be observed on the oscilloscope and the whole system can be finally balanced for maximum signal to noise (in particular the power to the crystal detector is varied, by adjusting the attenuator).

The 'stabilised superheterodyne' mode is the same as the unstabilised mode except that the sawtooth sweep to the klystron reflector is switched off and the klystron stabilisation circuit switched on. The maser oscillation now produces a steady D.C. signal on the oscilloscope.

e. Superheterodyne Detection[338]

The power output from the maser is only of the order of 10^{-11} watts so for this to be detected a low noise superheterodyne detector is used. With a microwave superheterodyne detector the noise figure depends on the mixer crystal, the intermediate frequency and the local oscillator level, but not on the power level of the signal. Now if the bandwidth of the intermediate frequency amplifier is B' and the bandwidth of the system after the second detector B" then the overall bandwidth of the system (and hence the noise performance) will depend on the operating conditions. If the power reaching the second detector is predominately noise then the effective bandwidth is $(2B'B")^{\frac{1}{2}}$, but if there is a sufficiently large intermediate frequency signal at the second detector and if this is operating on the linear portion of its characteristic, the overall bandwidth will be B"; which of course is very much less than $(2B'B")^{\frac{1}{2}}$ because $B" << B'$.

Thus for low noise operation of a superheterodyne system the signal

level must be carefully adjusted and the gain of the amplifier must be considerable, in practice 80 to 120 dB. It is desirable that the bandwidth of the I.F. amplifier should be reasonably large because any fluctuations in the centre frequency will cause an amplitude (and phase) change in the transmitted signal. Since it is difficult to construct an amplifier to be stable to better than ±25 KHz at 30 MHz a bandwidth of at least 2 MHz is desirable. For low noise operation of the first detector crystal a high intermediate frequency is desirable, but the frequency must not be too high for the construction of a low noise intermediate frequency amplifier, 30 MHz is a reasonable compromise.

120 dB gain at 30 MHz with 2 MHz bandwidth is most easily obtained with a combination of pre-amplifier and main amplifier. The noise figure of a microwave receiver is given by

$$NF_{dB} = 10 \log(NF_{IF} + NR - 1)L_c \qquad 49$$

where NF_{IF} is the intermediate frequency amplifier noise figure expressed as a ratio. NR is the first diode noise figure, also expressed as a ratio, that is the excess noise over resistance noise alone in the diode when in a microwave field and L_c is the conversion loss of the diode, also expressed as a ratio. Now the intermediate frequency amplifier has a noise figure of 1.4 and two crystal types have been used, the silicon IN26A and the Germanium D4089

	L_c	NR	NF	
IN26A	7.5 dB	x 2.0	11.5 dB	
D4089	6.5 dB	x 1.5	9.5 dB.	50

The more expensive D4089 has been used for the low noise experiments.

The noise of a well designed amplifier is given by

$$F = F_1 + \frac{F_2 - 1}{G} \qquad 51$$

where F_1 is the noise factor of the first stage of power gain G and F_2 is the noise factor of the remainder of the amplifier. The chief sources of noise are resistive noise in the input of the amplifier, this is reduced to a minimum by using 'good' resistors and a transformer correctly matching the valve input impedance to the crystal detector, secondly shot noise due to the random fluctuations in the number of electrons reaching the anode; thirdly flicker noise (1/f noise) and fourthly partition noise.

The last is very important in a multigrid valve; the cathode current is divided between the anode and grids and large fluctuations take place. These fluctuations are usually larger than shot noise (~ x5) and larger than flicker noise except at low frequencies (< ~ 1 KHz). Thus for a low noise amplifier a triode should be used, but this will have low gain if it is to be stable, so according to equation 51 the second and later stages of the amplifier might be important. To avoid this a cascode[339] first stage has been used. This consists of two triodes, the first with grounded cathode, the second with grounded grid, in a configuration suggested by Wallman, Macnee and Gadsden[339]. This arrangement, if appropriate neutralisation is used, has the noise properties of a triode and the gain of a pentode. Figure 7b is a circuit diagram of the cascode preamplifier which has been constructed with a noise figure of about 1.4 dB and gain of 35 dB.

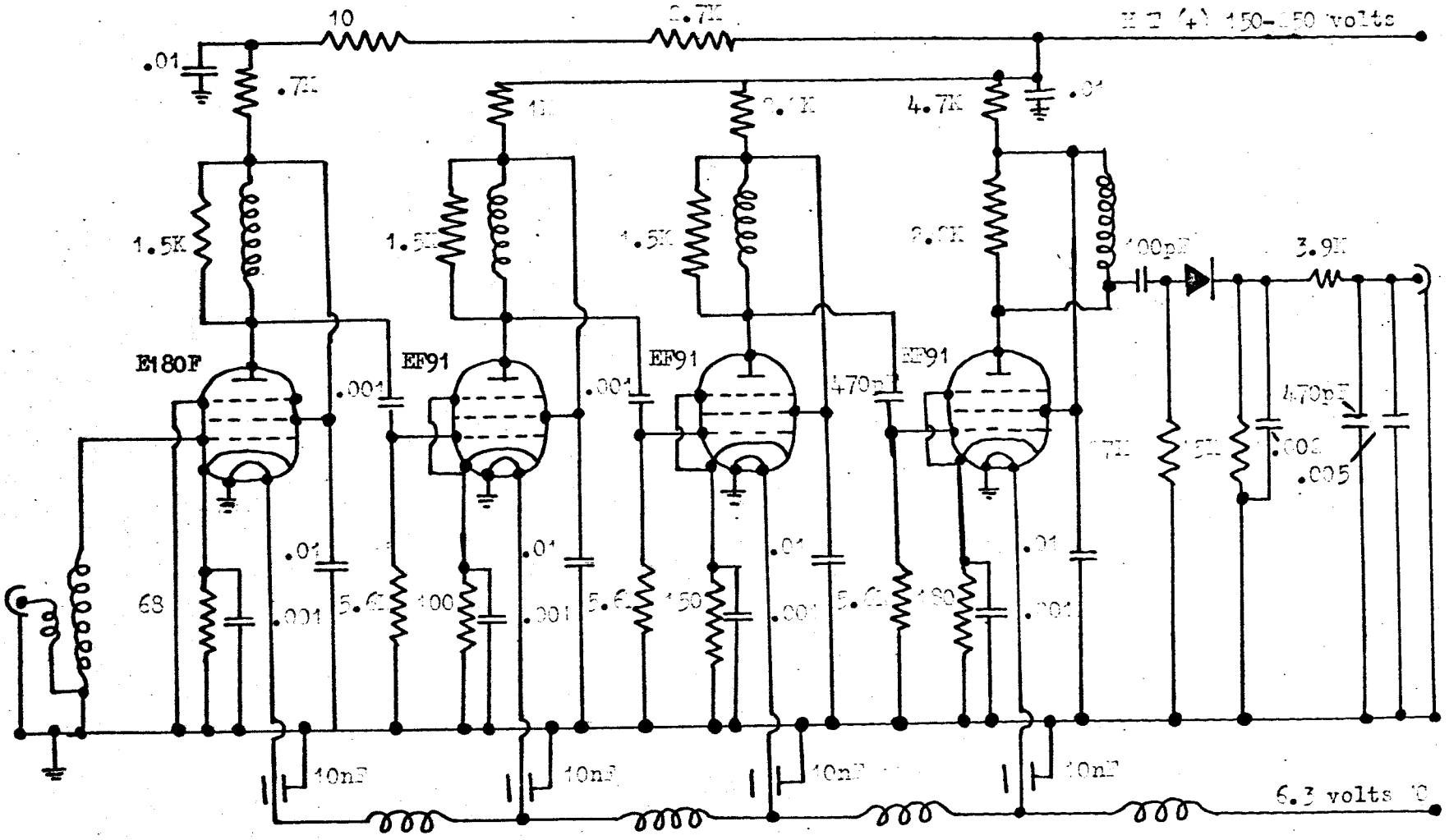

Unmarked resistors in ohms, unmarked capacitors in microfarads

Figure 5:9

30 MHz Intermediate frequency amplifier

Figure 9 is a circuit diagram of the main amplifier whose gain is varied from 40 to 80 dB by varying the high tension from 130 to 250 volts. The output smoothing capacitor is varied to suit the particular experiment taking place.

f. Klystron and Stabilisation

Initially the only K band klystron available as a local oscillator was a 2K33. This requires a resonator potential of 2 KV relative to cathode and a reflector potential of 2 to 2½ KV. This klystron was run from an 'A.P.T.' KP20 klystron power supply with the sawtooth sweep (20 to 1000 Hz) connected to the reflector by a 0.1 μF 5KV working condensor. The klystron produced 25 mW of power, but even when water cooled was only stable to about one part in 3×10^3 in frequency. This variation in frequency is too large for sensitive operation of the system so itwas decided to stabilise the klystron using a microwave frequency discriminator system. Figure 10a is a block diagram of this system; two wavemeters are used as microwave reference cavities, one set just below the klystron frequency, the other just above[340-341]. Their outputs are fed into a difference amplifier and the signal is amplified and passed through a 10,000 turn coil which is mounted axially round the klystron such that the field it produces alters the flight time of the electrons in the anode reflector region by causing them to take a helical path. Thus by varying the current the klystron frequency can be changed without the necessity of feeding a signal directly to the reflector at 2KV. Figure 10b is a photograph of the output of the difference amplifier when critically

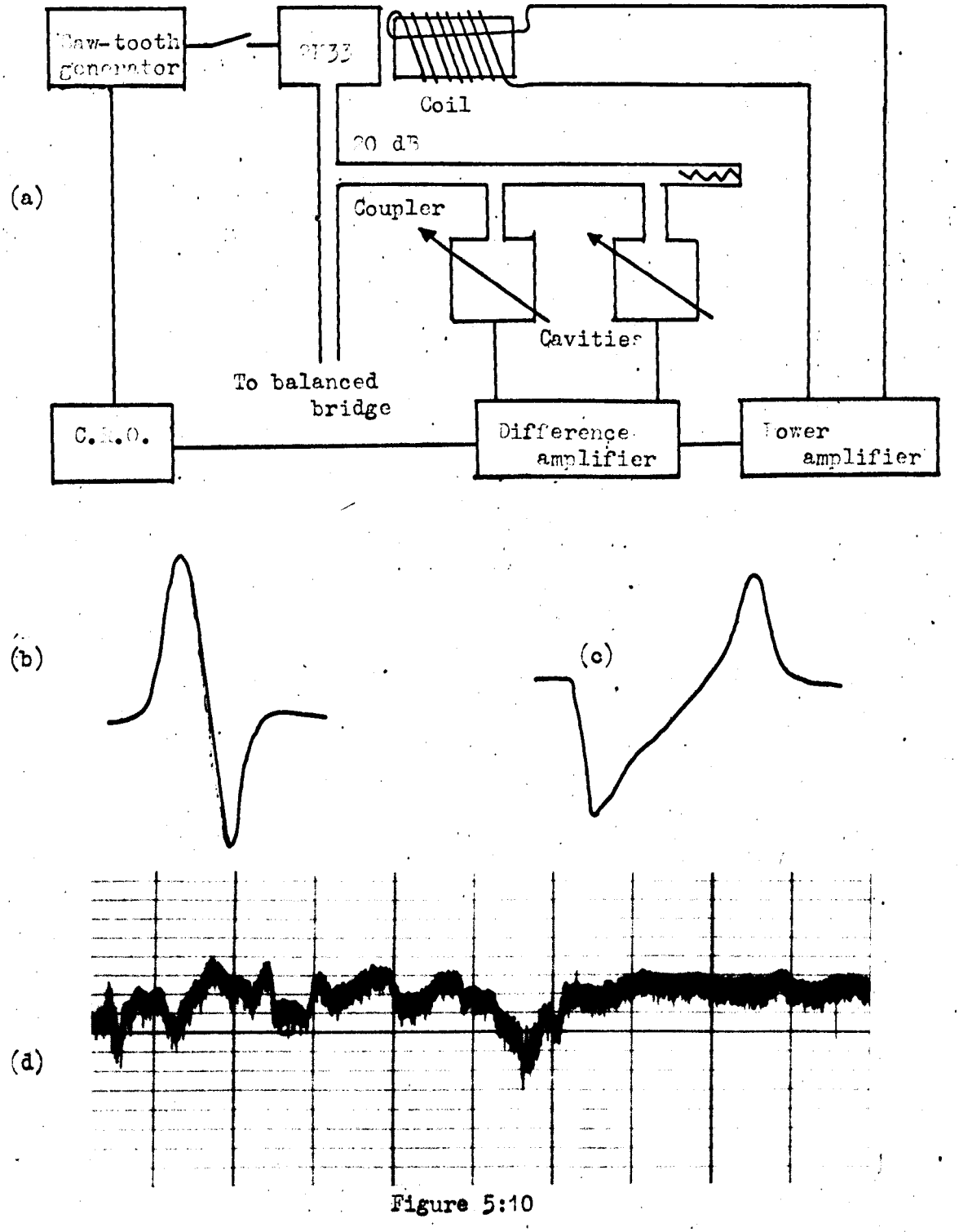

Figure 5:10

(a),2 cavity stabilisation block diagram.

(b) and (c),correctly and incorrectly set reference cavities.

(d),Stabilised and unstabilised klystron output

adjusted and a sweep potential applied to the klystron reflector. 10c is a similar photograph but with reference cavities separated by too great a frequency gap. This system locked the klystron (see Figure 10d), but the field produced by the coil not only changed the frequency of the klystron it also modulated the power output of the klystron. These variations were sufficiently large to cause maser signal level fluctuations at the second detector, so this method of stabilisation was unsatisfactory.

In place of this a stabilisation system using the ammonia maser itself as the frequency reference was constructed. A 30 MHz intermediate frequency amplifier was coupled to the anode coil of the last stage of the signal I.F. amplifier (at this stage the preamplifier had not been built so the output of the main signal amplifier was only at a level of about 1 mV), this amplifier with a maximum gain of 105 dB and 2 MHz bandwidth is shown in Figure 11. The fifth stage is grid bias limited (~ 1.5 volts p. to p.) and its output is coupled to a Foster-Seeley discriminator which produces a swing of ±1.5 volts for a swing of ±2 MHz in difference between the maser and local oscillator. The loss in the last stage (the anode coil varies by ±12 volts) is because the anode coil and secondary coil are 3 KV insulated from each other. The output is connected to a balanced transistor amplifier which is floated together with its battery supply at the klystron reflector potential, and when the klystron frequency changes the intermediate frequency signal changes and the frequency discriminator converts this to an amplitude change which is developed

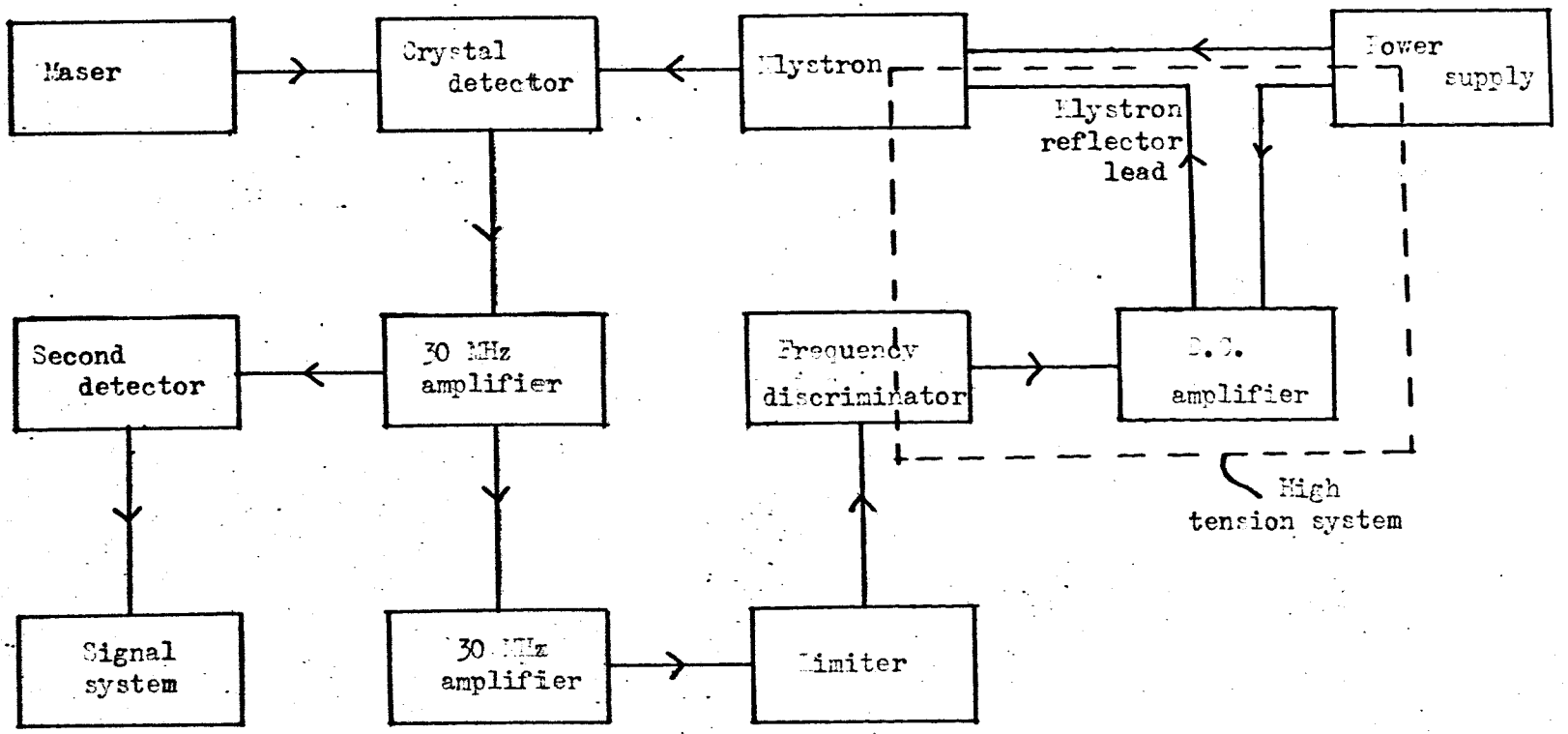

Figure 5:11

Klystron stabilisation using maser signal as reference

as a potential difference across a resistor in the reflector lead. Thus there is a maximum correction signal of ±20 volts for a ±1 MHz change in klystron frequency. For efficient operation this system requires the maser to be oscillating with sufficient amplitude to produce a signal to noise ratio of at least 20 to 1 at the second detector. Unfortunately, as will be seen in section 6 below, it is found that for maximum sensitivity of the detection of the maser oscillation detector the maser should be oscillating only just above threshold, such a signal is unable to act as the reference frequency, so it became necessary to use another frequency reference.

The 2K33 klystron was replaced by an 'Elliott-Litton' 12RK3 klystron, which is blower cooled and has its heater supplied by a 6 volt accumulator; the reflector sensitivity is 0.5 MHz per volt. The frequency, after 2 hours warm-up, is stable to one part in 2.5×10^4 short term (5 minutes), and the long term drift (4 hours) is 1 part in 10^5.

This klystron is stabilised to a high harmonic of a 5 MHz ± 0.5% tunable crystal controlled oscillator. This oscillator has been measured to be stable in frequency for several hours to one part in 10^6 and for 15 minutes to one in 3×10^7.

The output of the nominal 5 MHz (in use 4,998,535 ± 10 Hz) oscillator is multiplied in a valve chain to 450 MHz (nominal) ('MicroNow'type 101C) and this generates harmonics in a IN26A crystal giving up to 25mA of current. There is a harmonic at 23,842 MHz (actual) and this beats with the klystron frequency of 23,899 MHz

(29 MHz above the maser frequency) in another IN26A crystal to produce a 57 MHz difference signal which is amplified, limited and passed to a frequency discriminator and D.C. amplifier (MicroNow 201). The D.C. amplifier produces a signal of amplitude and sign such that when it is fed to the klystron reflector any klystron frequency change is corrected. The feed is performed by a 'Raytheon' raysistor which limits the time constant to about 1 millisecond with a stabilisation factor of 1000. The system can be seen in Figure 1. The klystron is isolated from the rest of the system by a 'F.X.R.' K157A ferrite isolator, with a V.S.W.R. of 1.15 and better than 24 dB isolation.

g. General Electronics

Most of the general electronic units are powered by a 240 volt 50 Hz mains constant voltage transformer. This is an 'Advance' 750 watt harmonic filtered unit with a constant output of 230 * 5 volt for an input of anywhere between 140 and 270 volts, the output filtering gives a true sinusoidal waveform with harmonic content of less than 5%. All the important electronic units are earthed to a single point (not the constant voltage transformer) and the various earth connections between units and frames have been adjusted to minimise 50 Hz pick-up.

Two E.H.T. units have been used to provide the 0-30 KV potentials difference for the separator, 'Hazlehurst Design' type 105PMB with a stability of 1% and latterly a 'Brandenburg' S0530 with a stability of better than 0.25%. Both are radio frequency units and even the latter has an output ripple of up to 30 volt peak to peak. A smoothing unit has been constructed (R.C. type, 130 M ohm series resistance, two

0.001 μF capacitors to earth), which both smoothes the ripple and reduces the current which can be drawn when a spark occurs in the separator, hence reducing any damage to the maser state separator.

The power units used to supply the D.C. potentials for the various intermediate frequency amplifiers are stabilised commercial supplies by 'Siemens-Ediswan' and 'A.P.T.'. A 'Mullard' transistor power supply giving 5 amps at 0-30 volts is used to supply various sub-circuits and two power amplifiers have been used, a 'Leak' and a 25 watt 'Cape'. Two audio amplifiers have been used, a 'Telequipment' two channel preamplifier type PA3, and a simple one using an EF86 and an ECC81.

Normally a 'Telequipment' single channel oscilloscope type S32 has been used together with an Elliott potentiometric pen recorder with 6" scale, 5 mV sensitivity, 1,000 ohm input impedance and 1.3 second full scale deflection response time.

In an earlier section it was seen that if the intermediate frequency system is operated correctly the total bandwidth (and hence noise) of the detection system is the bandwidth of the system after the second detector. Now the signal to be examined at the output will be at an audio frequency sufficiently large to avoid 1/f noise but small compared with the intermediate frequency. To reduce the bandwidth of the audio detection and recording stage a narrow bandwidth amplifier might be used, but it is difficult to make an audio amplifier with a Q of greater than about 100 and ensure the signal IF remains within the band pass of the IF amplifier. To reduce the noise

further a 'lock-in' amplifier may be used. Normally this has a tuned signal amplifier to reject harmonics of the expected signal freuqnency and any 'pick-up' frequencies, such as 50 Hz mains hum etc:, but with a Q such that there are no problems, phase or amplitude, due to frequency drift. The output from the signal amplifier is then mixed with a reference frequency provided direct from the source of the original modulation; this is thus at exactly the same frequency as the expected signal. Two side bands are produced, at the difference frequency (0 Hz) and at the sum frequency. The latter is rejected by filtering and the former has an amplitude depending on the phase relation between the signal and reference. The switching is so arranged that the signals from each half cycle add together, whereas any signal in the signal channel (such as noise) which is out of phase or at a different frequency from the reference will tend to cancel itself out, the degree of cancellation, and hence the resolution of the system, depending on the time constant of the subsequent smoothing circuit. The effective bandwidth of the system is given by B ~ 1/T where T is the time constant of the smoothing. For simple RC filtering T = 2.2 RC for a single stage and 3.4 RC for a double section filter (where T is the 10 to 90% rise time) with bandwidths of 1/2 RC and 1/4 RC. Thus with a time constant of ten seconds the bandwidth is 1/40 Hz, which will give a Q of 40,000 at 1 KHz, which is at least x100 better than the best tunable filter system.

Two similar lock-in amplifier (phase-sensitive detector) systems have been used, a 'Princeton' type JB-4, and later a Princeton JB-5.

These are fully transistorised tunable instruments, the former from 15 Hz to 15 KHz, the latter from 1.5 Hz to 150 KHz. Both have x50 gain, Q ~ 25 signal amplifiers and time constants up to 10 seconds. The reference can either be provided externally or an internal oscillator can be used as the internal signal source for external modulation. The output can either be read off a meter or monitored on a pen recorder.

5:5 Operation and Basic Characteristics

To obtain maser oscillation the following procedure is followed. The nozzle, separator and microwave cavity are all carefully aligned using a low voltage bulb below the cavity to provide illumination (the nozzle is sufficiently transparent to be seen through if enough illumination is used). The vacuum system is then reduced to 10^{-5} torr as described in section 4b and the ammonia reservoir filled with clean dry ammonia. The microwave system is tuned-up on the cavity absorption curve and the klystron is offset by 30 MHz. The system is switched from crystal-video to unstabilised superheterodyne detection and the ammonia beam pressure adjusted by the fine control valve until there is about 1.5 torr behind the nozzle. The EHT supply to the separator is then increased to about 25 KV and the maser oscillation signal observed on the oscilloscope screen. The system is then finally tuned as described in section 4f, the klystron reflector sawtooth sweep is switched off and the output of the 450 MHz harmonic chain (which has been switched on for several hours) is then increased until it beats with the klystron signal to give the 57 MHz correction

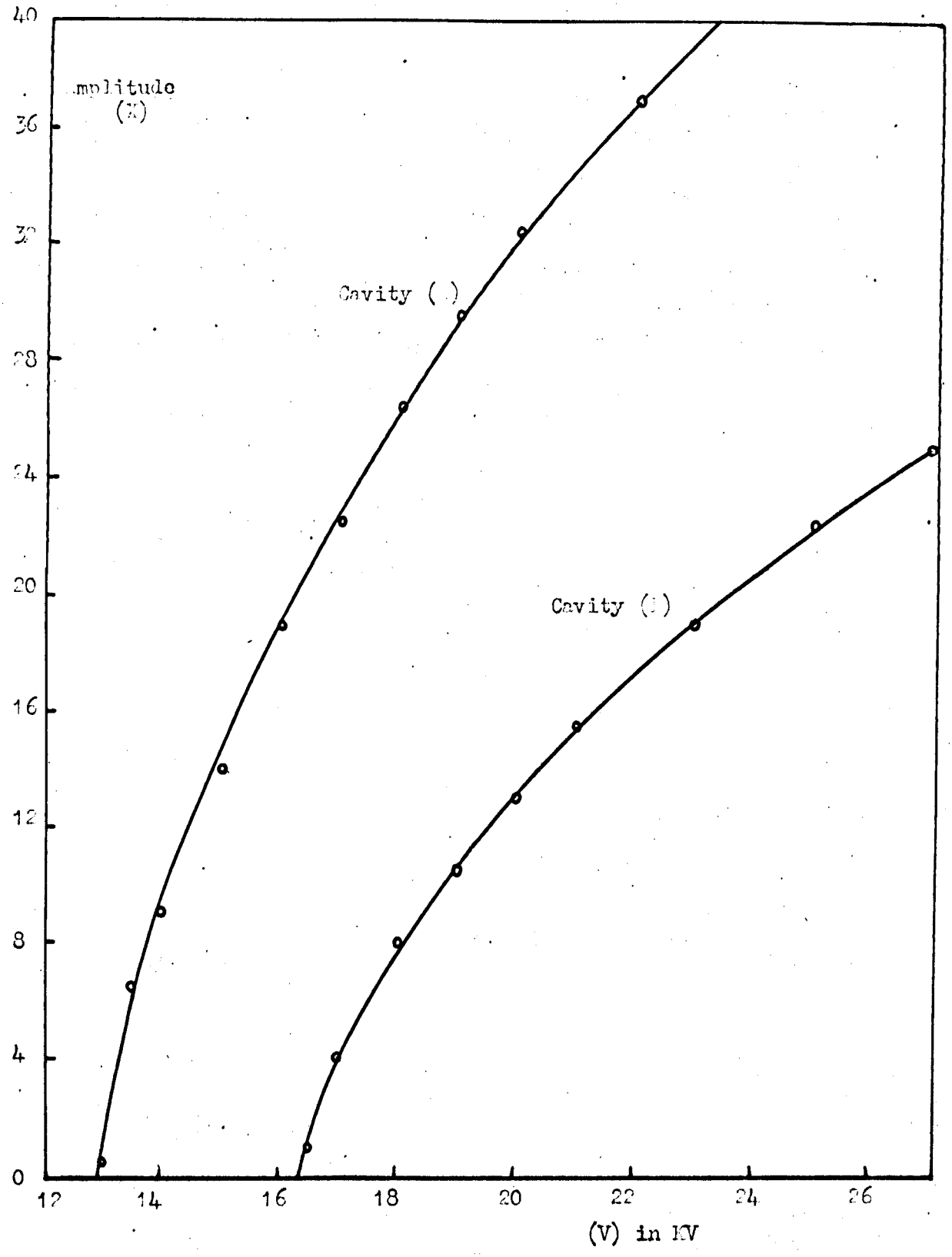

Figure 5:12

Maser oscillation amplitude (X) for cavities (A) and (B), variation with separator potential (V)

signal. The system is adjusted for maximum amplitude of the 57 MHz signal and the correction signal switched to the klystron reflector, the klystron is then 'locked' and maximum aplitude of maser beat-frequency is obtained by slightly adjusting the 5 MHz oscillator to pull the klystron until it is exactly the intermediate frequency away from the maser frequency (that is for maximum amplitude).

Since the detection system is being operated in the linear response region the output amplitude of oscillation (X) is directly proportional to the field in the cavity (E) and hence the oscillation parameter θ. The amplitude of oscillation can be varied by changing the EHT on the separator or the nozzle ammonia pressure. At high potentials and the correct pressure (see below) a signal to noise ratio of 100 to 1 is fairly easy to obtain. Figure 12 is a plot of the amplitude of oscillation (X, and the separator potential (V in KV) both for the upper (A) cavity and the lower (B) cavity (the former is 7 cms long and its end is 0.5 cm from the separator, the latter is 10 cm long and is 8 cm from the separator) at 1.3 torr beam pressure. It can be seen that both these are similar to the predicted form (see Figure 2b) of the characteristic, $n/n_{thresh} = \theta^2/\sin^2\theta$, but do not reach saturation. This was predicted by Shimoda[34] when he considered the effect of actual velocities rather than one constant RMS velocity. As might be expected by consideration of beam divergence the top cavity threshold of oscillation occurs at a lower potential difference (~ 13 KV) than that of the bottom cavity (~ 16.5 KV). Figure 13 is a similar series of plots for cavity B, but for various beam pressures from 0.75 to 2.0 torr.

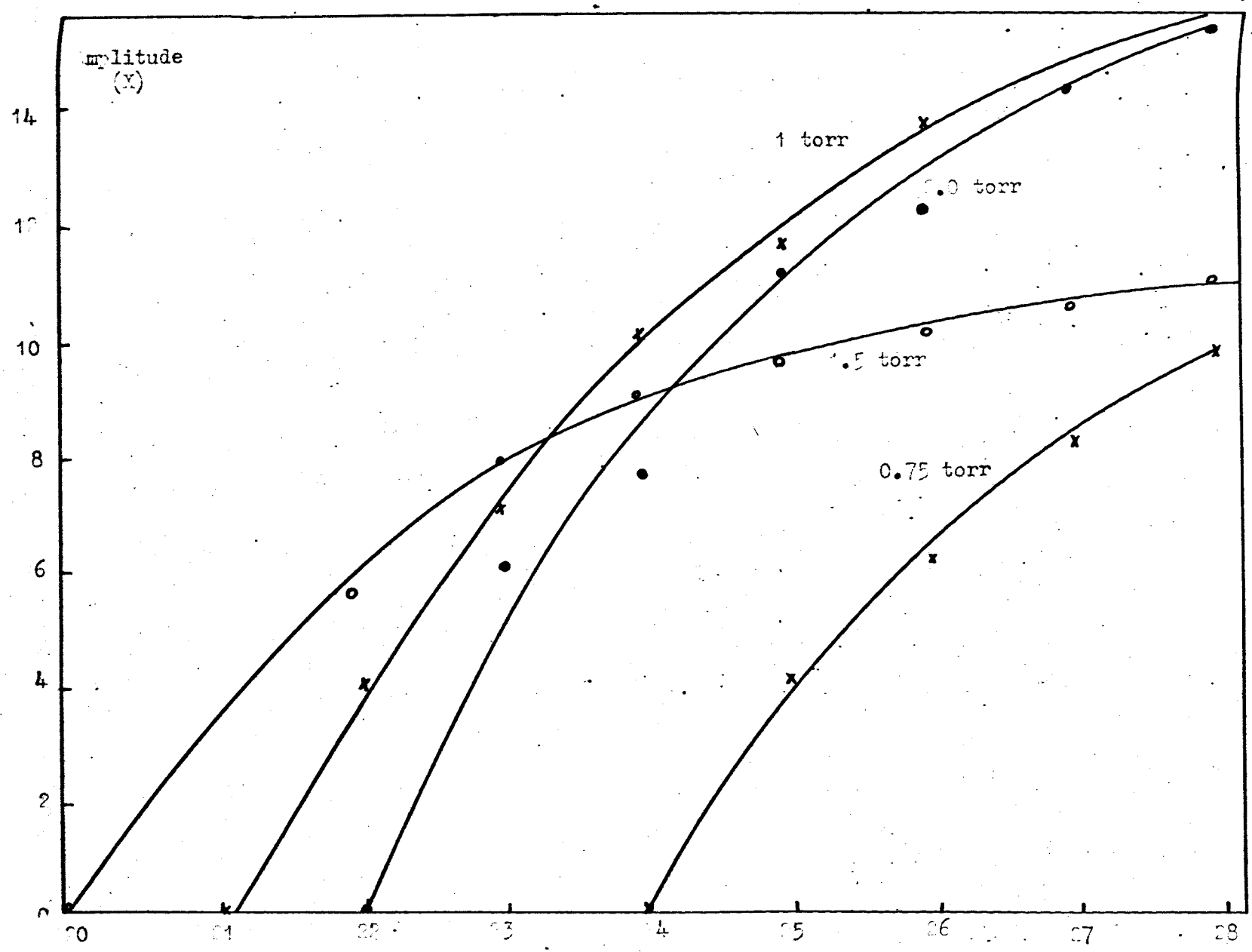

Figure 5:13

Single cavity maser amplitude of oscillation (X) variation with separator potential (V)

The Figure 14 plots the threshold of oscillation amplitude (X_{thresh}) variation with separator potential (V) and source pressure (P). It can be seen that for both cavities the system is best between 0.8 and 1.8 torr. The fall-off in performance at lower pressures is due to insufficient flux, and at high pressures due to increased collisions in the system, both close to the nozzle and in the beam. It can be seen that the minimum for the bottom cavity (which requires a higher flux from the separator) occurs at a lower pressure than the minimum for the top cavity. This shift could be due to either collisions in the nozzle and separator or in the separated beam. Figure 15 (see below) indicates that collisions in the nozzle and separator should decrease relatively with higher focuser potential and better separation, so it would appear that the optimum pressure for oscillation is dependent on collisions in the beam between the focuser and the exit of the appropriate cavity.

Figure 15 is a series of characteristics, for cavity B, of amplitude X and beam pressure P for different separator potentials V: it is apparent that the peaks of the curves move towards higher pressures at higher separator potentials. This indicates that the nozzle and separator combination works more efficiently at higher potentials (below breakdown) and confirms the indications of Barnes[342].

5:6 Velocity effects, separator modulation and sensitivity

It was established in section 4:2 that a parallel rod separator focuses into the microwave cavity molecules proportional to the square of

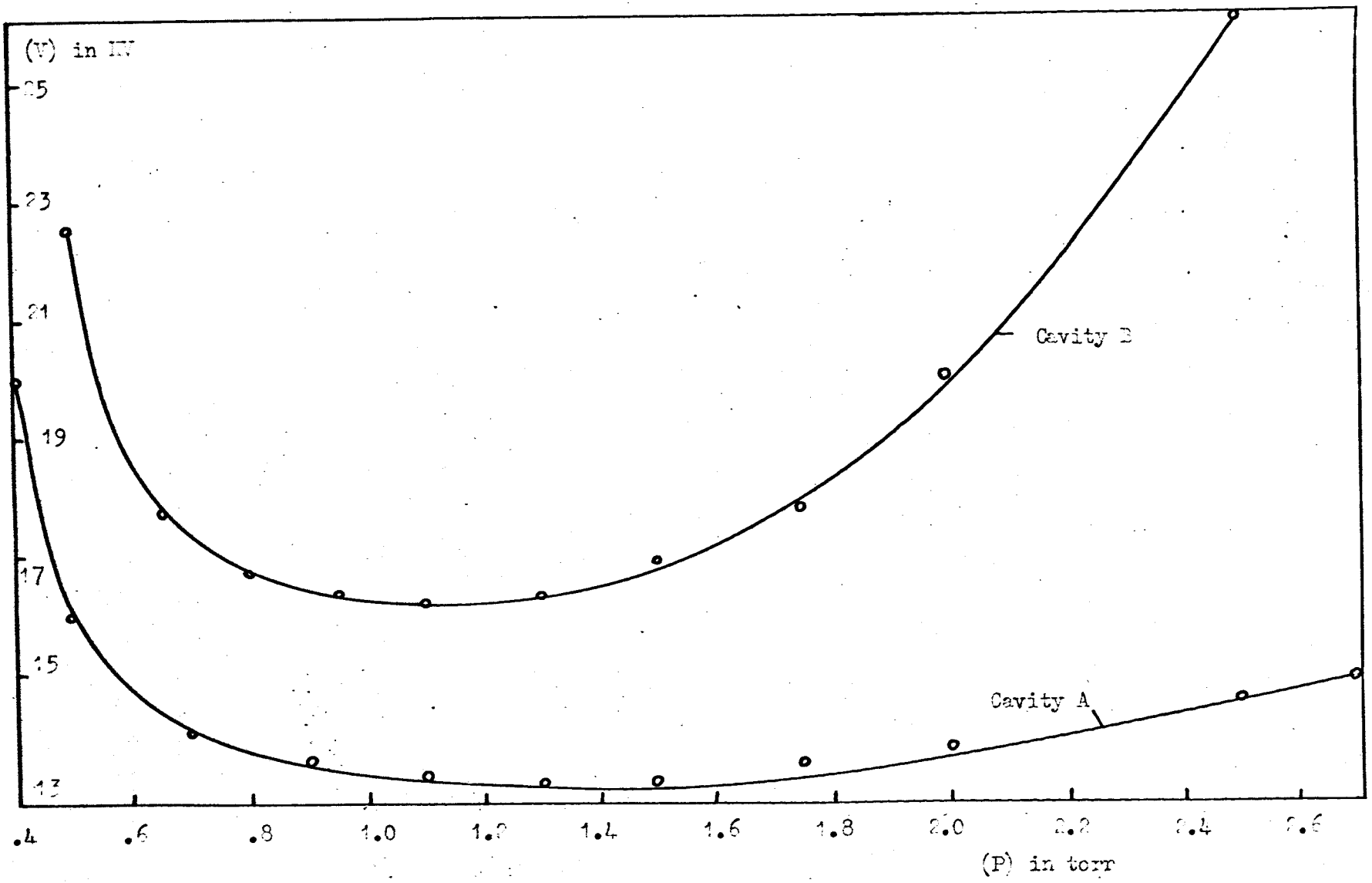

Figure 5:14

Laser threshold of oscillation characteristics. (A) top cavity, (B) bottom cavity

the magnetic state quantum number and proportional to the square of the electric field in the separator. Further the maximum radial velocity of molecules emerging from the separator is given by

$$\tfrac{1}{2}mv_{rc}^2 = pE_{max} M_J K/J(J + 1) . \qquad 52$$

The effects caused by the influence of the magnetic state quantum number will be considered in Chapter 7; but briefly it is seen that molecules with larger M states are more effectively focused. This can be seen in Figure 16a, which plots the density of focused molecules with different velocities for various M states and separator potentials[50, 342].

It is immediately apparent that the most probable velocities are considerably less than that predicted (a) for a thermal distribution, $\tfrac{1}{2}ma^2 = kt$, which gives for ammonia at 300° absolute a ~ 53,000 cm per second. This is because of the field focusing criterion and because the slower molecules spend a longer time in the separator and are thus more effectively separated. Shimoda[34, 37] has established that the effective average velocity is proportional to the critical radial velocity, $v_a = v_{cr}k$, so at lower separator potentials only the slower molecules are effectively separated. The value of the constant k depends on the geometry of both the separator and the cavity.

A multi-pole separator does not separate the molecules in velocity, state or direction uniformly across its exit. The slower molecules tend to be on the axis and paraxial and the faster molecules tend to be off axis and following a path at an angle to the axis. So if the

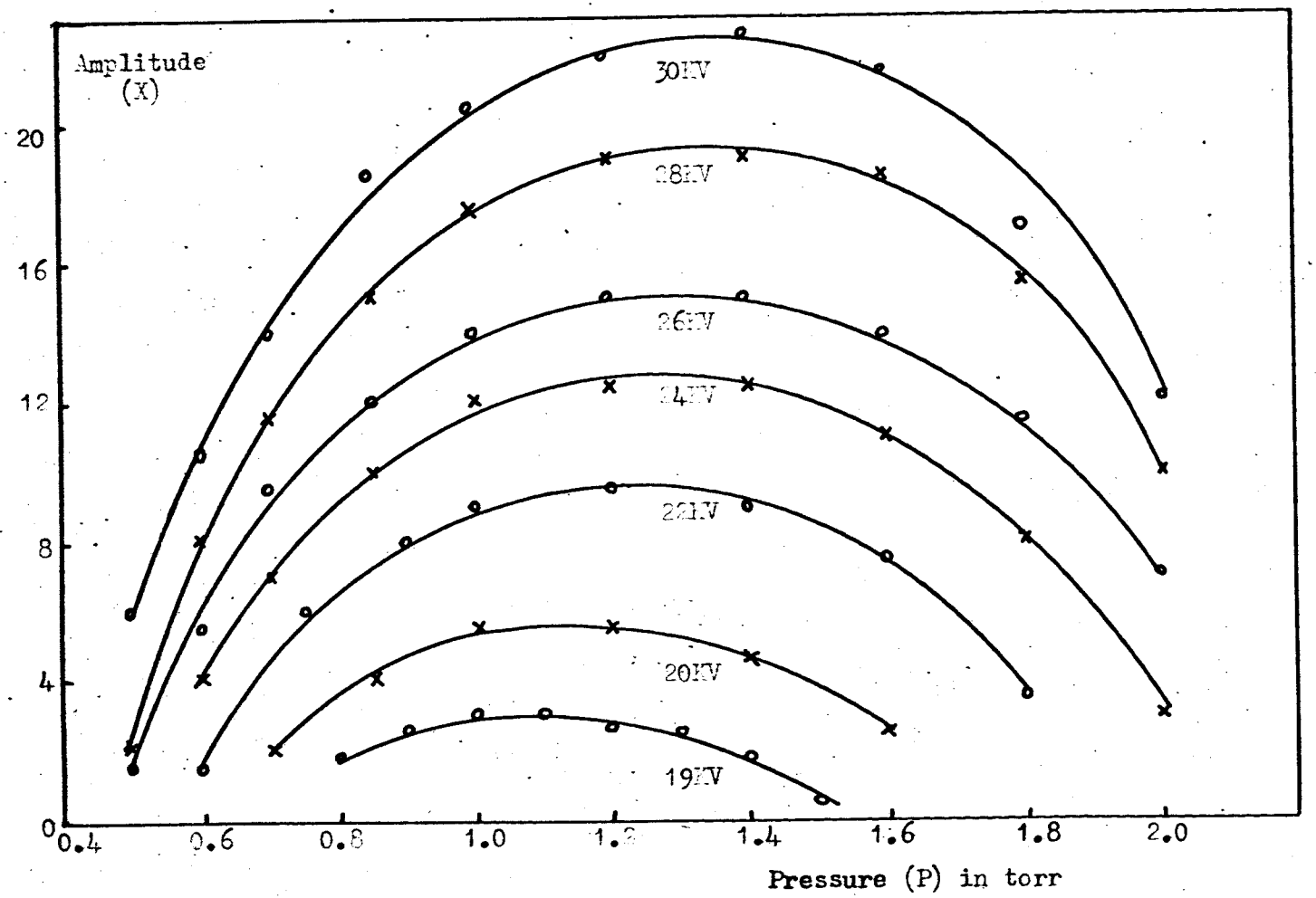

Figure 5:15

Sirgle cavity maser characteristics. Variation of amplitude of oscillation (X) with beam pressure (P) for various separator potentials

microwave cavity is situated some distance from the separator one would expect the effective average velocity to be less, both because it is accepting a narrower solid angle of molecules (tending towards the paraxial) but also because the microwave field in E_{010} cavity is greatest along the axis, so the transition probability is greatest for axial molecules. Since the slower molecules spend a longer time in the microwave cavity there will be a further decrease in the effective average velocity. Jaynes and Cummings[343] have computed the effect of some of these phenomena and predict that not only are the slowest molecules very important for stability and noise properties of the maser, but also the starting flux (amongst other parameters) is dependent on the slowest 5 to 10% of the molecules, which would suggest velocities of 4000 to 8000 centimeters per second.

The beam maser has been used to investigate both the effective average velocity at threshold and the average velocity for higher flux.

In section 4:2 it was shown that the number of focused molecules changed with variation in separator potential according to

$$dn/n = 2dE/E = 2dV/V \quad . \qquad 53$$

So if a small periodic variation (dV) is applied to the potential (V) on the electrostatic separator there should be an equivalent and similar period variation (dN) in the number of focused molecules (N).

The signal from an audio range variable frequency oscillator is amplified and coupled to the high potential electrodes of the electrostatic state separator through an E.H.T. capacitor (see Figure 11). This modulates the number of molecules focused into the microwave cavity

(a)

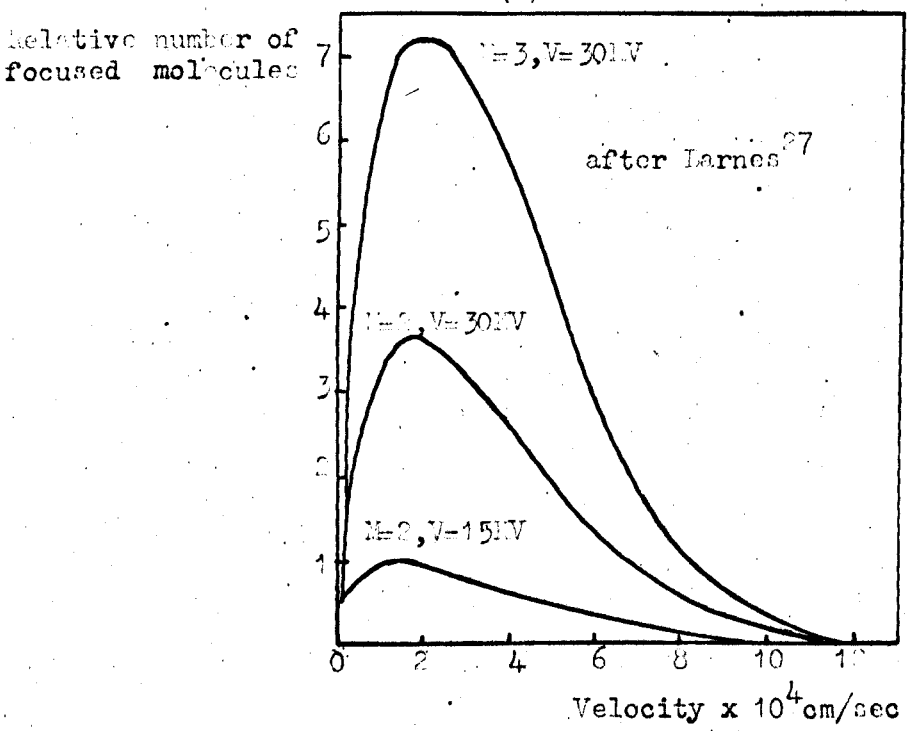

(b)

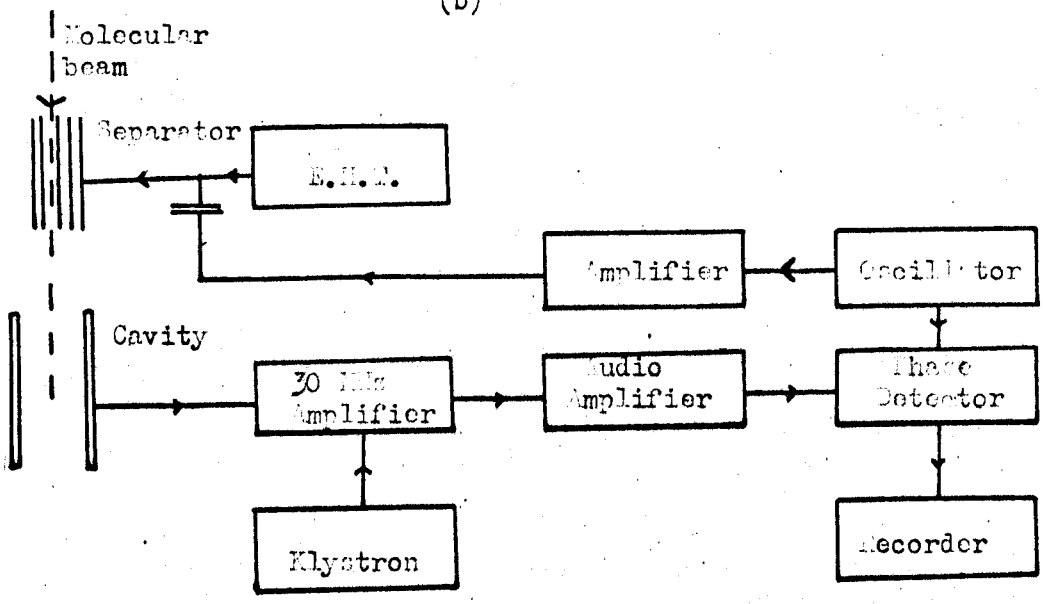

Figure 5:16

(a), Focused flux for different molecular states and operating conditions

(b), Block diagram of separator modulation experiment

and if the cavity is oscillating the amplitude of the oscillation, as detected through the 30 MHz I.F. superheterodyne amplifier, will be modulated at the appropriate audio frequency. This signal is synchronously detected with phase reference provided directly from the audio oscillator, the output is smoothed and observed on a meter and pen recorder.

It was expected that a low audio frequency would have to be used as the ammonia molecules are only travelling at an average velocity of the order of 10,000 cm/sec, which is equivalent to a flight time of 1 ms for a ten centimeter long cavity. For there to be reasonable uniformity in the number of molecules per unit volume along the length of the cavity there should not be more than an eighth of a cycle of modulated beam in the cavity at any one time. Thus the signal output from the phase sensitive detector should decrease rapidly as the modulation frequency approaches the order of 100 Hz. Figure 17a is a plot of maximum detected signal amplitude (Y max) and frequency of modulation (f) for constant separator modulation and constant beam flux. The D.C. separator potential is adjusted for maximum phase detected signal for each frequency. From this it is seen that the system is most sensitive at the lower modulating frequencies.

Figure 18 shows a series of graphs of synchronously detected audio signal amplitude (Y) plotted as a function of the amplitude of the ammonia microwave oscillation (X) for different frequencies of modulation of the electrostatic separator, all with constant nozzle pressure. It is from the amplitude maxima of these curves that

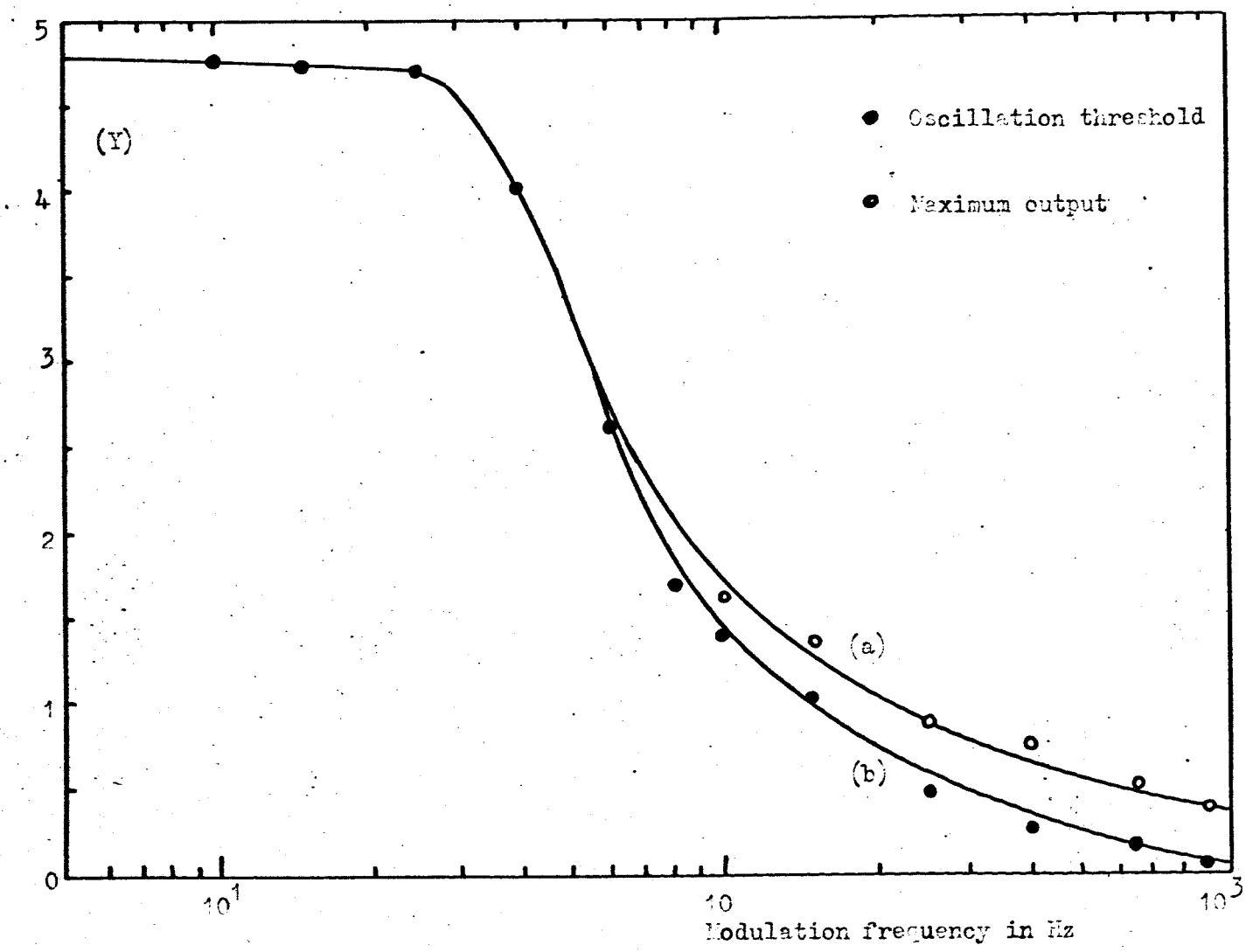

Figure 5:17
Variation of maximum detected maser modulation (Y_{max}) with operating frequency

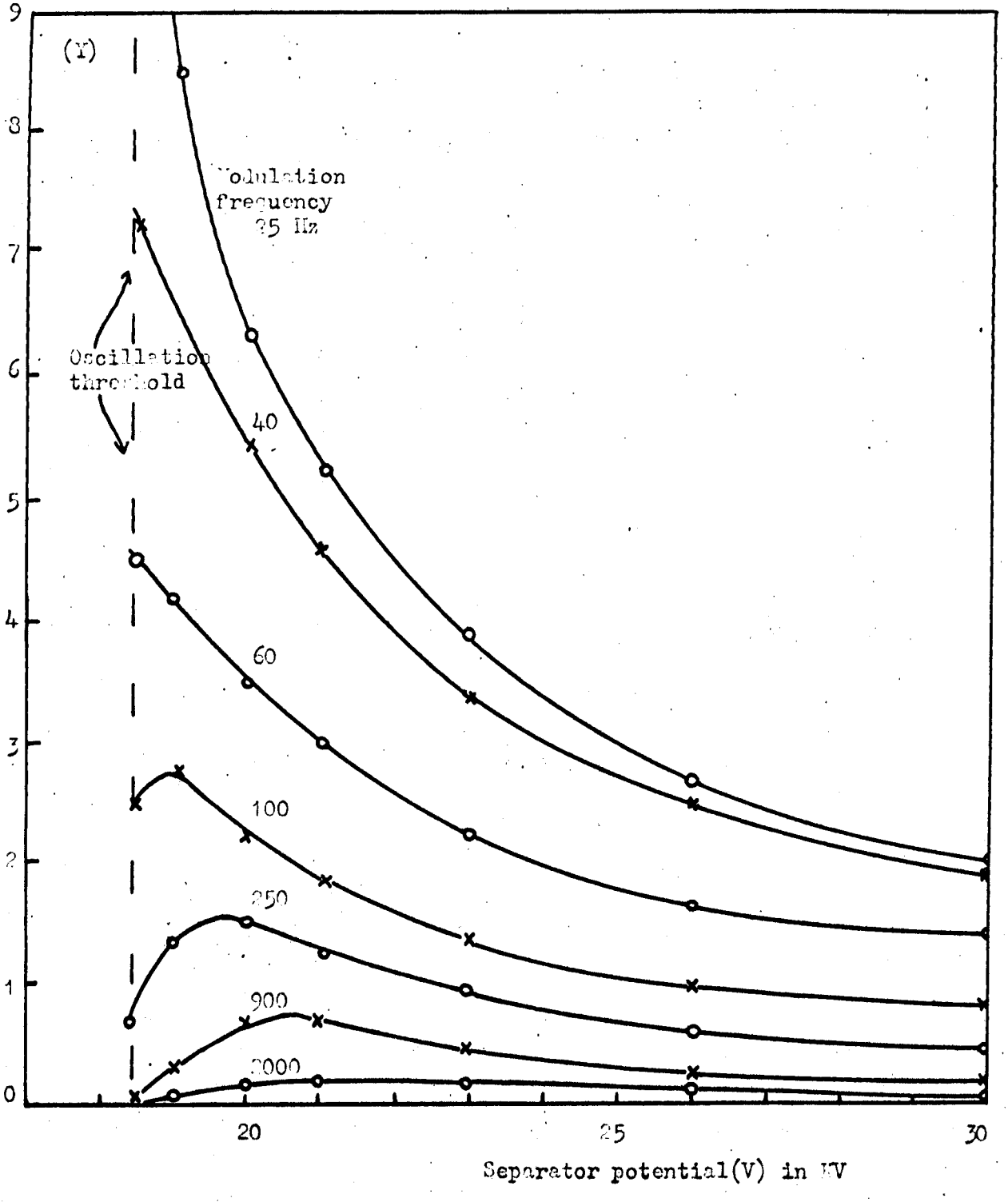

Figure 5:18

Variation of maser modulation output (Y) with operating frequency and (V)

Figure 17a was constructed. Figure 17b shows the graph of detected audio signal amplitude (Y) and frequency (f) for the case when the microwave maser is oscillating just above threshold. Figures 17a and 17b diverge when the maximum detected amplitude (Y) does not occur at oscillation threshold.

Figure 19 shows that the maximum sensitivity being constant below 25 Hz as illustrated in Figure 17 for threshold conditions is also true for higher beam flux conditions.

Figure 20 is a double plot for a beam of 1.5 torr ammonia beam pressure with 2 volts R.M.S. 30 Hz separator modulation. Both the amplitude of the synchronously detected 30 Hz signal (Y) and the amplitude of the microwave oscillation (X) are plotted against the mean D.C. potential applied to the separator (V). Figure 21 is obtained from 20; it is a plot of the 30 Hz detected amplitude and the slope of the microwave amplitude of oscillation against separator potential curve, dX/dV, this is a straight line and suggests that dX/dV is the dynamic operation curve for the detection system. At higher modulation frequencies this linearity no longer obtains because the time of molecular flight through the system becomes comparable with the period of the separator modulation. This effect will become most apparent at the lowest intensities of microwave oscillation, for a given modulation frequency, because near threshold the average molecular velocity is considerably less than the average molecular velocity near saturation.

The above results were obtained with the cavity B which is 8 cm

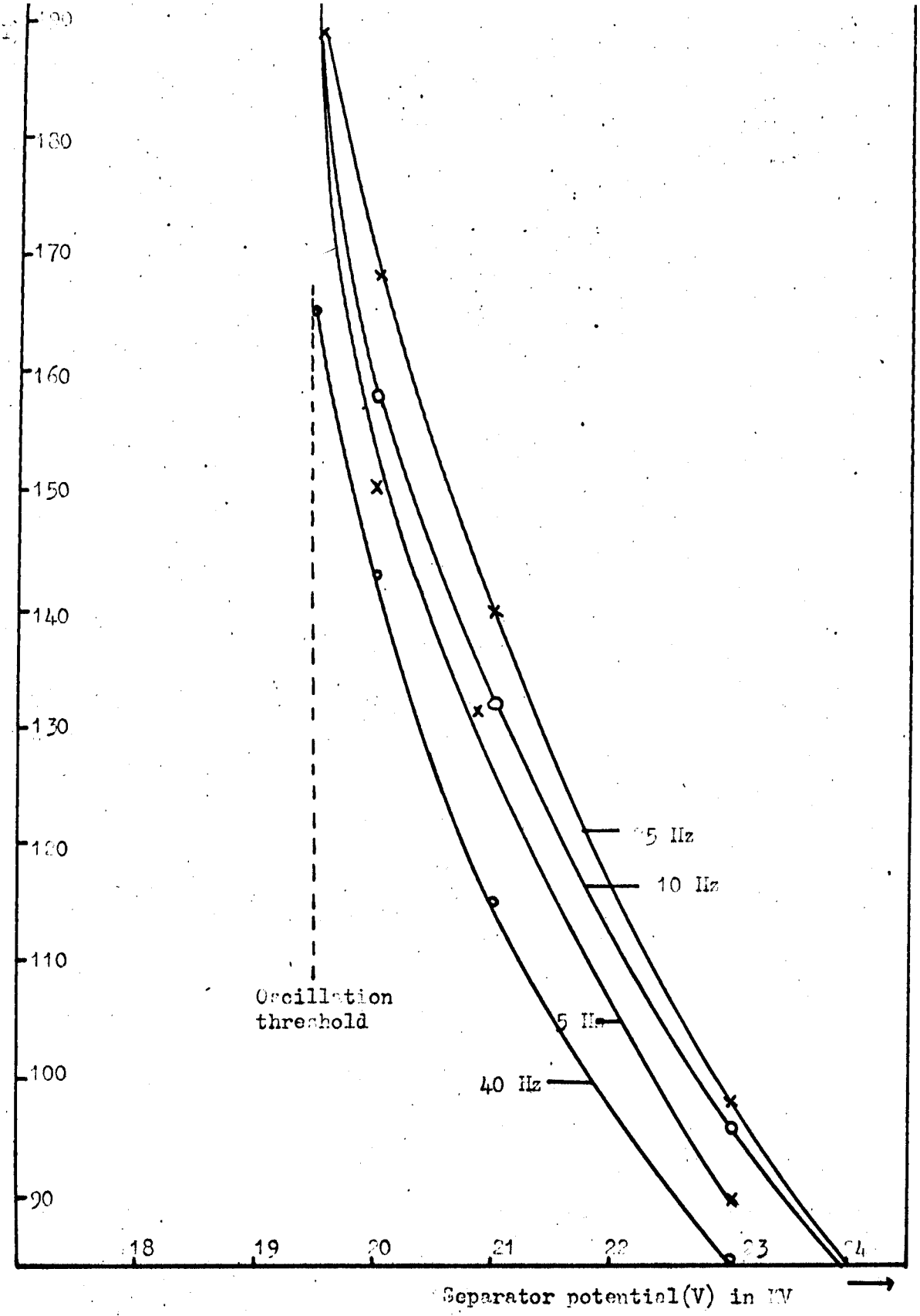

Figure 5:19

Variation of maser modulated output (Y) at low frequencies

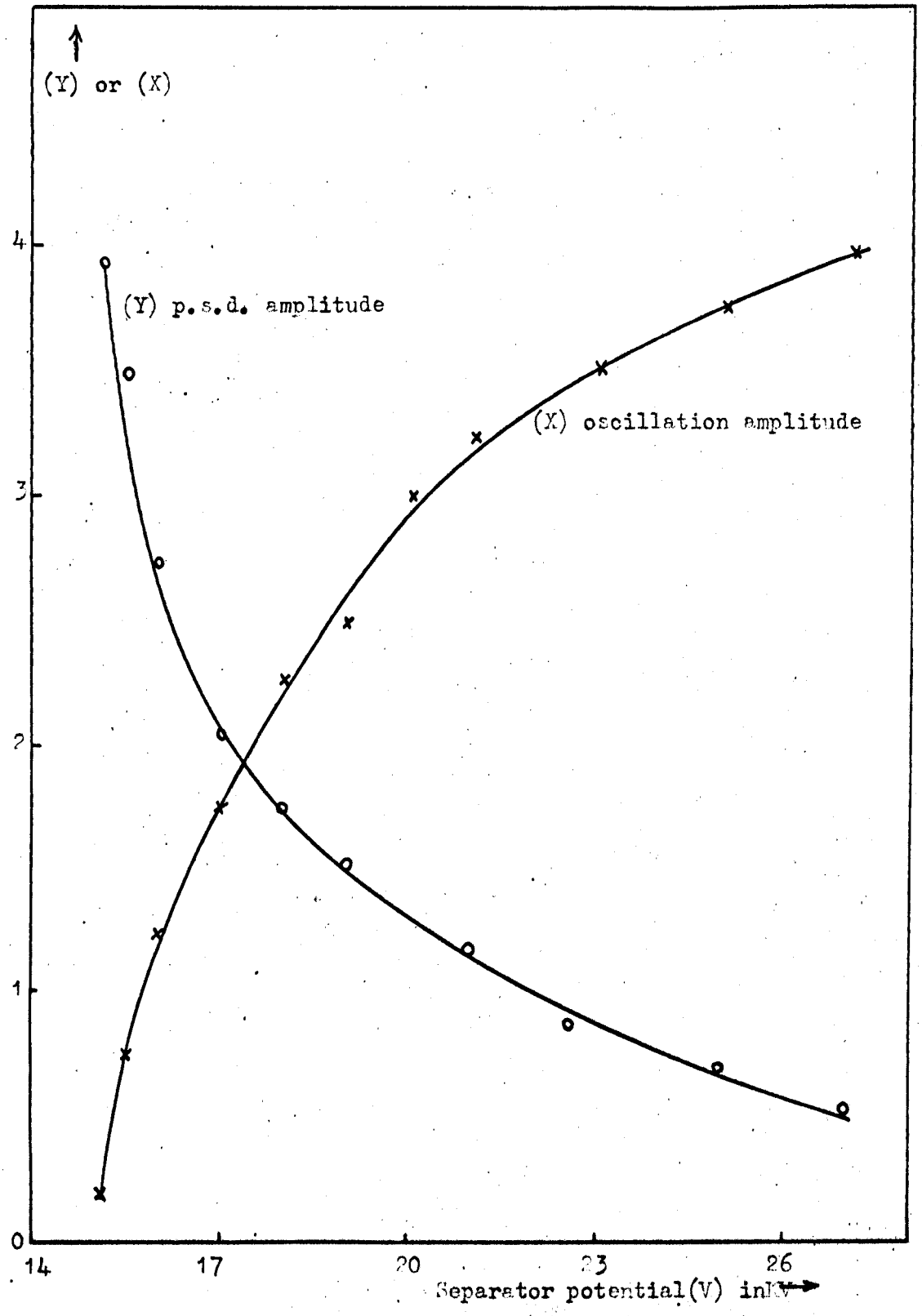

Figure 5:20

Variation of amplitude of maser oscillation(X) and detected modulation(Y) with separator potential (V)

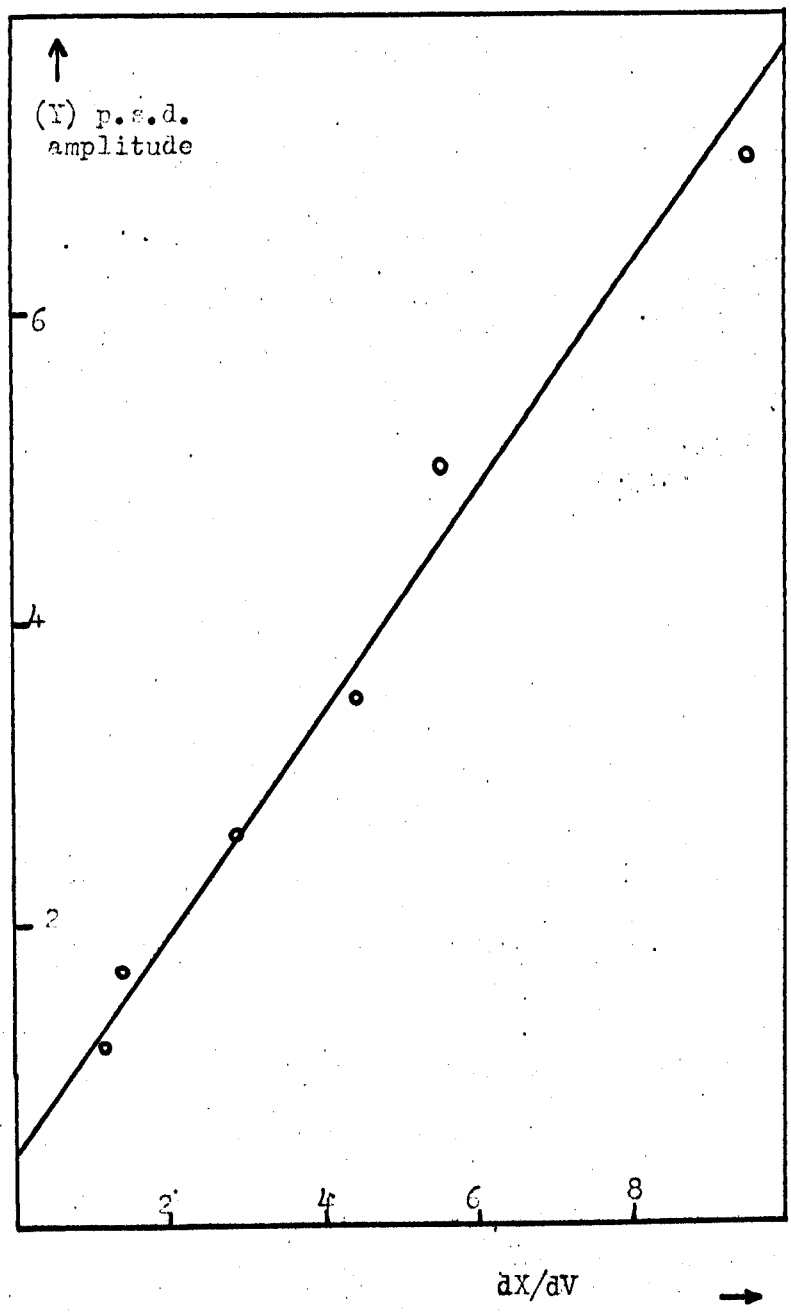

Figure 5:21

Variation of maser detected modulation(Y) with dX/dV

from the separator (nearest points). Because of the time of flight between the separator and the cavity there will be a phase shift between them, so the phase sensitive detector signal is maximised for each separate operating frequency (at 20 kv separator potential each time).

There will be effects due to the spread in times of flight between the separator and cavity, the times of flight in the cavity and the times of flight in the separator. The first two of these will tend to decrease the modulation signal strength as the separator potential is increased, the third will tend to increase the modulation strength because the average velocity will be greater and the beam modulation will be averaged less.

To compare the two former effects, results obtained for identical operating conditions were compared for cavity B (10 cm long) 8 cm from the separator and cavity A (7 cm long) 0.5 cm from the separator (phase peaked at 15 KV separator potential). Curves 22 and 23 give the results: it can be seen that the general pattern is the same, but the shapes of the curves are slightly altered and that for cavity A the inflection is at 80 Hz whereas for B it is at about 65 Hz. These effects should be able to be examined in more detail in the more flexible maser system described in Chapter 8, using a short spiral separator.

From Figure 18 it is apparent that (Y) decreases to a half when the modulation frequency is increased from the low frequency mean (the 25 Hz curve) to 55 ± 5 Hz at oscillation threshold (18½ KV).

If one assumes a univelocity beam, velocity v, then with a phase

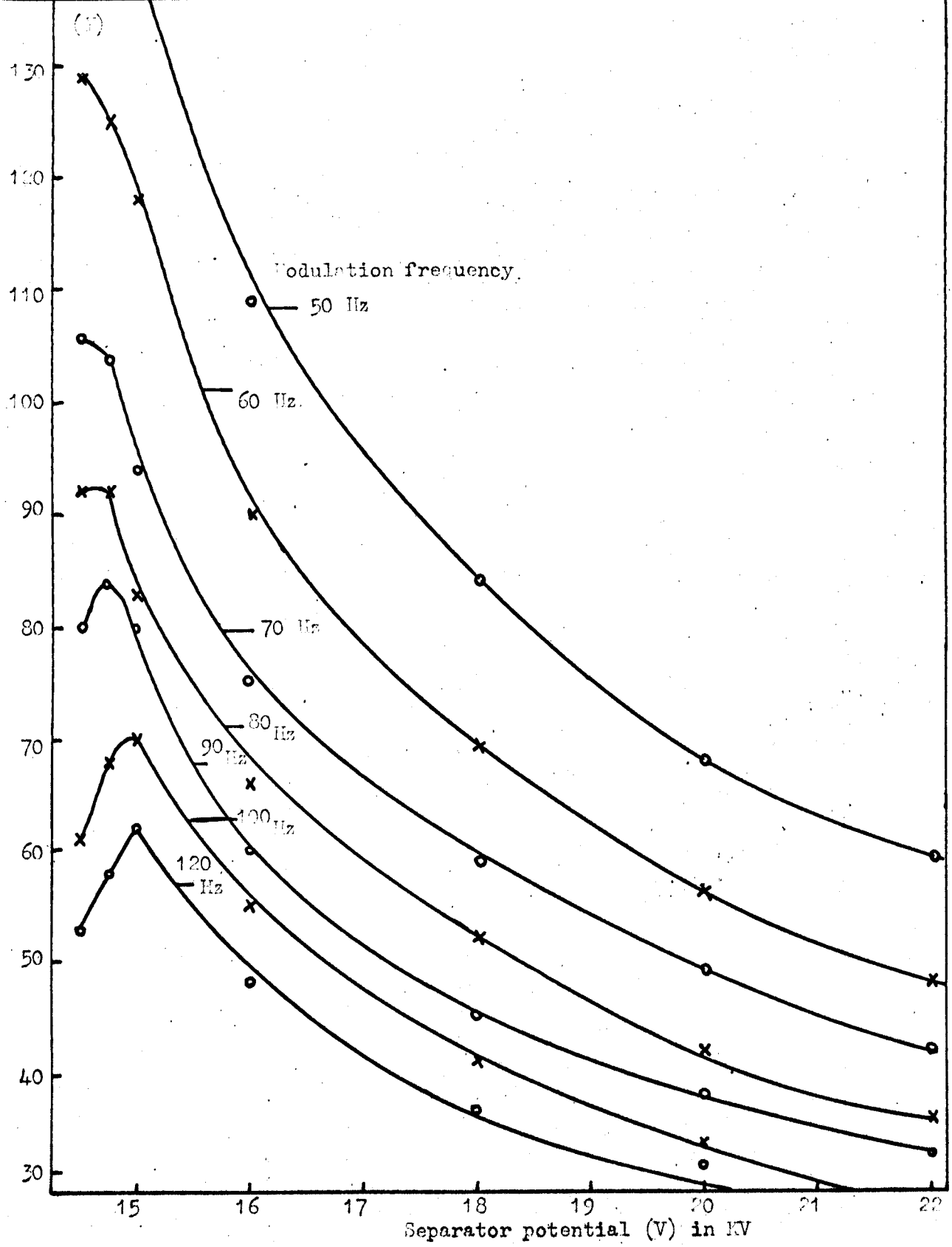

Figure 5:22
Variation of cavity A detected amplitude (Y) with potential (V) for different modulation frequencies

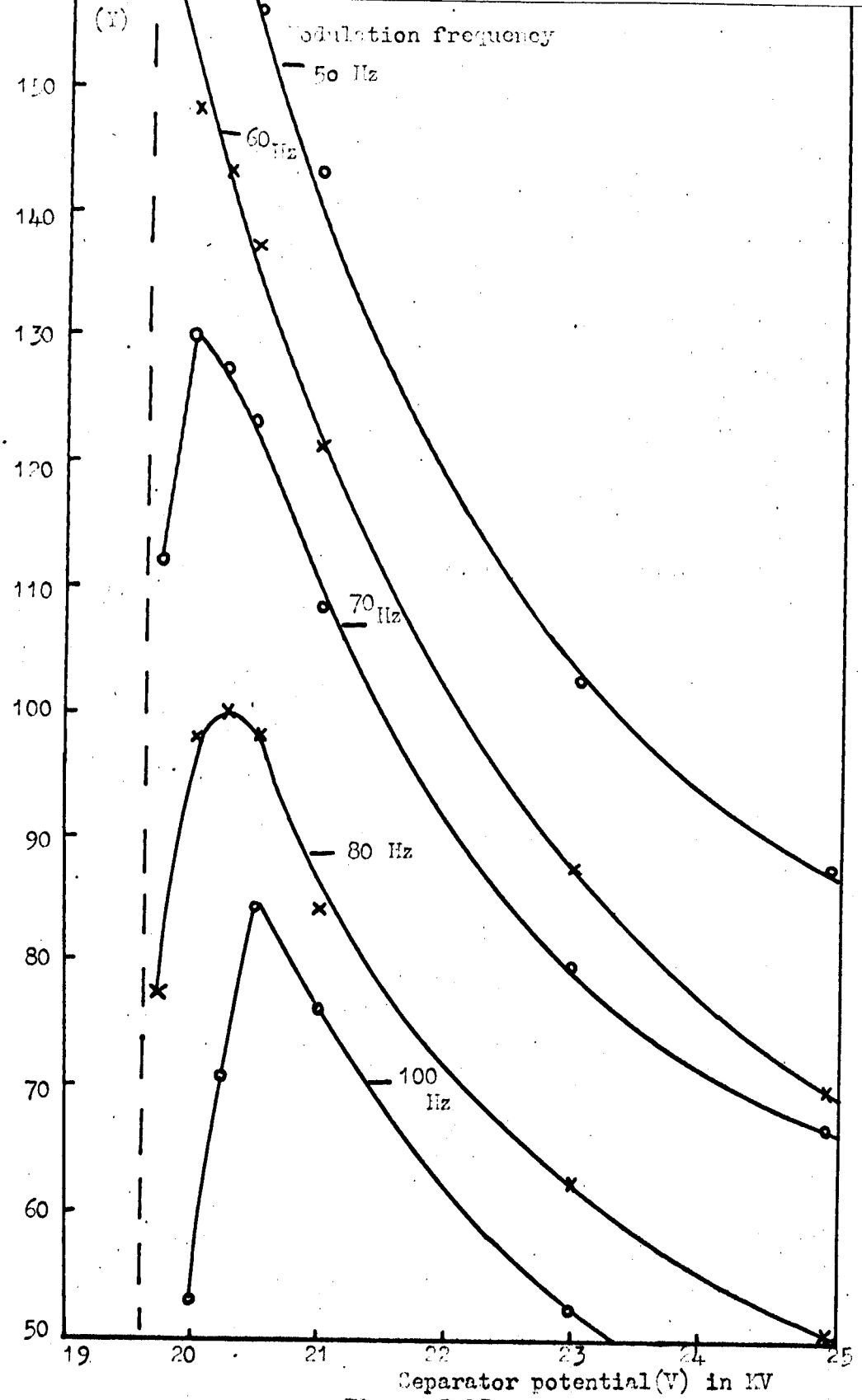

Figure 5:23

Variation of cavity B detected amplitude (Y) with separator potential (V) for different modulation frequencies

sensitive detector the signal strength should reduce to 50% when the phase is changed by about $2\pi/10$ degrees, so $L/v = 1/10f$ where L is the cavity length and f the frequency of modulation which is required to produce the 50% drop in modulation amplitude. Thus for the present system

$$v_{threshold} = 5{,}500 \pm 1000 \text{ cm/sec.}$$

This value agrees with the prediction of Jaynes and Cummings.

The variation of signal strength with beam flux for constant separator potential has been determined at 30 Hz, and in this case 1.5 torr ammonia pressure was found to give the best sensitivity for weak oscillation conditions.

The amplitude of the modulation on the separator has been varied at 30 Hz and is found to vary linearly with the phase detected signal over two orders of magnitude change. The smallest modulation on the separator which could be detected with a ten second time constant in the phase sensitive detector at 15 Hz was approximately 18 mv rms, this was at 14.5 KV separator potential; thus from equation 53

$$dn/n = 2 \times 18/(14.5 \times 1000 \times 1000) = 2.5 \times 10^{-6}.$$

This compares with $dn/n = 3 \times 10^{-5}$ for the theory given in section 5:2 for the case when the field in the cavity is independent of the molecular beam intensity, (when all stimulated emissions are sufficiently isolated that they can be considered as independent of each other). In the present case the microwave field seen by the molecules is created by

stimulated emission and a dynamic system exists. A sensitivity greater than that suggested by the Shimoda theory should be obtained, as is seen to be the case. But the Townes theory, also given in section 5.2, suggests that the sensitivity should be greater by at least an order of magnitude, if the maser is noise limited by thermal fluctuations. Section 5:3 indicates that it is so limited at low oscillation amplitudes. Thus the increase sensitivity of about × 10 due to 'Q narrowing' is rather less than the value of × 50 which Townes estimated Shimoda and Wang[69] obtained, and also less than the value which was obtained by Lecar and Okaya[344-345], but it has been obtained under conditions where the cavity and coupling hole are not optimised for maximum sensitivity.

Chapter 6. Multi-Cavity Microwave Maser

6:1 Introduction

It was seen in Chapter 2 that a two cavity beam maser might be used as a double resonance system to investigate far infrared transitions of the ammonia molecule with microwave detection. In the previous chapter the construction of a beam maser with space for the insertion of a second cavity, microwave or ultramicrowave, between the state separator and the microwave detection cavity was described. Some of the properties of the single cavity maser were investigated and the most sensitive operating conditions for its use as an oscillating detector were determined.

In section 4 of Chapter 2 it was assumed that the only interaction between the two resonant structures would be population effects: that is, the first cavity might alter the population distribution between the (+) and (-) inversion states of the 3,3 ammonia molecule and these changes, if large enough, would be observed as a change of oscillation amplitude in the second cavity. In 1957 Higa[346] found that for a two microwave cavity system the interaction was too complicated to be explained by simple population effects, since then several research groups have investigated the effects. The interest seems to be fourfold: first, the effects themselves seem to illuminate some very fundamental properties of two quantum state systems. Second, such a two microwave cavity system can be developed into a low noise amplifier with some very useful properties. Third, the system might be developed into a frequency standard. Fourth, such a system is a very sensitive spectrometer.

In the remainder of this section a brief historical and phenomenological survey of the main features of the observed effects will be presented and the difficulties of a comprehensive quantitative explanation examined. In section 2 some of the characteristics of a two microwave cavity system are measured and agreement is obtained with many of the previous results, but some discrepancies appear and various effects appear more complicated than expected. In section 3 the state separator potential difference is modulated, as in section 6 of Chapter 5, and the sensitivity of the two cavity system determined over a range of operating conditions. Then in section 4 the system is used as a two cavity spectrometer and previously unresolved hyperfine structure of the ammonia molecule is observed. This interpretation is confirmed by externally coupling the two microwave cavities to form a phased 'Ramsey like' system. In section 5 some of the preoperties of the two cavity amplifier are examined and the operating conditions determined.

Higa[346] cascaded two TE_{011} mode cavities and when both cavities were tuned to the line centre he observed a strong emission from the first (A) cavity and a small signal from the B cavity, both signals being at the same frequency. When cavity A was detuned the frequencies remained the same in each cavity until at a critical value of detuning the bottom cavity broke out into oscillation at its centre frequency modulated with the difference frequency between this and the A cavity oscillation frequency. When cavity A was further detuned it ceased to oscillate and the signal in the second cavity was no longer modulated. Higa noted that the beats were evidence both for the

non-linear properties of the maser and that the maser oscillator could act as an amplifier. Javan and Wang[347] and Sher[330] investigated the two cavity maser as an amplifier. Javan and Wang pointed out that if both cavities were tuned to the line centre the power emitted in the second cavity was proportional to the field intensity (for small E) not the square of the field intensity as in a normal beam maser (equation 17, Chapter 5) and that a threshold flux was not necessary for oscillation, power being emitted from cavity B however small the flux (N). Consider the two state quantum system at resonance ($f = f_o$) with $a_1(0) = 0$ and $a_2(0) = 1$, then from equations 4 and 5 of Chapter 5, provided that $\Delta a_1(t) << 1$ (that is the linear amplifier condition),

$$|a_1(t)|^2 = \sin^2(\pi y t) = \sin^2(\mu E \pi t/h) = (\pi \mu E t/h)^2 \qquad 1$$

and the average power emitted per molecule in the single cavity is

$$P = \frac{hf}{t} (\pi \mu E t/h)^2 \ . \qquad 2$$

But if the molecule has a small non-zero value of $a_1(0)$ then[1]

$$|a_1(t)|^2 - |a_1(0)|^2 = (\pi \mu E t/h)^2 + 2(a_1(0)) \pi \mu E t/h \qquad 3$$

and the emitted power is given by

$$P = \frac{hf}{t} \left[(\pi \mu E t/h)^2 + 2(a_1(0)) \pi \mu E t/h \right] \ . \qquad 4$$

Thus it can be seen from equations 4 and 2 that more power is generated from the superposition assembly than from the pure upper state assembly. If this prestimulation takes place in an initial microwave cavity then the two cavity system should be more sensitive

to changes in power matched to the first cavity than a single cavity maser amplifier would be (see section 5 below for investigation of this effect).

In 1960 Reder and Bickart[348] realised that the two cascaded cavity maser might be a very useful frequency standard because various difficulties encountered with the single cavity maser could be avoided. For example, since the ammonia beam maser is a low power device the coupling from the output cavity to the frequency measurer or translator has to be quite large, this means that the output frequency is likely to be altered due to load variations. However, with the two cavity maser the output frequency is determined by the first cavity only, and this cavity can be constructed without a coupling hole and can be externally isolated from the rest of the system. The second cavity appears to act only as a 'pick-up antenna' and if it is detuned only the output amplitude changes, not the frequency. For a narrow emission line the emitting cavity should be long so that the interaction time is long, but this leads to longitudinal doppler broadening (due to non-uniform emission of power along the cavity length) of the emission line. With the two cavity system the overall interaction time can be large even with a very short detector cavity (~ 4 cm).

In 1957 Wells[349] attempted an explanation of the Higa beats in terms of cooperative phenomena of the beam molecules. If the molecules in the first cavity assume an induced macroscopic polarisation due to individual microscopic transitions, then when they leave the cavity the beam will continue to 'ring'[350] for a period determined by the

linewidth, and on entering the second cavity an emission signal will be observed at the frequency of the first cavity transitions. When both cavities are tuned to the molecular resonance the inverted population reaching the second cavity is too small to sustain independent oscillations, but as the first cavity is detuned its oscillation amplitude decreases and enough upper energy state molecules enter the second cavity to support an independent oscillation. Thus there may be two signals detected by the system connected to the second cavity, these appear to mix in the non-linearities of the maser system to produce the 'Higa' beats. If the first cavity is detuned further it ceases to oscillate and the second cavity behaves like a normal single cavity maser. Wells used a geometric technique developed by Feynman, Vernon and Hellwarth[351], but he was only able to give qualitative arguments for the frequencies in the two cavities and did not consider the oscillation spectrum in the second cavity.

The oscillation spectrum of the second cavity output was examined independently by two groups, Strakhovskii and Tatarenkov[352] and Laine' and Srivastava[353] who obtained similar results. They found that if both cavities were tuned to the line centre and cavity A was strongly oscillating then the signal from B was small. As cavity A was slowly detuned (and its output decreased) the signal from B increased until the detuning was about 2 MHz when a peak value of oscillation power was reached; on further detuning the output from B decreased until in the region of 4 to 5 MHz detuning the Higa beats appeared and the oscillation amplitude rapidly increased. As the signal from B

became large the beats disappeared and cavity A ceased to oscillate, and the system performed as a single (B) cavity maser. The same pattern was observed for positive and negative detuning of the first cavity and the pattern was approximately symmetrical if cavity B was exactly tuned to the line centre, (in fact Lainé and Srivastava suggested this as a method of accurately determining the cavity setting for a frequency standard). Figure 1a is a graph of the complete pattern, (from now on referred to as the S-T pattern) and 1b is a photograph of the Higa beats.

Lainé and Srivastava gave a qualitative description of the spectrum and beats in terms of 'molecular ringing' and oscillator amplification and saturation. Srivastava[354] has also considered the effects of absorption. When cavity A is detuned outside the range A-A' and there is sufficient beam flux, cavity B oscillates as if a normal single cavity maser. As the detuning is decreased stimulated emission in cavity A increases until at A it starts to oscillate at the pulled frequency given by equation 47 of Chapter 5, p103. A ringing signal appears in cavity B due to the oscillation in A and beats with a natural (centre frequency f_o) oscillation in cavity B to produce the Higa effect. As cavity A is tuned nearer to f_o so the oscillation in cavity A increases in amplitude, fewer upper state molecules reach cavity B and it oscillation amplitude decreases, so one has the portions of the trace A-B and A'-B' in Figure 1a. At B (and B') the bottom cavity ceases to oscillate, so the beats cease and the ringing field becomes the driving field of cavity B (at the frequency of cavity A). The ringing signal in cavity B is amplified by 'surplus' upper state molecules in cavity B and thus increases as

(a)

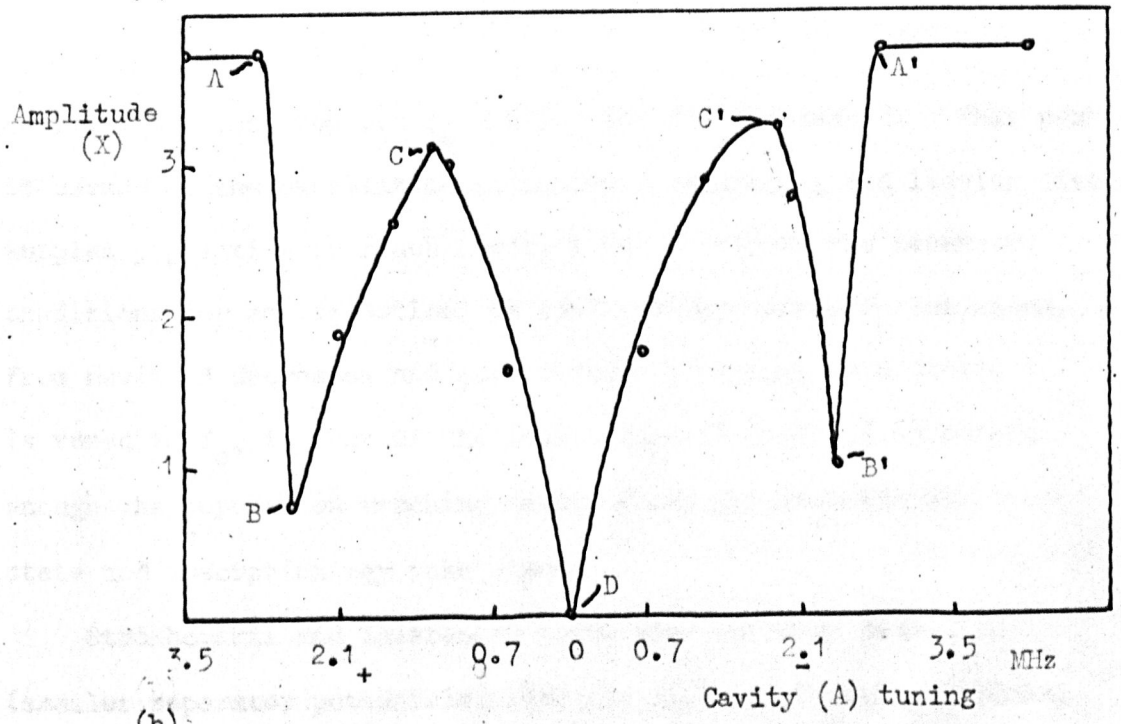

(b)

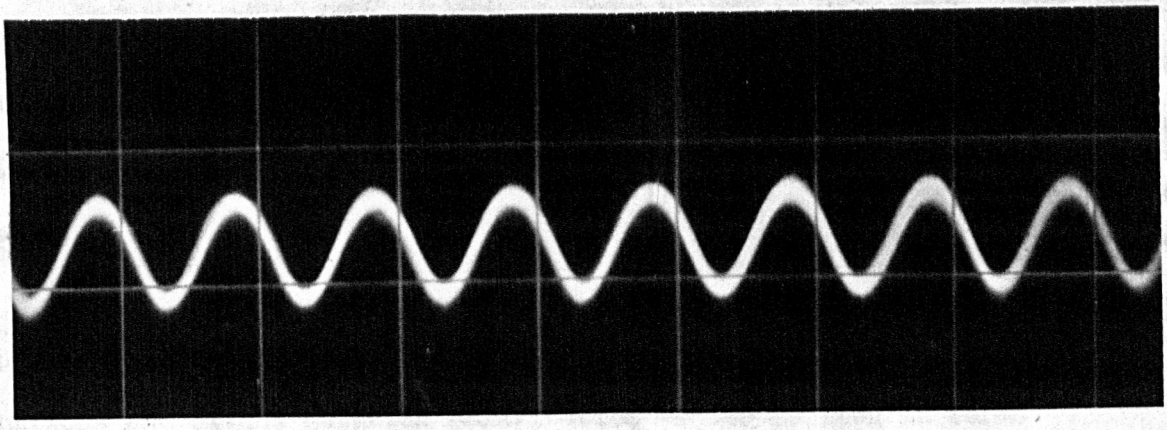

Figure 6:1

(a), S-T pattern. (b), Higa beats

cavity A is tuned towards f_o until C (or C') is reached. This peak is caused by the oscillation in cavity A saturating and leaving little surplus population to reach cavity B and so create the necessary conditions for amplification, as cavity A approaches f_o the signal from cavity B decreases and goes through a minimum when cavity A is tuned to f_o, in fact if the oscillation in cavity A is strong enough the population reaching cavity B may be predominately lower state and absorption may take place.

Strakhovskii and Tatarenkov noted that at lower beam flux (smaller separator potentials) when the flux of molecules reaching cavity B is not enough for oscillation even when cavity A is completely detuned, as cavity A is tuned across the molecular response the central portion of Figure 1a appeared, that is from B to B', but the wings, Higa beats and central dip were absent. Thus a signal can be obtained from cavity B when the flux is insufficient for independent oscillation, confirming equation 4.

Basov and Oraevskii[355] attempted a rather more quantitative explanation of the S-T patterns and Higa beats using Maxwell's equations and with a material polarisation vector defined in terms of the average dipole moment per unit volume of the beam. They were able to show that the frequencies of the oscillations in the two cavities were the same but they were unable to determine the S-T patterns. Belenov and Oraevskii[356] have extended this treatment to cover the two beam two cavity frequency standard and Strakhovskii, Tatarenkov and Tumanov[357] have operated such a device on the 3,2 line of ammonia with similar characteristics as for the

3,3 line. Basov et al[358-359] in two similar papers have presented some further characteristics of the two cavity system, noting some of the effects of variation of beam pressure and electric and magnetic fields. They also used a rather more rigorous quantum mechanical description but were unable to interpret the S-T pattern spectrum. More recently Li Tie-Cheng and Fang Li-Zhi[360] have attempted a full and rigorous quantum mechanical treatment but they are unable to find a quantitative solution except for $f = f_o$. However they attempt a qualitative explanation of the high intensity S-T pattern, but are unable to agree with the low intensity S-T pattern. In the next section the properties of a two cavity maser are examined and detailed characteristics presented and it is hoped that these will provide a rather more accurate basis for a future complete theoretical analysis.

6:2 Operation and Characteristics

The system used is that described in Chapter 5 with two E_{010} mode cascaded cavities. The first one (A) 7 cm long, the second one (B) 10 cm long and separated from the first by a 0.5 cm air gap, but probably 1.5 cm electrically because of the effects of the end-caps. Both cavities are controlled by copper resistance thermometers and Airmec N299 temperature controllers with glass fibre insulated heating coils. The top cavity has a loaded Q of 4,000, the bottom one 6,000.

Figure 2 is a representative selection of the S-T patterns obtained for constant beam nozzle pressure and various separator potentials. It is seen that at high potentials (Figure 2a) the trace is similar to that in 1a with Higa beats in the regions A-B and A'-B'. As the

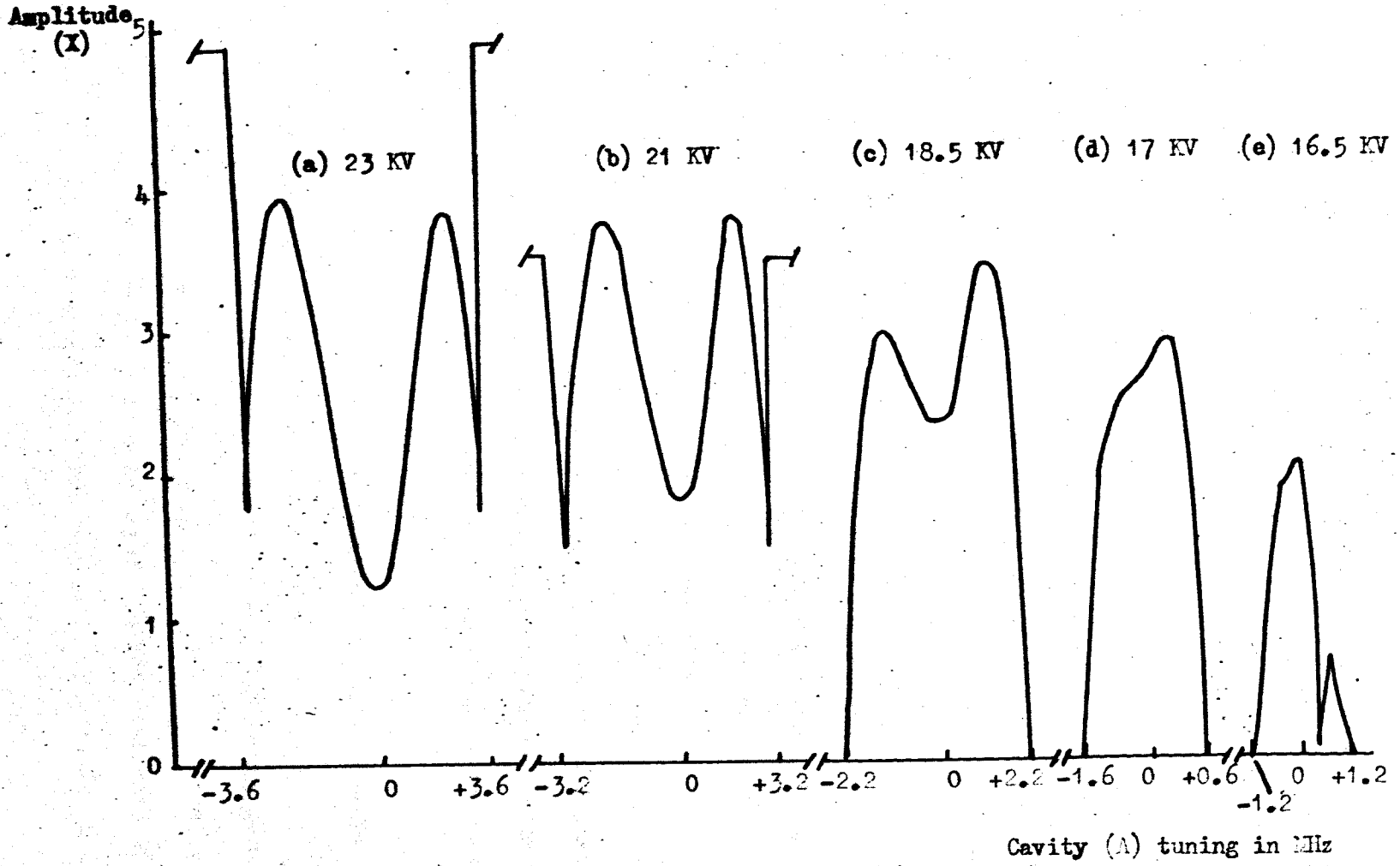

Figure 6:2

S-T curves for various separator potentials. All for 1.3 torr beam pressure

separator potential is reduced, the wings (A and A') are reduced in size (Figure 2b) but the central peaks C and C' remain almost constant in amplitude. As the flux is reduced further the wings disappear altogether (no single cavity oscillation in B) and eventually the central dip D disappears. This behaviour is plotted in Figure 3 (for another set of results). Two points are worthy of further notice, first, the amplitude C saturates. This is contrary to the results of Basov et al[358-359] but agrees with the results of reference 357. Second, the amplitude D tends to zero at high beam flux, which is not what Basov et al claim, but their results appear to be somewhat internally inconsistant, but can be reproduced if cavity B is slightly detuned, see Figure 4b. This was obtained with a slightly detuned B cavity, and it seems to match Figure 3 of reference 358 and Figure 7 of reference 359. It may be noted from Figure 2 that the width of the S-T pattern varies with flux. At high flux, with high separator potential, cavity A will oscillate over a greater detuning range than at low flux. Figure 4a is a graph of the variation of the S-T pattern width A-A' with separator potential V. The width values are determined by the settings of the temperature control unit and the assumption of 0.4 MHz per ^{o}C frequency change of the cavity.

The Higa beat frequencies have been examined by photographing the calibrated oscilloscope screen. As might be expected from the cavity frequency pulling equation (47 of Chapter 5) as the A-A' width gets greater so the Higa beat frequency increases. Beats take place over the ranges A-B and A'-B' varying both in amplitude and frequency with the amplitude of oscillation (X) in these regions. Figure 5a is a

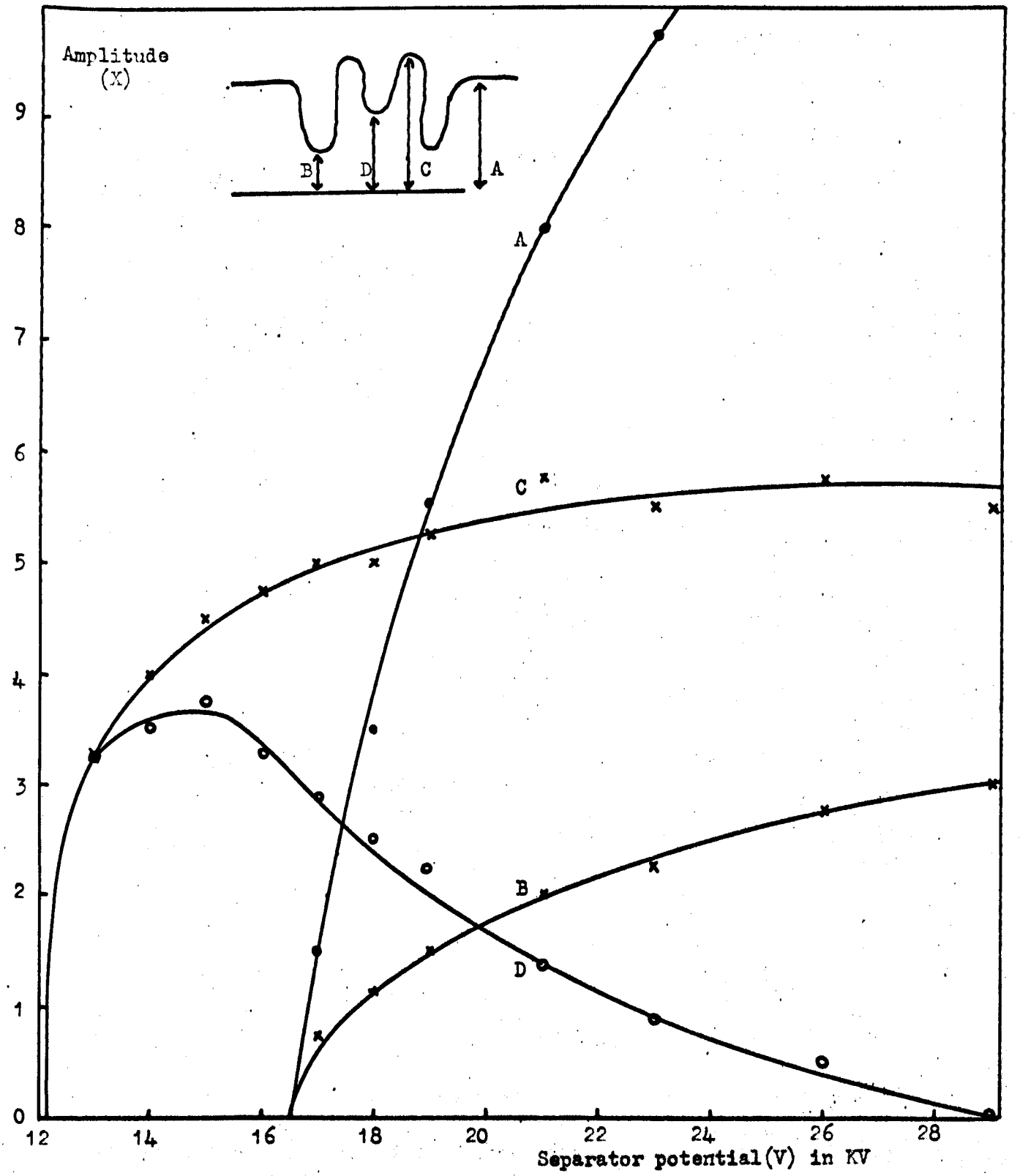

Figure 6:3

The variation of various key portions of the S-T curves with seperator potential,for 1.2 torr beam pressure

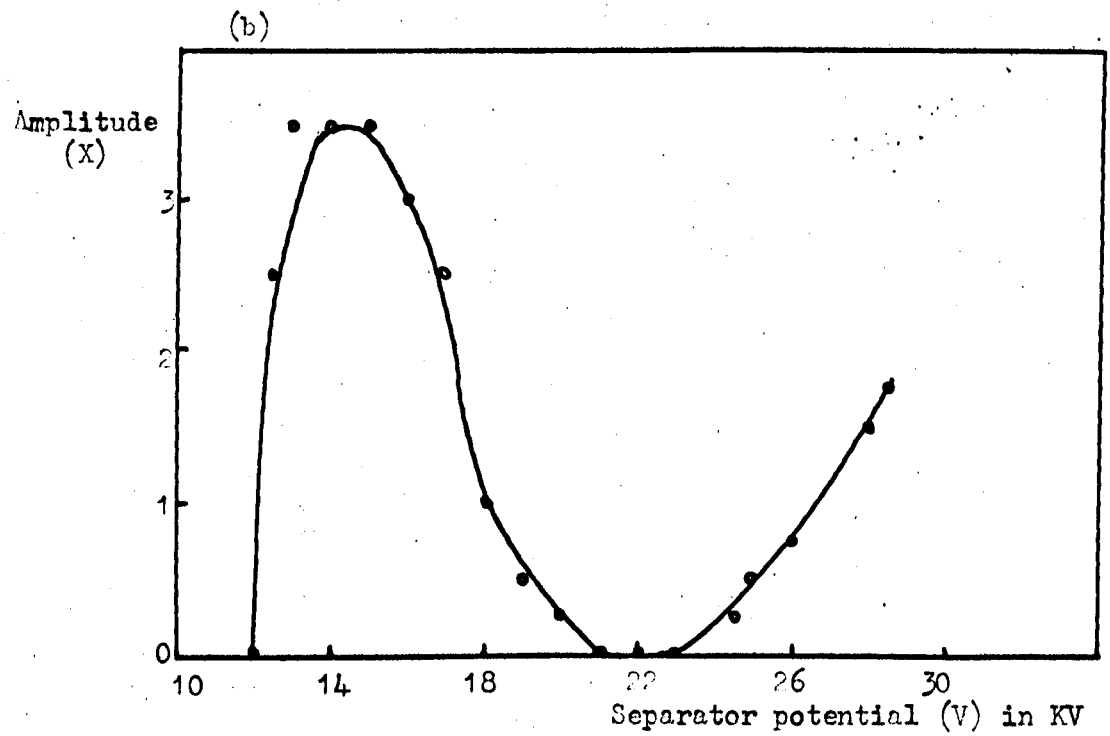

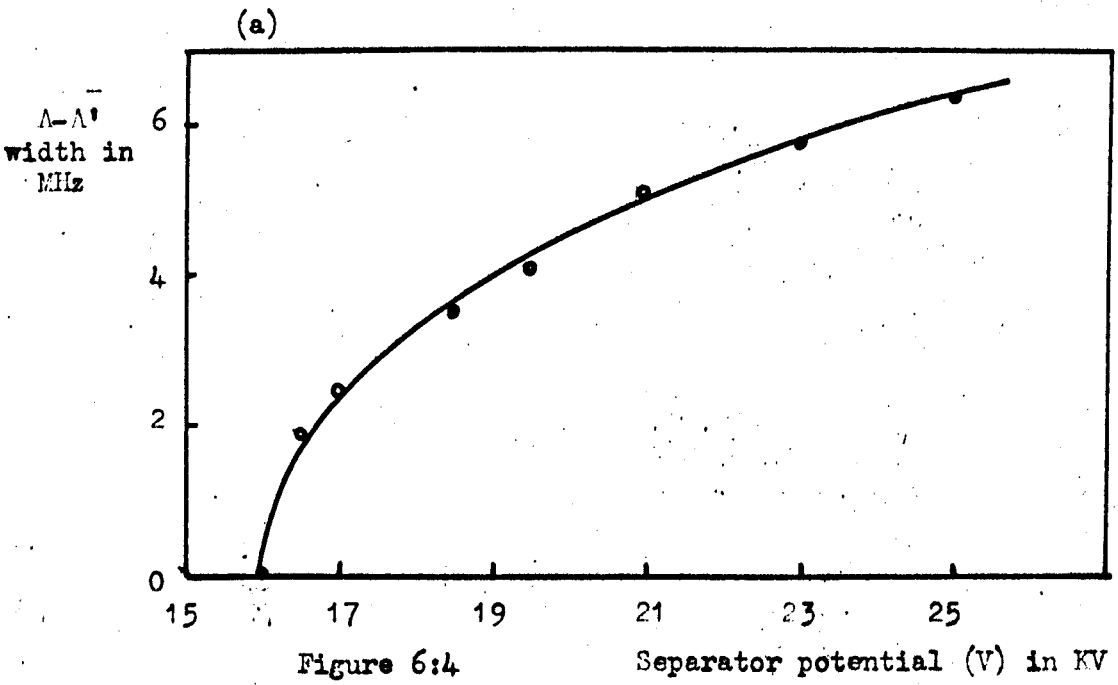

Figure 6:4

(a), Width of S-T pattern(Λ-Λ') variation with separator potential with 1.3 torr beam pressure. (a), See text, for 1.5 torr beam pressure

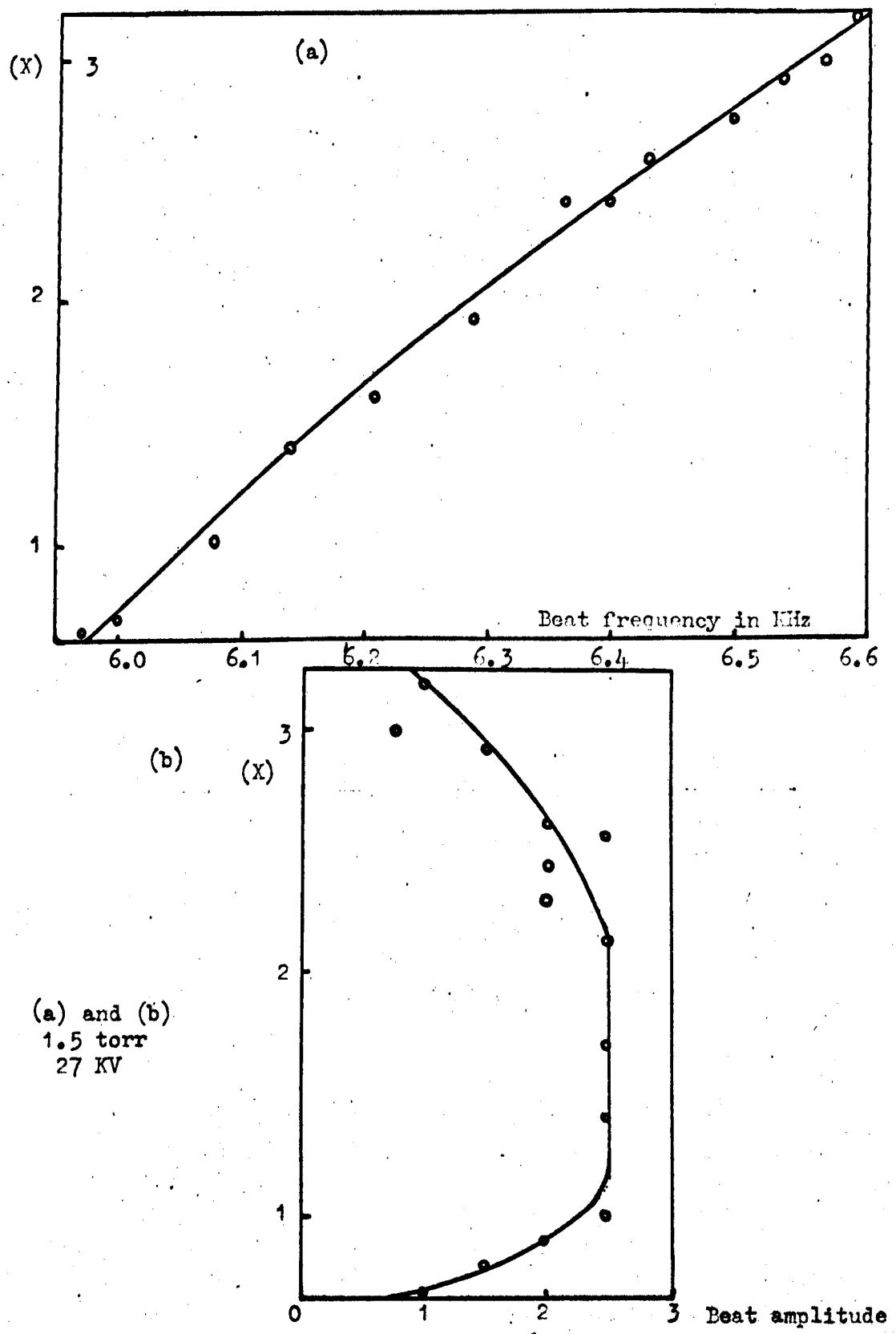

Figure 6:5

(a), Variation of Higa beat frequency with maser amplitude (X)
(b), Variation of Higa beat amplitude with maser amplitude (X)

plot of (X) in the region A-B and the frequency of the beats. The beat frequency increases with amplitude (greater detuning); it is interesting to note that this variation is nearly linear. Figure 5b is a graph of the amplitude of the beats variation with (X), it is apparent that the beat intensity reaches a maximum when (X) is 25 to 75% of maximum, the beat peak to peak amplitude is then about 25% of the maximum value of (X), A.

Since the width of the S-T pattern A-A' varies with separator potential it should be possible to sweep through portions of it without sweeping the cavity frequency. Thus if cavity A is tuned just outside A (or A') and the separator E.H.T. is increased, the effective width of the S-T pattern increases and the Higa beat region A-B together with some of the region B-C can be plotted out (see Figure 6a).

If the two cavity maser is to be used as a frequency standard, then it is essential that the effect of detuning the bottom cavity on the signal frequency and amplitude should be known. It has been established that the frequency varies by less than one part in 10^{12}, but no quantitative results of the amplitude change have been published. Figure 7 is a series of graphs of the amplitude of oscillation (X) in the bottom cavity for different tunings of both cavities. It is apparent that the amplitude of oscillation is far less dependent on correct tuning of the second cavity than for the single cavity case. Thus a single cavity maser detuned by about 3 MHz would cease to oscillate (at ~ 24.5 KV), whereas the second cavity of the 2 cavity

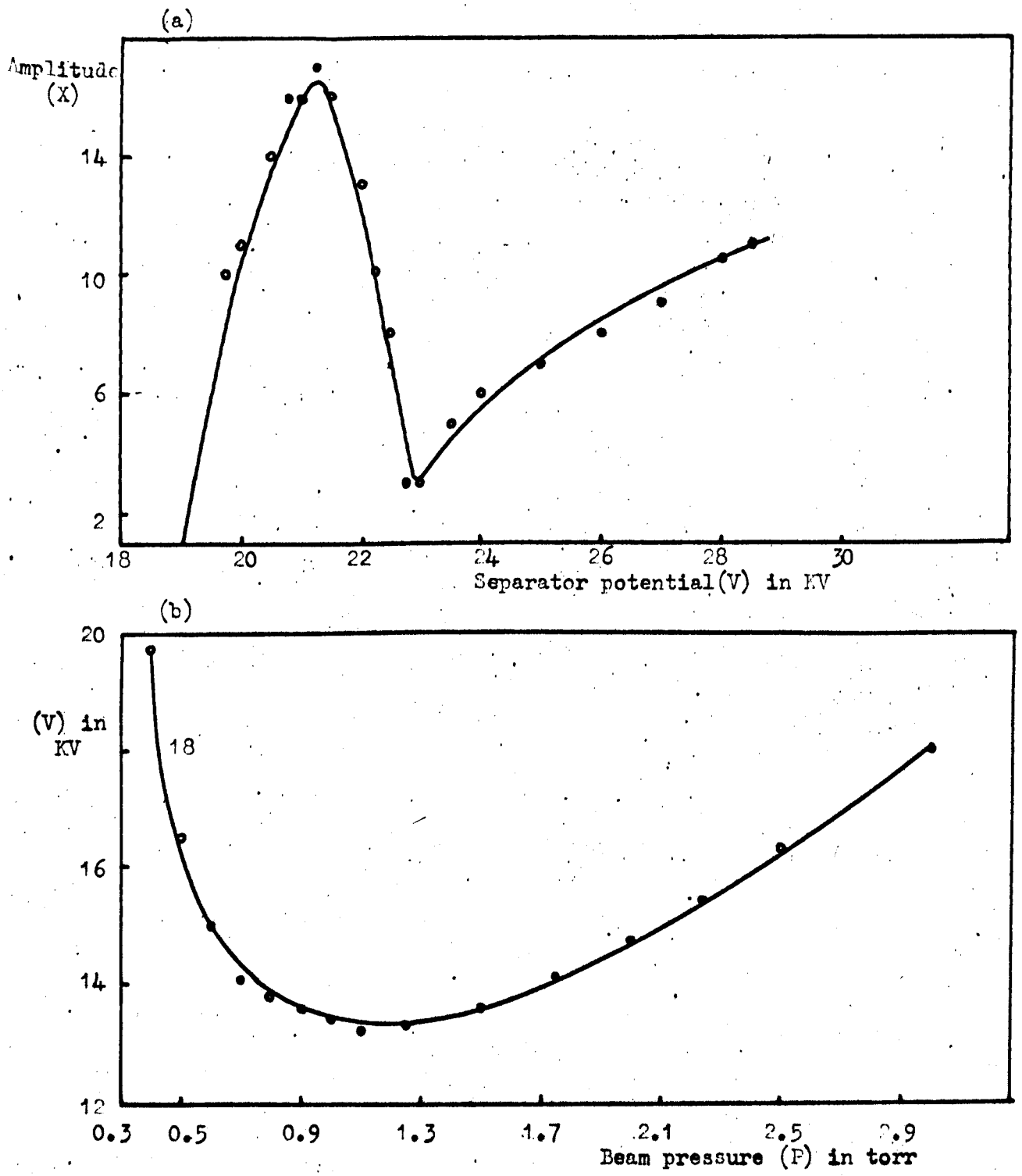

Figure 6:6

(a), Maser amplitude (X) variation with E.H.T. for cavity (A) set at S-T position A for low separator potential

(b), Threshold of oscillation plot for both cavities tuned to $f=f_o$

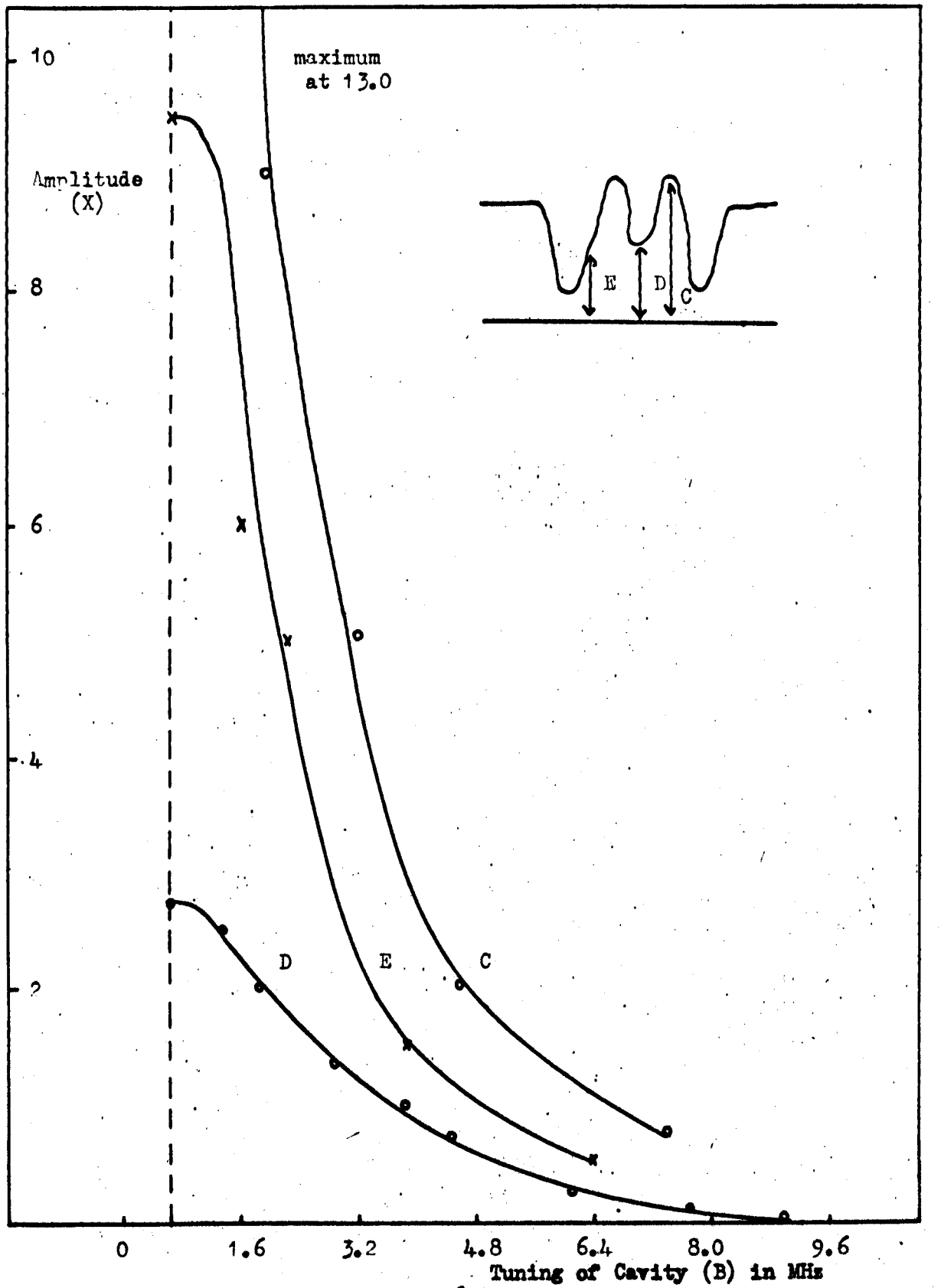

Figure 6:7

Cavity(B)detuning,amplitude(X) variation for 24.5KV separator potential and 1.4 torr ammonia beam pressure

system can be detuned by this amount and the output is only reduced by 50%. The cavity B has to be detuned by about 9 MHz for the power output to approach zero.

For the two cavity beam frequency standard both cavities would probably be tuned to the line centre, so as to reduce frequency pulling effects. Thus it is important to know the variation in output with changes of various parameters, such as separator E.H.T. and beam nozzle pressure, when both cavities are accurately tuned to the line centre. (This accurate tuning can be achieved by the following procedure. First approximately tune the bottom cavity, then sweep the top cavity through the S-T pattern; if the amplitudes B and B' are very different adjust the setting of cavity B and repeat the procedure. When the pattern is approximately symmetric set cavity A on the central minimum (D) of the S-T pattern, then increase the E.H.T. If the bottom cavity is on tune the amplitude should decrease, if it goes through a minimum then cavity B is still incorrectly tuned.)

With both cavities accurately tuned to the line centre three sets of characteristics have been measured. First the threshold of oscillation characteristic for different separator potentials (V) and beam pressures (P). Second, the amplitude of oscillation (X) variation with (V) for fixed values of (P). Third the (X) variation with (P) for fixed values of (V). Figure 6b shows the starting flux (threshold of oscillation) graph for different values of separator potential (V in KV) and ammonia beam nozzle pressure (P in torr); it can be seen that the lowest separator potentials are required for values of

P from 1.0 to 1.5 torr. Figure 8 is the amplitude of oscillation (X) variation with separator potential for four values of beam pressure (0.9, 1.3, 1.8 and 2.25 torr). It is seen that although the lowest threshold potential occurs for nozzle pressures in the region of 1.0 to 1.5 torr, maximum amplitude can be obtained with slightly higher pressures (~ 1.8 torr). Figures 9a to h indicate that the situation is rather more complicated, these are plots of amplitude (X) versus beam pressure (P) for different values of separator potential. For low potentials there is a single peak which at higher potentials splits into two peaks with the minimum value becoming more prominent and shifting to higher beam pressures as the separator potential (V) is increased. As the pressure is increased from a low value the onset of oscillation is very sharp, presumably due to large amplification in cavity B. These results do not agree very well with the rather more limited results of Basov et al[358-359] (which appear to be those of Strakhovskii and Tatarenkov[357] with changed separator potential values).

The effect of electric and magnetic fields on the system have not been examined in detail (see Basov et al[358-359]). Several other effects have been noted. First, with the high flux S-T pattern, the wing A' (at the high temperature end of the cavity sweep) sometimes has a smaller amplitude than A. This does not seem to be due to outgasing or other pressure effects, nor due to mistuning of cavity B, see section 6 below. Second, if the cavity B output is observed using the unstabilised superheterodyne mode of operation, then for certain flux values (with the 2 cavity system at A' in the S-T pattern)

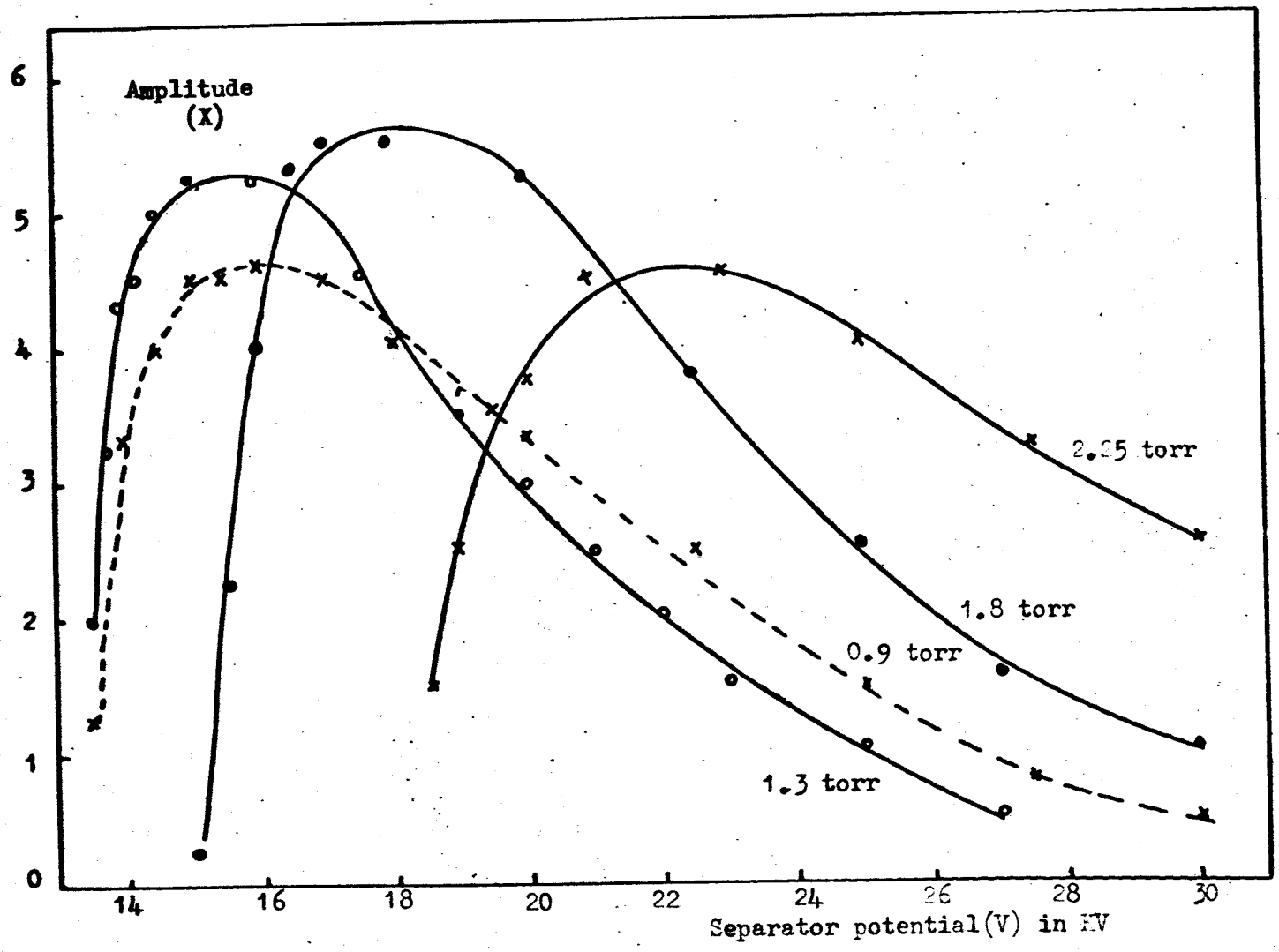

Figure 6:8

Both cavities tuned to f_o. Amplitude of oscillation(X) variation with separator potential for various beam pressures

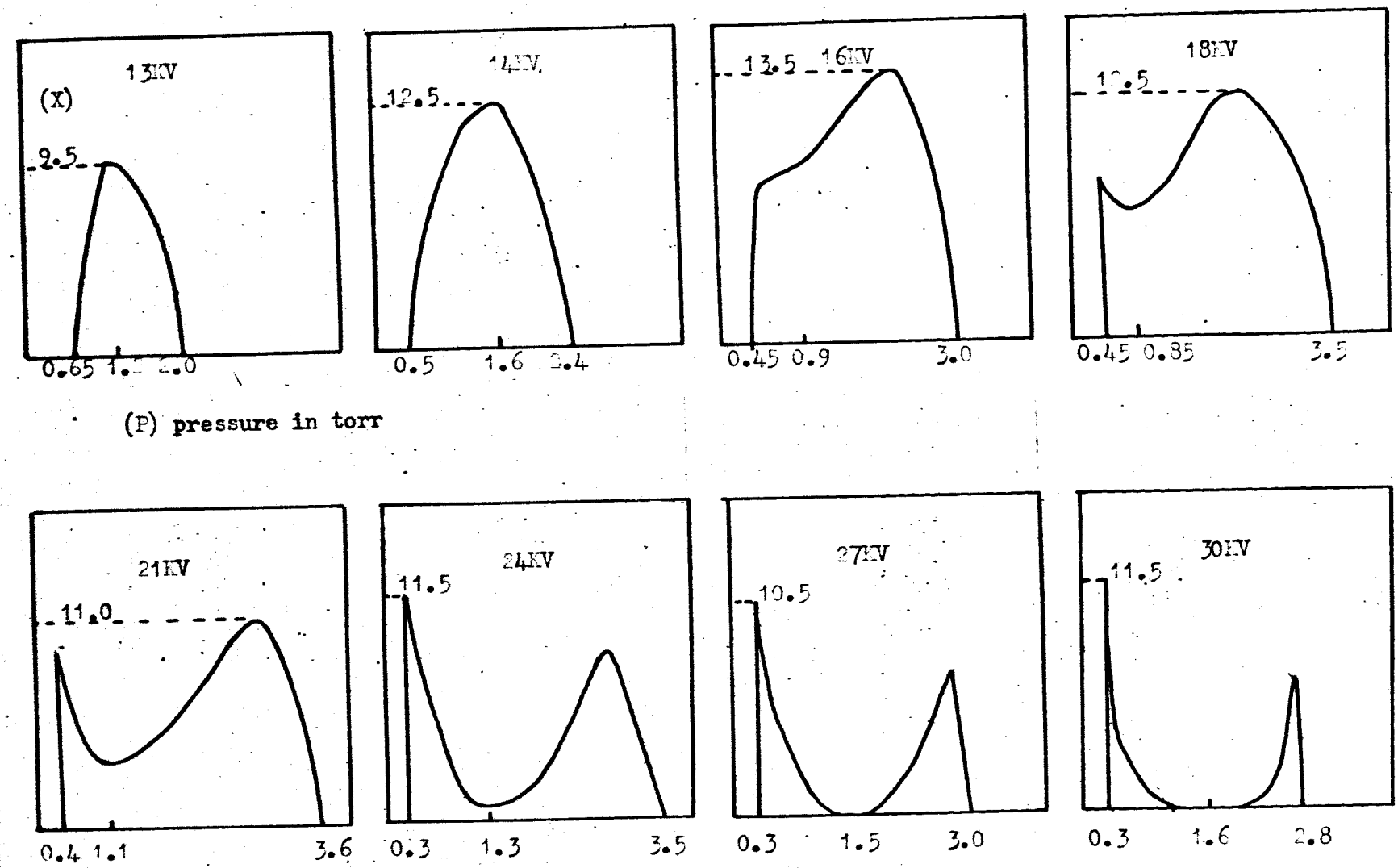

Figure 6:9

Both cavities tuned to f_o. Amplitude of oscillation(X) variation with beam pressure for various separator potentials

as the separator potential is increased a small signal appears and then disappears before the main signal appears. This initial signal seems to be offset in frequency by 3 ± 2 MHz from the main line. Unfortunately it was not possible to repeat the phenomenon often enough to accurately identify it. Third, again at threshold as the signal increases from noise, there appears to be a 'pulsation' of period about one second, which dies out when the signal is about 2x noise (this is also observed, to a lesser extent, with single cavity operation).

6:3 Separator Modulation and Sensitivity[361]

The effects observed, and velocity and sensitivity measurements obtainable by modulating the separator potential at a low audio range frequency for a single cavity system have been described in section 6 of Chapter 5. A similar electronic method can also be used to observe the sensitivity of the two cavity maser system over the complete S-T tuning range. A sinusoidal 70 volt peak to peak 30 Hz signal is coupled via an E.H.T. capacitor to the state separator high tension rods. The modulation of the amplitude of oscillation is detected with the phase sensitive system (see Figure 10).

Figure 11 consists of traces of the phase detected output (Y) for tuning of the top cavity (A) through the S-T patterns. 11a is obtained for high values of flux corresponding to the high flux S-T pattern. 11b corresponds to the low flux S-T pattern and 11c corresponds to the very low flux S-T pattern (just above threshold) when the central minimum, D in Figure 2, has disappeared. Two points should

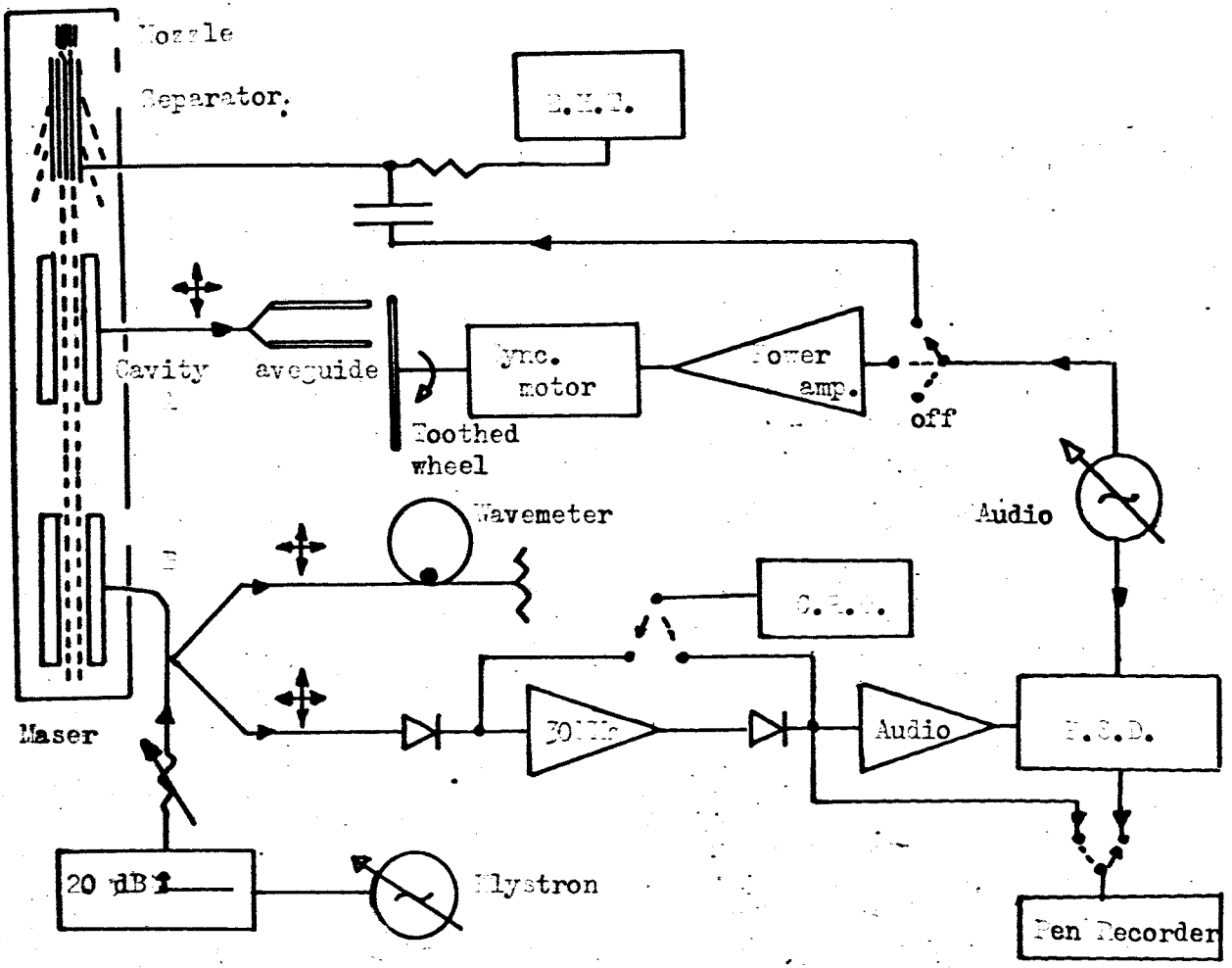

Figure 6:10

Block diagram of circuit for modulation experiments

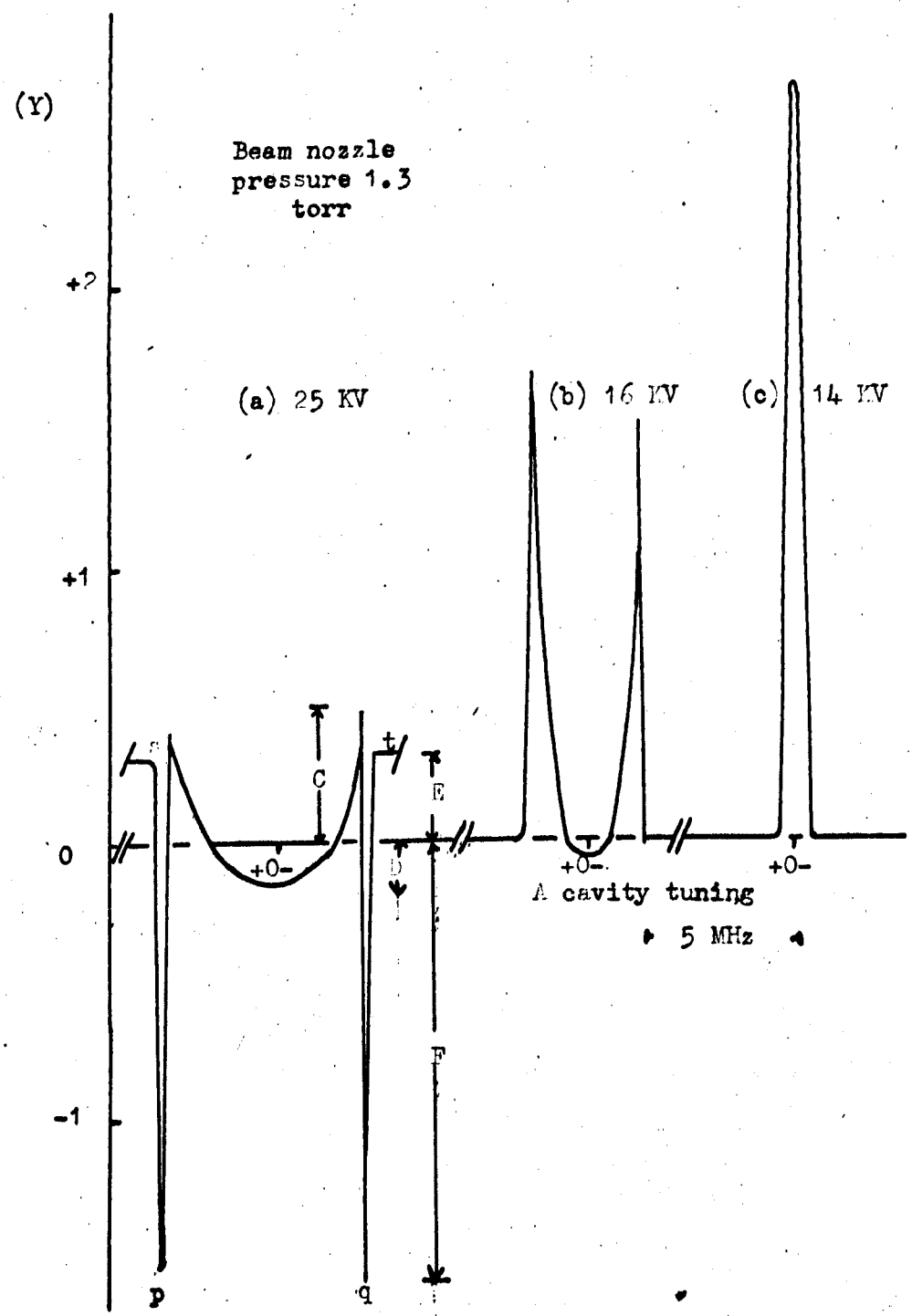

Figure 6:11

Phase detected separator modulation(Y) for tuning of Cavity(A) and different separator potentials

be noted, first, the amplitudes of the wings at s and t correspond to the normal single cavity case. Second, the phase of the output signal (Y) changes for portions of the S-T sweep from that experienced for the single cavity case.

Figure 12 is a graph of the amplitude and phase of various portions (of particular interest) of the sweep curves for variation of the separator potential. The various curves correspond to portions of the sweep curves as labelled in Figure 11a. Three regions I - III have been marked off by broken vertical lines. Region I corresponds to the high flux S-T pattern. Below 19 KV oscillation only occurs in cavity B when cavity A oscillates, Higa beats are not obtained, down to 15.25 KV; this is labelled as region II. Between 15.25 KV and threshold, region III, the behaviour is somewhat complicated. This will be explained in section 4 below. At high flux, in region I, curve E gives the amplitude modulation for single cavity operation and curve F the corresponding level of modulation for the 2 cavity system if it is tuned to the most sensitive operating position on the S-T curve. At low flux, in region II, the most sensitive operation is obtained with curve C, under these conditions a single cavity maser does not operate. Thus a two cavity maser can be operated as a beam flux change detector with greater sensitivity than for a single cavity maser (X4 at least) and at considerably lower flux levels (i.e. 15.5 KV rather than 19 KV separator potential), provided that the cavity of the single cavity maser is some distance from the state separator (8 cm). This would not normally be so, because of beam divergence the cavity

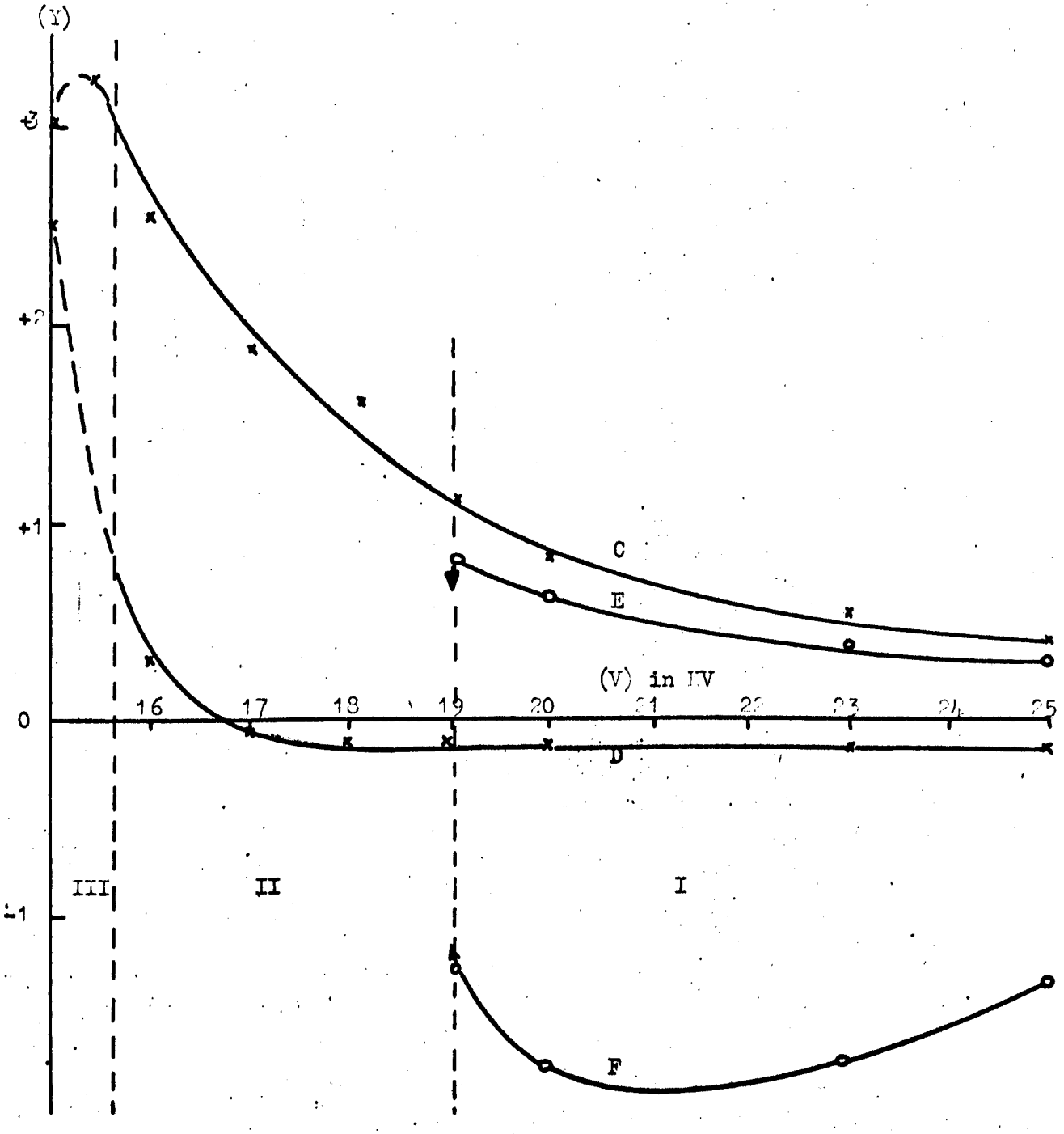

Figure 6:12

Amplitude of modulation (Y) in cavity B for certain key values of tuning of cavity A. The labelling follows from 6:11a

would be situated as close to the beam separator as possible. Thus the two cavity maser should be compared with a single cavity maser with its cavity close to the separator. The advantage of lowered operating flux then disappears, but the sensitivity of operation of the two cavity system is still at least twice that of the single cavity system.

The origin of the curves shown in Figure 11 can be explained as illustrated in Figure 13. Two curves, broken and solid, are drawn for two slightly different values of separator potential (and thus flux) for each of the three situations shown in Figure 11. The solid line corresponds to slightly lower separator potential and hence the S-T patterns are narrower. The differences are much exaggerated (for the small separator potential variation actually used), but the lengths of the arrows illustrate the relative magnitude of the modulation (Y) and the polarity is represented by their direction. Thus the dynamic modulation of the system can be represented as the difference between two static S-T curves and the general shapes of the phase detected modulation curves obtained.

6:4 Low beam flux operation and Cavity Coupling

It was seen in section 3 that as the beam flux is reduced so the central minimum of the S-T pattern (D in Figure 1a) gradually disappears (see Figure 2a - d) but at very low beam flux (just above threshold) the peak splits into two well resolved components (Figure 2e). At even lower flux there is a very small single component line again. The split peak can be obtained over a separator potential range of

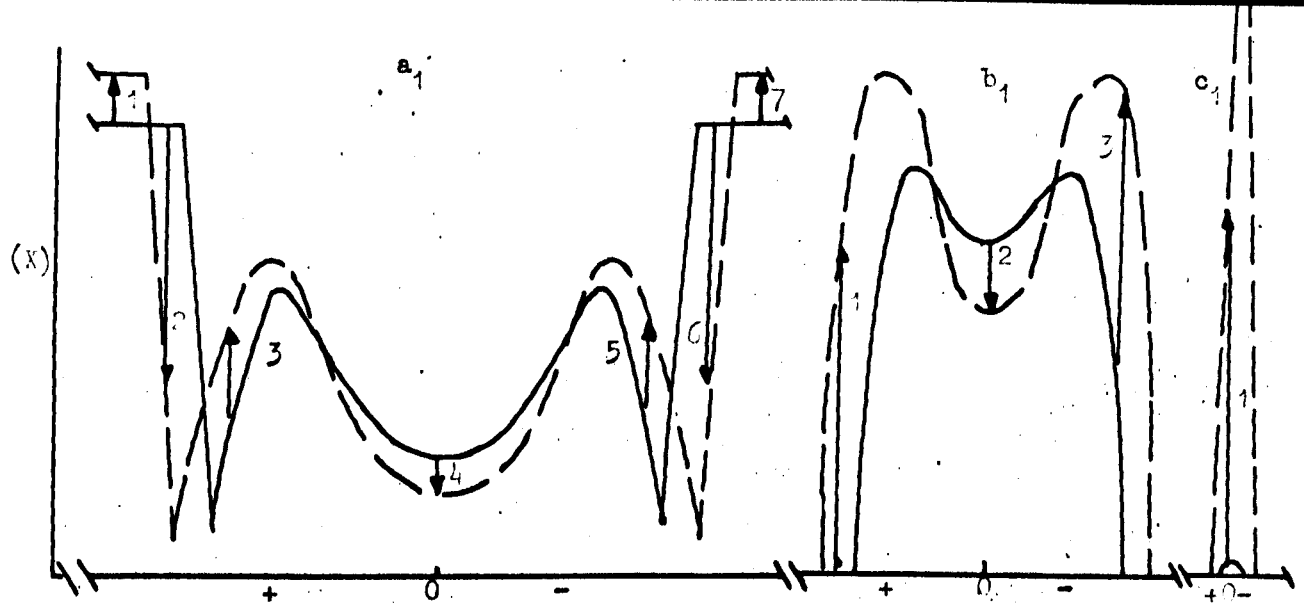

A cavity tuning

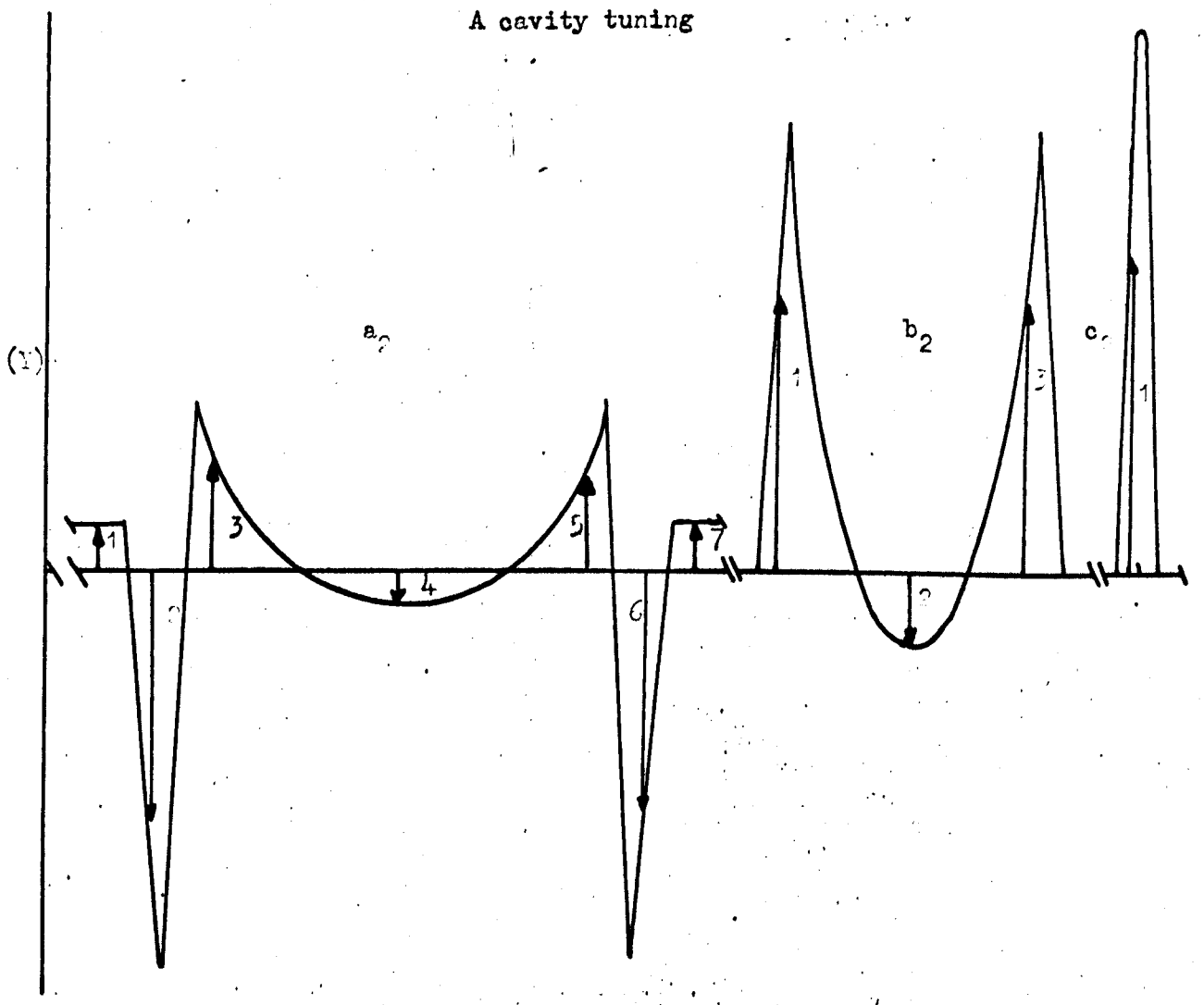

Figure 6:13

Suggested derivation of modulation curve amplitudes(Y) from S-T amplitudes(X)

about 200 volts, and the centre side of the larger component trace is very steep. This splitting leads to the complex behaviour referred to in the E.H.T. modulation experiments, corresponding to region III of Figure 3.

The above double cavity experiments were conducted with no microwave energy coupling between the two cavities except by the molecular beam. (This was tested for by coupling a large amount of power to one cavity and trying to detect it with the other). But if the two cavities, A and B, are strongly coupled by an external waveguide system the normal S-T patterns are not obtained. It is found that new and different behaviour takes place when more than about 50% of the output power is coupled from cavity A to cavity B. If the coupling is much less than this, the S-T pattern is not changed. The patterns obtained are quite complicated and have been rather difficult to observe accurately because of the lack of a calibrated K-band phase shifter or adequate directional couplers. However, using variable lengths of waveguide and 'magic T' coupling it would appear that the patterns observed are similar to Ramsey[362-363] separated field systems. Such an effect might be expected to arise when the field phase in cavity B is directly determined by the phase of the oscillation in cavity A, and not by the phase of the molecular beam passing from A to B. The following characteristics are those obtained for a phase adjustment between cavities which most closely correspond to the normal Ramsey patterns.

Figure 14 is a series of traces of the output amplitude (X) of cavity B as cavity A is frequency tuned across the molecular response

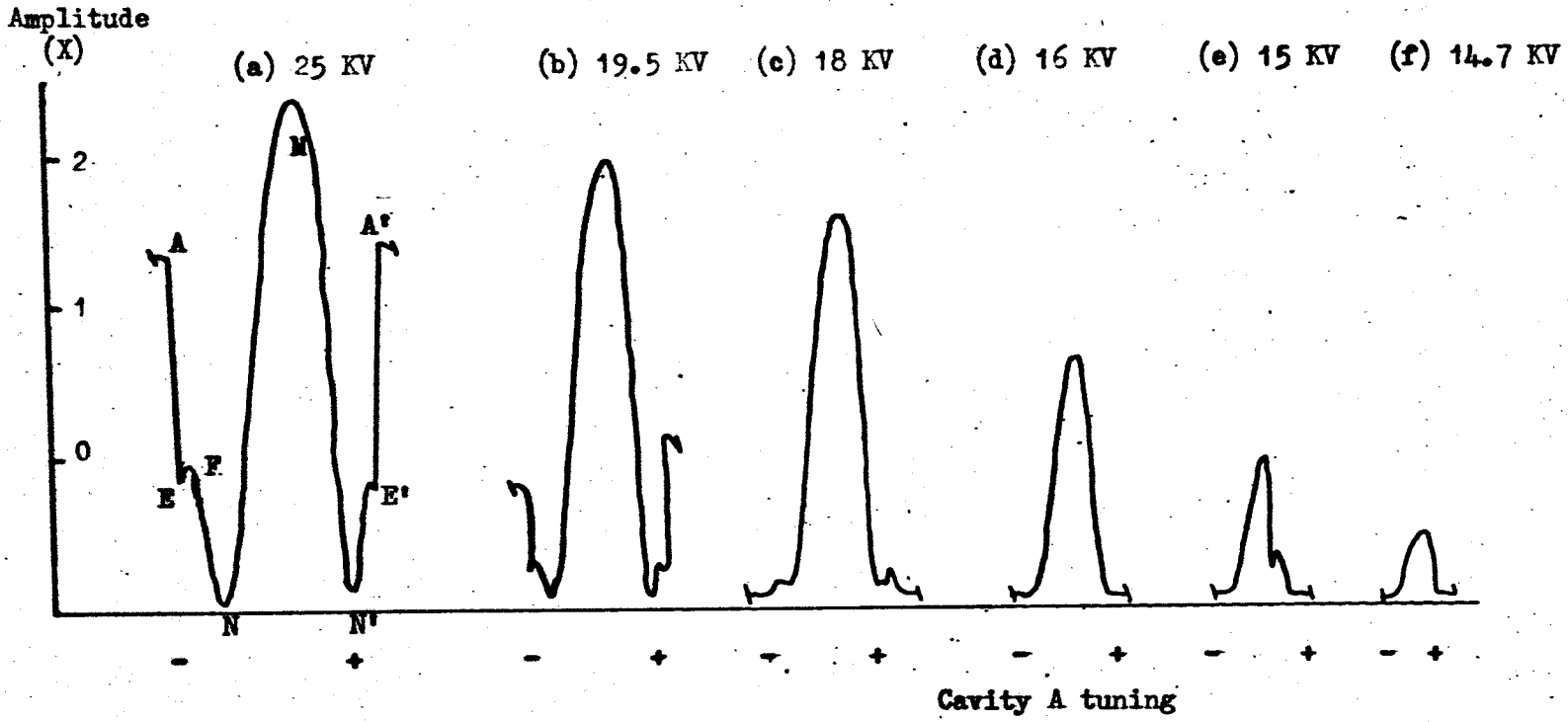

Figure 6:14

Suggested Ramsey 180° phase shift patterns, for variation in cavity A tuning

for what is similar to the 180° out of phase condition. It can be seen, Figure 14a, that at A the Higa beats start as usual, but at E they cease, presumably because the separate oscillations of the two cavities have become locked together to the frequency of the cavity (A) oscillation, and they stay locked together until the sweep reaches E' when the Higa beats recommence. Figures 14b - f correspond to lower separator potential curves and it can be seen that the split line is produced at low flux. Figure 15 is a series of graphs which show the behaviour of various portions of the sweep curves for a variation of spearator potential. It may be noted that the centre peak M appears to saturate (which is not so for the S-T pattern or for the single cavity maser) and that the separation of the two subsidiary peaks increases with separator potential. Now according to Ramsey the separation between the subsidiary peaks is given by

$$1.22 = \frac{L\Delta f}{\alpha} \qquad 5$$

where L is the separation of the oscillating fields, α the most probable molecular velocity and Δf the frequency of oscillation difference between the centre line and either subsidiary peak. This assumes that the phase of the two fields stays constant, assuming that that is so for the present system and realising that with the present system with the oscillating fields so close together it is difficult to choose an accurate value for L, but if L = 1.5 cm and α = 7,500 cm/sec, then the subsidiary peaks should be about 6 KHz away from the centre peak. In practice they vary from about 4.5 KHz to 7 KHz according to

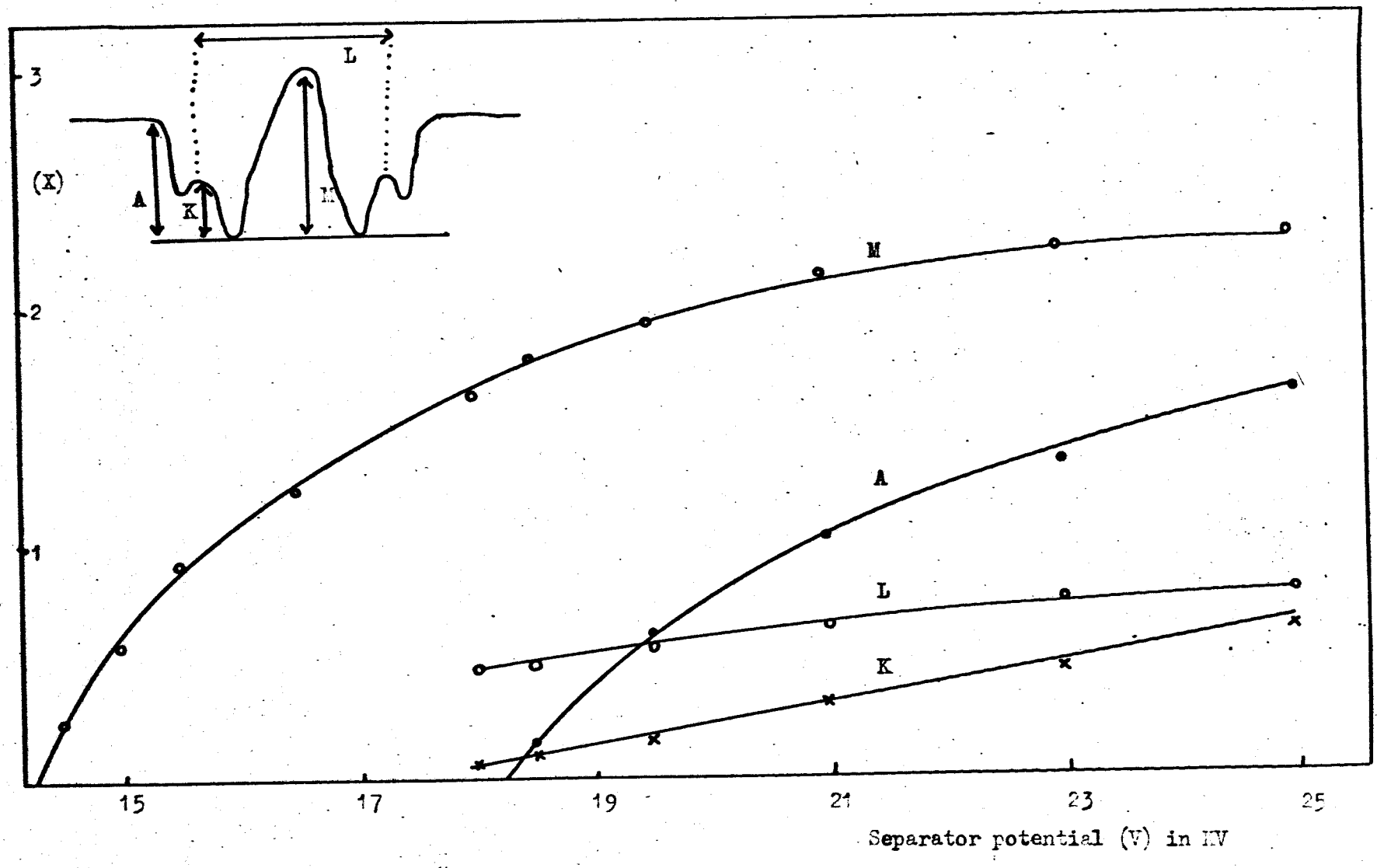

Figure 6:15

Amplitudes of various key values of suggested 180° Ramsey patterns. Beam pressure 1.3 torr

separator potential (and hence average beam velocity).

Figure 16 plots two graphs of amplitude of oscillation (M) versus beam pressure (P) for two different separator potentials, 18 and 24 KV, for the supposed 180° Ramsey patterns. It is probable that the maximum and subsequent decrease of (M) is due to beam collisions and a general increase in background pressure.

All the above results have been for two cavities probably being 180° out of phase, the other Ramsey phase situation which has been considerably studied is the 90° phase diffence situation. Inset in Figure 17 is a typical (fairly high flux) lower cavity amplitude output curve as the top cavity is swept across the molecular response. In the region A-E Higa beats, then a smooth double peak response is traced out until E' is reached and the Higa beats recommence. It is thought that at E the amplitude of oscillation in cavity A is sufficient to lock the B cavity phase to 90° from that of cavity A and that they stay locked between E and E'. Graph 17 (N) shows that the central dip decreases in relative intensity as the beam flux is increased, this is the reverse of what happens to the centre dip of the uncoupled S-T pattern.

It was mentioned in section 6:3 that at very low flux the single S-T peak for externally non-coupled cavities split into two components (Figure 2e). This splitting was also observed with the coupled cavities, as mentioned earlier in this section (Figure 14e). However, what was not mentioned was that the two lines are not now completely resolved and that there is a region of overlap (Figure 18a) and that

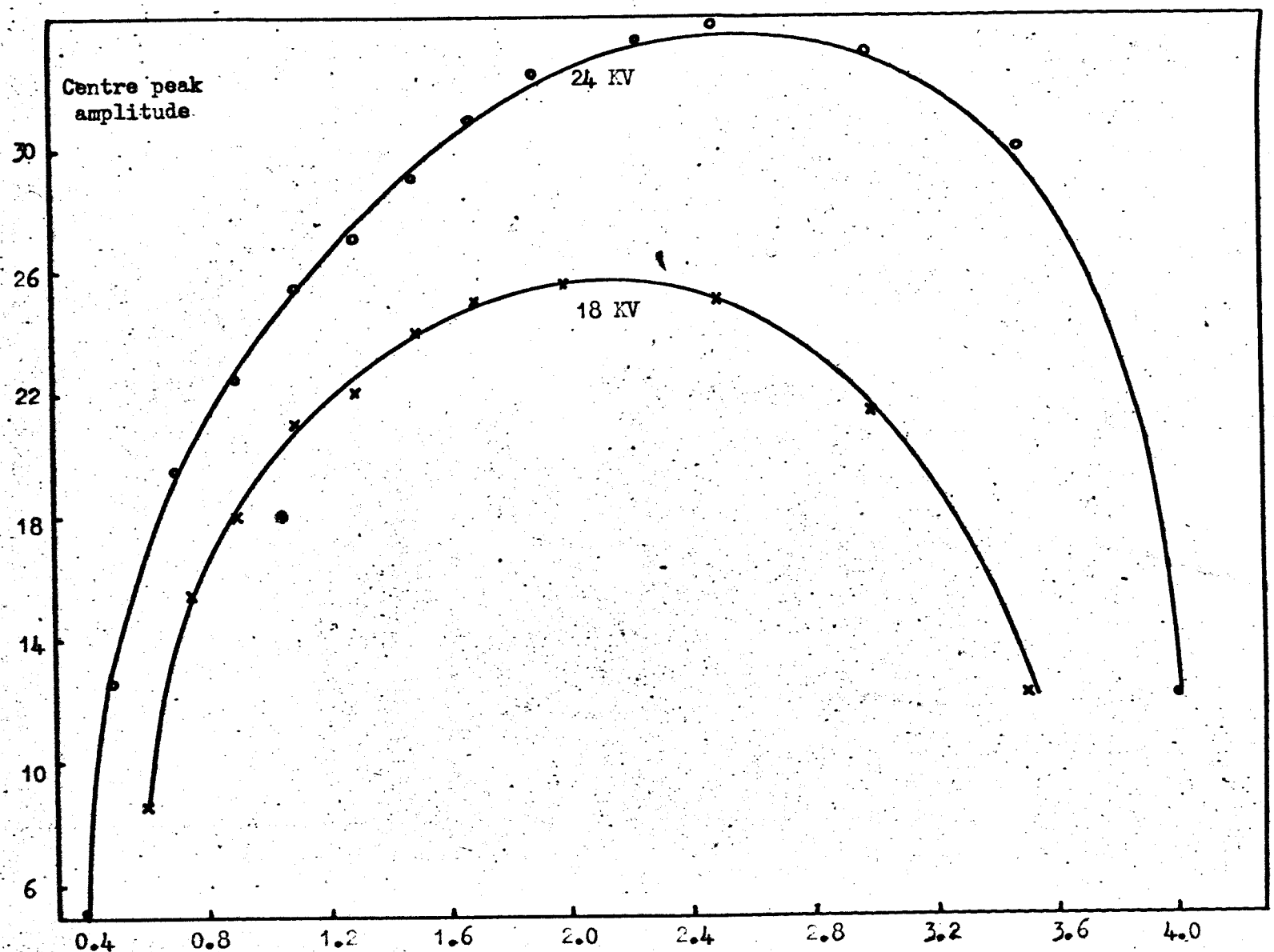

Figure 6: 16

Centre peak amplitude of suggested Ramsey 180° pattern, variation with beam pressure for 18 and 24 KV

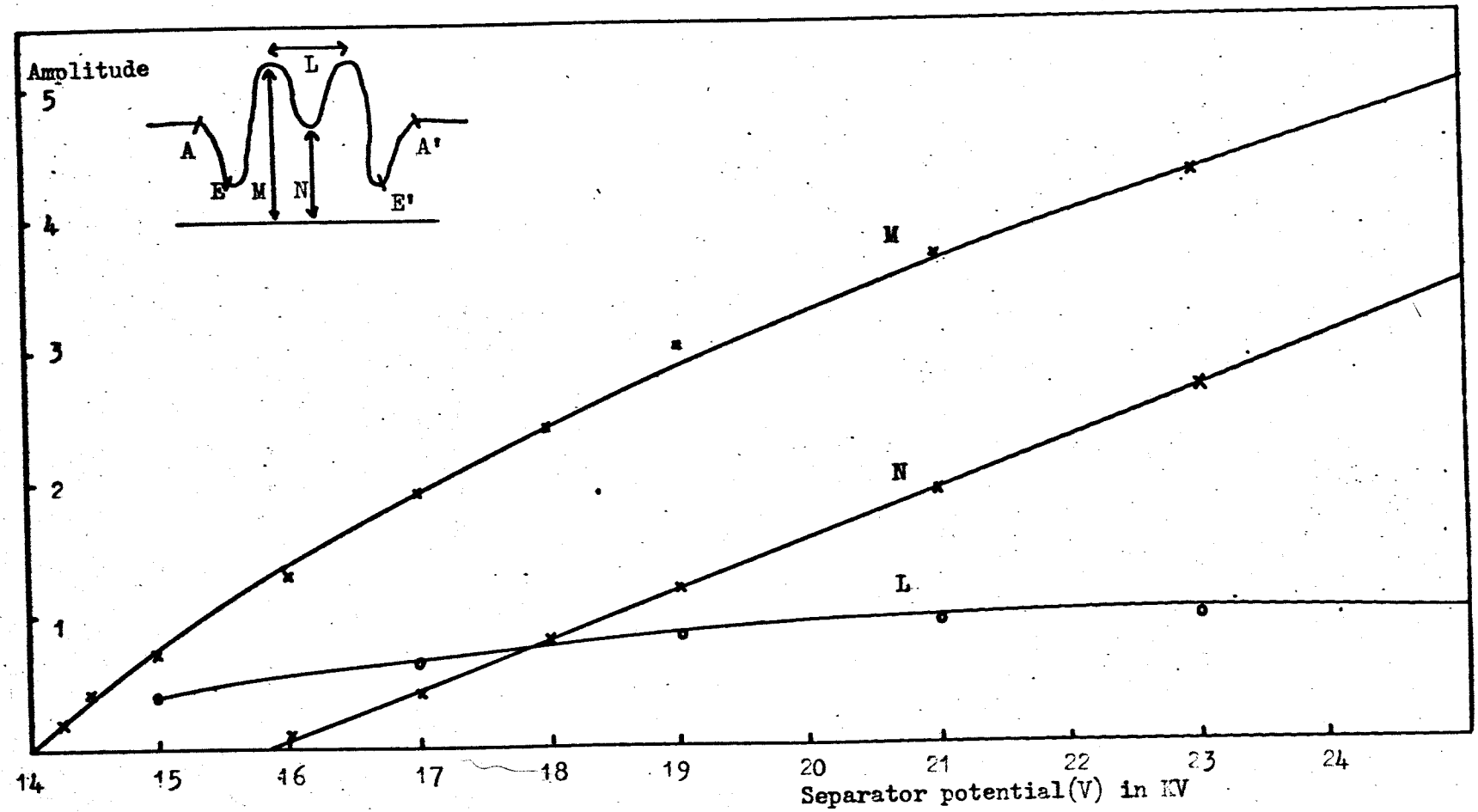

Figure 6:17

Amplitudes of various key values of suggested 90° Ramsey pattern, variation with (V) for 1.4 torr ammonia

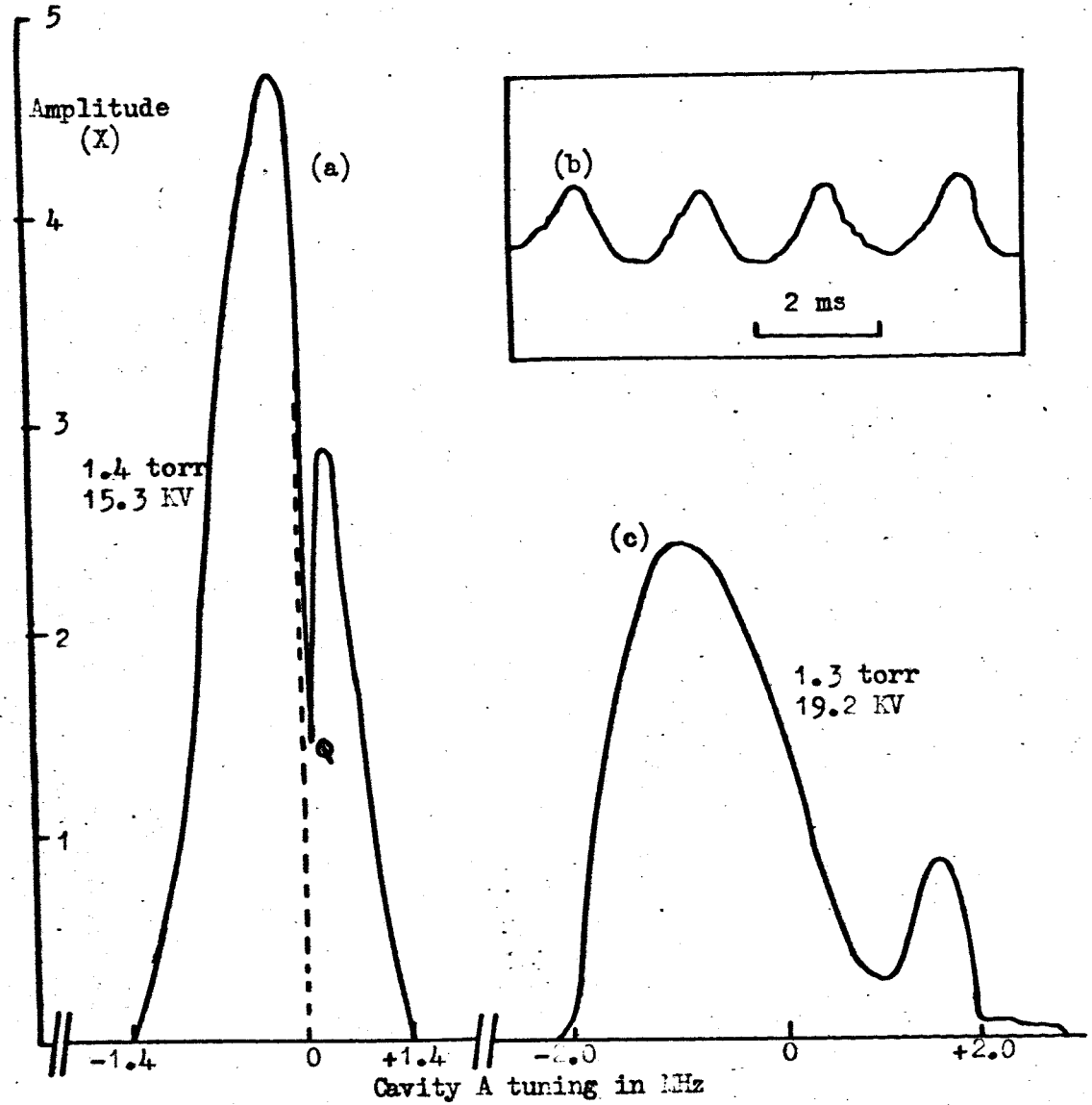

Figure 6:18

(a), and (c), Suggested hyperfine structure of ammonia. (b), beats between hperfine components

in addition amplitude modulation (18c) of the maser oscillation occurs which changes smoothly through the frequency range 300 to 1,000 Hz as cavity A is tuned through a critical point corresponding to the oscillation amplitude minimum (point Q on Figure 18). Further, if the matching to the top cavity is appropriately adjusted the low frequency amplitude modulation is quenched and a smooth response curve obtained (Figure 18b). The splitting between the peaks can be changed by up to 50% by applying a small magnetic field perpendicularly to the axis of the lower cavity. The separation increases with field until a maximum is reached, and then decreases. If too large a field is used the oscillation is quenched.

It is thought that both the splitting of the curve and the amplitude modulation effect may be explained if the hyperfine lines corresponding to the $J = K = 3, \Delta F = 0, \Delta F_I = 0$ inversion transition are at least partially resolved[364]. As was seen in section 5 of Chapter 3 (fig 4a (f.p.55)) this transition is composed of three lines: $F_I = 3$, 4 and 2 in order of increasing frequency; the weighted average frequency of these components after state separation is taken as f_o. As was seen in section 7 (p60 of) Chapter 3, in thermal equilibrium the populations of these three levels are in the ratios, 847 : 1225 : 640, but state separation is far more efficient for high M_J state molecules[34], such that after state separation the relative strengths of these lines in emission are in the ratios 1 : 0.92 : 0.05, so the weak $F_I = 2$ component may be ignored. The frequency difference between the $F_I = 3$ and $F_I = 4$ lines was discussed in section 5 of Chapter 3, p54-7.

It was seen that the best available value is 1.25 ± 0.3 KHz. If these hyperfine lines are to be resolved the average effective velocity of the molecules must be less than about 1.5×10^4 cm/sec, by consideration of the time of flight through both cavities. This velocity is consistent with the value of 5.5×10^3 cm/sec obtained in the last section of Chapter 5 for near threshold of oscillation conditions. This argument is supported by the fact that the splitting is only obtained at low beam flux, when this low average velocity is evident. Further, the longitudinal doppler effects due to travelling waves (which increase with cavity length) are reduced since two short cavities with isolated microwave fields are used rather than a single long one of equivalent total length.

The oscillation frequency in cavity A (and thus in B due to ringing) starts at a frequency near that of the strong $F_I = 3$ line when A is initially tuned below f_o. As A is tuned to a higher frequency the maser oscillation is pulled nearer to the frequency of the $F_I = 4$ line. Thus the maser derives its oscillation energy first from one hyperfine component, then from the other as cavity A is tuned, which would account for the variation in oscillation power as shown in Figures 2e and 18a. The smaller amplitude component is obtained over a narrower tuning range and is on the high frequency side of the larger component. This provides evidence that the smaller smaller component owes its origin to the weaker $F_I = 4$ line and the stronger to the $F_I = 3$ line. (These results should be compared with those of Poluj, Daams and Kalra[288], but they did not fully resolve any structure.)

When A and B are appropriately coupled externally and the resonant

frequency of A is increased from the low frequency side the oscillation power in B predominately due to the $F_I = 3$ line decreases rapidly as the emission from the $F_I = 4$ line increases: and the new oscillation on the $F_I = 4$ line starts before the $F_I = 3$ oscillation is suppressed. Consequently the amplitude modulation observed at Q in Figure 18a may arise from the mixing of these two signals in the non-linearities of the system. The actual beat frequency is determined by the differential frequency pulling effects associated with each component which compete with the tendency for mutual synchronism. A power interdependence of the two oscillations arising from partially resolved lines would account for the modulation frequency being less than the hyperfine splitting and for the departure of the modulation from a sinusoidal waveform, as shown in Figure 18c. In fact the highest value of the beat frequency of 1000 ± 200 Hz agrees reasonably well with the estimate of 1250 ± 300 Hz for the hyperfine splitting.

6:5 Modulation of first microwave cavity

Sher[330] investigated in some detail the properties of a two cavity beam maser used as an amplifier. The signal being coupled into the first cavity and out of the second cavity, with both cavities tuned to f_o. He used the system below oscillation threshold and obtained gains of up to 30 dB and noise figures of about 6 dB. The great advantage of the system as an amplifier was the isolation of the input and output signals. Higa[346] showed that the two cavity maser oscillator would act as an amplifier and the S-T patterns for low beam flux examined in section 6:3 confirm this. In this section the

variation of the amplitude and phase of the output is observed as the cavity A is tuned across the S-T pattern with cavity B tuned to f_o and the field in cavity A is modulated.

The impedance presented by the coupling of cavity A is varied cyclically at 15 Hz by using a mechanical arrangement as shown in Figure 10. A toothed metal wheel driven by a synchronous motor is rotated past the open end of the waveguide coupled to cavity A. The change from a tooth to a slot causes a change of impedance coupled to cavity A. The motor is driven by the frequency reference oscillator of the lock-in amplifier, after amplification in an audio power amplifier. A matching unit in the waveguide between the cavity A and the open end is used to produce equal changes of opposite polarity in the impedance when the wheel turns from a tooth to a slot. This arrangement produces the antisymmetric curve shown in Figure 19.

It is well known that any change in the loading of a maser cavity may pull the oscillation frequency. Thus the origin of the curve shown in Figure 19 may be seen by drawing two S-T curves which are shifted in frequency with respect to each other, corresponding to the limits of the modulation. See Figure $20a_1$ for high flux and $20b_1$ for the low flux condition. The curves a_2 and b_2 may then be constructed by taking the difference in the ordinates of the pair of curves a_1 and b_1, where the direction of the arrows indicate the polarity of the modulation signal. It is found in a static subsidiary experiment that when there is total reflection from a tooth, or zero reflection from a slot, the two S-T curves are tilted in opposite senses. Thus the two outer minima of Figure a_1 are drawn at different levels. This latter result

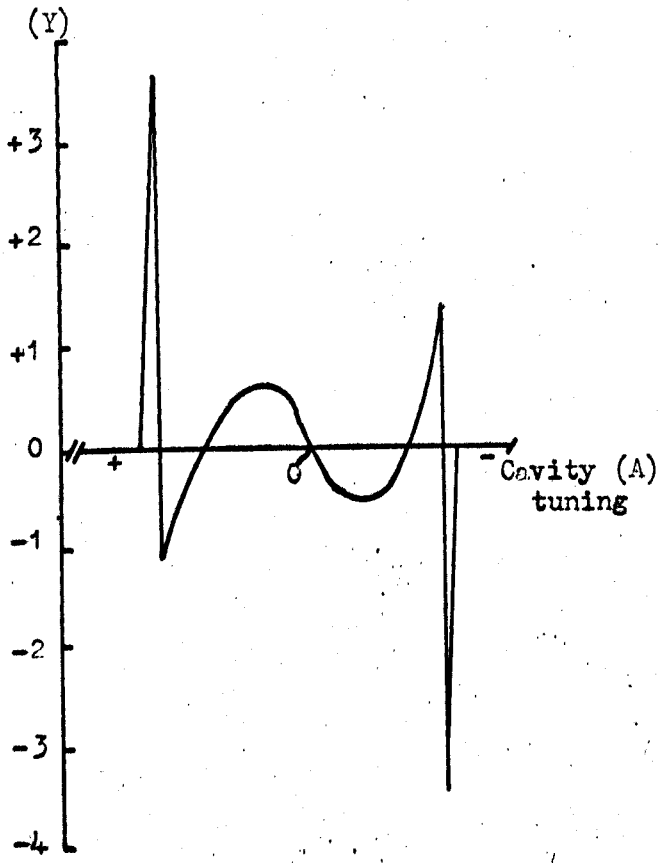

Figure 6:19

Modulation of cavity (A). Output (Y) of P.S.D. as cavity (A) is tuned across the molecular resonance

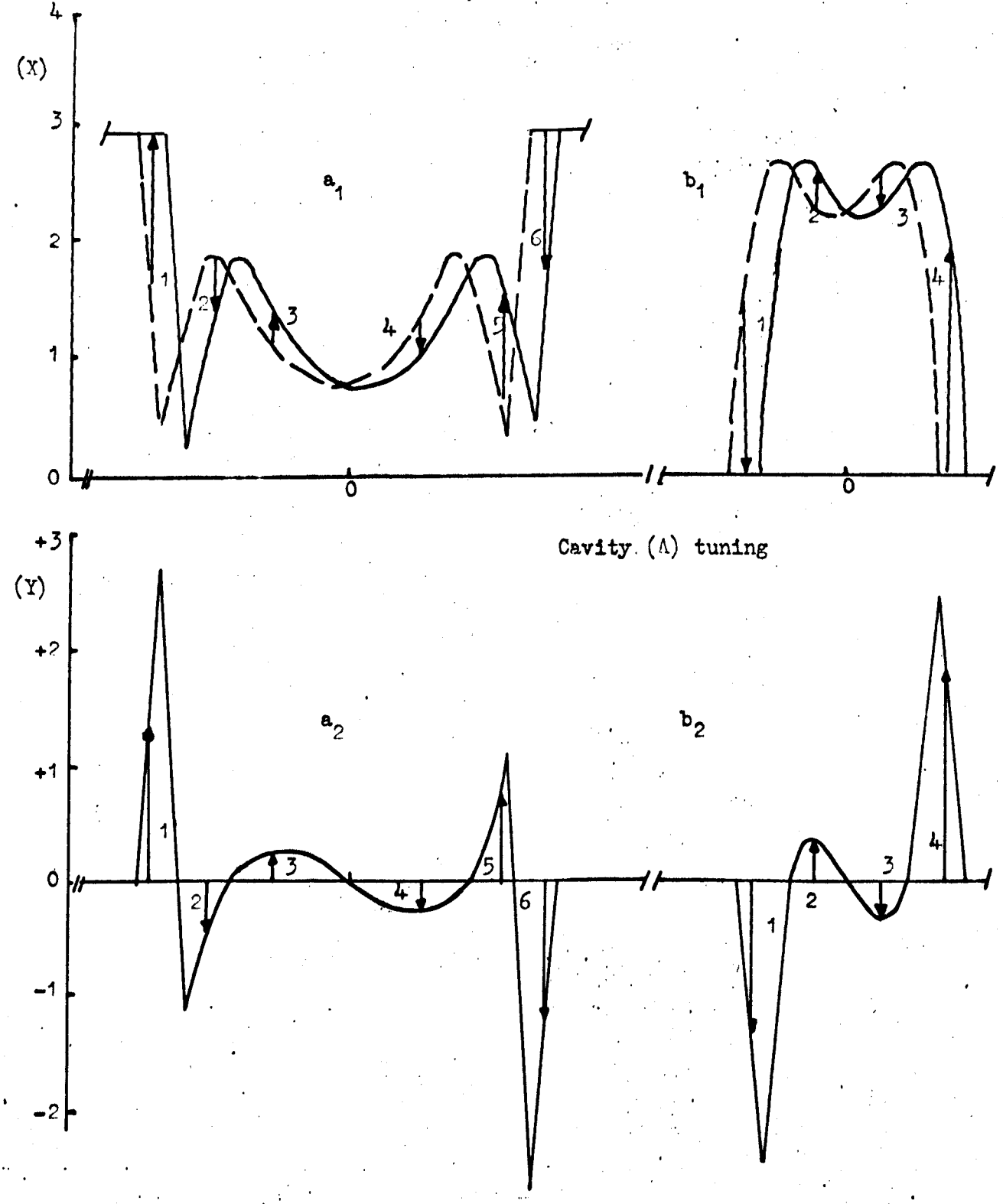

Figure 6:20

Cavity(Λ) modulation. Suggested derivation of modulation curve amplitudes(Y) from S-T amplitudes (X)

shows that the symmetry of the S-T curves depends not only on the tuning of cavity B, as suggested by Lainé and Srivastava[353], but also upon the matching of cavity A. Consequently the symmetry of the S-T pattern is not a reliable method of resetting the two cavity maser as a frequency standard if there is any chance of the top cavity loading being changed, thus for preference there should be no coupling hole to the top cavity. The method suggested in section 3 above is probably preferable, but the oscillating cavity method of Veselago et al[365] is probably best of all. This method makes use of the fact that (except when the first cavity is tuned to the molecular resonance) the phase of the signal in the second cavity varies with the distance between the cavities. So if this distance is regularly changed the phase of the second cavity output can be calibrated in terms of the detuning of the first cavity.

Chapter 7. Ultramicrowave/Microwave Double Resonance and future work

7:1 Introduction

In Chapter 2 a double resonance experiment was proposed. This uses a common energy level between a rotational and an inversion transition of the ammonia molecule in order to transfer the difficult problem of observation of the far infrared rotational transition to the rather easier problem of observing the microwave inversion transition. In the course of the beam maser experiments (Chapters 5 and 6) originally determined by concern with the double resonance experiment many results of considerable interest have been obtained and these have been further investigated because of their own significance. Unfortunately none of the double experiments have produced definite positive results. The first sections of this Chapter are concerned with these far infrared experiments and the reasons for their lack of success. It is somewhat difficult to describe in a logical sequence the experiments which have been performed because justification for particular experiments which was satisfactory at the time when they were planned or performed, has in several cases been superseded by more exact knowledge of far infrared radiation and resonator design. Thus in these four sections the description will be historical as well as phenomonological. In the remainder of this section the proposed double resonance experiment is described and the results obtained in earlier chapters fitted into the general pattern. In section 2 the threshold of oscillation, linewidth and expected signal patterns are investigated. Section 3 describes two sets of experiments devoted to detection of the rotational trans-

ition without systematic modulation of the cavity energy density. In section 4 the means of modulating the cavity energy density are assessed and some experiments described. The last two sections are devoted to summarising the results obtained and proposals for future work, both in the far infrared and with beam masers.

The energy levels which correspond to the two rotational states of ammonia J = 3, K = 3 and J = 4, K = 3 are split due to inversion (see Figure 1 of Chapter 2). Possible transitions are given by the selection rules

$$\Delta J = 0, \pm 1, \Delta K = 0 \quad (+) \leftrightarrow (-) \qquad 1$$

where the upper and lower inversion levels are designated (+) and (-).

The inversion transition $\Delta J = \Delta K = 0$, $(+) \leftrightarrow (-)$ for J = K = 3 has been extensively used in studies of the ammonia maser at 23.870 GHz. The splitting of the next rotational state J = 4, K = 3 corresponds to the inversion frequency of 22.688 GHz. Other higher rotational states are not of importance for the present project.

When ammonia molecules pass through a strong inhomogeneous electrostatic field, the molecules in the lower inversion level of each rotational state tend to be deflected out of the beam, and those in the upper inversion levels are preferentially focussed along the beam axis. Thus a net population excess is obtained between levels 4 and 1 and stimulated emission at 124.64 microns can occur.

The amplitude of the emitted signal in an ammonia beam maser is a function of the net excess population of molecules in the upper energy state. If n_1 and n_2 are the numbers of molecules in the lower and upper 3,3 state, then the population excess is given by $n = n_2 - n_1$.

If the ammonia beam passes through a resonator which is simultaneously tuned to the frequencies f_{12} and f_{14}, then induced ultramicrowave transitions will terminate on the lower inversion level of the 3,3 rotational state. Such rotational transitions increase n_1 and decrease n and consequently the microwave emission signal is weakened. It is feasible that stimulated emission from these transitions could be detected in a normal ammonia maser if a cavity could be made to support high Q modes at both frequencies.

Whilst it might be possible to construct a dual mode cavity, even for frequencies which differ by as much as two orders of magnitude, an alternative method is preferred so that each mode can be tuned independently. Such a method is to pass the ammonia molecules through two cavities, A and B, in cascade, tuned to the ultramicrowave and microwave frequencies respectively. Stimulated emission which occurs in A at frequency f_{14} can be detected by monitoring the stimulated emission in B at f_{12}. It can be seen from Figure 1 of Chapter 2 that absorption of radiation at f_{23} will also decrease n and therefore reduce the microwave power emitted in B.

Various types of ultramicrowave resonant structures have been considered and in Chapter 4 it was seen that the two most interesting were the high mode order cylindrical cavity, which would have a large filling factor but possibly would be resonant in several different modes and hence have a low quality factor in any one; and secondly the half confocal resonator which should have a limited number of modes and the possibility of coupling radiation into it from an outside source; but a poor filling factor (beam-field interaction time).

Two types of electrostatic beam separator were considered in Chapter 4, the conventional multi-pole and the ring separator. Both are suitable for a submillimetre maser (SMASER), but knowledge of the latter type has only become available during the course of this investigation so most of the work has used the former type: but one ring separator has been made and its use is described in section 3 below. In section 6 of Chapter 5 it was found that the average velocity of effective molecules at microwave oscillation threshold using an octapole separator was only 5,500 cm/sec, which is rather smaller than values used in previous calculations. Values based on this figure have been used in the calculations of section 2 below.

In Chapter 2 the general submillimetre spectral region was investigated and some familiarity with 100 to 150μ radiation obtained. In particular the transmission of specimens of crystal quartz, silica and polythene were obtained and the emission from a mercury-quartz lamp determined. These results are used in section 4, when external radiation is coupled into the half confocal ultramicrowave cavity.

In Chapter 6 it was found that a two microwave cavity detection system should be more sensitive than a single microwave cavity detector, but the difficulties of operation of such a scheme are such that only a single cavity detector has been used up to the present time. The sensitivity and best operating conditions of such a single cavity system were found in Chapter 5, together with the operating frequency for the modulation of the far infrared stimulating radiation.

7:2 Linewidths and oscillation threshold

The 125μ ammonia transition will be transverse doppler bandwidth limited, given by

$$\Delta f_t = fv \sin \theta / c \qquad 2$$

where v is the mean molecular velocity and θ the half beam-width angle, thus the bandwidth $2\Delta f_t$ = 200 KHz. This will be slightly modified by uncertainty effects, field intensity effects and microwave cavity receiver area.

In the 3,3 ammonia inversion maser the three transitions $\Delta F_I = 0$ are degenerate (see Figure 4b of Chapter 3) and together form the main line. This is because the quadrupole splittings of the upper and lower inversion levels are approximately the same for any one rotational level. Thus the J = 4, K = 3, $\Delta F_I = 0$ transitions are also degenerate (see Figure 4a of Chapter 3).

However the quadrupole splittings are not the same for the two rotational states and the J = 4 ↔ 3, K = 3, ΔF = 0, + ↔ -, $\Delta F_I = 1$ transitions will lie at different frequencies. The splitting is of the same order as the $\Delta F_I = 0$ transitions. Thus Figure 4c of Chapter 3 shows the 6 expected lines spread out over a range of 2.350 MHz; if the system of observation has a sufficiently high resolution these lines might be distinguished. It was seen in section 6 of Chapter 4 that a half confocal cavity as constructed might be expected to have a bandwidth of 10 to 50 MHz so it would be unable to resolve these lines. There should be a single peak response for the system as the Fabry-Perot is tuned through the molecular resonance, provided that the

cavity is resonant in only one mode. It was also seen in that section that the cavity would have resonances separated by $\lambda/8$, but the lowest loss modes would be separated by $\lambda/2$. For a resonator 13.2 cm long the separation of the $\lambda/8$ modes will be 300 MHz (and 1.2 GHz for the $\lambda/2$ modes), so the structure will be tuned to a resonator mode for one sixth to one thirtieth of its scan, and if the detector and recorder system has a time constant of 10 seconds then the structure should not be tuned faster than one $\lambda/8$ separation in 5 minutes or $\lambda/2$ in 20 minutes. In practice scan rates of a half to a quarter of this value have been used.

Shimoda[366] has obtained the condition for oscillation when a line is doppler limited in width,

$$N = \frac{3hVvv_t}{2\pi^2\mu^2 QL\lambda} \qquad 3$$

where N is the net excess population in the upper energy state flowing per second, V is the cavity volume, v the average molecular velocity, with transverse component v_t and path length L in the exciting field. Substituting the previously determined values, including 0.367×10^{-36} for the square of the dipole matrix element, μ, gives N as about 1×10^{13} molecules per second.

The microwave maser under similar conditions requires only 2×10^{11} molecules per second (see section 2/p95 of Chapter 5): thus the rotational transition requires about ×50 more excited state molecules per second for oscillation.

The situation is rather worse than this, first, in section 7, p95, of

Chapter 3 it was calculated that for thermal equilibrium populations that the ratio of the number of molecules in the 4,3 state and 3,3 state is 0.870 at 300 ^{o}K. Second, equation 14 of Chapter 4 p69 shows that the octapole separator is less efficient for higher rotational state molecules. The number of focused molecules is dependent on the factor $(M_J/(J + 1)J)^2$, where M_J is the high field quantum number. It is difficult to average over the M_J states because the low field M_J states do not necessarily transfer to the same value in high field. But it is clear that only about 4/9 as many molecules will be focused by the separator. Third, three $\Delta F_I = 0$ lines contribute to the microwave oscillation, whereas they are split for the ultramicrowave transition so that three times more flux will be required for oscillation on any one of these. Thus for the rotational transition the flux required for oscillation will be $\times$ 50 $\times$ 1/0.87 $\times$ 9/4 $\times$ 3 = ~ 375 greater than for the 3,3 inversion transition.

Further, in section 2 of Chapter 4 p69 it was seen that the number of molecules within a given solid angle is approximately proportional to $N_o^{2/3}$ where N_o is the total flux effusing from the source. Hence the total number of molecules will be increased by about four orders of magnitude. But the microwave oscillator requires a minimum total flux from the nozzle of about 5×10^{16} molecules per second, so the Smaser will require at least 10^{20} molecules per second, which is considerably more than can be provided by the most efficient nozzles, hence it is unlikely that any effects observed in the present stimulated emission detection system will be due to far infrared oscillations.

7:3 Thermal stimulation of far infrared transitions

The transition matrix element for the rotational transition is given by equation 34 of Chapter 3/p59 as 1.468×10^{-18} c.g.s. units. The Einstein B coefficient is given by equation 17 of Chapter 1/p8 as

$$B_{41} = \frac{8\pi^3}{3h^2} |\mu_{41}|^2 = 0.69 \times 10^{18} \text{ c.g.s. units} \qquad 4$$

and since according to Planck the density of thermal radiation U at $290^{\circ}K$ at 125 microns is 1.7×10^{-19} c.g.s. units, the rate of transfer[6] of molecules from levels 4 to 1, ΔN_{41} is given by

$$\Delta N_{41} = (N_4 - N_1) B_{41} U t = 1.2 \times 10^{-5} (N_4 - N_1) \qquad 5$$

where t the interaction time is taken as 10^{-4} seconds.

If $N_4 = 10^{12}$ molecules per second, then $\Delta N_{41} = 1.2 \times 10^{7}$ transitions/sec.

Consequently the half confocal resonator could only provide enough transitions for them to be detected at mode resonances. For these resonances thermally stimulated transitions will produce photons which may cause further transitions. If there was a gain of the order of unity, each thermal photon stimulating one further transition, then the double resonance system might be expected to permit observation of inter-rotational level effects.

Three systems have been used to try and observe the effect of far infrared thermally stimulated photons on the maser transition. The first system is that described in Chapter 5/p90, with the 13.2 cm half confocal cavity (described in Chapter 4/p83) acting as the first cavity, A.

This resonator is mounted with its axis horizontal, that is with its axis transverse to the molecular beam; with the beam passing through a one inch diameter hole drilled through the centre of the mirror spacer. The beam after leaving the state separator first passes through this ultramicrowave structure and then the microwave one. The microwave cavity is tuned to the 3,3 transition and the flux is adjusted for a signal to noise of 3 (to 5) to 1 of the maser microwave oscillation (10 to 15% of the maximum amplitude obtainable with 30 KV separator potential). This means operating the maser with a separator potential about 1 KV above that required for oscillation threshold. The detection system is operated in the stabilised superheterodyne mode and the output of the second detector is amplified by an audio amplifier, rectified, smoothed by a 5 second R-C time constant and recorded on a pen recorder. This system is sensitive to about 2.5% changes in operating beam flux. Occasional large spurious signals were produced by spark discharges in the state separator, these spikes could be monitored by their radio frequency emission and the resulting 'signals' ignored.

The half confocal resonator is scanned through the possible ultramicrowave resonant conditions by thermally expanding the spacer between the mirrors. The heater is bifilar wound and run from a low voltage D.C. supply, giving a temperature from 20 to 120°C and hence a scan range of at least $3\lambda/2$. Thus three $\lambda/2$ resonances should be observable in the two hour sweep time. Apart from the separator spark 'signals' no systematic pattern of results was obtained over a series

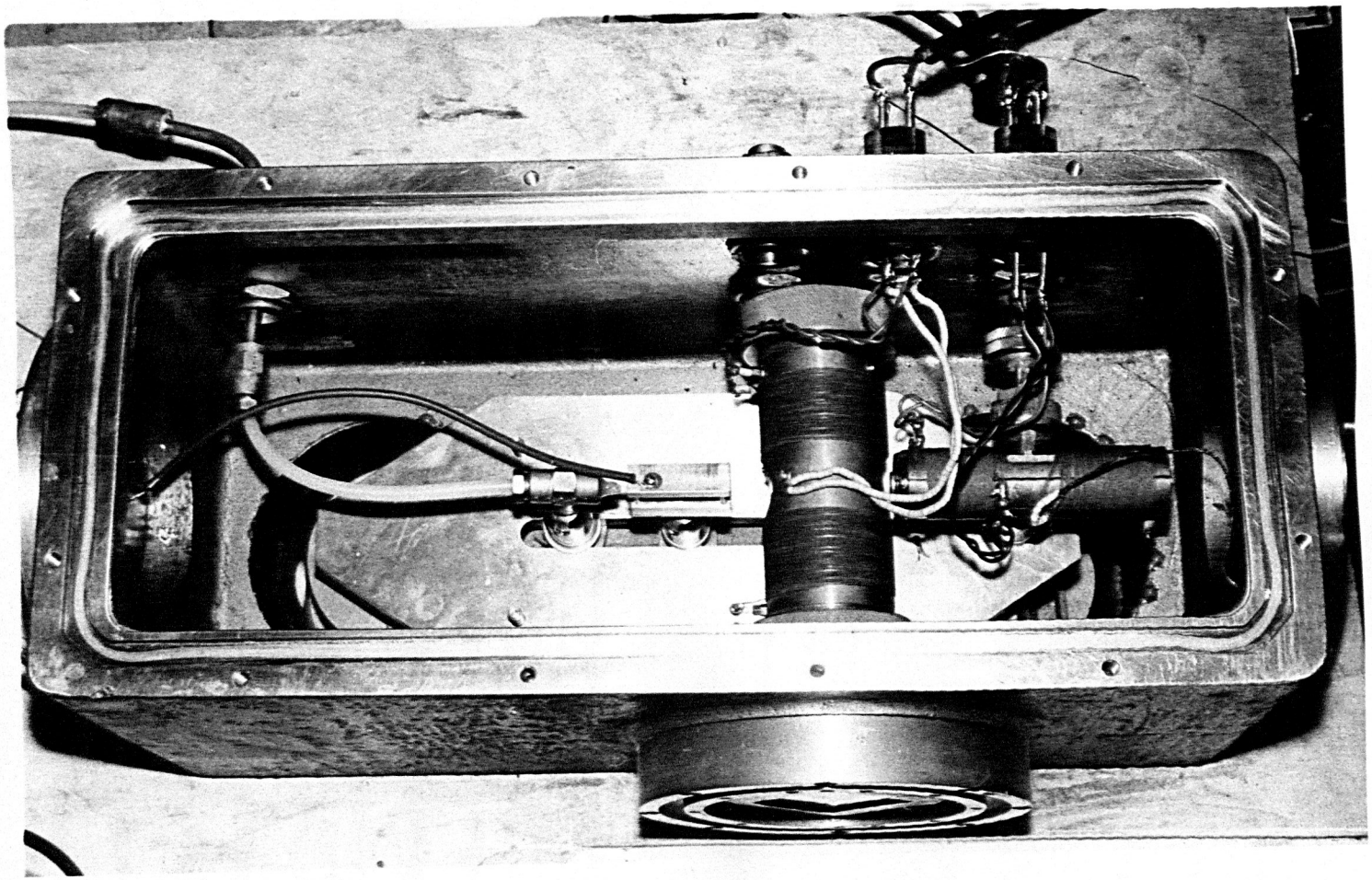

Figure 7:1

of runs, either under the low flux conditions or when the flux was increased to give a microwave oscillation signal to noise of about 40 to 1.

The second system used was designed and built to overcome various limitations in the first system. This first system (see Figure 4, [illegible].104, Chapter 5) consists of brass castings with rubber 'O' ring seals, and it was found that these castings could move relative to one another, both as the system was being evacuated and when in operation. Since the system was aligned whilst at atmospheric pressure this was a serious disadvantage and might lead to the beam of molecules accidentally failing to pass through the 0.5 cm diameter of the half confocal field pattern. A new maser housing and pumping system was subsquently built. The main body of the vacuum system was cast in aluminium bronze with various 'O' ring demountable plates and 'lead-ins'. All the maser components are mounted norizontally on a half inch thick brass optical bench, (see Figure 1) mounted inside the vacuum box. This system has four main advantages. First, once aligned the various components cannot move when the system is evacuated. Secondly, the components can be aligned with an accuracy of at least 0.1 cm. Thirdly, the system is horizontal rather than vertical so the good vision can be obtained along the axis of the system from the microwave cavity (rather than nozzle) end of the system. This last is of added importance because of the fourth reason, which is that this system has been operated with a ring type state separator and 0.35 mm diameter 1.0 cm long single capillary source. This has the advantage of much better operating efficienty, as was seen in section 3 of Chapter 4, but the capillary cannot be

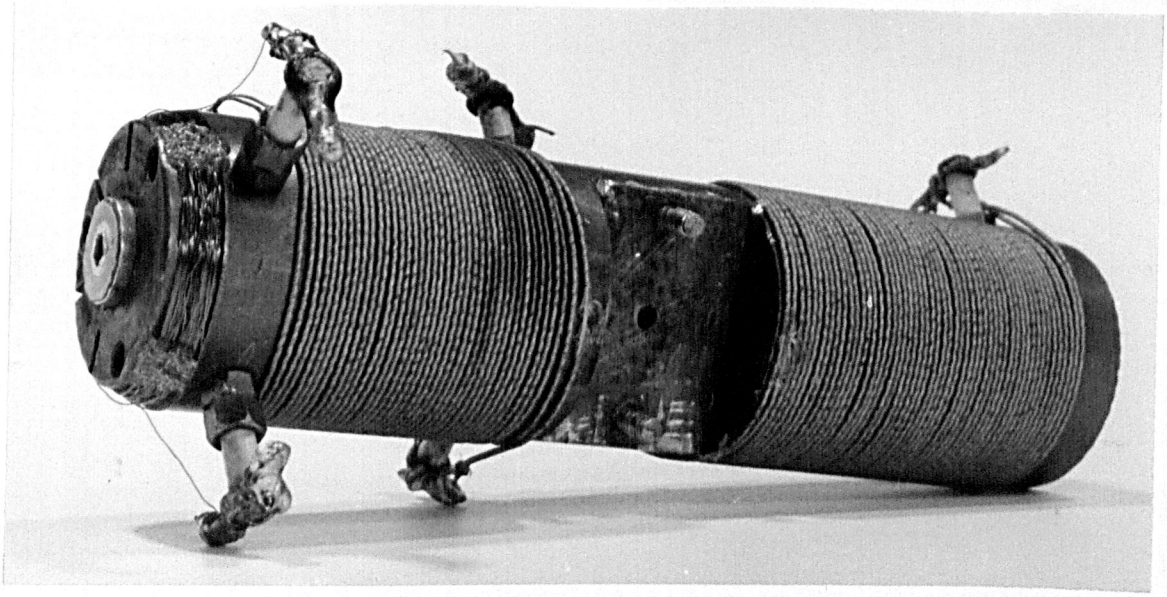

(a) Microwave cavity with stop

(b) Liquid nitrogen jacket

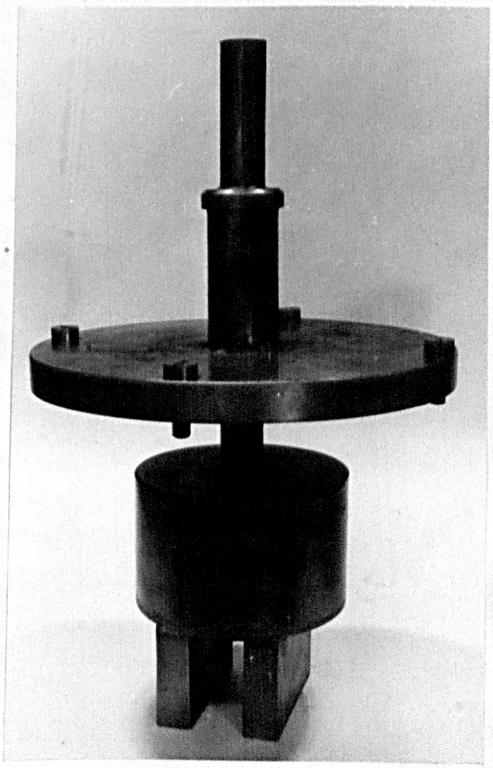

Figure 7:2

used for optical alignment purposes owing to the small hole diameter.

The nozzle and ring separator are positioned so as to focus molecules into the microwave cavity when there is a 6 cm separation between the nearest parts of the separator and microwave resonator. Thus according to the theory of section 3 of Chapter 4 for a ring separator with 0.25 cm separation between rings, of internal diameter 0.35 cm, the upper state molecules should be focused into a beam with a cross section of about 0.4 cm at the entrance to the resonator. A 0.3 cm diameter diaphragm is centrally placed across the entrance (Fig. 2a).

This nozzle, separator and microwave cavity system has been tested by operating it in the crystal-video mode as a normal microwave beam maser. Figure 3 is a graph of the threshold of oscillation separator potential (V) against the ammonia source pressure behind the nozzle, it is apparent that the lowest operating separator potential is 18 KV at 6.5 torr of ammonia. Figure 4 is a set of amplitude of oscillation (X) versus separator potential (V) traces for 4,7 and 10 torr beam pressures. It appears that there is some corona in the state separator which is reduced at lower beam pressures, so the optimum pressure for low noise operation is 4 to 5 torr.

The new maser vacuum housing is mounted on a portable trolley (see Figure 5) and uses all the electronic and control circuits of the earlier system, but has its own vacuum pumping system. This consists of two 2" diffusion pumps (~ 40 litres/sec) operating in parallel, backed by a Genevac two stage GRD4 (1.88 litre/sec) rotary pump. This system, together with the separator nitrogen jacket, reduces the approximately

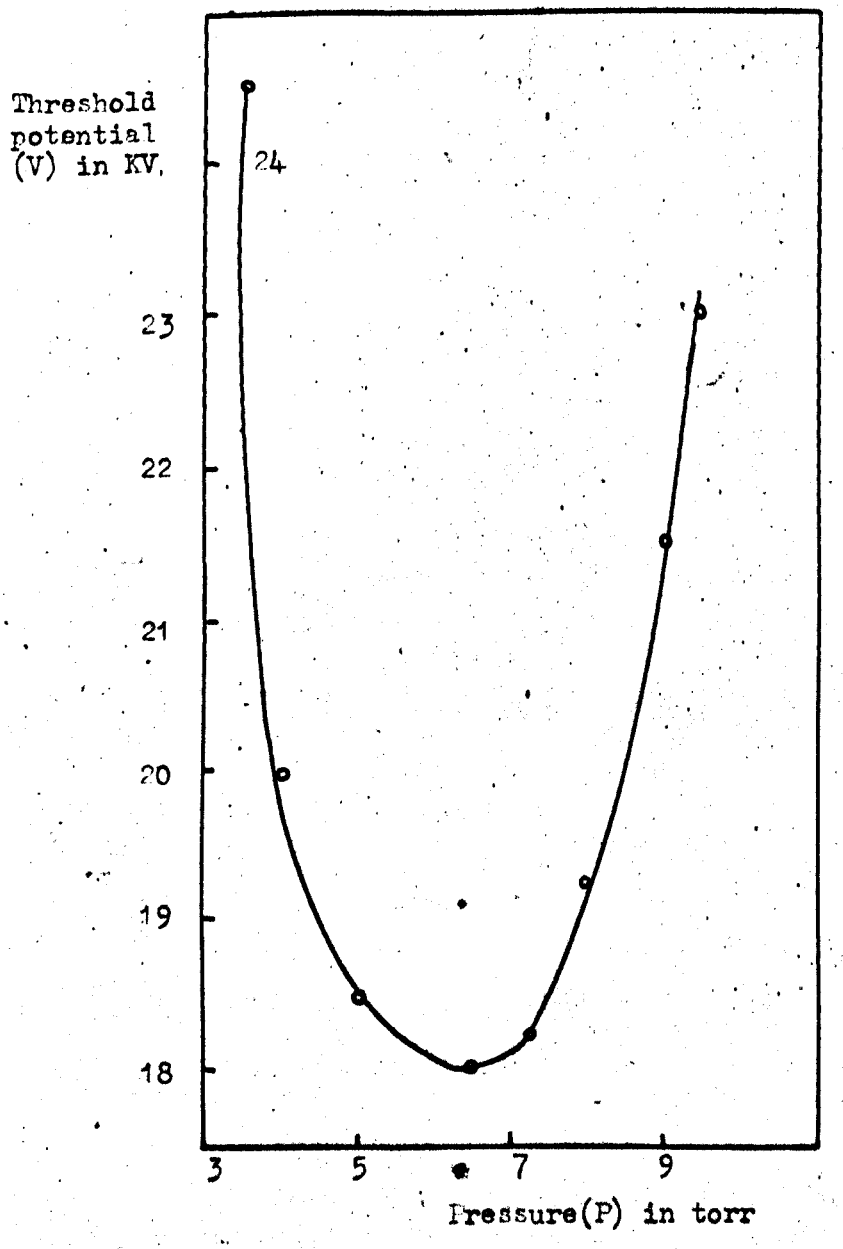

Figure 7:3

Separator potential(V) for threshold of oscillation variation with ammonia beam pressure(P) for a ring separator

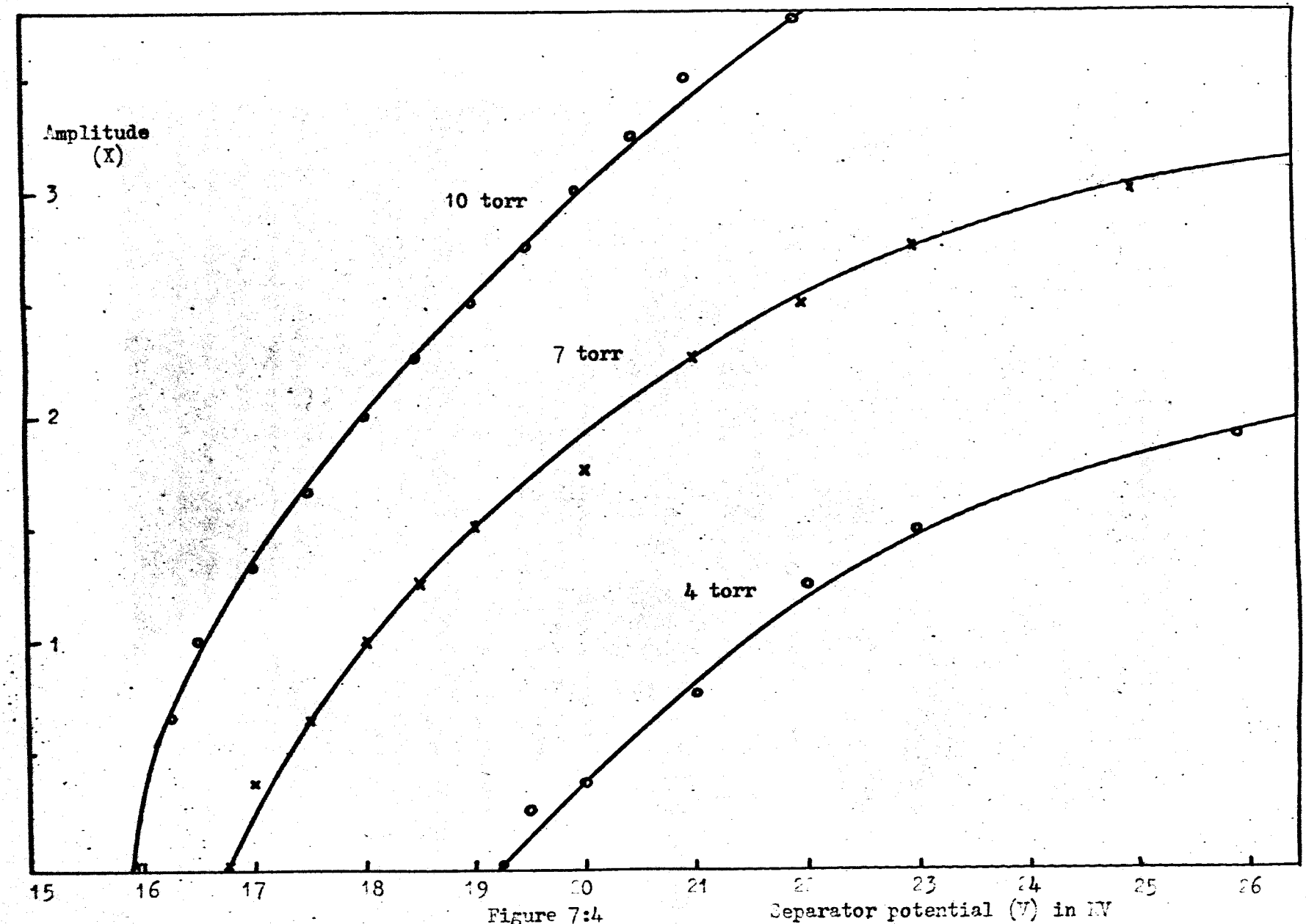

Figure 7:4

Amplitude of oscillation(X) variation with separator potential for a ring separator for three beam pressures

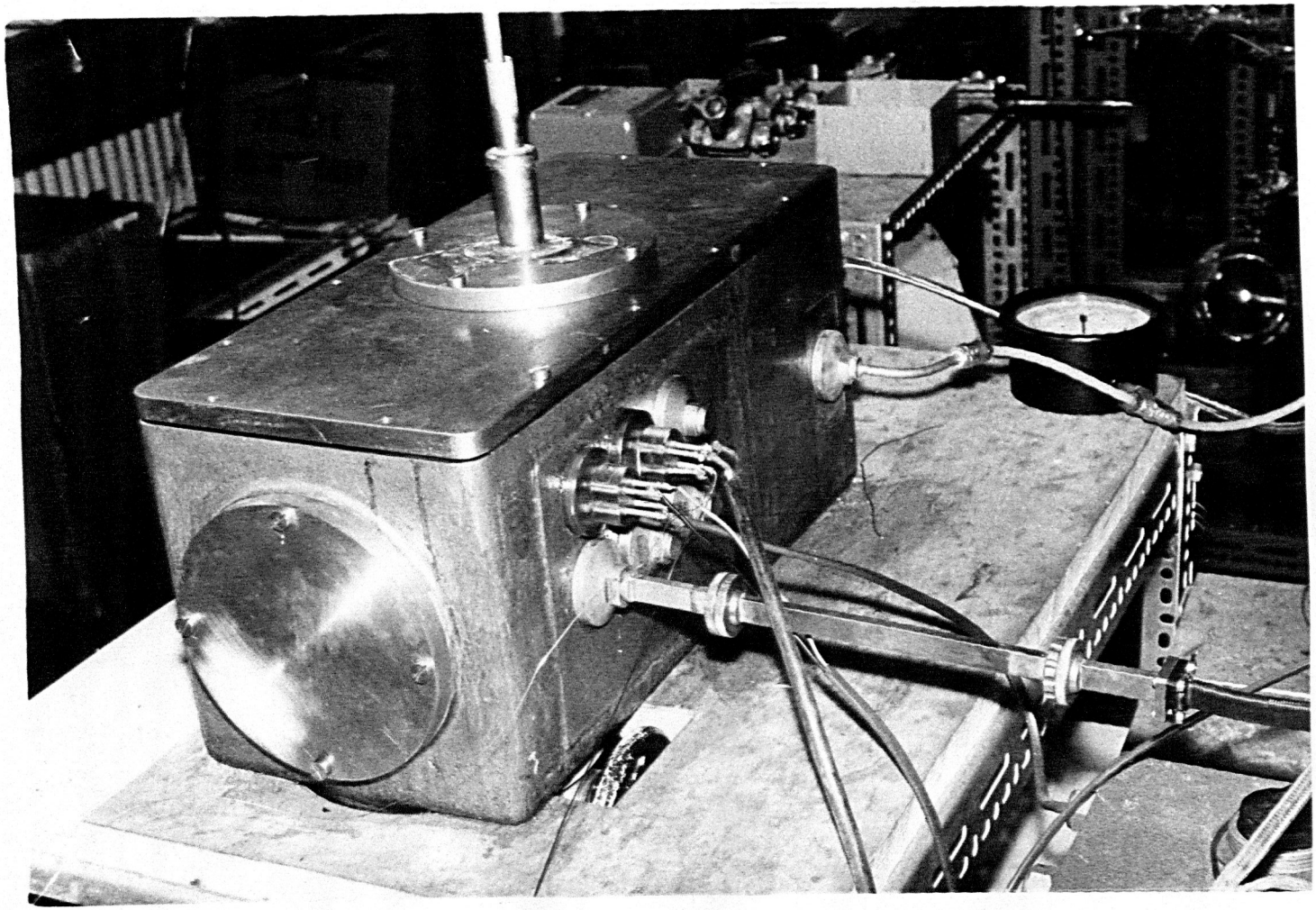

Figure 7:5

3 cubic feet volume of the high vacuum system to 2×10^{-6} torr pressure in about 3 hours and to less than 10^{-6} torr in 6 hours. The nitrogen jacket consists of two hollow fins (which fit either side of the ring separator) attached to the base of a liquid nitrogen reservoir, which is 'double-insulated' from its surroundings by copper-nickel tube (see Figure 2b).

This, the second, system has been used to try and observe the ultramicrowave transitions in the half confocal cavity in exactly the same way as with the first system. The half confocal cavity is mounted transversely between the nozzle and detector cavity (see Figure 1). The microwave maser is operated at 1.5 KV above oscillation threshold at 4.5 torr ammonia pressure. There were few sparks in the separator, but what was thought to be corona in the separator limited the sensitivity of the system to 4% fluctuations in detected amplitude. The only responses greater than 4% during cavity frequency sweeps with the system did not correlate with the expected signals.

The third system used is that with an ultramicrowave cylindrical cavity in place of the half confocal cavity. Thus a 0.9687 cm diameter cavity (as described in section 5 of Chapter 4) has been used. It should be resonant in the 77th mode at a moderate temperature. The previously described 'old' maser system was used and it was swept through a 200°C temperature range without success. There are two possible reasons why this system is unsuccessful, first it may be resonant in several different modes, second, its dimensions may be such that it does not tune to the correct wavelength in the course of

p75

the 200°C sweep (a complete sweep would require a 700°C range). The failure of the first two systems is probably due to lack of sensitivity of the detection system. It was calculated earlier that the population of the 3,3 (-) level would only be altered by one part in 10^5 by the far infrared cavity, assuming no gain in either cavity. It was seen in Chapter 5 that a gain of about $\times 10$ should be obtained in the microwave cavity, thus a field about 10^3 greater than black-body thermal is required in the far infrared cavity for detection of the ultramicrowave transition. This assumes a detector sensitivity of 10%. This detector sensitivity can be greatly increased by using an A.C. system as described in the next section. For such a system, in Chapter 5, p128 the sensitivity was found to be one part in 4×10^5.

7:4 Modulated thermal stimulation

As was mentioned immediately above, much greater sensitivity of the double resonance detection system to change of molecular flux can be obtained by modulating the thermal field in the ultramicrowave cavity such that A.C. detection techniques can be used. Thus the detection scheme shown in Figure 6 has a sensitivity of 1 part in 4×10^5 compared with one part in 40 for the D.C. system, an improvement of four orders of magnitude. If the thermal field in the far infrared cavity is that of a room temperature radiator completely modulated at the A.C. frequency the detection system should be able to record its presence.

The system used is shown in Figure 6, the 'old' maser housing is used with the half confocal resonator between the octapole separator and microwave cavity. The plane mirror of the half confocal resonator

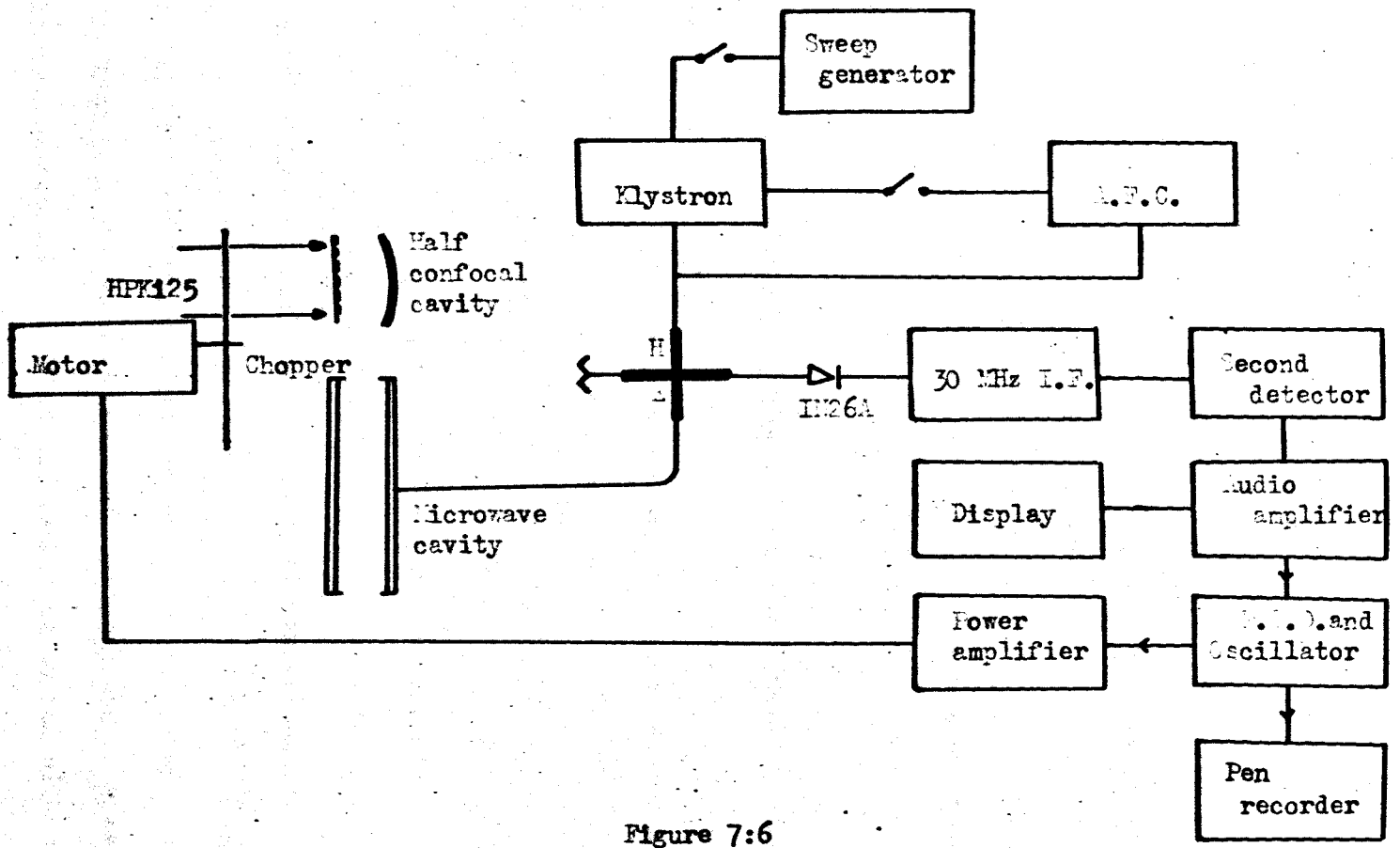

Figure 7:6

Block diagram of modulation of upper cavity radiation density

is partially transmitting (see below) and modulated radiation from an HPK 125 mercury quartz lamp is coupled through this mirror into the resonator. The lamp is run off an A.C. supply under conditions determined in Chapter 2. The radiation from the lamp is collected by a 6" diameter concave surface aluminised mirror and focused onto the plane plate of the half confocal resonator. Between the lamp and the resonator there is a 4 mm crystal quartz plate and a rotating vane connected to the shaft of a synchronous electric motor. The quartz acts as a window and vacuum seal between the high vacuum of the maser system (10^{-5} to 10^{-6} torr) and the much higher pressure (10^{-1} torr) which is satisfactory for removing the water vapour in the source lamp region.

The electric infrared chopper motor is powered by the output from the oscillator in the JB4 phase sensitive detector, via a suitable amplifier. The oscillator is set at 15 Hz and it also acts as the reference oscillator for the phase detector. The phase of the chopped far infrared radiation is checked by using an OCP71 photo detector in place of the superheterodyne detector. It was found that the superheterodyne system gave a 'signal' output when the microwave beam maser was oscillating, whatever the tuning of the far infrared cavity. This was identified as microphonic pick-up of vibrations from the motor by the state separator, the phase of this pick-up coinciding with the phase of the OCP71 detected signal.

Thus with the phase determined, the lamp and chopper working and the superheterodyne detection and recording system with a ten second time constant, various frequency sweeps of the half confocal cavity were made,

as described in section 3; that is each one taking at least an hour for a $3\lambda/2$ sweep. This system was operated both for low flux (about 1 KV above oscillation threshold) and high flux (~ 25 KV separator potential) maser oscillation, both with the lock-in amplifier phased as above and with it phased 90° from this. No results which can be interpreted as the expected signal pattern were obtained.

Several different coupling systems were considered and used and the relative merits of the various methods were considered in section 7 of Chapter 4. The schemes which have been used are:-

(a) 0.7 and 1.0 mm diameter hole drilled in the centre of the aluminium surfaced plane mirror.

(b) 0.67 mm diameter hole in aluminium surface of a crystal quartz plate.

(c) 1.0 cm diameter aluminium mirror on a crystal quartz plate, with diffraction coupling round the mirror.

(d) 600 mesh to the inch stainless steel grid.

(e) 125°A thin aluminium film on a crystal quartz plate.

The holes in (a) should couple to a few percent of the modulation in the TEM_{00q} modes in the cavity, but unfortunately as was seen in Chapter 4, it now appears that the losses of this mode will be more than several of the transverse modes[321], and a very low Q and uncertain configuration will result. The same applies to (b), with the addition that there will be added coupling losses due to the transmission through the quartz. (c) is a different coupling method and has been used successfully for far infrared gas lasers to couple power out of the resonator, but no theory has been developed for its use and it is

difficult to couple the mode patterns to the radiation beam direction and angle. The metal mesh of (d) might make a very efficient reflection/transmission combination (see Chapter 4 p30 if it were possible to obtain such a mesh in a high reflectivity metal, and if the effect of non-coplanarity of the wires was known. The very thin aluminium film of (e) was suggested by Strain[367], but has been unsuccessful.

7:5 The Far Infrared Situation

Thus it is seen that no definite observation of the effects of far infrared transitions have been observed in the double resonance experiments. That they should be observed with the D.C. observation system of section 7:3 is marginal, but the fact that no such effects were observed with the A.C. modulated radiation is rather more difficult to explain. Recent evidence tends to suggest that an explanation should be sought in terms of the following factors:-

(a) The alignment of the molecular beam and the resonator fields.

(b) The molecular and radiation field interaction times.

(c) The use of a single beam with an octapole separator.

(d) Doppler line broadening in the half confocal resonator.

(e) Only a low power stimulating source available.

(f) The confocal cavity coupling.

(g) The alignment and quality factor of the ultramicrowave resonator.

(h) The mode configuration in the ultramicrowave resonator.

(a), (b) and (c). Interaction of upper state molecules and field

In all the earlier work the octapole state separator was used,

p63

and it was seen in section 2 of Chapter 4 that this means that the axial molecules are not adequately state separated. This is not important for the normal microwave beam maser because the diameter of the cavity and microwave field is about the same as that of the separator, and the cavity accepts a large number of off axis molecules which are well state separated, but for the half confocal cavity with a TEM_{00q} diameter of only 0.5 cm the axial molecules become very important. This problem should be overcome by the use of a ring or spiral state separator, but unfortunately time has not been available to perform any of the above A.C. experiments with the ring separator as used in section 3 above. The same time element explains why the 'new' maser housing and system with the greatly improved alignment has not been used for any of the modulation experiments. With the original system it is quite possible that the 0.5 cm diameter field of the half confocal cavity only partially overlaps the molecular beam. Also it should be noted that even if the beam is perfectly aligned with the field the field beam interaction is only over a path length of 0.5 cm not about 10 cm as for the microwave cylindrical cavity maser. (This last factor (b) was of course taken into account in the calculations, but (a) and (c) are not so easily accounted for in the theory.)

(d). Doppler line broadening of the far infrared resonance

With a spherical mirror system, as opposed to a plane mirror one, the molecules move in a path at a slight angle to the radiation wavefront in the resonator and the doppler width is somewhat increased. This effect will be reduced if the beam passes close to the plane

mirror of the half confocal resonator, rather than through the centre.

(e). Low power far infrared stimulation

For operation of the A.C. modulation experiments a mercury quartz lamp with a black-body equivalent temperature of about 1000°C has to be used. This means that the maximum possible increase in field in the ultramicrowave resonator is × 3, with perfect coupling. The situation would be greatly improved if a high power gas laser could be used as the stimulating source, but as was seen in Chapter 1 the only Smasers available near 125 microns are very low powered and not exactly at the ammonia wavelength.

(f). Cavity coupling

It was seen above and in Chapter 4 that the efficient coupling of radiation into a half confocal cavity is difficult. It is now apparent that what appeared to be the best coupling scheme (the single central hole) seriously effects the mode patterns in the resonator. At the present time the systems most likely to succeed would seem to be those with 'beyond cut-off' arrays of holes, either in the form of a mesh as in section 4 above, or as an array of etched holes in a metal film on a dielectric base (as discussed in section 7,p84-9. of Chapter 4), or an array of holes in a thin metal membrane, as has been proposed by Goldick[368]. Such fine structures are very difficult to make.

The other problem concerned with coupling is ensuring that not only does the coupling arrangement effect the cavity field configuration but that the direction of the incident radiation should match the mode shape of the cavity; Auston and others[316] have done some preliminary

work on this problem.

(g) and (h). Cavity modes and mirror alignment

All the evidence for the expected 'Q' of the half confocal resonator has been based on theory or millimetre wave experiments. Thus the mirror spacer was very accurately machined, polished and measured so as to align the mirrors within acceptable geometric limits. However, working with an 8 mm plane parallel resonator it has been found that the resonator does not normally have the highest 'Q' when the mirrors are measured to be parallel, and the only way to optimise the Q is to have a power source and direct observation of the alignment. This has not been possible for the 125μ resonator.

If the resonator has considerable energy in more than one mode then the Q of the modes will be very much reduced. It is now clear that most of the 'above cut-off' coupling schemes will lead to numerous higher order modes and without visual alignment the resonator is unlikely to have its highest Q in the TEM_{00q} modes. That this is so for the plane parallel resonator has been observed by Krupnov and Skvortsov[57] (c.f. Barchukov, Prokhorov and Savransky[369]) at 4 mm when working on their CH_2O maser. They found that the emission line split and that this could be best explained in terms of a split field pattern. They used an explanation similar to that of Feynman et al[351] (see Chapter 6). If a molecule goes through two fields equal in magnitude but opposite in phase any transition probability in the first field will be reversed in the second and thus rotation of the polarisation vector due to the first field will be annulled by retero-rotation in

the second field. Now a transverse mode in a resonator has at least one such field reversal in a path through its mode. Thus it is possible that there can be quite a strong interaction between beam and field without the population levels outside the resonator being significantly altered. This effect has also been noted by Strauch et al[314] in a half confocal resonator at 2 mm wavelength. If this explanation is correct then the separated oscillating field results of Chapter 6 are directly applicable to the half confocal cavity, in fact the half confocal cavity can be regarded as a multi cavity system. The complicated results recorded for the cascaded microwave cavity case indicate that there is little hope of operating a spherical mirror geometry resonator at 125μ with the correct mode pattern unless the structure can be aligned and tested with a source of considerable power.

The cavity problem is further aggravated by the fact that Barchukov et al[369] have found that the highest resonator quality factors are obtained when the mirrors are separated by at most a few wavelengths, which is contrary to the established theory. One explanation of this would seem to be that diffraction and 'walk-off' losses are much greater than expected. Thus Goldick[368] has planned to use a mirror separation of only a few half wavelengths for a 250μ ammonia maser and Prokhorov[370] has tried to use such a system to make a 125μ ammonia oscillator without success.

To summarise, if the far infrared double resonance system is to work, much further knowledge is required about spherical mirror structures, mode patterns and cavity coupling schemes. High power sources are needed for stimulation, alignment and general diagnostic procedures.

Further work should also be done to find out why thin metal films are so strongly reflecting in the far infrared and microwave regions.

7:6 Beam maser results and future work.

There appear to be five areas in which the results obtained with the beam maser can usefully be extended.

(a) Molecular Velocities

In Chapter 5 it was found that the average molecular velocity at threshold for a microwave beam maser using an octapole state separator was only 5,500 ± 1000 cm/sec, agreeing with the predictions of Jaynes and Cummings. The method of measurement, modulation of the state separator potential, can easily be extended to measure the velocity of the molecular flux from other types of state separator, such as ring and spiral. It would be improved by using resonators and separators short in length compared with their separation. Variation of this separation distance should yield information about the divergence of the molecular beam.

This method of measurement is much simpler than those using mechanical means, and with some care could be extended to measure the average velocities for higher than threshold flux conditions.

(b) Multi-cavity detection systems

The sensitivity of the superheterodyne detection system was measured for both single and double cavity systems. The two cavity system can be superior if it is carefully tuned for optimum performance. Further work is required to find out the effects of cavity lengths, separation and quality factors.

(c) Two field systems

These can be created either in a single cavity (such as a half confocal) or with two separate microwave cavities, phase matched in various ways. The characteristics of such systems have been extensively examined. Such information should both lead to a better understanding of the processes involved and to a possible frequency standard.

(d) Beam maser noise

The noise output of a single cavity beam maser has been measured and its general behaviour found to agree with that predicted by theory. More accurate equipment is needed for adequate quantitative information.

(e) High Resolution Spectroscopy

The two cavity oscillating maser system has been found to be an exceptionally high resolution device for beam spectroscopy, and the technique may be adaptable for measurement of structure with a resolution of about 500 Hz (or less with slow molecule systems). In particular previously unresolved hyperfine structure of the ammonia centre line has been observed. It would be useful to measure the frequency output of this split line for final confirmation of the interpretation suggested.

REFERENCES

The References are ordered according to their first mention in the text. The following abbreviations have been used:-

Trans. I.R.E. (and Trans. I.E.E.E.) - Transactions of the Institute of Radio Engineers (later, Institute of Electric and Electronic Engineers) - followed by specialist volume designations:-

P.G.E.D. - Professional Group on Electron Devices

P.G.I. - Professional Group on Instrumentation

I. - Instrumentation

M.T.T. - Microwave Theory and Technique

I.G.A. - Industrial and General Applications.

Soviet Journals. The English translation reference is normally given, the reference being preceded by S.P. standing for Soviet Physics:-

S.P. J.E.T.P. - Journal of Experimental and Theoretical Physics

S.P. Opt. and Spec. - Optics and Spectroscopy

S.P. R.E. and E.P. - Radio Engineering and Electron Physics.

Ap. Opt. - Applied Optics.

J.O.S.A. - Journal of the Optical Society of America.

Z.A.M.P. - Zeit. f. angewante Math. und Phys.

1 Wittke, J. P., Proc. I.R.E. 45, 1957, p. 291.

2 Weber, J., Rev. Mod. Phys. 31, 1959, p. 681.

3 Smith, R. A., Brit. J. Ap. Phys. 12, 1961, p. 197.

4 Heavens, O. S., 'Optical Masers', 1964, Methuen, London.

5 Troup, G., 'Masers and Lasers', 1963, Methuen, London, 2nd. ed.

6 Singer, J. R., 'Masers', 1960, Wiley, London.

7 Weber, J., Trans. I.R.E. P.G.E.D. 3, 1953, p. 1.

8 Gordon, J. P., Zeiger, H. J., Townes, C. H., Phys. Rev. 95, 1954, p. 282.

9 Einstein, A., Phys. Zeit. 18, 1917, p. 121.

10 Geusic, J. E., Scovil, H. E. D., Rep. Prog. Phys. 27, 1964, p. 241.

11 Bloch, F., Phys. Rev. 70, 1946, p. 460.

12 Purcell, E. M., Pound, R. V., Phys. Rev. 81, 1951, p. 279.

13 Basov, N. G., Prokhorov, A. M., S.P. Doklady 101, 1955, p. 47.
Basov, N. G., Prokhorov, A. M., S.P. J.E.T.P. 27, 1954, p. 431.

14 Gordon, J. P., Trans. I.R.E. P.G.I. 4, 1955, p. 155.
Gordon, J. P. Zeiger, H. J., Townes, C. H., Phys. Rev. 99, 1955, p. 1264.

15 Combrisson, J., Honig, A., Townes, C. H., Compt. Rend. 242, 1955, p. 2451.

16 Basov, N. G., Prokhorov, A. M., S.P. J.E.T.P. 1, 1955, p. 184.

17 Bloembergen, N., Phys. Rev. 104, 1956, p. 324.

18 Scovil, H. E. D., Feher, G., Seidel, H., Phys. Rev. 105, 1957, p. 762.

19 Goldenberg, H. M., Kleppener, D., Ramsey, N. R., Phys. Rev. Letters 5, 1960, p. 316.

20 Schawlow, A. L., Townes, C. H., Phys. Rev. 112, 1958, p. 1940.

21 Basov, N. G., Krokhin, O. N., Popov, Yu M., S.P. Uspekhi 3, 1961, p. 702.

22 Maiman, T. H., Nature, 187, 1960, p. 493.

23 Javan, A., Bennett, W. R., Herriott, D. R., Phys. Rev. Letters 6, 1961, p. 106.

24 Gordon, J. P., Phys. Rev. 99, 1955, p. 1253.

25 Gambling, W. A., Wilmshurst, T. H., Phys. Letters 5, 1963, p. 228.

26 Helmer, J. C., J. Ap. Phys. 28, 1957, p. 212.

27 Barnes, F. S., Proc. I.R.E. 47, 1959, p. 2085.

28 Basov, N. G., Strakhovskiy, G. N., Cheremiskin, I. V., S.P. R.E. and E.P. 6, 1961, p. 905.

29 Mitchell, A. M. J., Roots, K. G., Phillips, G., Elect. Tech. 37, 1960, p. 136.

30 Yamamoto, M., Memoirs, College of Science, Kyoto, A, 30, 1962, p. 69.

31 Shimoda, K., J. Phys. Soc. Jap. 13, 1958, p. 939.

32 Shimoda, K., J. Phys. Soc. Jap. 16, 1961, p. 1728.

33 Shimoda, K., Wang, T. C., Townes, C. H., Phys. Rev. 102, 1956, p. 1308.

34 Shimoda, K., J. Phys. Soc. Jap. 12, 1957, p. 1006.

35 Venkates, H. G., Strandberg, M. W. P., J. Ap. Phys. 31, 1960, p. 396.

36 Jaynes, E. T., Cummings, F. W., Proc. I.E.E.E. 51, 1963, p. 89.

37 Shimoda, K., Trans. I.R.E. I, 11, 1962, p. 195.

38 Shimoda, K., Kohno, N., Jap. J. Ap. Phys. 1, 1962, p. 5.

39 Prins, J. de, Trans. I.R.E. I. 11, 1962, p. 200.

40 McCoubrey, A. O., Proc. I.E.E.E. 54, 1966, p. 116.

41 Kleppner, D., Goldenberg, H. M., Ramsey, N. F., Phys. Rev. 126, 1962, p. 603.

42 Ramsey, N. F., Trans. I.R.E. I. 11, 1962, p. 177.

43 Vessot, R. F. C., Peters, H. E., Trans. I.R.E. I. 11, 1962, p. 184.

44 Kleppner, D., Berg, H. C., Crampton, S. B., Ramsey, N. F., Vessot, R. F. C., Peters, H. E., Vanier, J., Phys. Rev. 138, 1965, p. A292.

45 Arditi, M., Carver, T. R., Phys. Rev. 124, 1961, p. 800.

46 Arditi, M., Carver, T. R., Phys. Rev. 136, 1964, p. A643.

47 Arditi, M., Carver, T. R., Proc. I.E.E.E. 51, 1963, p. 190.

48 Arditi, M., Carver, T. R., J. Ap. Phys. 36, 1965, p. 443.

49 Davidovits, M., Novick, R., Proc. I.E.E.E. 54, 1966, p. 155.

50 Shimoda, K., Takuma, H., Shimizu, T., J. Phys. Soc. Jap. 15, 1960, p. 2036.

51 Shimizu, T., Scientific Papers of the Institute of Phys. and Chem. Res. 57, 1963, p. 37.

52 Shimizu, T., Shimoda, K., J. Phys. Soc. Jap. 16, 1961, p. 777.

53 Thaddeus, P., Krisher, L. C., Rev. Sci. Instr. 32, 1961, p. 1083.

54 Thaddeus, P., Krisher, L. C., Loubser, J. H. N., J. Chem. Phys. 40, 1964, p. 257.

55 Krupnov, A. F., Skvortsov, V. A., S.P. J.E.T.P. 18, 1964, p. 74.

56 Krupnov, A. F., Skvortsov, V. A., S.P. J.E.T.P. 18, 1964, p. 1426.

57 Krupnov, A. F., Skvortsov, V. A., S.P. J.E.T.P. 20, 1965, p. 1079.

58 Marcuse, D., J. Ap. Phys. 32, 1961, p. 743.

59 Marcuse, D., Proc. I.R.E. 49, 1961, p. 1706.

60 Marcuse, D., Trans. I.R.E. I. 11, 1962, p. 187.

61 Barnes, F. S., Maley, D., Electronics, 17 March, 1961, p. 45.

62 Barnes, F. S., Proc. I.E.E.E. 51, 1963, p. 115.

63 Lainé, D. C., Srivastava, R. C., Smith, A. L. S., Ingram, D. J. E., Proc. Symp. on Optical Masers, Brooklyn, 1963, p. 617.

64 Wells, W. H., J. Ap. Phys. 36, 1965, p. 2838.

65 Gorog, I., U.S. Government Report A.F.O.S.R. 1978 (AD275 428) 1961.

66 Basov, N. G., Letokhov, V. S., S.P. J.E.T.P. Letters 2, 1965, p. 3.

67 Gordy, W., Cowan, M., J. Ap. Phys. 31, 1960, p. 941.

68 Bergmann, S. M., J. Ap. Phys. 31, 1960, p. 275.

69 Shimoda, K., Wang, T. C., Rev. Sci. Instr. 26, 1955, p. 1148.

70 Schulten, G., Philips Research Reports 19, 1964, p. 395.

71 Lainé, D. C., Proc. Phys. Soc. 87, 1966, p. 855.

72 Bolef, D. I., Chester, P. F., Trans. I.R.E. M.T.T. 6, 1958, p. 47.

73 Chester, P. F., Bolef, D. I., Proc. I.R.E. 45, 1957, p. 1287.

74 Hirshfield, J. L., Wachtel, J. M., Phys. Rev. Letters 12, 1964, p. 535.

74a Marcuse, D., Proc. 3rd Int. Quantum Electronics Conference, Paris 1963, p. 1161.

75 Lainé, D. C., Elect. Tech. 37, 1960, p. 174.

76 Matthei, W. G., Microwave Journal 9, 1966, p. 39.

77 Shimoda, K., Takahasi, H., Townes, C. H., J. Phys. Soc. Jap. 12, 1957, p. 686.

78 Muller, M. W., Phys. Rev. 106, 1957, p. 8.

79 Ditchfield, C. R., Solid State Elect. 4, 1962, p. 171.

80 Minkowski, J. M., Phys. Rev. 119, 1960, p. 1577.

81 Hughes, W. E., Proc. I.R.E. 50, 1962, p. 1691.

82 Odehnal, M., Czech. J. Phys. B13, 1963, p. 8.

83 Hughes, W. E., Richards, W. E., J. Quantum Electronics 1, 1965, p. 221.

84 Hughes, W. E., Deal, R. E., Proc. I.E.E.E. 52, 1964, p. 857.

85 Walling, J. C., Solid State Elect. 4, 1962, p. 225.

86 Yngvesson, S., Kollberg, E., Proc. I.E.E.E. 53, 1965, p. 1737.

87 Matveenko, L. I., Misezhnikov, G. S., Mukhina, M. M., Shteinshleiger, V. B., S.P. Doklady 10, 1965, p. 320.

88 Morris, L. C., Miller, D. J., J. Quantum Electronics 1, 1965, p. 164.

89 Arams, F. R., Peynton, B. J., Proc. I.E.E.E. 53, 1965, p. 12.

89a McEvoy, J. P. Miller, D. J., Morris, L. C., Solid State Elect. 4, 1965, p. 443.

90 Harris, K. D., Elect. Tech. 39, 1962, p. 86.

91 Sanders, J. H., J. Brit. I.R.E., 24, 1962, p. 365.

92 Ingram, D. J. E., Contemporary Physics 3, 1962, p. 435.

93 Applied Optics Supplement on Optical Masers, 1962.

94 Yariv, A., Gordon, J. P., Proc. I.E.E.E. 51, 1963, p. 4.

95 Kassel, S., Proc. I.E.E.E. 51, 1963, p. 216.

96 Schawlow, A. L., Contemporary Physics 5, 1963, p. 81.

97 Lax, B., Microwave J. 9, 1966, p. 24.

98 Rosenthal, J. E., Ap. Opt. 1, 1962, p. 169.

99 'Lasers and their Applications', Conference Proceedings I.E.E. London, September, 1964.

100 Heavens, O. S., Brit. J. Ap. Phys. 17, 1966, p. 287.

101 Wright, J. K., Contemporary Physics 6, 1964, p. 1.

102 Miller, R. C., Ap. Phys. Letters 5, 1964, p. 17.

103 Franken, P. A. Ward, J. F., Rev. Mod. Phys. 35, 1963, p. 23.

104 Gilliano, C. R., Ap. Phys. Letters 5, 1964, p. 137.

105 Megla, G. K., Ap. Opt. 2, 1963, p. 311.

106 Jones, O. C., J. Sci. Instr. 41, 1964, p. 653.

107 Anderson, L. K., Microwaves, January, 1955, p. 42.

108 Kogelnik, H., Yariv, A., Proc. I.E.E.E. 52, 1964, p. 165.

109 Koestler, C. J., Snitzer, E., Ap. Opt. 3, 1964, p. 1182.

110 Bridges, W. B., Picus, G. S., Ap. Opt. 3, 1964, p. 1189.

111 Marcuse, D., Proc. I.E.E.E. 53, 1965, p. 687.

112 Freed, C., Haus, H. A., Ap. Phys. Letters 6, 1965, p. 85.

113 Mathias, L. E. S., Rock, N. H., Ap. Opt. 4, 1965, p. 133.

114 Steele, E. L., Davis, W. C., J. Ap. Phys. 36, 1965, p. 348.

115 Moos, H. W., Imbusch, G. F., Mollenhauer, L. F., Schawlow, A. L., Ap. Opt. 2, 1963, p. 817.

116 Gerardo, J. B., Verdeyen, J. T., Proc. I.E.E.E. 52, 1964, p. 690.

117 Adams, C. M., Hardnay, G. A., Trans. I.E.E.E. I.G.A. 1, 1965, p. 90.

118 Meisels, M., Microwaves, December, 1964, p. 6.

119 Macek, W. M., Davis, D. T. M., Ap. Phys. Letters 2, 1963, p. 67.

120 Sinclair, D., Given, M. P., J.O.S.A. 54, 1964, p. 795.

121 Pennington, K. S., Microwaves, October, 1965, p. 35.

122 Brinton, J. B., Microwaves, March, 1966, p. 8.

123 Rigden, J. D., Gordon, E. I., Proc. I.R.E., 50, 1962, p. 2387.

124 Oliver, B. M., Proc. I.E.E.E. 51, 1963, p. 220.

125 Langmuir, R. V., Ap. Phys. Letters, 2, 1963, p. 29.

126 Allen, L., Jones, D. G. C., Phys. Rev. Letters 7, 1963, p. 321.

127 Goldfischer, L. I., J.O.S.A. 55, 1965, p. 247.

128 Chiao, R. Y., Garmire, E., Townes, C. H., Phys. Rev. Letters 13 1964, p. 479.

129 Lewis, B. L., Proc. I.E.E.E. 53, 1965, p. 1768.

130 Wang, C. C., Phys. Rev. Letters 16, 1966, p. 344.

131 Garmire, E., Chiao, R. Y., Townes, C. H., Phys. Rev. Letters 16, 1966, p. 347.

132 Garrett, C. G. B., Proceedings 3rd Int. Quantum Electronics Conference, Paris, 1963, p. 971.

133 Gurs, K., Z.A.M.P. 16, 1965, p. 49.

134 Applied Optics supplement on Chemical Lasers, 1965.

135 Nieuwpoort, W. C., Bleekrode, R., Z.A.M.P. 16, 1965, p. 101.

136 Stockman, D. L., Mallory, W. R., Tittel, K. F., Proc. I.E.E.E. 52, 1964, p. 318.

137 Zernike, F., Berman, P. R., Phys. Rev. Letters 15, 1965, p. 999.

138 Dumke, W. P., Phys. Rev. 127, 1962, p. 1559.

139 Burns, G., Natham, M. I., Proc. I.E.E.E. 52, 1964, p. 770.

140 Lax, B., I.E.E.E. Spectrum, July, 1965, p. 62.

141 Holonyak, N., Bevacqua, F., Ap. Phys. Letters 1, 1962, p. 82.

142 Melngailis, I., Ap. Phys. Letters 6, 1965, p. 59.

143 Butler, J. F., Calawa, A. R., Phelan, R. J. Jr., Harman, T. C., Strauss, A. J., Rediker, R. H., Ap. Phys. Letters 5, 1964, p. 75.

144 Hurwitz, C. E., Keyes, R. J., Ap. Phys. Letters 5, 1964, p. 139.

145 Rabinonitz, P., Jacobs, S., Gould, G., Ap. Opt. 1, 1962, p. 513.

146 Allen, L., Jones, D. G. C., Advances in Phys. 14, 1965, p. 479.

147 Patel, C. K. N., Bennett, W. R., Faust, W. L., McFarlane, R. A., Phys. Rev. Letters 9, 1962, p. 102.

148 Faust, W. L., McFarlane, R. A., Patel, C. K. N., Garrett, C. G. B., Ap. Phys. Letters 1, 1962, p. 85.

149 Faust, W. L., McFarlane, R. A., Patel, C. K. N., Garrett, C. G. B., Phys. Rev. 133, 1964, p. A1476.

150 Faust, W. L., McFarlane, R. A., Patel, C. K. N., Garrett, C. G. B., Ap. Phys. Letters 4, 1964, p. 18.

151 Faust, W. L., McFarlane, R. A., Patel, C. K. N., Garrett, C. G. B., Proc. I.E.E.E. 52, 1964, p. 318.

152 Faust, W. L., McFarlane, R. A., Patel, C. K. N., Garrett, C. G. B., Proc. I.E.E.E. 52, 1964.

153 Labuda, E. F., Gordon, E. I., Miller, R. C., J. Quantum Electronics 1, 1965, p. 273.

154 Cheo, P. K., Cooper, H. G., J. Ap. Phys. 36, 1965, p. 1862.

155 Kasper, J. V. V., Pimentel, G. C., Phys. Rev. Letters 14, 1965, p. 352.

156 Becker, C. H., Cox, G. C., McLennan, D. B., Proc. I.E.E.E. 51, 1963, p. 358.

157 Fink, E. L., Ellison, G. N., Proc. I.E.E.E. 51, 1963, p. 951.

158 Turner, T. E., Electronics, November, 1963.

159 Bazhulin, P. A., Knyazev, I. N., Petrash, G. G., S.P. J.E.T.P. 23, 1965, p. 649.

160 Marcuse, D., Proc. I.E.E.E. 51, 1963, p. 849.

161 Mathias, L. E. S., Parker, J. T., Ap. Phys. Letters 3, 1963, p. 16.

162 " " , Phys. Letters 7, 1963, p. 194.

163 Patel, C. K. N., Phys. Rev. Letters 12, 1964, p. 588.

164 Patel, C. K. N., Phys. Rev. 136, 1964, p. A1187.

165 " , Phys. Rev. Letters 13, 1964, p. 617.

166 Mathias, L. E. S., Crocker, A., Wills, M. S., Phys. Letters 13, 1964, p. 303.

167 Patel, C. K. N., Ap. Phys. Letters 7, 1965, p. 273.

168 Moeller, G., Rigden, J. D., Ap. Phys. Letters 7, 1965, p. 274.

169 Patel, C. K. N., Tien, P. K., McFee, J. H., Ap. Phys. Letters 7, 1965, p. 290.

170 Crocker, A., Gebbie, H. A., Kimmitt, M. F., Mathias, L. E. S., Nature 201, 1964, p. 250.

171 Gebbie, H. A., Findlay, F. D., Stone, N. W. B., Robb, J. A., Nature 202, 1964, p. 169.

172 Mathias, L. E. S., Crocker, A., Phys. Letters 13, 1964, p. 35.

173 Witteman, W. J., Bleekrode, R., Phys. Letters 13, 1964, p. 126.

174 Large, L. N., Hill, H., Ap. Opt. 4, 1965, p. 625.

175 Mathias, L. E. S., Crocker, A., Wills, M. S., Phys. Letters 14, 1965, p. 33.

176 Gebbie, H. A., Stone, N. W. B., Findlay, F. D., Nature 202, 1964, p. 685.

177 Chantry, G. W., Gebbie, H. A., Chamberlain, J. E., Nature 205, 1965, p. 377.

178 Mathias, L. E. S., Crocker, A., Wills, M. S., Elect. Letters 1, 1965, p. 45.

179 Steffen, H., Steffen, J., Moser, J. F., Kneubuhl, F. K., Phys. Letters 20, 1966, p. 20.

180 Devor, D. P., O'Haenens, I. J., Asawa, C. K., Phys. Rev. Letters 8, 1962, p. 432.

181 Devor, D. P., Trans. I.E.E.E. M.T.T. 11, 1963, p. 251.

182 Szabo, A., Proc. I.E.E.E. 51, 1963, p. 1037.

183 Zverev, G. M. Prokhorov, A. M. Shevchenko, A. K., S.P. J.E.T.P. 17, 1963, p. 952.

184 Strain, R. J., Coleman, P. D., Trans. I.E.E.E. M.T.T. 11, 1963.

185 Phelan, R. J. Jr., Rediker, R. H., Ap. Phys. Letters 6, 1965, p. 70.

186 Varsanyi, F., American Physical Society Spring Meeting, 1965, Paper AH7.

187 Varsanyi, F., Phys. Rev. Letters 14, 1965, p. 786.

188 Bloembergen, N., Phys. Rev. Letters 2, 1959, p. 84.

189 Krupke, W. J., J. Quantum Electronics 1, 1965, p. 20.

190 Brown, M. R., Shand, W. A., Phys. Rev. Letters 12, 1964, p. 367.

191 " " , Phys. Letters 18, 1965, p. 95.

192 Bell, W. E., Bloom, A., Rempel, R. C., Proceedings 3rd Int. Quantum Electronics Conf., Paris, 1963, P1347.

193 Scalapino, D. J., Vassiliadis, A., Wilson, R. N., I.E.E.E. Int. Conv. Rec. 12, 1964, p. 18.

194 Fontana, J. R., Pantell, R. H., Smith, R. G., Proc. I.R.E. 50, 1962, p. 469.

195 Akitt, D. P., Coleman, P. D., J. Ap. Phys. 36, 1965, p. 2004.

196 Andresen, H. G., U.S. Gov. Res. Rep. AD-426 998, Sept. 1963.

197 Sorokin, P. P., Braslau, N., I.B.M. Journal 8, 1964, p. 177.

198 Shiren, N. S., Ap. Phys. Letters 7, 1965, p. 142.

199 Martin, D. H., Contemporary Physics 4, 1963, p. 139.

200 Martin, D. H., Contemporary Physics 4, 1963, p. 187.

201 Bloor, D., Dean, T. J., Jones, G. O., Martin, D. H., Mawer, P. A., Perry, C. H., Proc. Roy. Soc. 260A, 1961, p. 510.

202 Jones, G. O., Martin, D. H., Mawer, P. A., Perry, C. H., Proc. Roy. Soc. 261A, 1961, p. 10.

203 Bastin, J. A., Gear, A. E., Jones, G. O., Smith, H. J. T., Wright, P. J., Proc. Roy. Soc. 278A, 1964, p. 543.

204 Ramsay, J. F., Proc. I.R.E. 46, 1958, p. 405.

205 Nichols, L., Edwards, R., Krahn, H. J., Elect. Tech. 41, 1964, p. 63.

206 Coleman, P. D., Trans. I.E.E.E. M.T.T. 11, 1963, p. 271.

207 Kaufman, I., Proc. I.R.E. 47, 1959, p. 381.

208 Twersky, V., Ap. Opt. 4, 1965, p. 1213.

209 King, D. D., I.E.E.E. Spectrum 2, 1965, p. 64.

210 'Proc. Symp. on Millimetre Waves' March-April, 1959, Brooklyn, New York.

211 Wall, M. E., Kuhn, T. G., Microwaves 5, 1966, p. 18.

212 Hadni, A., Decamps, E., Munier, J., Revue d'Opt. 11, 1963, p. 584.

213 Boldt, W., Reimann, H., Ann. der Phys. 7, 6, 1960, p. 293

214 Plyler, E. K., Yates, D. J. C., Gebbie, H. A., J.O.S.A. 52, 1962, p. 859.

215 Filippov, O. K., Pirovarov, V. M., S.P. Opt. and Spec. 15, 1963, p. 282.

216 Plyler, E. K., Blaine, L. R., J. Res. N.B.S. 64c, 1960, p. 55.

217 Hadni, A., Wyncke, B., Strimer, P., Decamps, E., Claudel, J., Proc. Int. Conf. Q. Elect. Paris, 1964, p. 731.

218 Kropotkin, M. A., Kozysev, B. P., S.P. Opt. and Spec. 17, 1964, p. 136.

219 Hadni, A., Claudel, J., Gerbaus, X., Morlot, G., Munier, J. M., Ap. Opt. 4, 1965, p. 487.

220 Richards, P. L., J.O.S.A. 54, 1964, p. 1474.

221 Czerny, M., Turner, A. F., Zeit. Phys. 61, 1930, p. 792.

222 Schafer, A. B., Megill, L. R., Droppleman, L., J.O.S.A. 54, 1964, p. 879.

223 Fastie, W. G., J.O.S.A. 42, 1953, p. 641.

224 Willis, H. A., Miller, R. G. J., Adams, D. M., Gebbie, H. A., Spect. Acta 19, 1963, p. 1457.

225 Filippov, O. K., Yaroslavskii, N. G., S.P. Opt. and Spec. 15, 1963, p. 299.

226 Roberts, S., Coon, D. D., J.O.S.A. 52, 1962, p. 1023.

227 Mitsuishi, A., Yamada, Y., Yoshinaga, H., J.O.S.A. 52, 1962, p. 14.

228 " " " , J.O.S.A. 52, 1962, p. 17.

229 Turner, A. F., Chang, L., Martin, T. P., Ap. Opt. 4, 1965, p. 927.

230 Happ, H., Hofmann, H. W., Lux, E., Seger, G., Zeit. f. Physik 166, 1962, p. 510.

231 Möller, K. D., McKnight, R. V., J.O.S.A. 53, 1963, p. 760.

232 Mitsuishi, A., Otsuka, T., Fujita, S., Yoshinaga, H., Jap. J. Ap. Phys. 2, 1963, p. 574.

233 Renk, K. F., Genzel, L., Ap. Opt. 1, 1962, p. 643.

234 Möller, K. D., McKnight, R. V., J.O.S.A. 55, 1965, p. 1075.

235 Proc. Symp. on Quasi-Optics, Brooklyn, New York, 1964.

236 Dekany, M., Elect. Design, June, 1964, p. 12.

237 Williamson, D. E., J.O.S.A. 42, 1952, p. 712.

238 Ohlman, R. C., Richards, P. L., Tinkham, M., J.O.S.A. 48, 1958, p. 531.

239 Chen, M. M., Berkowitz-Mattuck, J. B., Glaser, P. E., Ap. Opt. 2, 1963, p. 265.

240 Pargamanik, L. E., Daich, A. R., Tsirlin, Yu. A., S.P. Opt. and Spec. 17, 1964, p. 418.

241 Putley, E. H., Proc. I.E.E.E. 51, 1963, p. 1412.

242 Golay, M. J. E., Rev. Sc. Instr. 18, 1947, p. 357.

243 Kamiya, K., Yoshihara, K., Science of Light 8, 1959, p. 1.

244 Bott, I. B., Proc. I.E.E.E. 52, 1964, p. 330.

245 Bott, I. B., Phys. Letters 14, 1965, p. 293.

246 Jones, G., Gordy, W., Phys. Rev. 135, 1964, p. A295.

247 Laine, D. C., Nature 191, 1961, p. 795.

248 Mahan, G. D., Hopfield, J. J., J. Ap. Phys. 34, 1963, p. 1531.

249 Fox, A. J., Smith, N. W. W., Proc. I.E.E.E. 52, 1964, p. 429.

250 Zernike, F., Berman, P. R., Phys. Rev. Letters 15, 1965, p. 999.

251 Laine, D. C., Srivastava, R. C., Smith, A. L. S., Ingram, D. J. E., 'Proc. Symp. Optical Masers', Brooklyn, New York, April, 1963, p. 617.

252 Plyler, K., Acquista, N., J. Res. N.B.S. 56, 1956, p. 149.

253 Plyler, E. K., Blaine, L. R., J. Res. N.B.S. 60, 1958, p. 55.

254 " " , J. Res. N.B.S. 64, 1960, p. 55.

255 Rao, K. N., Vore, R. V de, Plyler, E. K., J. Res. N.B.S., 67a, 1963, p. 351.

256 Palik, E. D., N.R.L. Bibliography No. 21.

257 Strong, J., J.O.S.A. 39, 1949, p. 320.

258 McCubbin, T. K., Sinton, W. M., J.O.S.A. 42, 1952, p. 113.

259 McCubbin, T. K., J. Chem. Phys. 20, 1952, p. 668.

260 Russell, J. W., Strauss, H. L., Ap. Opt. 4, 1965, p. 1131.

261 Murrell, J. N., Kettle, S. F. A., Tedder, J. M., 'Valence Theory', Wiley, London, 1965.

262 Seel, F., 'Atomic Structure and Chemical Bonding', Methuen, London, 1963.

263 Herzberg, G., 'Infrared and Raman Spectra', Van Nostrand, New York, 1945.

264 Townes, C. H., Schawlow, A. L., 'Microwave Spectroscopy', McGraw-Hill, New York, 1955.

265 Vuylsteke, A. A., 'Elements of Maser Theory', Van Nostrand, Princeton, 1962.

267 Mould, H. M., Price, W. C., Wilkinson, G. R., Spect. Acta 14, 1959, p. 313.

268 Barrow, G. M., 'Introduction to molecular spectroscopy', McGraw-Hill, New York, 1962.

269 Wright, N., Randall, H. M., Phys. Rev. 44, 1933, p. 391.

270 Cleeton, C. E., Williams, N. H., Phys. Rev. 45, 1934, p. 234.

271 Dennison, D. M., Uhlenbeck, G. E., Phys. Rev. 41, 1932, p. 313.

272 Dennison, D. M., Rev. Mod. Phys. 3, 1931, p. 280.

273 Good, W. E., Phys. Rev. 70, 1946, p. 213.

274 Sheng, H., Barker, E. F., Dennison, D. M., Phys. Rev. 60, 1941, p. 786.

275 Newton, R. R., Thomas, L. H., J. Chem. Phys. 16, 1948, p. 310.

276 Swalen, J. D., Ibers, J. A., J. Chem. Phys. 36, 1962, p. 1914.

277 Bagdanskis, N. I., Bulanin, M. O., S.P. Opt. and Spec. 19, 1965, p. 128.

278 Costain, C. C., Phys. Rev. 82, 1951, p. 108.

279 Hansler, R. L., Oetjen, R. A., J. Chem. Phys. 21, 1953, p. 1340.

280 Barnes, R. B., Phys. Rev. 47, 1935, p. 658.

281 McCubbin, T. K., J. Chem. Phys. 20, 1952, p. 668.

282 McCubbin, T. K., Sinton, W. M., J.O.S.A. 40, 1950, p. 537.

283 Gunther-Mohr, G. R., White, R. L., Schawlow, A. L., Good, W. E., Coles, D. K., Phys. Rev. 94, 1954, p. 1184.

284 Gunther-Mohr, G. R., Townes, C. H., Van Vleck, J. H., Phys. Rev. 94, 1954, p. 1191.

285 Van Vleck, J. H., Rev. Mod. Phys. 23, 1951, p. 213.

286 Bonanomi, J., de Prins, J., Herrmann, J., Kartaschoff, P., Rossel, J., Archives des Science, 10, 1957, p. 187.

287 Bonanomi, J., De Prins, J., Herrmann, J., Kartaschoff, P., Helv. Phys. Acta 30, 1957, p. 288.

287a Oraevskii, A. N., 'Soviet Maser Research' ed. D. V. Skobeltsyn, (translation of P. N. Lebedev Physics Institute Proceedings Vol. 21), Consultants Bureau, New York, 1964, p. 1.

288 Holuj, F., Daams, H., Kalra, S. N., J. Ap. Phys. 33, 1962, p. 2370.

289 Coles, D. K., Good, W. E., Bragg, J. H., Sharbaugh, A. H., Phys. Rev. 82, 1951, p. 877.

290 Jauch, J. M., Phys. Rev. 72, 1947, p. 715.

291 Vonbun, F. C., J. Ap. Phys. 29, 1958, p. 632.

292 Shimoda, K., Rendiconti S.I.F. 17, 1960, p. 1.

293 Giordmaine, J. A., Wang, T. C., J. Ap. Phys. 31, 1960, p. 463.

294 Shimoda, K., Takuma, H., Shimizu, T., J. Phys. Soc. Jap. 15, 1960, p. 2036.

295 Hirono, M., J. Radio Res. Lab. 6, 1959, p. 515.

296 Helmer, J. C., Jacobus, F. B., Sturrock, P. A., J. Ap. Phys. 31, 1960, p. 458.

297 Becker, G., Zeit. angew Phys. 15, 1963, p. 13.

" , " " " 15, 1963, p. 281.

" , " " " 13, 1961, p. 59.

" , Proc. 3rd Int. Quantum Electronics Conference, Paris, 1963, p. 393.

298 Pickara, A., Stankowski, J., Smolinska, S., Galica, J., Postepy Fizyki 15, 1964, p. 565.

299 Basov, N. G., Zuev, V. S., S.P. Instruments and Experimental Techniques 1, 1961, p. 122.

300 Kazachok, V. S., S.P. Technical Physics 10, 1965, p. 882.

301 Moreno, T., 'Microwave Transmission Design Data', Dover, New York, 1948.

302 Connes, P., Revue d'Optique 35, 1956, p. 37.

" , J. Phys. Radium 19, 1958, p. 262.

303 Jackson, D. A., Proc. Roy. Soc. A263, 1961, p. 289.

304 Fox, A. G., Li, T., Bell System Tech. J. 40, 1961, p. 453.

305 Zimmerer, R. W., Proc. I.E.E.E. 51, 1963, p. 475.

306 Welling, H., Andresen, H. G., Tran. I.E.E.E. M.T.T.-12, 1964, p. 249.

307 Kogelnik, H., Rigrod, W. W., Proc. I.E.E.E. 50, 1962, p. 220.

308 Vanyukov, M. P., Isaenko, V. I., Kalinin, V. P., Lyubimov, V. V., S.P. Opt. and Spec. 19, 1965, p. 161.

309 Sinclair, D. C., Ap. Opt. 3, 1964, p. 1067.

310 Boyd, G. D., Kogelnik, H., Bell System Tech. J. 41, 1962, p. 1347.

311 Boyd, G. D., Gordon, J. P. Bell System Tech. J. 40, 1961, p. 489.

312 Sochoo, R. F., Proc. I.E.E.E. 51, 1963, p. 70.

313 Fox, A. G., Li, T., Proc. I.E.E.E. 51, 1963, p. 80.

314 Strauch, R. G., Cupp, R. E., Lichtenstein, M., Gallagher, J. J., Proc. Symp. on Quasi Optics, Brooklyn, New York, 1964, p. 581.

315 Brannen, E., Proc. I.E.E.E. 53, 1965, p. 2134.

316 Auston, D. H., Primich, R. I., Hayami, R. A., Proc. Symp. on Quasi Optics, Brooklyn, New York, 1964, p. 273.

317 Davis, S. P., Ap. Opt. 2, 1963, p. 727.

318 Akselrad, A., Kiss, Z. J., Lewis, H. R., U.S. Gov. Res. Rep. No. AD 432 058, 20 December, 1963.
Mormen, H., J. Physik, 59, 1929, p. 791.

319 Korolev, F. A., Gridnev, V. I., S.P. Opt. and Spec. 16, 1964, p. 181.

320 Schlossberg, H., Javan, A., Am. Phys. Soc. Spring Meeting, April, 1965, Paper AH5.

321 McCumber, D. E., Bell System Tech. J. 44, 1965, p. 333.

322 Morokuma, T., J. Res. N.B.S., 68C, 1964, p. 25.

323 Culshaw, W., Trans. I.R.E. M.T.T.-7, 1959, p. 221.

324 " , " " M.T.T.-8, 1960, p. 182.

325 " , " " M.T.T.-9, 1961, p. 135.

326 " , " " M.T.T.-10, 1962, p. 331.

327 Zimmerer, R. W., Anderson, M. V., Strine, G. L., Beers, Y., Trans. I.E.E.E. M.T.T.-11, 1963, p. 142.

328 Balakhanov, V. Ya., S.P. Doklady 10, 1966, p. 783.

" , " " 10, 1966, p. 788.

329 Vinogradov, E. A., Dianov, E. M., Irisova, N. A., S.P. J.E.T.P. Letters 1, 1965, p. 205.

330 Sher, N., I.R.E. National Convention Record Part 1, A.P. M.T.T. 1958, p. 27.

331 Townes, C. H. Geschwind, S., J. Ap. Phys. 19, 1948, p. 795.

332 Townes, C. H., Phys. Rev. Letters 5, 1960, p. 428.

333 Wang, T. C., J. de Phys. et le Radium 21, 1960, p. 261.

334 Alsop, L. E., Giordmaine, J. A., Townes, C. H., Wang, T. C., Phys. Rev. 107, 1957, p. 1450.

335 Beers, Y., Rev. Sci. Instr. 32, 1961, p. 23.

336 Gordon, J. P., White, L. D., Proc. I.R.E. 46, 1958, p. 1588.

337 Bonanomi, J., Hermann, J., De Prins, J., Kartasshoff, P., Rev. Sci. Instr. 28, 1957, p. 879.

338 Robinson, F. N. H., 'Noise in Electrical Circuits', Oxford, 1962.

339 Wallman, H., Macnee, A. B., Gadsden, C. P., Proc. I.R.E. 36, 1948, p. 700.

340 Smith, M. J. A., J. Sc. Instr. 39, 1962, p. 127.

341. Ginston, E. L. (ed.), 'Microwave Measurements', p. 44-49, McGraw-Hill, 1957.

342 Barnes, F. S., Proc. I.R.E. 47, 1959, p. 2085.

343 Jaynes, E. T., Cummings, F. W., Proc. I.E.E.E. 51, 1963, p. 89.

344 Lecar, H., Okaya, A., 'Paramagnetic Resonance' ed. W. Low, Academic Press, New York, 1963, p. 675.

345 Troup, G. J., Worner, J., Proc. 3rd Int. Conf. Quantum Electronics, Paris, 1963, p. 943.

346 Higa, W. H., Rev. Sc. Instr. 28, 1957, p. 726.

347 Javan, A., Wang, T. C., Bull. Am. Phys. Soc. 2, 1957, p. 209.

348 Reder, F. H., Bickart, C. J., Rev. Sc. Instr. 31, 1960, p. 1164.

349 Wells, W. H., J. Ap. Phys. 29, 1958, p. 714.

350 Bloom, S., J. Ap. Phys. 27, 1956, p. 785.

351 Feynman, R. P. Vernon, F. L., Hellwarth, R. W., J. Ap. Phys. 28, 1957, p. 49.

352 Strakhovskii, G. M., Tatarenkov, V. M., S.P. J.E.T.P. 15, 1962, p. 625.

353 Lainé, D. C., Srivastava, R. C., J. Brit. I.R.E. 26, 1963, p. 173.

354 Srivastava, R. C. Univ. of Birmingham unpublished thesis, 1962.

355 Basov, N. G., Oraevskii, A. N., S.P. J.E.T.P. 15, 1962, p. 1062.

356 Belenov, E. M., Orayevskiy, A. N., S.P. R.E. and E.P., 1963, p. 140.

357 Strakhovskiy, G. M., Tatarenkov, V. M., Tumanov, O. A., S.P. Isvestiya Vuziya Radiophysica 6, 1963, p. 1279.

358 Basov, N. G., Oraevskii, A. N., Strakhovskii, G. M., Tatarenkov, V. M., S.P. J.E.T.P. 18, 1964, p. 1211.

359 Basov, N. G., Oraevskii, A. N., Strakhovsky, G. M., Tatarenkov, V. M., Proc. 3rd Int. Quantum Electronics Conference, Paris, 1963, p. 377.

360 Li Tie-Cheng, Fang Li-Zhi, Acta Physica Sinica 20, 1964, p. 753.

361 Lainé, D. C., Smith, A. L. S., Proc. 4th Int. Quantum Electronics Conference, Phoenix, 1966, and J. Quant. Elect. to be published.

362 Ramsey, N. F., 'Molecular Beams', Oxford, 1956.

363 Kukolich, S. G., Proc. I.E.E.E. 52, 1964, p. 211.

364 Laine, D. C., Smith, A. L. S., Physics Letters 20, 1966, p. 374.

365 Veselago, V. G., Oraevskii, A. N., Strakhovskii, G. N., Tatarenkov, V. M., S.P. J.E.T.P. Letters 2, 1965, p. 49.

366 Shimoda, K., Scientific Papers of the Institute of Phys. and Chem. Res. 55, 1961, p. 1.

367 Strain, R. J., Private Communication, 1965.

368 Goldick, H. D., Private Communication, 1966.

369 Barchukov, A. I., Prokhorov, A. M., Savransky, V. V., Proc. 3rd Int. Conf. Quantum Electronis, Paris, 1963, p. 419.

370 Prokhorov, A. M., Private Communication, 1965.